28th edition

ISSN 1454 - 8003

Proceedings of International Conference on HYDRAULICS, PNEUMATICS, SEALING ELEMENTS, TOOLS, PRECISION MECHANICS, SPECIFIC ELECTRONIC EQUIPMENT & MECHATRONICS

HERVEX 2024

November 13-15 | Băile Govora, ROMANIA

HERVEX

November 2024
28th Edition

INTERNATIONAL CONFERENCE

HERVEX 2024

Hydraulics| Pneumatics|
Sealing Elements| Tools| Precision Mechanics|
Specific Electronic Equipment & Mechatronics

Baile Govora, ROMANIA | November 13 - 15, 2024

ORGANIZERS

HYDRAULICS AND PNEUMATICS RESEARCH INSTITUTE BUCHAREST, ROMANIA

CHAMBER OF COMMERCE AND INDUSTRY VALCEA, ROMANIA

ORGANIZING PARTNERS

WROCLAW UNIVERSITY OF SCIENCE AND TECHNOLOGY, POLAND

KOMAG INSTITUTE OF MINING TECHNOLOGY, POLAND

TECHNICAL UNIVERSITY OF MOLDOVA IN CHISINAU, REPUBLIC OF MOLDOVA

NATIONAL INSTITUTE OF RESEARCH & DEVELOPMENT FOR MACHINES AND INSTALLATIONS DESIGNED TO AGRICULTURE AND FOOD INDUSTRY – INMA BUCHAREST, ROMANIA

“POLITEHNICA” BUCHAREST NATIONAL UNIVERSITY OF SCIENCE AND TECHNOLOGY

“POLITEHNICA” UNIVERSITY OF TIMISOARA, ROMANIA

TECHNICAL UNIVERSITY OF CLUJ-NAPOCA, ROMANIA

“DUNAREA DE JOS” UNIVERSITY OF GALATI, ROMANIA

MEDIA PARTNERS

HERVEX 2024

INTERNATIONAL CONFERENCE

HERVEX 2024

HELD UNDER HONORARY AEGIS OF

Comité Européen des Transmissions Oléohydrauliques et Pneumatiques

SUPPORTED BY

Ministry of Research, Innovation and Digitalization in Romania (MCID)

National Professional Association of Hydraulics and Pneumatics in Romania - "FLUIDAS"

Conference Proceedings is **indexed by**

Published by Hydraulics and Pneumatics Research Institute, Bucharest, Romania

COMMITTEES

HONORARY COMMITTEE

PhD.Eng. Hubertus MURRENHOFF – Institute for Fluid Power Drives and Controls at Aachen University, Germany

Prof. PhD. Eng. Viorel BOSTAN – Rector of Technical University of Moldova, Republic of Moldova

PhD.Eng. Petrin DRUMEA – President of National Professional Association of Hydraulics and Pneumatics – FLUIDAS, Romania

Dipl.Eng. Valentin CISMARU – President of Chamber of Commerce and Industry Valcea, Romania

ORGANIZING COMMITTEE

Dipl. Eng. Gheorghe RIZOIU – General Manager of Chamber of Commerce and Industry Valcea, Romania

PhD. Eng. Gabriela MATACHE – Hydraulics and Pneumatics Research Institute in Bucharest, Romania

PhD. Eng. Krzysztof KEDZIA – Wroclaw University of Technology, Poland

Prof. PhD. Eng. Dan OPRUȚA – Technical University of Cluj-Napoca, Romania

Prof. PhD. Eng. Ilare BORDEAȘU – Politehnica University of Timisoara, Romania

Prof. PhD. Eng. Adrian CIOCĂNEA – Politehnica University of Bucharest, Romania

PhD. Phys. Mihai VARLAM - General Manager of National Research & Development Institute for Isotope & Cryogenics Technologies (ICSI) Râmnicu Vâlcea, Romania

PhD.Eng. Sergiu NICOLAIE – General Manager of R&D National Institute for Electrical Engineering ICPE-Advanced Researches, Bucharest, Romania

PhD.Eng. Nicolae-Valentin VLĂDUȚ – General Manager of National Institute of Research and Development for Machines and Installations Designed to Agriculture and Food Industry – INMA Bucharest, Romania

PhD.Eng. Ioan LEPĂDATU – Hydraulics and Pneumatics Research Institute in Bucharest, Romania

PhD.Eng. Cătălin DUMITRESCU – Director of Hydraulics and Pneumatics Research Institute in Bucharest, Romania

SCIENTIFIC PROGRAMME COMMITTEE

PhD.Eng. Zygmunt DOMAGALA – Wroclaw University of Technology, Poland

Prof. PhD.Eng. Valeriu DULGHERU – Technical University of Moldova, Republic of Moldova

PhD.Eng. Cătălin DUMITRESCU – Director of Hydraulics and Pneumatics Research Institute in Bucharest, Romania

D.Sc. Eng. Dariusz PROSTAŃSKI – KOMAG Institute of Mining Technology, Gliwice, Poland

Ph.D. Eng. Bartosz POLNIK – KOMAG Institute of Mining Technology, Gliwice, Poland

Ph.D. Eng. Krzysztof NIEŚPIAŁOWSKI – KOMAG Institute of Mining Technology, Gliwice, Poland

Ph.D. Eng. Artur DYCZKO – KOMAG Institute of Mining Technology, Gliwice, Poland

Ph.D. Eng. Radosław MARLĘGA – KOMAG Institute of Mining Technology, Gliwice, Poland

PhD.Eng. Wilhelm KAPPEL – Scientific Manager of R&D National Institute for Electrical Engineering ICPE-Advanced Researches, Bucharest, Romania

Prof. PhD.Eng. Mihai AVRAM – Politehnica University of Bucharest, Romania

Assoc. Prof. PhD.Eng. Nicușor BAROIU – "Dunarea de Jos" University of Galati, Romania

PhD.Eng. Mircea CHINTOANU – Director of Research Institute for Analytical Instrumentation INCDO INOE 2000 - ICIA Cluj-Napoca, Romania

Prof. PhD.Eng. Cristian PAVEL – Technical University of Civil Engineering in Bucharest, Romania

Lect. PhD.Eng. Mihail SAVANIU – Technical University of Civil Engineering in Bucharest, Romania

PhD.Eng. Cornelia MURARU-IONEL – National Institute of Research and Development for Machines and Installations Designed to Agriculture and Food Industry – INMA Bucharest, Romania

Prof. PhD.Eng. Neculai Eugen SEGHEDIN – Vice-Rector of "Gheorghe Asachi" Technical University of Iasi, Romania

PhD.Eng. Andrei DRUMEA – Politehnica University of Bucharest, Romania

Prof. PhD.Eng. Sorin CĂNĂNĂU – Politehnica University of Bucharest, Romania

Prof. PhD.Eng. Ion DAVID – Technical University of Civil Engineering in Bucharest, Romania

Prof. PhD.Eng. Edmond MAICAN – Politehnica University of Bucharest, Romania

PhD.Eng. Mihai Gabriel MATACHE – National Institute of Research – Development for Machines and Installations Designed to Agriculture and Food Industry – INMA, Bucharest- Romania

PhD.Eng. Mircea PRICOP – S.C. HESPER S.A., Bucharest, Romania

Lect. PhD.Eng. Ioan Lucian MARCU – Technical University of Cluj-Napoca, Romania

Lect. PhD.Eng. Daniel-Vasile BANYAI – Technical University of Cluj-Napoca, Romania

Dipl. Eng. Ioan CÂMPEAN – S.C. HIDROSIB S.A. Sibiu, Romania

PhD.Eng. Daniel MARIN – S.C. FAST ECO S.A., Bucharest, Romania

PhD.Eng. Adrian MIREA – S.C. FAST ECO S.A., Bucharest, Romania

Dipl. Eng. Ioan MOLDOVEANU – Festo S.R.L., Bucharest, Romania

PhD.Eng. Iulian-Claudiu DUȚU – Politehnica University of Bucharest, Romania

Dipl. Eng. Laurențiu NICOLAE – PROFLEX SERVICE S.R.L. Bucharest, Romania

Dipl. Eng. Nicolae TASU – HANSA FLEX Romania

EXECUTIVE SECRETARIAT

Ana-Maria POPESCU – Hydraulics and Pneumatics Research Institute in Bucharest, Romania

PhD. Chem. Adriana Mariana BORȘ – Hydraulics and Pneumatics Research Institute in Bucharest, Romania

Dipl. Eng. Ștefan-Mihai ȘEFU – Hydraulics and Pneumatics Research Institute in Bucharest, Romania

CONTENTS

ISSN 1454 - 8003
Proceedings of 2024 International Conference on Hydraulics and Pneumatics - HERVEX
November 13-15, Băile Govora, Romania

REALIGNING OF HYDRAULIC ENGINEERING EDUCATION TO ACTUAL INDUSTRIAL REQUIREMENTS

Peter HEIDRICH[1], Niklas WEISS[1], Mirko ROTHHAAR[1]

[1] University of Applied Sciences Kaiserslautern, Schoenstraße 11, 67659 Kaiserslautern, Germany, peter.heidrich@hs-kl.de; niklasweiss1@gmx.de; mirko.rothhaar@hs-kl.de

Abstract: *Fluid technology is an ever-changing technology influenced by actual trends like up-and-coming mechatronics or digitization of signals. Further influence is given by occurring new technologies like augmented and/or virtual reality as well as artificial intelligence. Hence, engineering education has to be adapted to these new requirements continuously. In this work we report on redesigning hydraulic lab exercises according to different curricula. Widespread hardware was purchased to cover all necessary technologies like solenoid valve circuits, servo valve operation with externally given velocity profiles and finally closed loop controller circuits. Based on included short hydraulic exercises comprehensive lab exercises of 30 to 60 minutes duration were developed and tested. Focus was here to involve knowledge of other course contents with adherence to the different curricula of Bachelor and Master studies. Finally, templates for all lab exercises were written and tested by ourselves. Future step will be to test new lab exercises with appropriate groups of students. Based on their feedback and additional feedback of supervising lab staff optimisation should be carried out – if necessary.*

Keywords: *Hydraulic engineering, hydraulic education, basic lab exercises, enhanced lab exercises*

1. Introduction

Fluid technology, including hydraulics as well as pneumatics, remains one of the most used drive train system in automation technology and automotive applications. Since its beginnings around 250 B.C. by Greek people like Archimedes or Heron of Alexandria [1, 2] continuous improvements led from simple machinery of the early days to today's high-tech applications of hydraulics and pneumatics.
Current trends are including fluid technology into mechatronics, digitization of signals and signal processing, integration into Industry 4.0 philosophy as well as testing of environmentally friendly pressure media like water-based liquids and using renewable energy sources like solar power to support hydraulic power trains [3, 4, 5]. Another topical field of interest is combining fluid technology with Augmented Reality (AR) and/or Virtual Reality (VR) [6, 7, 8]. Hence, it is possible to replace – especially for teaching and training purposes – expensive hardware by simulation tools embedded into augmented and/or virtual surroundings. Newly, benefits of linking fluid technology with Artificial Intelligence (AI) are researched and implemented to first industrial applications [9, 10].
Based on this awareness it is obviously, that hydraulic engineering education has to be realigned to these new requirements. Here it is important to find a proper balancing between basic understanding of hydraulics and introducing new technologies in lectures as well as in lab exercises. Otherwise students are not well prepared for professional life. Hence, in this paper we report on our experience in developing new lab exercises that would fulfill both specifications – train basic hydraulics and introduce new technologies.

2. Related Work

The first step was to carry out a comprehensive literature review regarding actual trends and opportunities in fluid technology education.
Generally, there is a constant need to adapt and enhance training systems and training methods of fluid technology to new and future requirements. Very important in this content is, that all improvements has to be specific to the target audience. For example, learning goals of future design

engineers are completely different to those who will work in maintenance or close to production [11, 12, 13].
A big challenge every now and then is, that commercially available training systems with appropriate technology are often either not available or only at tremendous cost. A simple relief could be to develop and design lab scale equipment in student work projects. As an example, miniature excavator arms were constructed and operated by electro-pneumatics or electro-hydraulics [14, 15]. Here, pneumatics is less dangerous and less oily compared to hydraulics. On the other side, hydraulics is more realistic to excavators. Additionally, controller based operation and even remote control by an app via blue tooth connection is possible [15].
Regarding teaching philosophy there seems to be a turning away from the classic fragmentation of lecture and lab exercises, at least for all fields of teaching, where theory is supported by practical contents. It begins with introducing active and cooperative teaching and learning methods to train soft skills along with knowledge, too [11, 16, 17, 18]. All references mention that student's abilities to cooperate, to solve problems and to be creative are promoted. Hence, students are better prepared for today's competitive working world. This trend continuous with Outcome Based Education (OBE) [19] and could finally result in gamification of lab exercises to catch student's attention [20]. Another possibility is to replace the classic written exam by project based workload with periodic self-assessment in combination with assessment by teaching staff [21]. Here students will train their self-reflection and their self-criticism, two important soft skills in today's working world. Finally, with all options there should always be an adaption of levels of difficulty to the level of studies, e.g. Bachelor versus Master [13, 22]. During the first semesters of Bachelor studies students need more guidance at lab time. At higher semesters of Bachelor studies the guidance should be replaced by space for development of own ideas. Additionally, tasks like planning, preparing and critical assessment should be taken into account. At Master studies students should get just problem descriptions and information on available lab equipment. Then, they should be able to solve the problem – with help from supervisors if necessary.
For several years there was a strong interest in developing and establishing remote and/or virtual lab exercises. One reason therefore is that training system hardware is not available with actual functionality, especially regarding needs of Industry 4.0 like electronical control of valves and digital data acquisition units [23]. Another reason is that more students could participate in virtual labs at any time – even at night or at the weekends – and with less cost for training equipment [24]. Especially due to COVID pandemic in 2020 there was need to offer non-contact lab exercises as well as non-contact assessment of lab activities. Hence, remote lab exercises were the one and only option to continue with education [25, 26].
Some lecturers integrate lab exercises like demonstrations into their lectures to replace boring slides and/or videos. Their experience shows more interest of students and hence, better marks [27, 28]. However, here the hardware must be transportable from lab to lecture hall or lectures has to take place directly in the lab. Sometimes special light weight equipment, in the referenced case even enhanced by augmented reality, has to be designed and produced [28].
A last conclusion is that in addition to academic fluid technology education the training of industrial people should be taken into account, too [11, 29]. Here training equipment as well as content of training courses should be adapted to the different knowledge base of industrial participants.

3. Hardware Selection

Based on all information of the literature review a requirement specification of the new hydraulic training system was finalised. The main items are:

- Exercises with manual operated valves – as basic hydraulics – should be performed with the actual training system;
- Exercises with solenoid operated valves should be performed with the new training system. Hence, appropriate operation units with low voltage power supply, a sufficient amount of push buttons, switches, electromagnetic relays (including switch-on delay and dropout delay) as well as audible alarms and visual displays must be available;

- Exercises with servohydraulic valves should be performed with the new training system. Therefore, actual controller units with features like zero balancing, slope time adjustment and test jacks of given value and actual value must be available;
- For all controller units the option of external generated given values – like sinusoidal wave, square wave or even sawtooth waveform – must be available;
- A hydraulic accumulator must be part of training system;
- Measurement equipment for pressure and flowrate must be part of training system;
- The hydraulic pump unit must be integrated into to training system;
- Due to safety reasons maximum system pressure should be 50 bar;
- All electrical equipment has to fulfil CE and GS mark requirements;
- For further enhancement of the system in future, an appropriate computer interface must be either integrated or could be upgraded easily.

With these items a noncommitted specification was created. After an open competitive bidding and an accurate assessment of all submitted proposals the new training system as shown in Figure 1 was purchased.

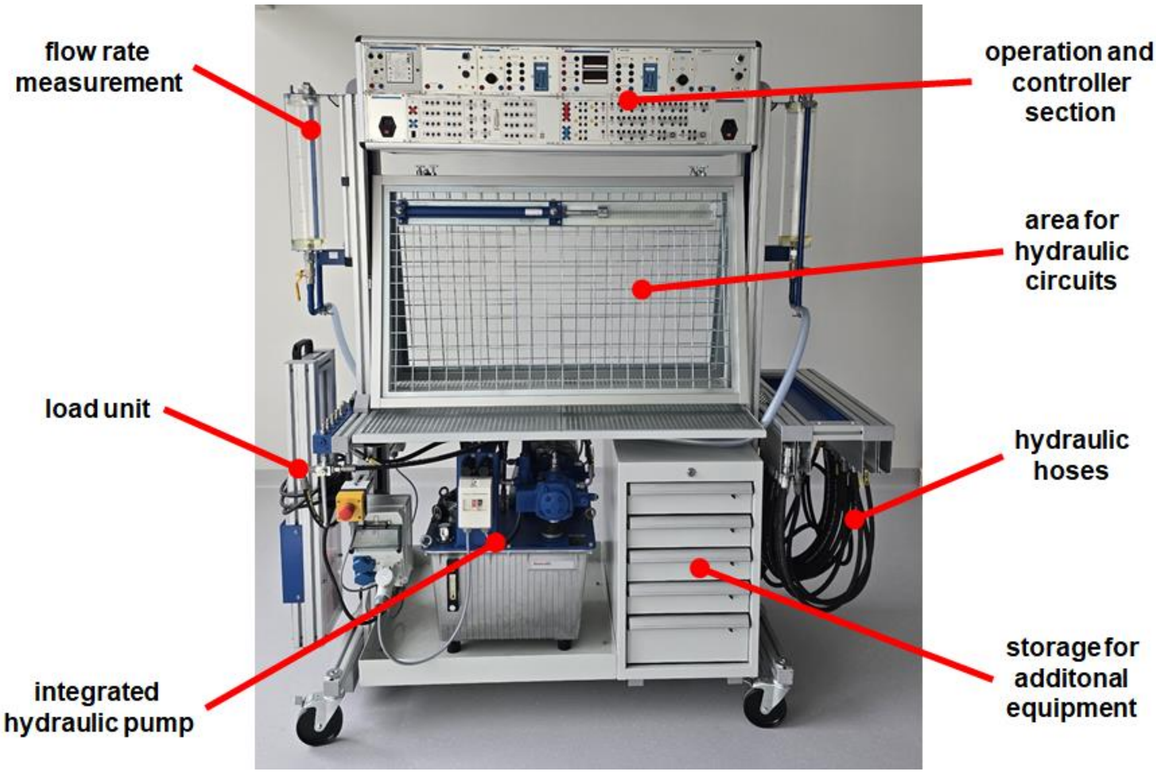

Fig. 1. New hydraulic training system at UAS Kaiserslautern

4. Testing, Validation and Assessment of Included Exercises

Together with the hardware of the new training system three folders with hydraulic exercises corresponding to technical apprenticeship requirements of Federal Institute of Vocational Training (Bundesinstitut für Berufsbildung, BIBB) were delivered. These folders cover the fields of “basic circuits with solenoid valves (24 exercises)”, “electro hydraulic servo valves (13 exercises)” and “closed loop controller circuits (6 exercises)”. The test record for each exercise consists of a basic introduction, explanations to all components used, the hydraulic and wiring diagram including parts lists and finally prepared templates for results documentation. Additionally most exercises contain information on typical risks and on prevention of accidents.

Hence, the next step was to conduct all 43 exercises, recognise content and duration as well as level of difficulty and correlate these results to requirements of related curricula. In Table 1 the assessment of suitability of all 43 exercises is shown in compressed form.

Table 1: Assessment of exercises regarding related curricula

Description	**Assessment**
Basic circuits with solenoid valves:	
Familiarize oneself with equipment (1 exercise)	yes
Operate hydraulic pump (1 exercise)	no
Operate hydraulic actors (3 exercises)	yes
Operate different hydraulic valves (8 exercises)	yes
Operate hydraulic accumulator (1 exercise)	yes
Assemble and operate basic circuits (2 exercises)	yes
Operate manometric switch (1 exercise)	yes
Operate rarely used and/or very special valves (1 exercise)	no
Operate very special circuits (4 exercises)	no
Commissioning and error diagnostics (1 exercise)	no
Electro hydraulic servo valves:	
Operate cylinder with preselected target value (4 exercises)	yes
Influence braking distance of cylinder (2 exercises)	yes
Velocity control of differential cylinder (1 exercise)	yes
Velocity profile control by proximity switch (2 exercises)	yes
Influence of operation pressure (2 exercises)	yes
Four-quadrant operation (2 exercises)	no
Closed-loop controller circuits	
Basic circuits of exact positioning (3 exercises)	yes
Positioning by limit switches (2 exercises)	no
Set-up operation (1 exercise)	no

All exercises assessed with “yes” are adequate to engineering education. All others are not suitable. They either are covered by other modules – like pump operation is part of fluid flow engine lab – or don’t fit to content of this module – like commissioning and error detection or very special circuits with rarely used valves.

5. Classification of Exercises Corresponding to Curricula

As most exercises assessed with “yes” in Table 1 are of short duration like 5 to 10 minutes and introduce just one single hydraulic component and its typical function, it was decided to group some of these exercises together with the goal of getting challenging exercises on Bachelor respectively Master level with a minimum of 30 minutes and up to 60 minutes duration.
Together with grouping the exercises, it was necessary to take the previous knowledge of the different curricula of mechanical engineering and mechatronics on Bachelor level as well as those on Master level into account. Main focus is here lectures and exercises in control theory and their relative position in curricula, as knowledge of this topic is absolutely necessary to participate in exercises with closed-loop controller circuits. Results are shown in Table 2.

Table 2: Extraction of Bachelor and Master curricula regarding control theory

Curriculum	Control theory	Hydraulics	Closed-loop controller circuits
Bachelor "Mechanical Engineering"	6th semester	5th semester	not suitable
Bachelor "Mechatronics"	4th semester	5th semester	suitable
Master "Mechanical Engineering and Mechatronics"	unconstrained	unconstrained	student's responsibility

Hence, lab exercises with closed-loop controller circuit are only suitable for Bachelor students of mechatronics. With Master students it is in their own responsibility to have appropriate previous knowledge if they want to participate in corresponding hydraulic Master modules.
Furthermore, technical skills regarding measurement technology should be integrated into the exercises. Usually with hydraulics this is pressure and flow rate measurement. These options are implemented in the training system a priori. In addition, rotational speed measurement was taken into account. Here, a simple measurement application consisting of power supply, speed sensor and oscilloscope has to set up by the students (see Figure 2). Hence, students learn to create measurement systems on their own instead of using just plug-and-play technology.

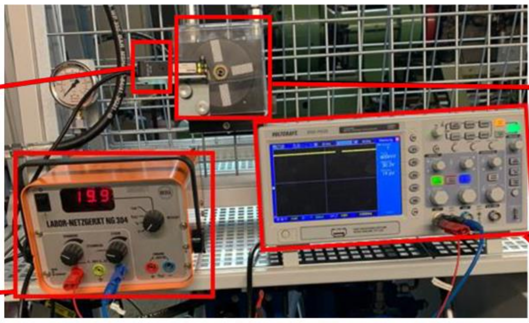

Fig. 2. Setup of speed measurement

As the rotating disk of hydro motor has 4 reflectors as visible in Figure 2, the frequency of the measured signal is four times the rotation frequency (see Figure 3). This has to be taken into account while evaluating.

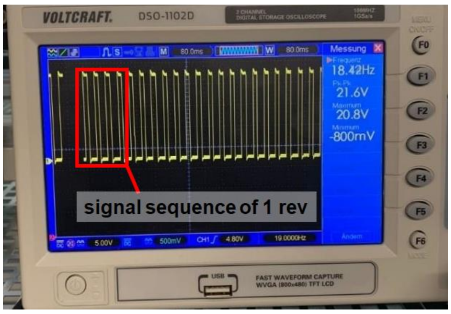

Fig. 3. Frequency signal of speed measurement

Further options for training measurement skills could be analysis of controller signals like given values and actual values via oscilloscope. Here students will learn to set proper sampling rates, scaling of display axis and to operate with trigger signals to start/stop data collection. Experience confirms that especially these skills could only be learned "do it yourself".

Based on all these requirements a set of 12 challenging exercises was defined as shown in Table 3. Additionally, the classification to the different curricula is included.

Table 3: Challenging exercises and classification

<table>
<tr><th rowspan="2">Exercise</th><th rowspan="2">Duration (min)</th><th colspan="3">classification</th></tr>
<tr><th>Bachelor Mech. Eng.</th><th>Bachelor Mechatron.</th><th>Master</th></tr>
<tr><td>Manual hydraulics (old training system)</td><td>30</td><td>yes</td><td>yes</td><td>no</td></tr>
<tr><td>Simple circuit with solenoid valves (hydraulic and electric installation)</td><td>40</td><td>yes</td><td>yes</td><td>no</td></tr>
<tr><td>Basic circuit with servohydraulics (connection of valve and controller as well as measurement of valve characteristic)</td><td>60</td><td>yes</td><td>yes</td><td>yes (introduction)</td></tr>
<tr><td>BIBB-exercise differential cylinder</td><td>20</td><td rowspan="2">yes (option)</td><td rowspan="2">yes (option)</td><td>no</td></tr>
<tr><td>BIBB-exercise homokinetic cylinder</td><td>20</td><td>no</td></tr>
<tr><td>BIBB-exercise hydro accumulator</td><td>30</td><td rowspan="2">yes (option)</td><td rowspan="2">yes (option)</td><td>no</td></tr>
<tr><td>BIBB-exercise load unit</td><td>30</td><td>no</td></tr>
<tr><td>Circuit with two cylinders in parallel/serial arrangement</td><td>40</td><td rowspan="2">yes (option)</td><td>no</td><td rowspan="2">yes (option if no previous knowledge)</td></tr>
<tr><td>Circuit with electrical pressure control</td><td>30</td><td>no</td></tr>
<tr><td>Analysis of hydro motor (pressure, pressure difference and flow rate including appropriate diagrams)</td><td>60</td><td>(perhaps option)</td><td rowspan="3">yes (option)</td><td>yes</td></tr>
<tr><td>Control of hydraulic cylinder with external sinus curve as given value (combination of microcontroller, servo controller, servo valve and cylinder)</td><td>40</td><td>(perhaps option)</td><td>yes</td></tr>
<tr><td>Automatic sequence of cylinder operation with velocity profile (fast motion, braking, slope timing)</td><td>50</td><td>no</td><td>yes</td></tr>
<tr><td>Closed loop controller circuit with load dependent positioning accuracy</td><td>80</td><td>no</td><td>no</td><td>yes</td></tr>
<tr><td>Approximate total lab time</td><td>---</td><td>210 - 220
(250 - 280)</td><td>220 - 240</td><td>290
(360)</td></tr>
</table>

For the two Bachelor studies total lab time results in 210 to 240 minutes. According to 1 ECTS for the whole lab exercises this duration for just the hydraulic part is reasonable. Hence, hydraulic lab exercises could be done in one part, e.g. one afternoon from 2 to 6 PM. On the other hand splitting lab exercises into two shorter sessions of about 2 hours is possible, too. This gives the student more flexibility in matching the lab exercises to their individual schedules.
For Master studies at minimum lab time of nearly 5 hours is necessary. As Master students do the more complex lab exercises combined with project work as examination type this longer time is absolutely necessary and appropriate. Master students should merge deeper into the hydraulic matter driven by a higher fraction of intrinsic motivation.
For all exercises a first version of single instruction manuals were prepared. Single instruction manuals were chosen as this gives more flexibility regarding varying lab exercises between different

studies and/or consecutive years. The content and structure are very alike the delivered manuals. However, all information regarding safety at work and avoidance of accidents are summarized in one common document to safe space and if printed out to safe paper.

6. Conclusion and Future Work

New technologies intruding into fluid technology made it necessary to adapt the hydraulic engineering education. Based on a comprehensive literature review of nearly 30 actual scientific publications requirements for a new training system were defined. Finally a new training system was purchased. Together with the training system a set of more than 40 basic lab exercises covering solenoid valves, servo valves and closed loop controller circuits were delivered. Out of this pool of exercises 12 enhanced lab exercises were developed to cover needs of different curricula involved into hydraulic engineering education. For all enhanced lab exercises appropriate hand-outs were prepared.

Future steps will be to test all the enhanced exercises with corresponding student groups. All student groups have to fill out feedback questionnaires. Additionally, the supervising staff members have to give feedback, too. After at maximum of two optimization loops of mentioned kind, a final set of lab exercises for all curricula involved should be established. Nevertheless, if necessary new technologies should be integrated into curricula respectively lab exercises as fast as possible.

Another option that should be taken into account is, with actual available training set industrial focused hydraulic training is possible, too. This might be of interest in context of new degree programs like “professional training and academic studies”. The system of education seems to be very volatile in this context, actually.

References

[1] Chondros, T.G. “Archimedes life works and machines.” *Mechanism and Machine Theory* 45, no. 11 (2010): 1766-1775.

[2] Fabre, A.-J. "Pneumatic Machines in Antiquity (Air as Source of Energy in the Treatise on Pneumatics of Heron of Alexandria)." *Analecta Historico Medica* (2008): 67-70.

[3] Drumea, P., C. Dumitrescu, I. Bordeasu, L. Vaida, and D. Opruta, “Trends in the Development of Hydraulic Drives.” Paper presented at the 2018 International Conference on Hydraulics and Pneumatics, HERVEX 2018, Baile Govora, Romania, November 7-9, 2018.

[4] Majdic, F. “Possibilities and Challenges on the Field of Water Hydraulics.” Paper presented at the 2019 International Conference on Hydraulics and Pneumatics, HERVEX 2019, Baile Govora, Romania, November 13-15, 2019.

[5] Popovici, I. A., M. Savaniu, O. Tonciu, M Culcea, and A. Teodorescu. ”Various Operation Mode of Construction Machinery Using Energy Obtained from Renewable Sources.” Paper presented at the 2022 International Conference on Hydraulics and Pneumatics, HERVEX 2022, Baile Govora, Romania, November 9-10, 2022.

[6] Rivera, E. F., E. E. Morales, C. C. Florez, and R. M. Toasa. “Development of an Augmented Reality System to Support the Teaching-Learning Process in Automotive Mechatronics.” Paper presented at the 8th International Conference on Augmented Reality, Virtual Reality and Computer Graphics, AVR 2021, Virtual Event, September 7-10, 2021.

[7] Antonya, C., F. Girbacia, C. Postelnicu, D. Voinea, and S. Butnariu. “Saliency Detection in a Virtual Driving Environment for Autonomous Vehicle Behaviour Improvement.” Paper presented at the 8th International Conference on Augmented Reality, Virtual Reality and Computer Graphics, AVR 2021, Virtual Event, September 7-10, 2021.

[8] Montalvo-Lopez, W., P. Catota, C. A. Garcia, and M. V. Garcia. “Development of a Virtual Reality Environment Based on the CoAp Protocol for Teaching Pneumatic Systems.” Paper presented at the 8th International Conference on Augmented Reality, Virtual Reality and Computer Graphics, AVR 2021, Virtual Event, September 7-10, 2021.

[9] Sefu, S. M., and B. A. Tudor. “Intelligent Hydraulics Using Artificial Intelligence.” Paper presented at the 2022 International Conference on Hydraulics and Pneumatics, HERVEX 2022, Baile Govora, Romania, November 9-10, 2022.

[10] Savaniu, M. I., O. Tonciu, R. Panaitescu-Liess, C. Sescu-Gal, M. Culcea, and A. R. Sasu. “Aspects of the Use of AI (Artificial Intelligence) Technology in Construction Equipment Management.” Paper presented at the 2023 International Conference on Hydraulics and Pneumatics, HERVEX 2023, Baile Govora, Romania, November 8-10, 2023.
[11] Lovrec, D. “Education in the Field of Fluid Power Technology – Challenges, Opportunities and Possibilities.” Paper presented at the 2019 International Conference on Hydraulics and Pneumatics, HERVEX 2019, Baile Govora, Romania, November 13-15, 2019.
[12] Banesz, G., A. Haskova, and D. Lukacova. "Pneumatic and hydraulic systems in tertiary education." Paper presented at the 2018 IEEE 12th International Conference on Application of Information and Communication Technologies, AICT 2018, Almaty, Kazakhstan, October 17-19, 2018.
[13] Rojas Suarez, J. P., J. A. Pabon Leon, and M. S. Orjuela Abril. "Development of an electro-pneumatic system for the practical training of pneumatic processes in the university environment." *Journal of Physics: Conference Series* 2073 (2021): 012016.
[14] Azaka, O. A., K. U. Igboka, A. A. Okafor, and C. P. Odeh. "Design and development of a laboratory scale hydraulic arm for engineering education." *Unizik Journal of Technology, Production and Mechanical Systems (UJTPMS)*, Maiden Edition, 2023.
[15] Pate, K., J. Garcia, and F. Breidi. “Enhancing the Learning Experience of Engineering Students Through Digitized Interactive Tools.” Paper presented at the 2021 ASEE Annual Conference, Virtual Meeting, July 26-29, 2021.
[16] Desai, S. R. "Impact of Active Learning Methods on Students’ Learning and Course Results." *Journal of Engineering Education Transformations* 35, no. 3 (January 2022): 133-142.
[17] Chen, W., H. Wang, and L. Zheng. “Research on the Teaching Method Reform of Automobile Related Courses: Take the Vehicle Hydraulic System as an Example.” Paper presented at the 7th Annual International Conference on Network and Information Systems for Computers, ICNISC 2021, Guiyang, China, July 23-25, 2021.
[18] Sheng, X., and X. Hu. “Teaching Method Reform of the Hydraulic and Pneumatic Course Based on Engineering Application Cases.” Paper presented at the IEEE Workshop on Advanced Research and Technology in Industry Applications, WARTIA 2014, Ottawa, Canada, September 29-30, 2014.
[19] Xu, L., L. Cai, and X. Nan. “Research on Teaching Reform of Hydraulic and Pneumatic Transmission Based on OBE.” Paper presented at the 7th International Conference on Education, Management, Computer and Medicine, EMCM 2016, Shenyang, China, December 29-31, 2016.
[20] Sandyk, I., M. Müür, V. Kuts, Y. Bonderenko, S. L. Pizzagalli, and T. Rüütmann. “Pneumatics Laboratory Interactive Educational Experience Development.” Paper presented at the 19th International CDIO Conference, Trondheim, Norway, June 26-29, 2023.
[21] Peng, P., Y. Sun, L. Tang, and H. Yang. “Teaching reform plan for hydraulic and pneumatic transmission courses based on experimental platform.” Paper presented at the 3rd International Conference on Humanities, Wisdom Education and Service Management, HWESM 2024, Atlantis Press, 2024.
[22] Perez-Sanchez, M., and P. A. Lopez-Jiminez. "Continuous Project-Based Learning in Fluid Mechanics and Hydraulic Engineering Subjects for Different Degrees." *Fluids* 95, no. 5 (June 2020): 1-15.
[23] Assaf, H., and A. Vacca. “Hydraulic Trainer for Hands-on and Virtual Labs for Fluid Power Curriculum.” Paper presented at the 17th Scandinavian International Conference on Fluid Power, SICFP’21, Linköping, Sweden, May 31 – June 2, 2021.
[24] Ji, T., B. Ren, and S. Huang. "Hydraulic and Pneumatic Transmission Three-Dimensional Virtual Training System Research." *Journal of Physics: Conference Series* 2219 (2022): 012064.
[25] Ostrowski, I., J. Mozaryn, J. Wang, and D. Cukier. "Lesson Learned from Semester of Online Teaching of Automation Using Simulators." *IOP Conf. Series: Materials Science and Engineering* 1016 (2021): 012005.
[26] Song, J., Z. Chen, Y. Li, and J. Liu. "Teaching System of Hydraulic Transmission Combined with Virtual Reality Technology." *Information* 14, no. 147 (2023): 1-14.
[27] Ismail, A. M. M., N. A. S. Manssor, and H. Abu Kasim. "The Basic of Hydraulic and Pneumatic Teaching Innovation Kit for Application in Fluid Power Technology Course." *Innovative Teaching and Learning Journal* 2, no. 1 (November 2018): 26-36.
[28] Soad, M. M., I. Hanizam, and H. I. Siti. "Design and Development of Portable Pneumatic with Augmented Reality for Teaching and Learning Purposes." *Journal of Advanced Research in Applied Mechanics* 74, no. 1 (2020): 1-9.
[29] Caiza, G., M. Riofrio-Morales, A. Robalino-Lopez, O. R. Toscano, M. V. Garcia, and J. E. Naranjo. “An Immersive Training Approach for Induction Motor Fault Detection and Troubleshooting.” Paper presented at the 8th International Conference on Augmented Reality, Virtual Reality and Computer Graphics, AVR 2021, Virtual Event, September 7-10, 2021.

ISSN 1454 - 8003
Proceedings of 2024 International Conference on Hydraulics and Pneumatics - HERVEX
November 13-15, Băile Govora, Romania

FLUID-MECHATRONIC SYSTEMS IN SEA AND OCEAN WAVE POWER-TAKE-OFF PROCESSES

Alexander SKVORCHEVSKY[1,*]

[1] Research Centre of Robotics, Mechatronics and Production Informatization, Kharkiv, Ukraine

* sircrmpi@gmail.com

Abstract: *The study aimed to identify problems in the development of fluid-mechatronic systems for wave energy converters and to propose solutions to these problems. The problem was solved by heuristic methods using the theory of automatic control, technical hydraulics and fluid mechatronics. The proposed study is based on the hypothesis that power capture can be increased through the use of wave energy converters` power take-off systems with variable parameters and structures. Using the specified hypothesis and methods were proposed power flow diagram of the fluid-mechatronic system of power-take-off of wave energy converters, as well as a float arm with hydraulic drive. The directions of proposed fluid-mechatronic systems of sea and ocean wave power-take-off future development were discussed.*

Keywords: *Fluid-mechatronics, wave energy converter, power-take-off process, float arm, buoy*

1. Introduction

Ocean and sea waves are the world's largest untapped energy source [1]. The Intergovernmental Panel on Climate Change (IPCC) puts the potential annual global electricity production from ocean and sea waves at 29,500 TWh. This is almost ten times Europe's annual electricity consumption of 3,000 TWh. It is also a clean, effective alternative to polluting and expensive diesel for remote islands and offshore industries, such as fish farms or oil & gas platforms [1]. The article [2] shows that in some regions, for example in the Mediterranean, the wave energy potential correlates with the wind energy potential. In general, wave energy can be considered as concentrated wind energy, which in turn is a derivative of solar radiation energy. The high density of wave energy necessitates the usage of engineering systems capable of creating high power density for taking it off. Today, such systems are hydraulic devices. Despite the enormous potential of renewable wave energy, wave power capture technologies are still emerging. Economically efficient power take-off can be achieved by wave energy converters' adaptive control according to the maximum power capture criteria. The application of hydraulic systems with their adaptive control involves the usage of fluid-mechatronics [3] methods. Fluid mechatronics is an integrative engineering and scientific field that combines hydraulics, fluid mechanics, control theory, mechanics, electrical engineering, electronics and other disciplines.

2. Literature review and problem statement

Hydraulic power take-off (PTO) systems for wave energy usually fall into two broad categories. These are, firstly, variable pressure systems where control of the primary force/torque is achieved by pressure modulation, and secondly, constant pressure systems where control of the primary force/torque is achieved by valve transitions that select between discrete effort levels determined by the approximately constant accumulator pressure and alternative piston areas. Energy storage is integral to the constant pressure category while, in the purest form of the variable pressure category, it is not provided. Hybrid systems which combine elements of both categories are also possible. The paper [4] reports an analysis of the most elementary of systems from each of these categories. The analysis uses a coupled hydrodynamic-hydraulic time domain model. The model is used to assess the effectiveness of the hydrodynamic power absorption and the efficiency of the hydraulic power transmission. The results show that, in each case, the hydraulic motor performance is a critical consideration and the optimal configuration of any one system is dependent on motor selection. In the best instances of both categories of PTO, the indicated performance is sufficiently high to facilitate the commercial viability of such systems [4].

From the analysis, the next conclusion was made: of the combinations of system concept and motor technology presented in [4], notwithstanding the spread in efficiencies, all possibilities are worthy of further investigation and development. However, the results are calculated for a single short-term sea state rather than for a complete year [4].

In the PhD dissertation [5] shown that despite 40 years of research activities within wave energy, the PTO is still a hindrance. No matured designs exist. The lack of advances in PTO research a contributing factor to wave energy remaining in a pre-commercialisation phase - a phase where electrical power production has been demonstrated but needs to find a road to larger power scales and effective production. One of the difficulties in PTO design is performing the trade-off between contradicting PTO characteristics, e.g. controllability, efficiency and peak power capacity. A PTO system for wave energy converters (WEC) is a classic example of a mechatronic design problem, where all aspects of the design couples.

PTO solution is based on the discrete control of a hydraulic cylinder and is assessed in [5] to be the most promising solution. It is therefore analysed in depth. The solution is named a Discrete Displacement Cylinder (DDC). The developed DDC allows discrete force control of a multi-chambered cylinder driven by the absorber, while efficiently transferring the generated power directly into a battery of high-pressure accumulators. The concept allows DDCs of multiple absorbers to supply the same accumulator battery, where a hydraulic motor may use the stored energy to drive a generator at a near-constant load.

In addition, dissertation 5 substantiates the following statements:

- Mechanical solution as for example ball screws may show the required force density and efficiencies, but are viewed as not having the durability.
- A hydraulic cylinder around Ø 25 cm and 1600 kg may give 420 kN. The problem is to control the force of the cylinder while efficiently converting the produced flow into electricity.
- Hydraulic accumulators are viewed as best suited storage technology for wave energy. It may cover both wave-to-wave and wavegroup-to-wavegroup power smoothing. It has a high-power density and low cost, combined with a round trip efficiency of about 94%.
- Discrete control of a hydraulic cylinder by pressure shifting seems to give the required efficiency while providing force control.
- Efficient and durable hydraulic PTOs with constant force control exist, but have a poor extraction.

The dissertation [5] is a fundamental work in the field of WECs` PTO and certainly deserves recognition. However, it should be noted that many of the statements made in [5] are still valid even at the time of its publication in 2013.

Multi-chamber cylinders, studied in detail in [5], do not look like a promising part of the fluid-mechatronic system of the PTO. This is due to their increased complexity, increased dimensions, the impossibility of converting standard, serially produced products (like conventional hydraulic cylinders), and a complex hydraulic control system with many valves. Hydraulic accumulators are considered the most promising storage of captured wave energy. However, the dissertation mainly considers hydro-gas accumulators. In [5], it was not possible to identify studies on the applicability of weight-loaded hydraulic accumulators, while gravity energy storage is considered one of the most promising in recent years [6, 7].

Discrete control of a hydraulic cylinder by pressure shifting can array the next problems:

1. The power flow carried by the sea wave is smooth, although it has peaks. Any attempts at discrete control of a smooth power flow will lead to significant power losses due to the need for modulation.

2. Discrete pressure control will lead to pressure surges in the hydraulic system, which in turn will increase the risk of pipeline rupture, damage to the membrane of the hydro-gas accumulator, damage to the seals of the hydraulic cylinders and generally reduce the reliability of the system. In addition, the presence of two elastic elements in the system - hydraulic fluid and compressed gas in the hydro-gas accumulator can lead to the system entering a self-oscillating mode during a discrete transition from one pressure level to another. In the dissertation [5], many WECs are considered. They have different kinematic diagrams. However, not a single WEC scheme was found in which the hydrokinematic diagram could change and adapt to the wave parameters - frequency, amplitude, and wavelength. This could be achieved, for example, by changing the length of the float arm. In this way, the pressure and speed of the piston of the hydraulic cylinder of the PTO could be changed adaptively.

Analysis of recent scientific publications [6-11] and practical examples of WEC [12, 13] did not show significant progress in the development of hydrokinematic and electrohydraulic (fluid-mechatronic) schemes of WECs` PTO. Mainly wave energy converters are built on the same principle, namely, there is a buoy that makes reciprocating movements under the action of waves. The buoy is mechanically connected by a constant-length float arm to hydraulic cylinders, which convert mechanical energy into hydraulic energy accumulated in hydro-gas accumulators. The flow of fluid rotates the shaft of the hydraulic motor, which rotates the shaft of the electric generator. McCabe Wave Pump (MWP), Pelamis Wave Energy Converter [12] and Eco Wave Power Company`s Converters [13] are built on this principle. The stagnation in the mass application of WEC, despite the enormous potential of sea and ocean waves as a source of renewable energy, is apparently caused by the use of typical hydrokinematic and electrohydraulic (fluid-mechatronic) diagrams for WECs` PTO. Using similar principal fluid-mechatronic PTO systems limits the potential for wave power captures and reduces the fault tolerance of WECs. This is because waves can vary greatly in frequency, amplitude, and length, with a significant random component.

3. The aim of the study

The study's aim is scientific foundation development for the structural and parametric synthesis of hydro-cinematic and fluid-mechatronic systems of WECs` PTO according to the maximum power capture and fault-tolerance criteria.

4. The study materials and methods

Heuristic methods were used for the structural synthesis of the WECs` PTO. Simplified block models of hydraulic and electro-hydraulic components were used during the concept and system-level design stages. The proposed study is based on the hypothesis that power capture can be increased through the use of WECs` PTO with variable parameters and structures. For example, an adaptive change of the float arm length can control the pressure in the hydraulic PTO. PTO`s fluid-mechatronic systems will be equipped with pressure and flow sensors included in feedback loops using proportional valves. Such PTO`s fluid-mechatronic systems will be controlled using PID regulations and other advanced control methods depending on changes in the frequency and amplitude of waves, taking into account random wave processes. In addition, this approach will increase the fault tolerance of wave energy converters due to the use of disturbance feedback loops. The next research hypothesis is that applying weight-loaded accumulators instead of hydro-gas accumulators will lead to a more stable pressure regime in the fluid-mechatronic system of PTOs and the ability to store more energy than in the case of a hydro-gas accumulator. This is because the weight-loaded accumulator produces constant pressure, and not pressure associated with gas expansion processes. The research materials were ideas, innovations, hydraulic and hydro kinematic diagrams of power-take-off systems of wave energy converters. The author's publications in fluid mechatronics [14-18] were used for the conducting of this project.

5. Results of the structural synthesis of fluid-mechatronic systems of sea and ocean wave power-take-off

The creation of cost-effective WECs rests on three core questions:

1. How to capture wave energy?

2. How to store the captured energy?

3. How to transfer energy to the electric grid? Moreover, doing this in the right amount and at the right time is desirable.

To solve these three problems, the author proposes some approaches, which are illustrated in Fig. 1.

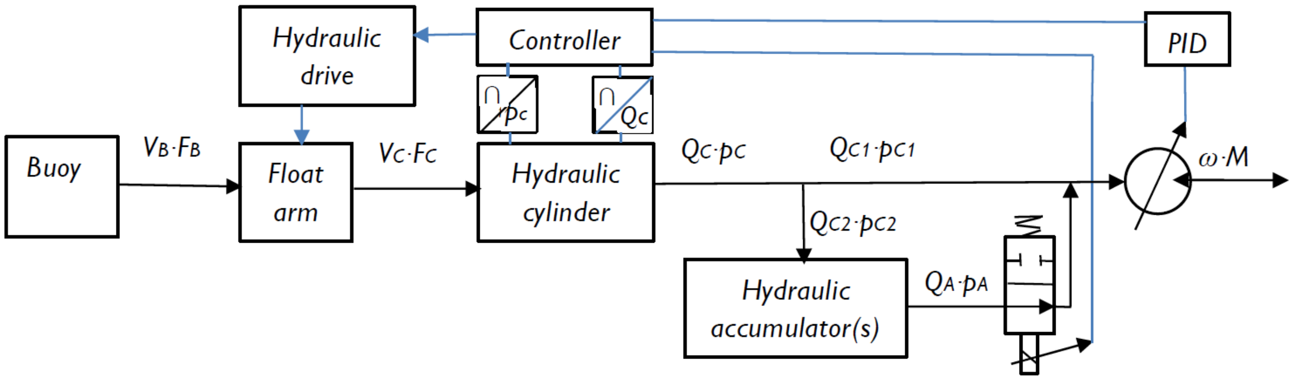

Fig. 1. Power flow fluid-mechatronic PTO of WECs

The parameters in Fig. 1 are variables of the "flow" type and the "potential" type, the product of which gives the power (Table 1). It is necessary to accept that all these values are constantly changing over time and to generate electricity of a given voltage and current, the power flow must be controlled in real time. A PID controller is well suited for this.

Table 1: The parameters in Fig. 1

"Flow" type variables	"Potential" type variables
V_B– buoy velocity	F_B – force on the buoy
V_C·– cylinder velocity	F_C – cylinder force
Q_C·– cylinder flow	p_C – cylinder pressure
Q_{C1}·– flow cylinder-motor	p_{C1} – pressure in line cylinder-motor
Q_{C2} – flow cylinder-accumulator	p_{C2} – pressure cylinder-accumulator
Q_A – flow accumulator-motor	p_A – pressure accumulator-motor
ω – motor`s frequency	M – motor`s torque

Fig. 2 illustrates how the parameters of the hydrokinematic diagram of the WEC can be controlled. Changing the float arm length makes it possible to stabilize the force on the hydraulic cylinder, and therefore the pressure. The basis of Fig. 2 is taken from the dissertation [5], and then modified by the author according to his proposals for improving the WEC.

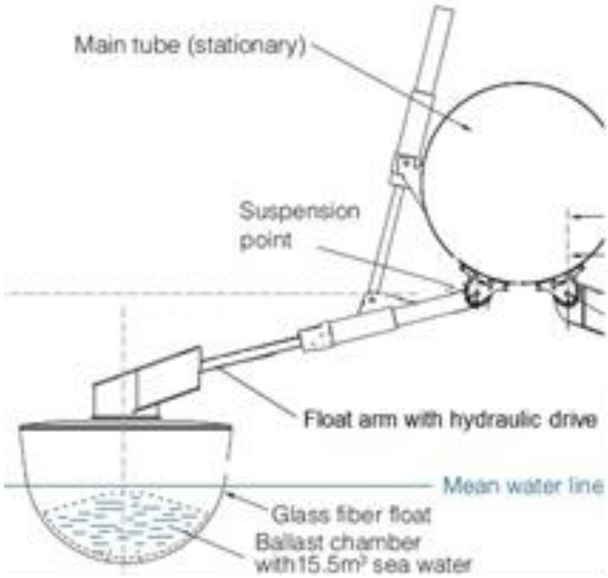

Fig. 2. Float arm with hydraulic drive

6. Discussion of the directions of fluid-mechatronic systems of sea and ocean wave power-take-off future development

The future direction of proposed fluid-mechatronic systems of sea and ocean wave power-take-off development should be the next:

1. Adaptive control of the pressure and flow rate of the fluid-mechatronic system of WECs` PTO to maximize the capture of wave power depending on the frequency, amplitude and length of sea waves;
2. Creation of WECs` PTO with the geometry of their moving parts, which will adaptively change depending on the frequency, amplitude and length of sea waves, thus ensuring more efficient capture of wave power;
3. Usage of the methods of machine learning and artificial intelligence for WECs control depending on changes in the frequency, amplitude and length of waves, taking into account random wave processes.
4. Usage of fluid-mechatronic systems not only as an intermediate link for converting wave power into electrical power but also as a drive for bringing the WECs into a more compact state (possibly submerging them under water) to counteract the destruction of converters during storms and hurricanes;
5. Detection of foreign objects getting between the moving parts of WECs to increase their fault tolerance, as well as reduce the risks of harm to marine mammals and birds by convectors;
6. Wider application of more environmentally friendly liquids (for example, rapeseed oil, polyethylene glycol and aqueous emulsions of these substances) in WECs` PTO.
7. Evaluation of using technologies for gravitational storing of sea wave energy by applying weight-loaded accumulators instead of hydro-gas accumulators.

5. Conclusions

Despite many decades of research, the development of WEC is at the stage of emerging technologies for many reasons. One of the most important, in the author's opinion, is that similar hydraulic circuits are used in various WECs. Further development of the concepts of fluid-mechatronic systems of WECs proposed in the paper will contribute to a more complete power take-off and more reliable operation of wave energy converters.

References

[1] Ocean Energy Europe. "Wave Energy." Accessed October 22, 2024. https://www.oceanenergy-europe.eu/ocean-energy/wave-energy/.

[2] Ponce de León, Sonia, João Horta Bettencourt, John V. Ringwood, and Jérôme Benveniste. "Review of Assessment of Combined Wind and Wave Energy in European Coastal Waters Using Satellite Altimetry." *Applied Ocean Research* 152 (2024): 104184. https://doi.org/10.1016/j.apor.2024.104184.

[3] Chair of Fluid-Mechatronic Systems (Fluidtronic), TU Dresden. Start page. Accessed October 22, 2024.. https://tu-dresden.de/ing/maschinenwesen/imd/fms.

[4] Costello, Ronan, John Ringwood, and Jochem Weber. "Comparison of two alternative hydraulic PTO concepts for wave energy conversion." Paper presented at the 9th European Wave and Tidal Energy Conference (EWTEC), Southampton, United Kingdom, September 5-9, 2011.

[5] Hansen, Rico Hjerm. *Design and control of the powertake-off system for a wave energy converter with multiple absorbers*. PhD thesis. Department of Energy Technology, Aalborg University, Denmark, 2013.

[6] Emrani, Anisa, and Asmae Berrada. "A comprehensive review on techno-economic assessment of hybrid energy storage systems integrated with renewable energy." *Journal of Energy Storage* 84 (2024): 111010.

[7] Li, Fang-Fang, Jia-Zhe Xie, Yu-Fan Fan, and Jun Qiu. "Potential of different forms of gravity energy storage." *Sustainable Energy Technologies and Assessments* 64 (2024): 103728.

[8] Barone, Piofrancesco, Teresa Castiglione, and Sergio Bova. "Wave Energy Converters and Hydraulic Power Take-off: analysis of a possible control strategy." *Journal of Physics: Conference Series* 2648, (2023): 012006.

[9] Soares, C.G., and T.A. Santos (eds.). *Advances in Maritime Technology and Engineering*, vol. 2, 1st Edition. London, CRC Press, 2024. Gaspar, J.F., C. Zeng, H.T. Xu, T.S. Hallak, C. Guedes Soares, and M.J.G.C. Mendes. "Wave energy converter power take-off with active oil-hydraulic accumulator", pp. 427-433.

[10] Wang, Hao, J. Sun, Z. Xi, S. Dai, F. Xing, and M. Xu. "Recent Progress on Built-in Wave Energy Converters: A Review." *Journal of Marine Science and Engineering* 12, no. 7 (2024): 1176.

[11] Jusoh, Mohd Afifi, Zulkifli Mohd Yusop, Aliashim Albani, Muhamad Zalani Daud, and Mohd Zamri Ibrahim. "An innovative dry-lab test rig for mechanical-hydraulic power take-off of wave energy conversion system." *International Journal of Power Electronics and Drive Systems* 15, no. 2 (2024): 715-724.

[12] EMEC - European Marine Energy Centre. "Pelamis Wave Power." Accessed October 23, 2024. www.emec.org.uk/about-us/wave-clients/pelamis-wave-power/.

[13] Eco Wave Power. "How It Works." Accessed October 23, 2024. www.ecowavepower.com/our-technology/how-it-works/.

[14] Skvorchevsky, Alexander. "Comparative Analysis of Current Approaches to Digital Twins of Electro-Hydraulic Mechatronic Systems Creations." Paper presented at the 27th International Conference on Hydraulics and Pneumatics – HERVEX 2023, Baile Govora, Romania, November 8-10, 2023.

[15] Skvorchevsky, Alexander. "The Possibilities Evaluation of Replacing Electro-Hydraulic Actuators with Planetary Roller Screws Linear Actuators." Paper presented at the 5th International Scientific Conference (KTM) KhNADU, Kharkiv, Ukraine, May 24, 2023. *Computer Technologies and Mechatronics* (2023): 89–93.

[16] Skvorchevsky, Alexander. "Electronic Load Sensing for Integrating Electro-Hydraulic Mechatronic Actuators with Industry 4.0 and 5.0 Components." Paper presented at the International Conference on Reliable Systems Engineering (ICoRSE), Bucharest, Romania, September 7-8, 2023. *Lecture Notes in Networks and Systems* 762 (2023): 440–455. https://doi.org/10.1007/978-3-031-40628-7_37.

[17] Skvorchevsky, A. "Identification of the Directions of Self-contained Linear Electrohydraulic Actuators' Development in the Context of Smart-Hydraulics Concept Emerging." Paper presented at the International Conference on Reliable Systems Engineering (ICoRSE), Bucharest, Romania, September 5-6, 2024. *Lecture Notes in Networks and Systems* 1129 (2024): 328–338. https://doi.org/10.1007/978-3-031-70670-7_28.

[18] Volontsevich, D., and A. Skvorchevsky. "Restoration and transformation of high-tech machine building industry by implementing the principles of the CALS-concept in the context of Industry 4.0 development." *Східно-Європейський журнал передових технологій / Eastern-European Journal of Enterprise Technologies* 3, no. 1 (117) (2022): 15-24. https://doi.org/10.15587/1729-4061.2022.260045.

ISSN 1454 - 8003
Proceedings of 2024 International Conference on Hydraulics and Pneumatics - HERVEX
November 13-15, Băile Govora, Romania

IMPROVING THE RELIABILITY OF AN AUTOMATED PNEUMATIC BEARING PRESS EQUIPMENT USED IN THE AUTOMOTIVE INDUSTRY

Roxana-Luiza BAHNA[1], Ioan-Lucian MARCU[1], Daniel-Vasile BANYAI[1]

[1] Technical University of Cluj-Napoca, Faculty of Automotive, Mechatronics and Mechanical Engineering, Department of Mechanical Engineering, Lucian.Marcu@termo.utcluj.ro

Abstract: *The process of pressing the bearings in the pressing stations, although a simple process at a first approach, requires pneumatic, hydraulic, mechanical and electrically operated equipment, with a corresponding reliability, which meets the quality requirements. The paper deals with a technical solution regarding the pressing of axial bearings in the gearboxes of motor vehicles. Since the initial process caused both the destruction of the bearings and subsequent problems with the operation of the gearbox, the concept of the pressing station was modified and improved.*

Keywords: *Bearing, press equipment, pneumatic, automotive industry*

1. Introduction

A technological assembly process means a sequence of operations and actions in certain time intervals and in a well-established order, resulting in an assembly or product that is functional at certain parameters and that meets certain requirements at the highest possible level. [1], [2]
In the assembly process we can find three types of automation levels and they are:

- Manual - when only the action of an operator/worker is needed in the assembly process
- Mechanized - when the operator, with the help of a mechanical system (for example: mechanical press), carries out an assembly process
- Automated - by automated process is understood the equipping of some installations with devices that ensure the completion of assembly operations, without the intervention of an operator. In most cases, in the assembly process there are workstations that belong to all three categories.

Press assembly of bearings is an operation by which a shaft-type part and a bore-type part are brought to the physical state in which tightening forces appear between them, to lead to the locking of the assembly. [3 - 5]
Bearings are used to support parts that perform rotational or oscillating movements. In their assembly, the following stages must be considered:

- The bearings and the other elements that make up the assembly will be chosen according to the gauge and the force applied to the respective assembly
- The symbolization, the radial beat and/or the frontal beat will be checked
- Checking the cracks and the slots where the bearings are inserted
- It will be considered that the elements to be assembled are positioned correctly
- The actual mounting of the bearings
- Checking the adjustment and the clearance
- Inserting the shaft into the body of the bearings
- Fitting the covers

Each mounting method presents a different degree of complexity, which brings with it a series of advantages and disadvantages. [4], [5]
Manual assembly It is done by an operator or worker and consists in the fact that he performs the assembly operation by hand, without the need for auxiliary tools.
Usually, the pieces that will be mounted in this way have clips in their construction to be able to press easily or the assembly between the borehole and the shaft does not require high pressing forces.

We find advantages like • Low costs, but also disadvantages like: • Low reliability; • Low process repeatability; • Possible assembly errors.
Mechanized assembly aims to replace manual work with technical means (machines, devices, stations, tools and mechanisms, etc.) to be able to perform some operations, with the worker only having to adjust and control the operation of the machines.
In the assembly activity, simple mechanization is achieved by using tools, instruments, devices and stations, which make work easier or even replace it.
It has the advantage that it ensures high productivity, and a better quality of the work performed.
Complex mechanization consists in the introduction of assembly lines, on which actual assembly work is performed, but also preparatory, auxiliary or final work.
Automated pneumatic assembly, the highest level of mechanization, and within it, control functions are also performed, with the operator only having the attribution of adjustment and supervision.
This automation technique has applicability in all technological fields.
To measure certain values, a series of special automation procedures have been developed that have led to the production of a wide variety of sensors (flow, pressure, temperature).
As a control, instead of fixed links between the execution elements and sensors, a PLC (programmable logic controller) is used, which is a flexible system.
The higher the degree of automation, the higher the need for sensors and actuators (execution elements). Different types of local networks have been created for communication between them.
In order to have high-speed connections, some installations have implemented closed local systems that work to process the signal in real time without delays.
It is necessary for the operator to be informed sufficiently and in a timely manner, without errors, to be able to make the right decisions.
The control panel must be easily accessible and intuitive for easy understanding.
As safety methods, compliance with all regulations is an important condition for creating safe machines and systems.

2. Improving the reliability of the automated bearing press equipment

Improving the reliability of the pneumatic bearing pressing station required changing the initial working concept, the modified press station is shown in figure 1.

Fig. 1. Modified press station

The process was very extensive and required the redesign of the pneumatic actuation schemes, specific sizing calculations for the equipment used, the inclusion of sensors and command and control systems.
The actuation schemes of the pressing cylinders for the bearings that will be mounted in the housing in figure 2, is presented in figures 3 (door cylinder) and 4 (main cylinder), respectively.

Fig. 2. Bearing housing

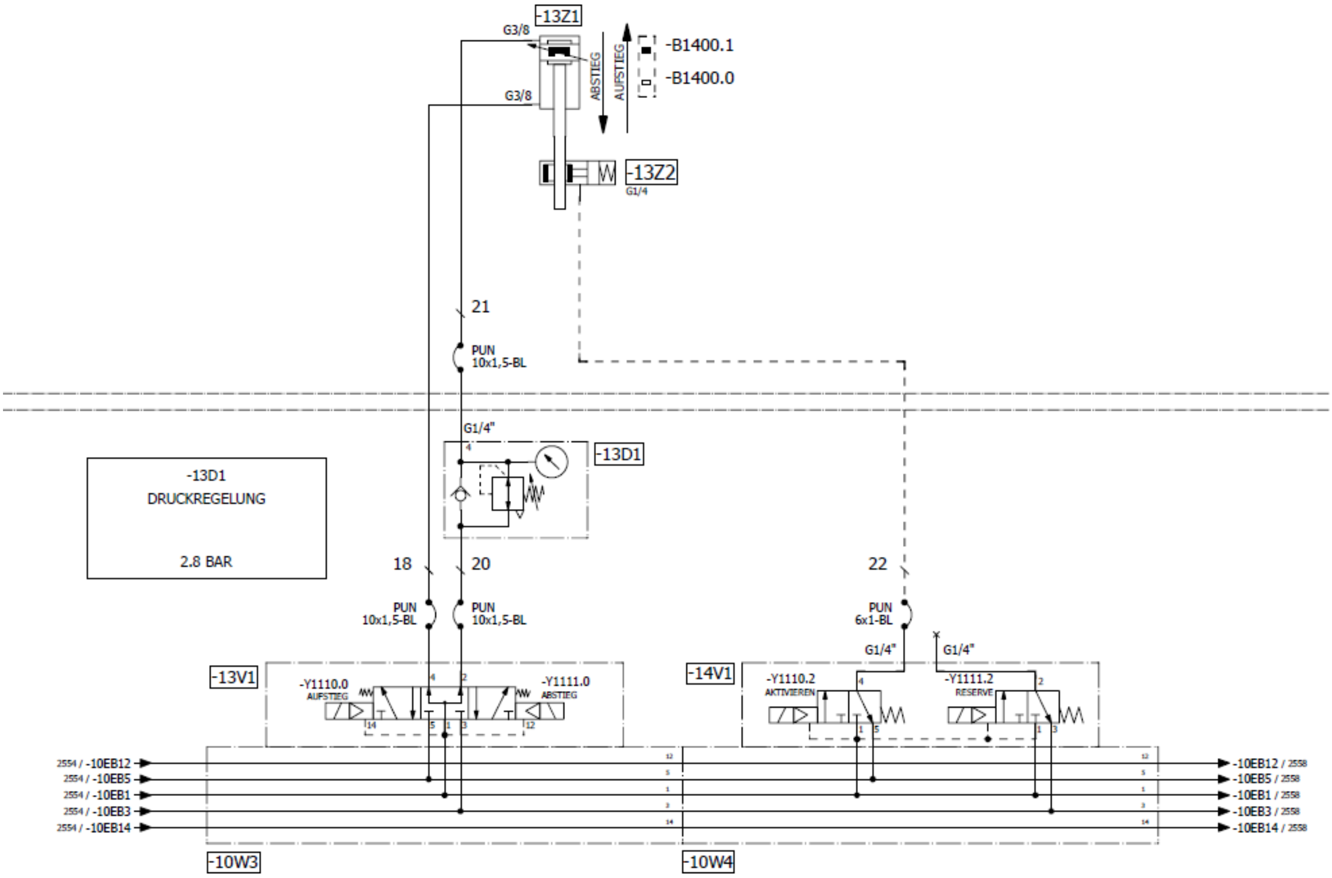

Fig. 3. Pneumatic diagram for cylinder 1A

On the first stage, the air flow needed in the pressing process was theoretically evaluated for each individual cylinder, considering the change in pressures and temperatures during operation, like figure 5 shows for the cylinder 1A.

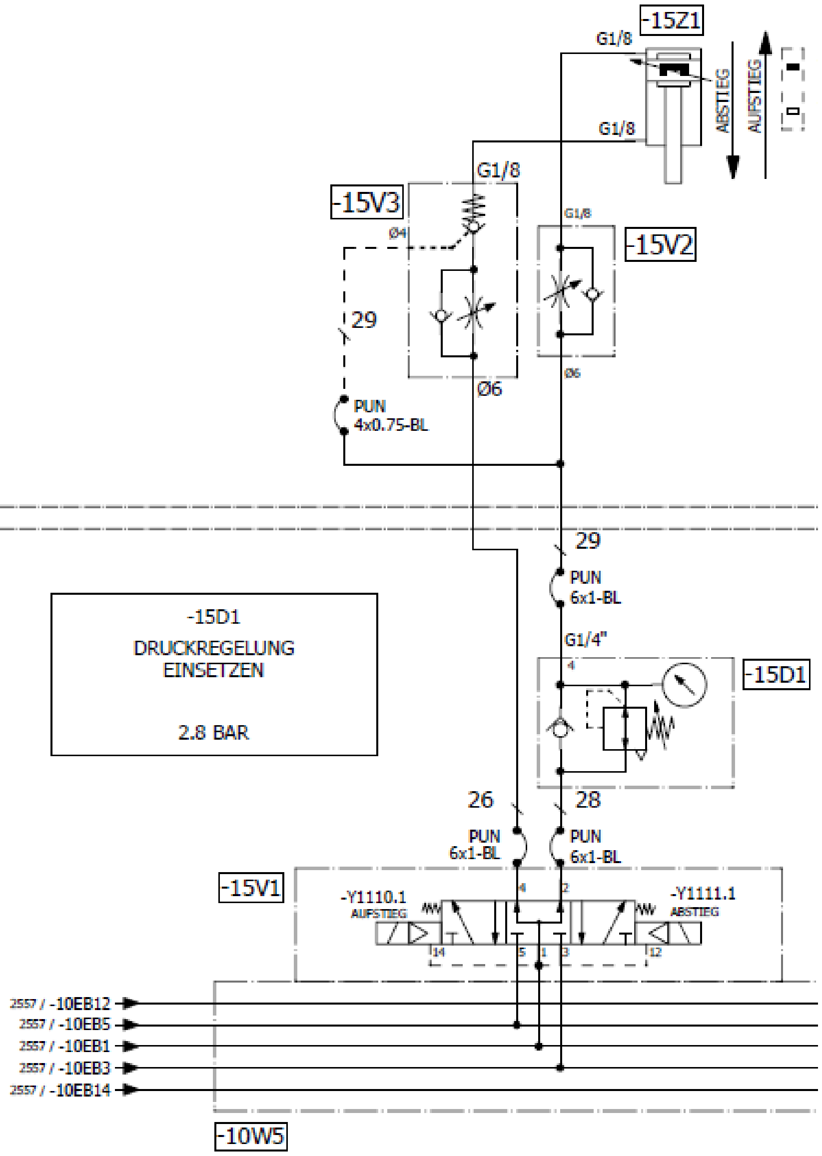

Fig. 4. Pneumatic diagram for cylinder 2A

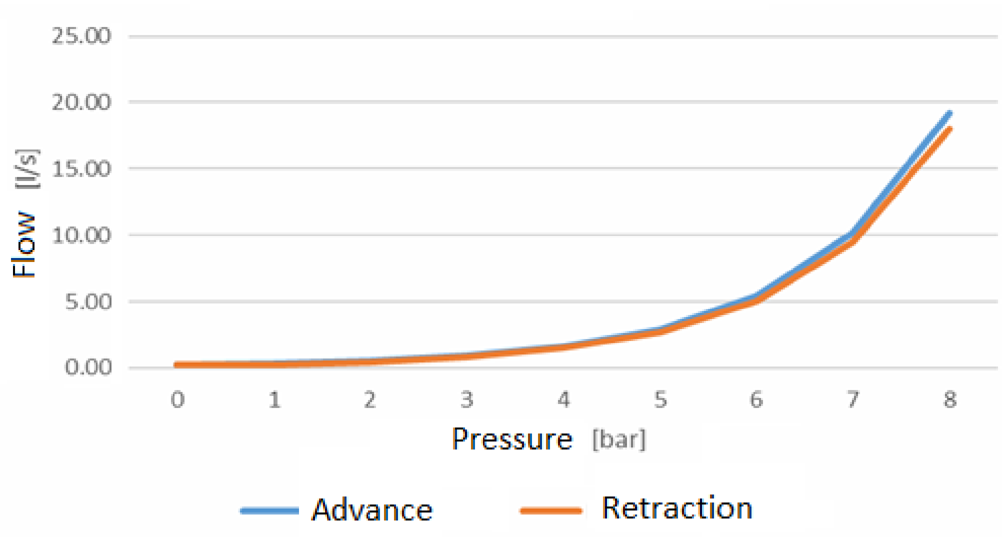

Fig. 5. Required air flow in cylinder 1A

In the pneumatic actuation version, the cylinder that performs the pressing operation of the two axial bearings is controlled on the advance and retreat stroke by a directional control valve, the force on the advance stroke being set by a pressure regulator valve. The studies carried out on the equipment led to the conclusion that it is very difficult to control the exact pressing process, the mounted bearings being with a high probability in incorrect positions.
Since the modernization of the pneumatic system would have generated quite high costs, without having a clear perspective on the quality of the pressing process, the use of an electric, automated system was considered.
Figure 6 basically shows the electric servo motor used for tests on the pressing station. [6]

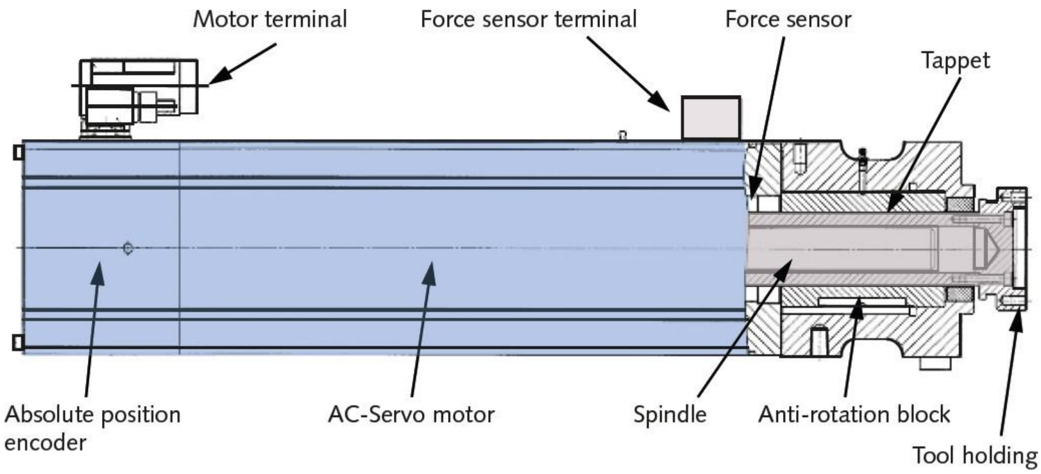

Fig. 6. The electric servo motor

Such a servomotor, of special construction, has high dynamics and drives a ball screw, so that the rotation is transformed into a forward movement through an integrated ball groove. The drive is based on the tubular shaft motor principle. The extremely compact design is achieved so that the screw drive passes through both the force sensor and the drive motor.
The integrated force sensor can absorb compression and tension forces, so that jointing processes with subsequent tensile testing are possible, and the monitoring and evaluation system is a maXYmos NC type 5847A. The pressing process is controlled by machine PLC.
The use of maXYmos NC allows the inclusion in the program of the pressing speeds and times, which can later be checked, so that we can know if the pressing was carried out under the required conditions, figure 7.

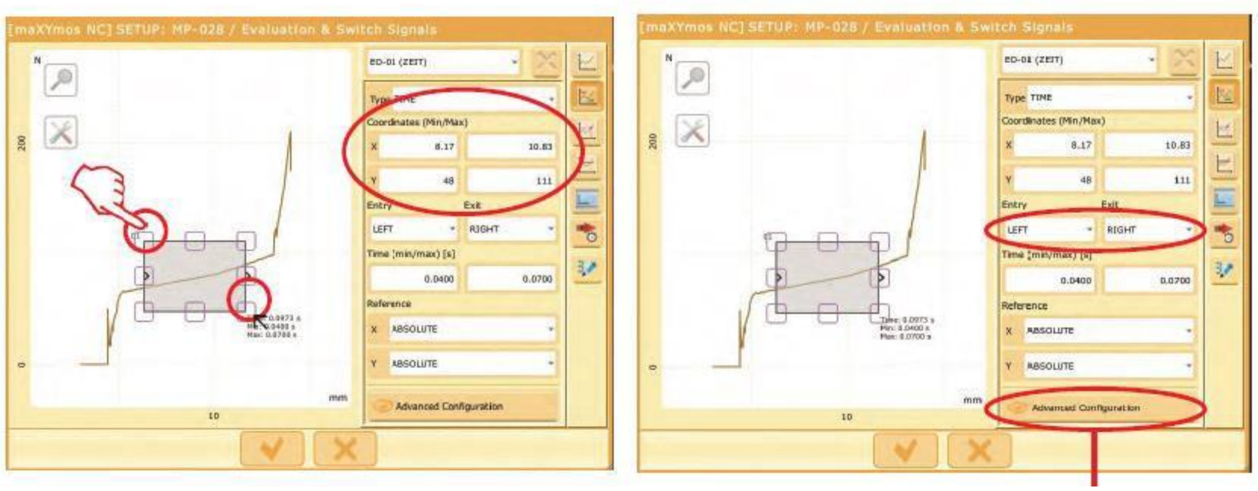

Fig. 7. Screens for entering speed and time parameters

The result of the pressing process is evaluated through the specific windows, in which the system returns the result OK, if a complete movement has been made, that is, the curvature of the curve and its course are in accordance with the tolerance specifications, figure 8. If the press has made an incomplete movement, due workpiece jam, maXYmos makes the decision that the press cycle is NOK, because the maximum press point is reached earlier, which means that the press force has increased far above the preset force graph.

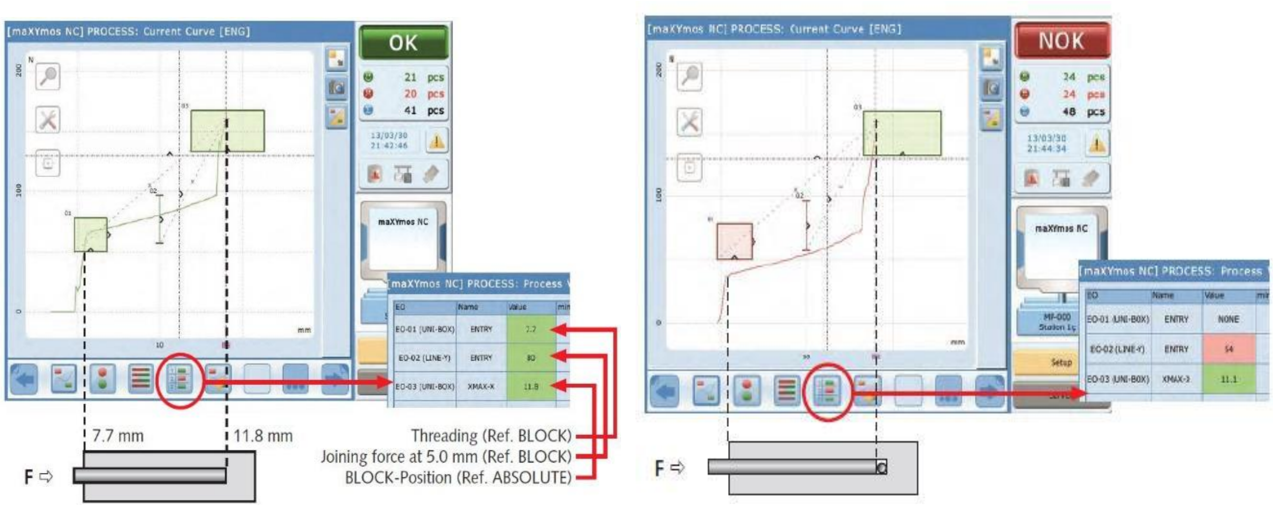

Fig. 8. Screens for entering speed and time parameters

3. Conclusions

The new pressing concept meant major changes both from the point of view of the station's reliability, as well as from the qualitative point of view and from the point of view of the safety of the pressing process.

The analysis of the functionality highlighted the fact that the pressing process was improved.

From the point of view of the maintenance of the installation, the maintenance of the equipment is very easy to do, because the system is a simple constructive one. Preventive maintenance (visual check, greasing, function check) can be performed by maintenance personnel only with the help of instructions and maintenance plans from the equipment supplier.

References

[1] Jula, Aurel, and Mihai Lateş. *Machine Parts*/*Organe de maşini*. Braşov, Transilvania University Publishing House, 2004.

[2] ***. “General Concepts of Automation, Cybernetization and Robotization of Technological Processes. 4.1 Automation of Technological Processes.”, Accessed October 10, 2024. https://www.academia.edu.

[3] ***. “Bearings. General Info.” Accessed October 10, 2024. http://urb-s.ro/products/docs/Rulmenti_info_general.pdf.

[4] NTN-SNR. Rulmenti – Romania/Bearing Mounting.” Accessed October 10, 2024. https://www.ntn-snr.com/ro/montarea-rulmentilor.

[5] ***. “Mechanisation and Automation of Assembly Work/Mecanizarea si automatizarea lucrarilor de asamblare.” *ePedia*. Accessed October 10, 2024. https://epedia.ro/2012/02/16/mecanizarea-si-automatizarea-lucrarilor-de-asamblare/.

[6] Kistler Group. “Servo presses.” Accessed 15, 2024. https://www.kistler.com/INT/en/servo-presses/C00000153.

ISSN 1454 - 8003
Proceedings of 2024 International Conference on Hydraulics and Pneumatics - HERVEX
November 13-15, Băile Govora, Romania

ASPECTS RELATED TO AXIAL PISTON PUMP OPERATION WITHIN A HYDRAULIC CIRCUIT

Fănel Dorel ȘCHEAUA[1]

[1] "Dunarea de Jos" University of Galati, fanel.scheaua@ugal.ro

Abstract: *An axial piston pump is a type of positive displacement pump that uses multiple pistons arranged axially in a circular array around a rotating shaft to displace fluid. This design allows for high-pressure operation, making it popular in hydraulic systems for applications such as construction machinery, aircraft hydraulics, and industrial equipment. Basic assembly components of an axial piston pump are represented by cylinder rotating block which contains the pistons and rotates with the drive shaft, a set of pistons that move inside the cylinder block's bores, swash-plate (angled plate) as a tilted plate that controls the stroke of the pistons by dictating their reciprocating motion, a drive shaft which transmits rotational motion to the cylinder block, valve stationary plate with ports for the inlet and outlet of the fluid and it controls the fluid flow into and out of the cylinder block. For variable displacement pumps, the swash-plate angle can be adjusted in order to control the pump's displacement. The efficient design makes axial piston pumps widely used in various industries where high-pressure and variable flow control is required. The basic parameters and the principle of operation are described in this work for axial piston pumps. The mathematical model describing the operation is also presented, as well as a numerical approach in order to highlight the operating characteristics.*

Keywords: *Hydraulic actuation, axial piston pump, swash plate, bent-axis, fluid flow rate, operational parameters, numerical analysis*

1. Introduction

The axial pistons pump works based on the reciprocating motion of pistons as they move within the bores of the rotating cylinder block. The drive shaft (usually powered by an electric motor or engine) rotates the cylinder block, which contains multiple pistons axially positioned parallel to the shaft's axis. As the cylinder block rotates, each piston follows the angle of the swash-plate, which is fixed at a certain inclination. The swash-plate causes the pistons to move back and forth within the cylinder block. As the piston moves away from the valve plate (upstroke), the volume inside the piston chamber increases, creating suction that draws hydraulic fluid into the chamber through the inlet port of the valve plate. As the piston moves toward the valve plate (down stroke), the volume inside the piston chamber decreases, forcing the hydraulic fluid out through the outlet port of the valve plate. This cycle of suction (inlet) and discharge (outlet) happens continuously as the cylinder block rotates. In a variable displacement axial piston pump, the swash-plate's angle can be adjusted, so a greater swash-plate angle means a higher piston stroke, resulting in higher displacement (more fluid flow rate pumped per rotation), while a reduced swash-plate angle means a shorter piston stroke, resulting in lower displacement. Zero value of inclination angle means that the pistons do not reciprocate, and the pump essentially stops displacing fluid. This feature allows for control over the flow rate of the pump, making it highly versatile in hydraulic applications where the fluid flow needs to vary. The main constructive and functional axial piston types are as variable displacement which allows control over the flow rate by adjusting the swash-plate angle, providing flexibility and efficiency and as fixed displacement where the swash-plate angle is fixed, meaning the pump delivers a constant amount of fluid flow rate per revolution. In a fixed displacement axial piston pump, the swash-plate angle is fixed, meaning the pump has a constant displacement volume for every revolution of the cylinder block.
The flow rate in this type of pump is dependent on the rotational speed (RPM) of the drive shaft and cannot be adjusted without changing the pump's speed. In terms of efficiency and operation

considerations must be presented the high pressure capability as axial piston pumps can generate high-pressure output 40-45 MPa, making them ideal for demanding hydraulic systems.
Variable displacement versions allow precise control of flow, making them suitable for energy-efficient operations. These pumps are highly efficient due to their positive displacement mechanism and ability to maintain steady pressure. The main applications of axial piston pumps are related to construction equipment for hydraulic systems in excavators, bulldozers, and cranes, aircraft hydraulics for control surfaces, landing gear, and braking systems, industrial machinery like presses, injection moulding machines and hydraulic motors and also marine and offshore equipment for steering systems and deck machinery.

2. Constructive variants of fixed displacement axial piston pumps

Both constructive variants considered have different designs and operating principles, but they achieve similar outcomes in terms of converting mechanical energy into hydraulic energy.
In swash plate volumetric unit, the pistons are arranged in a circular pattern within a rotating cylinder block, while the pistons have a translational movement within the special bores.
The pistons are connected to the swash plate angled relative to the cylinder block.
As the cylinder block rotates, the angle of the swash plate causes the pistons to reciprocate. The angle of the swashplate determines the piston stroke. During half of the rotation, the pistons move outward (suction stroke), and during the other half, they move inward (discharge stroke), creating flow of hydraulic fluid.

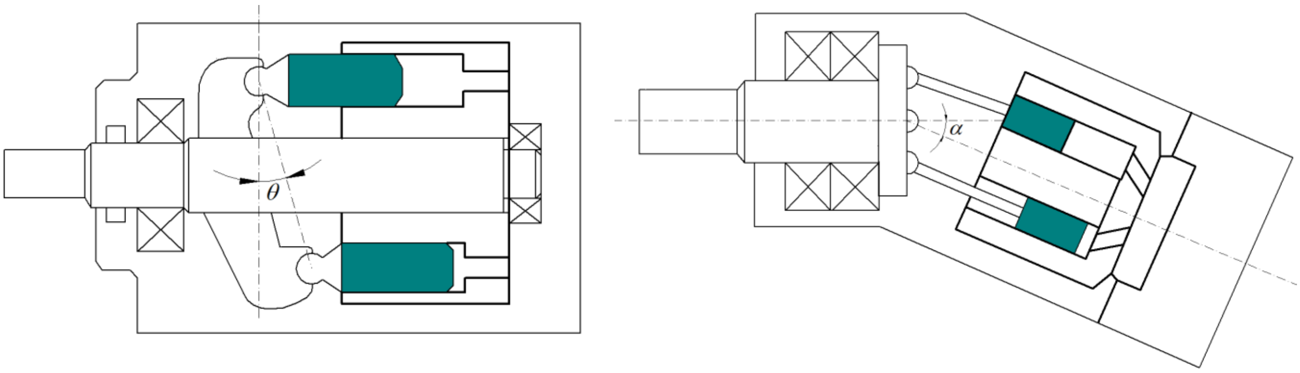

Fig. 1. Fixed displacement axial piston pump variants (swash plate and bent axis)

In a bent axis pump, the pistons are also arranged in a circular pattern, but the cylinder block is oriented at an angle to the drive shaft (bent axis).
The pistons are directly connected to the drive shaft via piston rods. As the shaft rotates, the angle between the drive shaft and the cylinder block causes the pistons to reciprocate within the bores.
The reciprocating action of the pistons results in the suction and discharge of hydraulic fluid.

3. Mathematical model for axial piston pump constructive variants

For a swash plate axial piston pump, the pistons move linearly in and out of the cylinders as the rotating cylinder block is driven by the drive shaft. The swash plate angle value determines the pistons stroke, which in turn controls the pump's displacement and flow rate values.
At a bent-axis axial piston pump, the cylinder block is positioned at an angle relative to the drive shaft axis, so the pistons are connected to the drive shaft by means of a universal joint and during operation, as the block rotates, the pistons are pushed in and out of the cylinder. [1-7]

Both models share some similarities, as they both depend on parameters such as the number of pistons (n), piston diameter (d_p), angular velocity (ω), and displacement (V_r). However, the swash plate pump uses a swash plate angle *θ*, while the bent-axis pump uses the bent angle *α*.

The key parameters can be calculated using the following equations for piston stroke (l_c), displacement per revolution (V_r), flow rate (Q_p) and torque (T_p):

$$l_c = 2r\sin(\theta) \tag{1}$$

$$V_r = n \cdot A_p \cdot l_c \tag{2}$$

$$Q_p = \frac{\omega}{2\pi} \cdot V_r = \frac{\omega}{2\pi} \cdot \frac{\pi \cdot n \cdot d_p^2}{4} \cdot 2r\sin(\theta) = \frac{n \cdot d_p^2 \cdot r \cdot \omega \cdot \sin(\theta)}{4} \tag{3}$$

$$T_c = \frac{n \cdot d_p^2 \cdot p \cdot r \cdot \sin(\theta)}{8} \tag{4}$$

The flow rate will be directly proportional to the swash plate angle *θ*, the pump shaft angular velocity *ω* and the piston diameter. For the torque value it is considered the pressure force acting on the piston head and also the moment with the distance *r* between the pistons position.
For the bent axis constructive variants the parameter equations are as follows:

$$l_c = 2r\sin(\alpha) \tag{5}$$

$$V_r = n \cdot A_p \cdot l_c = \frac{n \cdot \pi \cdot d_p^2}{4} \cdot 2r \cdot \sin(\alpha) \tag{6}$$

$$Q_p = \frac{\omega}{2\pi} \cdot V_r = \frac{\omega}{2\pi} \cdot \frac{\pi \cdot n \cdot d_p^2}{4} \cdot 2r\sin(\alpha) = \frac{n \cdot d_p^2 \cdot r \cdot \omega \cdot \sin(\alpha)}{4} \tag{7}$$

$$T_c = \frac{n \cdot d_p^2 \cdot p \cdot r \cdot \sin(\alpha)}{8} \tag{8}$$

4. A numerical analysis for axial piston pump constructive variant

In order to model the axial piston pump operation, the time-varying dynamics of key physical parameters are considered, with focus on fluid flow rate, pressure, and displacement. The models are derived from the physical principles governing fluid mechanics, pressure-volume relations and the mechanicals of pistons movement (table 1).

Table 1: Axial pump modeling parameters

Axial Piston Pump		
	Swash Plate	Bent-Axis
State variables	$x(t) = \begin{bmatrix} p(t) \\ \theta(t) \\ \omega(t) \end{bmatrix}$	$x(t) = \begin{bmatrix} p(t) \\ \alpha(t) \\ \omega(t) \end{bmatrix}$
Hydraulic pressure dynamics	$\frac{dp(t)}{dt} = \frac{Q(t)}{C_t} - \frac{p(t)}{R_h}$	

Angle dynamics	$\frac{d\theta(t)}{dt}=-k_1\cdot\theta(t)+k_2\cdot u(t)$	$\frac{d\alpha(t)}{dt}=-k_1\cdot\alpha(t)+k_2\cdot u(t)$
Angular velocity dynamics	$\frac{d\omega(t)}{dt}=\frac{T_m(t)-T_h(t)}{J}$	

The derived state-space models for both the swash plate and bent-axis axial piston pumps can be solved numerically to simulate their behavior over time.
Initial conditions are based on the initial values for *p(0), θ(0)* or *α(0),* and *ω(0).*
The analysis model used a direct numerical simulation based on analytical expressions for sinusoidal motion, with a transient response factor.
The piston positions were calculated using a sinusoidal function corresponding to their periodic movement. This analytically method is using trigonometric functions to directly compute the displacement over time.
The transient behavior was modeled using an exponential term which was multiplied by the sinusoidal function to simulate a gradual increase in piston displacement.
The flow rate and pressure were computed directly from the piston displacement using arithmetic relations, assuming linear dependencies.
The simulation results would be the time-varying operation behaviour from pressure, fluid flow rate and position over time for each piston.
This numerical approach allows analyzing how the pump will respond under varying loads, control inputs, and operating conditions. The models can also be used for designing controllers or optimizing pump performance [8-10].
The obtained results are presented in figure 2, highlighting the swash plate constructive variant in 5 piston configuration design.

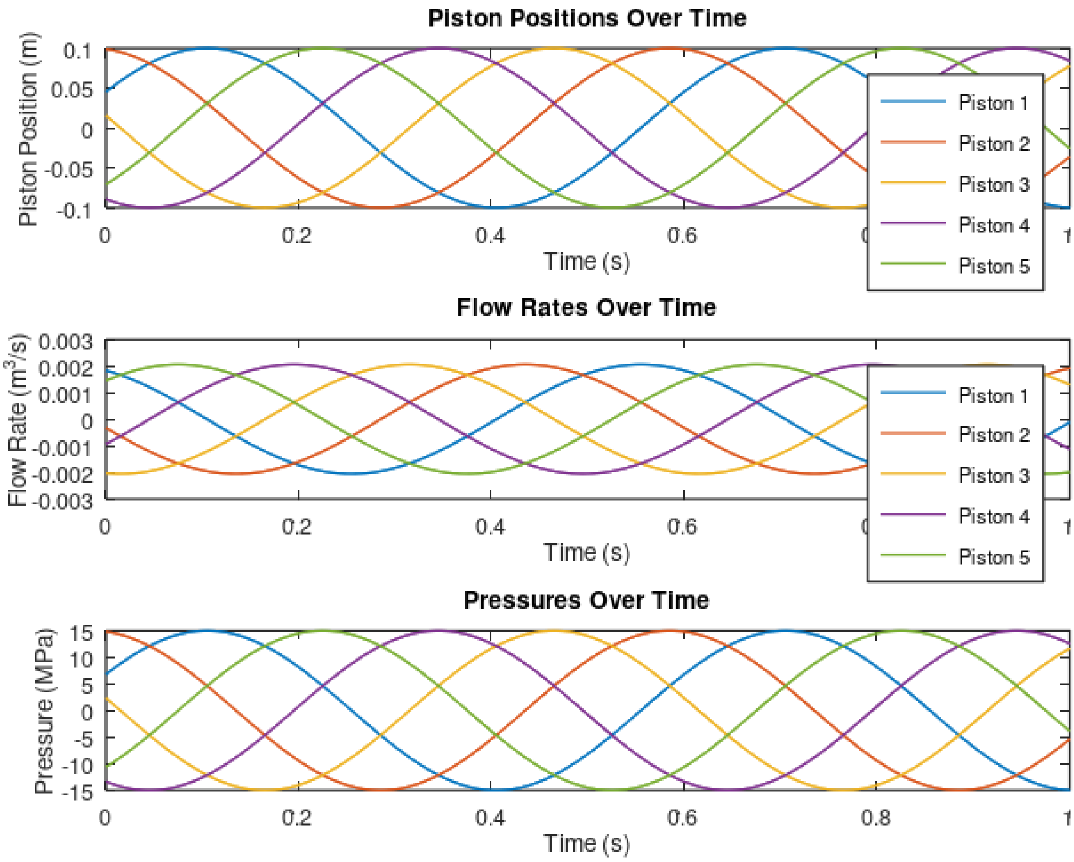

Fig. 2. The analysis results for the axial 5 piston pump

The numerical analysis method is providing solution especially when handling nonlinear dynamics such as those seen in the axial piston pump operation. The swash-plate angle is directly controlled by the time-varying control input, which in turn affects the pressure and angular velocity. The time-varying nature of the control input simulates real-world scenarios where the pump's swash-plate angle is adjusted in order to control the flow rate dynamically.
The bent-axis model behaves similarly to the swash plate model, but there are subtle differences regarding the pistons interaction with the shaft. The response of the pressure, angle and angular velocity encounter slight modification based on this geometry type.

5. Conclusions

The axial piston volumetric units are vital components in hydraulic systems due to their unique design and performance characteristics. These constructive variants are known for their high volumetric efficiency, which means they can transfer high amounts of hydraulic fluid with less energy loss and this efficiency is crucial for applications where power and energy conservation are important. They are commonly used in industrial machinery, construction equipment, aerospace, automotive applications, and other hydraulic systems. The pumps can handle high pressure levels, typically up to 450 bar (6,500 psi) and beyond, making them suitable for heavy-duty applications where substantial force is required, while this ability allows for compact and powerful system designs.
Many axial piston pumps come with variable displacement capabilities, allowing the user to adjust the output flow rate as needed and this adaptability provides better control over the hydraulic system, enhancing system responsiveness and efficiency.
The design of axial piston pumps is compact compared to other pump types, such as gear or vane pumps, making them suitable for applications where space and weight are critical factors.
Axial piston pumps offer smoother fluid flow and can be designed for low noise operation. This characteristic is especially beneficial in industrial settings where noise reduction is essential.
With proper maintenance, axial piston pumps can have a long service life. Their design enables high durability even under harsh operating conditions, making them cost-effective over time.
For the swash plate design, the pistons move linearly back and forth along a cylinder block due to the angled swash plate and the displacement is directly proportional to the swash plate angle.
The piston position follows a more regular sinusoidal pattern as it is driven directly by the rotation and the swash plate's fixed angle.
The flow rate will typically show a smoother sinusoidal pattern with less fluctuation between pistons.
In a bent-axis pump, the pistons are connected at an angle between the drive shaft and the cylinder block; the piston displacement depends of the bent axis angle and is driven by the rotation of the shaft. This can result in slightly different sinusoidal patterns for piston positions and flow rates due to the combined effect of the axis angle and rotational motion.
Variations in flow rate might be more pronounced due to the changing effective stroke over the pump cycle.
A constructive design axial volumetric unit swash plate with 5 pistons had been analyzed in this paper, highlighting the piston position, flow rate and pressure values corresponding to operation. The transient response was introduced in the models using an exponential term. This simulates the gradual stabilization of the pump's performance after starting up. The value of the time constant can significantly affect the initial behavior.
In both swash plate and bent-axis configurations, this transient effect shows a rise in flow rate, pressure, and piston positions, but the patterns of stabilization might slightly be different.
Swash plate pump tend to stabilize more uniformly due to the consistent motion induced by the swash plate, while the bent-axis variant may exhibit slight variations in transient behavior due to the varying effective stroke length at different piston positions over the cycle.

For swash plate volumetric units, the flow rate for each piston follows a consistent pattern because of the uniform driving mechanism.
Swash plate design offer more uniform sinusoidal behavior across piston positions, flow rates, and pressures.
The practical implications are that swash plate pumps are generally preferred for applications requiring smooth, consistent flow and pressure characteristics.
These values are related to the mechanical design of the pumps and become evident in simulations that account for transient behavior, displacement, and flow characteristics.

References

[1] Axinti, G., and A. S. Axinti, *Hydraulic and pneumatic drives – Components and systems, Functions and features / Acţionări hidraulice şi pneumatice – Componente și sisteme, Funcții și caracteristici.* Vol. 1. Chişinău, Tehnica-Info Publishing House, 2008.
[2] Axinti, A. S., and F. D. Șcheaua. *Introduction to industrial hydraulics/Introducere în hidraulica industrială*. Galati, University Press, 2015.
[3] Axinti, G., and A. S. Axinti. *Hydraulic and pneumatic drives – Bases of Calculation, Design, Operation, Reliability and Drive Diagrams /Acţionări hidraulice şi pneumatice – Baze de Calcul, Proiectare, Exploatare, Fiabilitate și Scheme de Acționare*. Vol. 3. Chişinău, Tehnica-Info Publishing House, 2009.
[4] Li, Ruichuan, Qi Liu, Yi Cheng, Jilu Liu, Qiyou Sun, Yisheng Zhang, and Yurong Chi. "Analysis of the Influence of Structure and Parameters of Axial Piston Pump on Flow Pulsation." *Processes* 10, no. 10 (2022): 2138.
[5] Todić, Nenad, Slobodan Savić, Dušan Gordić, and Radovan Petrović. "Experimental Research of the Hydrodynamic Processes of an Axial Piston Water Hydraulic Pump." *Machines* 10, no. 9 (2022): 728.
[6] Sun, Zhiyuan, Qingliang Zeng, Lirong Wan, and Hanzheng Dai. "Control and dynamic characteristics analysis for the double-compound axial piston pump based on working conditions." *Machines* 10, no. 6 (2022): 411.
[7] Kauranne, Heikki. "Effect of operating parameters on efficiency of swash-plate type axial piston pump." *Energies* 15, no. 11 (2022): 4030.
[8] Liu, Jiamin, Shuai Meng, Xintao Zhou, and Lichen Gu. "A hydraulic axial piston pump fault diagnosis based on instantaneous angular speed under non-stationary conditions." *Lubricants* 11, no. 9 (2023): 406.
[9] Xu, Shunhai, Chunxiao Zhao, Dian He, Nan Xu, Bin Zhang, and Guofang Gong. "Research on Bearing Mechanism of Spherical Valve Pairs of Axial Piston Pumps." *Actuators* 13, no. 4 (2024): 147.
[10] Shi, Junqiang, Jiaxing Shi, Jingcheng Gao, Dongjing Chen, Xiaotao Li, Ying Li, and Jin Zhang. "The Influence of Complex Piston Movement on the Output Flow Rate of a Hingeless Bent-Axis Axial Piston Pump." *Processes* 12, no. 6 (2024): 1141.

ISSN 1454 - 8003
Proceedings of 2024 International Conference on Hydraulics and Pneumatics - HERVEX
November 13-15, Băile Govora, Romania

COMPARISON OF EXPERIMENTAL RESULTS WITH SIMULATION STUDIES OF "DIGITAL" HYDROSTATIC TRANSMISSION

Ahmed Zubair JAN[1], Krzysztof KĘDZIA[1], Paweł ŚLIWIŃSKI[2]

[1] Wroclaw University of Science and Technology, POLAND, ahmed.jan@pwr.edu.pl, krzysztof.kedzia@pwr.edu.pl

[2] Gdansk University of Technology, POLAND, pawel.sliwinski@pg.edu.pl

Abstract: *The publication presents the results of experimental research on a "digital" hydrostatic transmission conducted at INOE 2000 IHP within the framework of the grant "Method of effective use of the digital hydraulics concept in multi-source hydrostatic drive systems". The primary goal of the research is to compare the effectiveness (efficiency) of using different methods of controlling the pump capacity and the hydraulic motor capacity in multi-source, hydrostatic drive systems and to compare the experimental results with simulation studies obtained in the MATLAB Simulink program.*

Keywords: *“Digital” hydrostatic transmission, modelling and simulation, experimental tests*

1. Introduction

Hydrostatic drives, also referred to as hydrostatic transmissions, are typically created by hydraulically connecting pumps and motors. A motor with constant displacement and a pump with variable displacement make up a standard hydrostatic gearbox. The system typically operates at maximum efficiency when the motor is operating at its highest volumetric displacement. When power is needed, hydraulic systems use fluids under pressure to convey power or perform tasks at a desired area. The history of technology has shown that fluid power is a valuable medium. It has been utilised in construction, agricultural, and aerospace equipment as well as more complicated designs like the water wheel. The following are some benefits of fluid flow over other power transmission technologies, such as electrical, pneumatically, and mechanical systems:

- Compared to its equivalents, hydraulic pumps and motors are substantially lighter and smaller than electric or petrol motors with the same horsepower.
- Due to their extreme flexibility, hydraulic hoses can send power to nearly any spot and route fluid lines around other pieces of equipment.
- Compared to a mechanical system that can generate the same amount of force, a hydraulic system is far smaller.
- A fixed gear ratio is not necessary because speeds may be readily adjusted for every operating circumstance.

The efficiency of a hydraulic system can be somewhat poor, which is a drawback. "Most mechanical systems are more efficient than hydraulic systems, even if hydraulic systems are far more efficient than electrical systems. The pump is the main part of the hydraulic system that supplies power. Axial-piston pumps, gear pumps, and vane pumps are only a few examples of the numerous varieties of pump arrangements. The most often used pumps are axial-piston pumps because they have great operating efficiency (up to 85%), can withstand high pressures, and can be controlled via variable displacement. We can further divide these pumps into two types: variable displacement and fixed displacement. For each cycle, fixed displacement pumps transport the same volume of fluid. Only when the pump's speed has been changed can the volume be altered. Pumps with variable displacement have the ability to regulate the flow without regard to the speed of the pump.

1.1. A "Digital" Hydrostatic Drive System Model

The “digital” pump is made up of a number of parallel arrays of constant displacement pumps (e.g. gear pumps) of various sizes. A grid of on-off valves allows the individual pumps to be switched between the load and idle states as the flow requirement varies (fig.1).

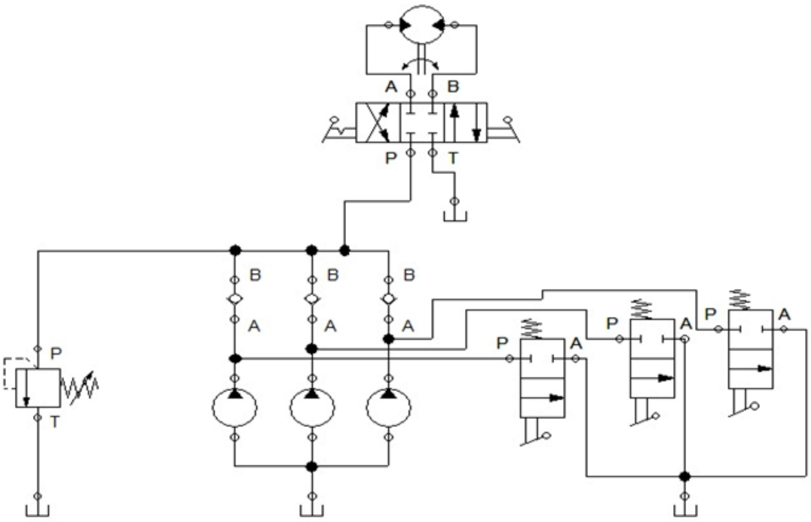

Fig. 1. Schema of “digital” hydraulic circuit

2. Scientific Goal of The Project

The scientific goal of this project is to compare the effectiveness (efficiency) of using different methods of controlling the pump flow rate and hydraulic motor capacity in multi-source, hydrostatic drive systems. Currently, the point is to compare a traditional hydrostatic system composed of multi-piston, axial hydrostatic unit with a "digital” hydrostatic transmission that allows for changing the liquid flow rate in the system with an appropriate displacement pumps (4 gear pumps on one shaft of an electric motor).

After comparing the results, it will be possible to answer the questions:

1. Will replacing a pump with the ability to change the flow rate (e.g. multi-piston axial pump with a tilting disc) and proportional control (implemented using a proportional valve) with a system consisting of a "digital" hydraulic transmission meet the requirements for the power supply units and control used for the construction of multi-source hydrostatic drive systems?

2. What will be the energy efficiency above the change described?

3. Will the dynamic parameters of the hydraulic system subjected to such modifications meet the requirements for multi-source systems?

4. What types of savings will result from this modified arrangement?

5. What will be the impact of replacing a typical hydraulic system with a system built according to the concept of "digital hydraulics" in the area of efficiency, reliability, safety and ecology (carbon footprint, emissions of harmful substances, e.g. in the case of using an internal combustion engine: carbon dioxide, nitrogen oxides, particulate matter)?

2.1 Technical Data of the Experimental Testing Pumping System

- Three – phase induction motor power …… 11 kW;
- 3-phase supply voltage ……………………. 380 V 50 Hz;

• Motor speed …………………………………. 1475 rev/min;

• Variable speed drive ………………………. Altivar 71; 15 kW;

• Motor speed adjustment range …………… 10÷50 Hz ;

• Max. flow ……………………….………….... Q = 45 l/min ;

• Max. pressure ……………………………… f(Q): 100÷200 bar;

• Pumps displacement ………………..……… 2, 4, 8, 16 cm3 /rev.

2.2 Technical Means Used During Experimental Test

Fluid working environment:

- Working fluid: HP 46 hydraulic oil;
- Filter fineness: 10m;
- Maximum temperature of the working fluid: 40 ± 5^{o}C.

Equipment used:

- Flow transducer accuracy class 2.0;
- Speed transducer accuracy class 1.0;
- Torque meter accuracy class 1.0;
- Thermometer 0 to 100ºC, accuracy class 2.0;
- Pressure transducer 0 to 160 bar;
- Power supply 24 V / 10A.

a) General view of valves connection

b) The view of electric motor with pumps

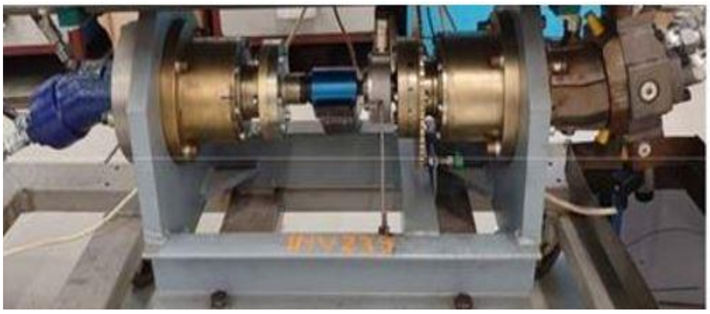

c) The view of hydraulic motor with load

Fig. 2. Experimental Equipment

2.3 Hydraulic Schematic Diagram of Experimental Testing Stand

Figure 3 displays the “digital” hydraulic schema used in the experiment.

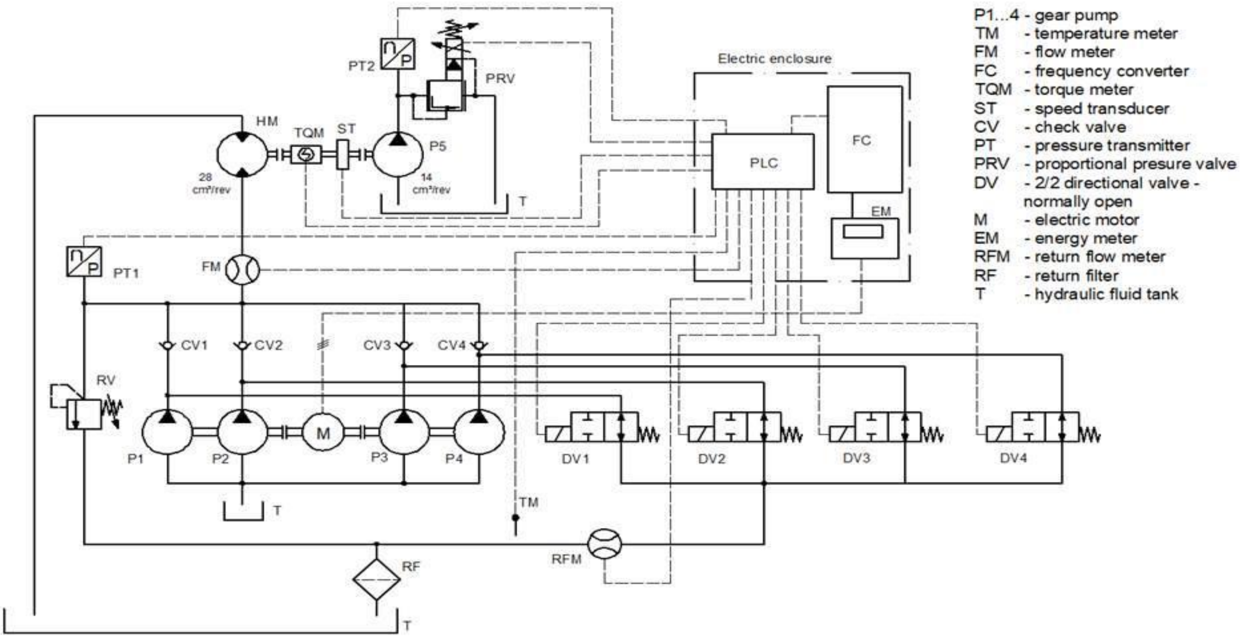

Fig. 3. Schema of “digital” hydrostatic transmission testing stand

2.4 Equipment Characteristics

No.	Equipment	Product type	Manufacturer	Charateristics
1	Pressure transducer	S-10	Wika	- Supply 10…30 VDC - Range 0…400 bar - Output sig. 4…20 mA
2	Flow transducer 1 (output flow)	EVS3100	Hydac	- Supply 10…30 VDC - Pmax. 400 bar - Range 6…60 l/min - Output sig. 4…20 mA
3	Flow transducer 2 (return flow)	VT1541VADNSOA4	Sika	- Supply 4.5…24 VDC - Range 2…40 l/min - pulses/liter 915 - Pmax. 300 bar - Meas. instrument TD 32500 - Output sig. 4…20 mA
4	Temperature trans.	TSOCB1	Comeco	- Range 0…100 °C - Output sig. 4…20 mA
5	Torque transducer	DR-2493	Lorenz messtechnik	- Supply 12…28 VDC - Range 500 Nm - Output sig. ± 10 V
6	Speed transducer	8.A020.3132.0360	Kubler	- Supply 10…30VDC, 150 mA - 360 pulses/rev
7	Solenoid controlled valve	HK EMDV 10 NO1 24DC	Hansa Flex	- MN10 - Rated flow 30 l/min - Pmax. 350 bar

3. Traditional Hydrostatic Transmission Simulation Model

The simulation model's creation aims to analyze the hydrostatic transmission (fig. 4), specifically the flow through the overflow valve during start up (Q_z) in relation to valve opening pressure (p_o), hydraulic motor angular velocity (ω_s), hydraulic pump side pressure (p_p), and hydraulic motor side pressure (p_s). The aim of simulation research is an answer whether the "digital" hydraulics can be used in a multi-source hydrostatic drive system? Are their parameters similar to the clasic hydrostatic transmission?

3.1 The Mathematical and Numerical Data of the Model:

a) Torque equation for hydraulic motors (1):

$$q_s p_s = M_0 + R_0\omega_s + I\frac{d\omega_s}{dt} \tag{1}$$

The initial state: $\omega_s(0)=0$, circumstances of the boundaries: for $q_s p_s \le M0$ and $\omega_s=0$, $\frac{d\omega_s}{dt}=0$

b) Equation for pump flow (2):

$$q_p\omega_p = G_p p_p + G_r(t)\sqrt{p_p - p_s} + Q_z + \frac{V_p}{E_c}\cdot\frac{dp_p}{dt} \tag{2}$$

Conditions at the beginning: $p_p(0) = \left[\frac{q_p\omega_p}{G_r}\right]^2$

c) Equation of flow for distribution valves (3):

$$G_r(t)\sqrt{p_p - p_s} = q_s\omega_s + G_s p_s + \frac{V_s}{E_c}\cdot\frac{dp_s}{dt} \tag{3}$$

Conditions at the beginning: $p_s(0) = 0$

d) Flow from an overflow valve Qz formula (4), (5):

A non-inertial valve:

$$\text{For } p_p < p_o:\quad Q_z = 0$$
$$\text{For } p_p > p_o,\ Q_z = K(p_p - p_o) \tag{4}$$

The inertial valve:

$$T_z\frac{dQ_z}{dt} = K_z(p_p - p_0) - Q_z \tag{5}$$

Data:

$q_p\omega_p$=723*10^{-6}[m^3/s], E_c=1.5*10^9[N/m^2], p_o=19*10^6[N/m^2], q_s=4.76*10^{-6}[m^3/rad], R_o=0.03[Nm/s], G_p=G_s=5.4*10^{-12} [m^4s/kg], T_z=0.2 [s], V_p=150*10^{-6} [m^3], V_s=230*10^{-6} [m^3], K_z=0.52*10-9 [m5/Ns], I_0=54*10^{-4}[Nm/s^2], M_0=60[Nm], G_r=7.23*10^{-7} [m^4/$N^{0.5}$].

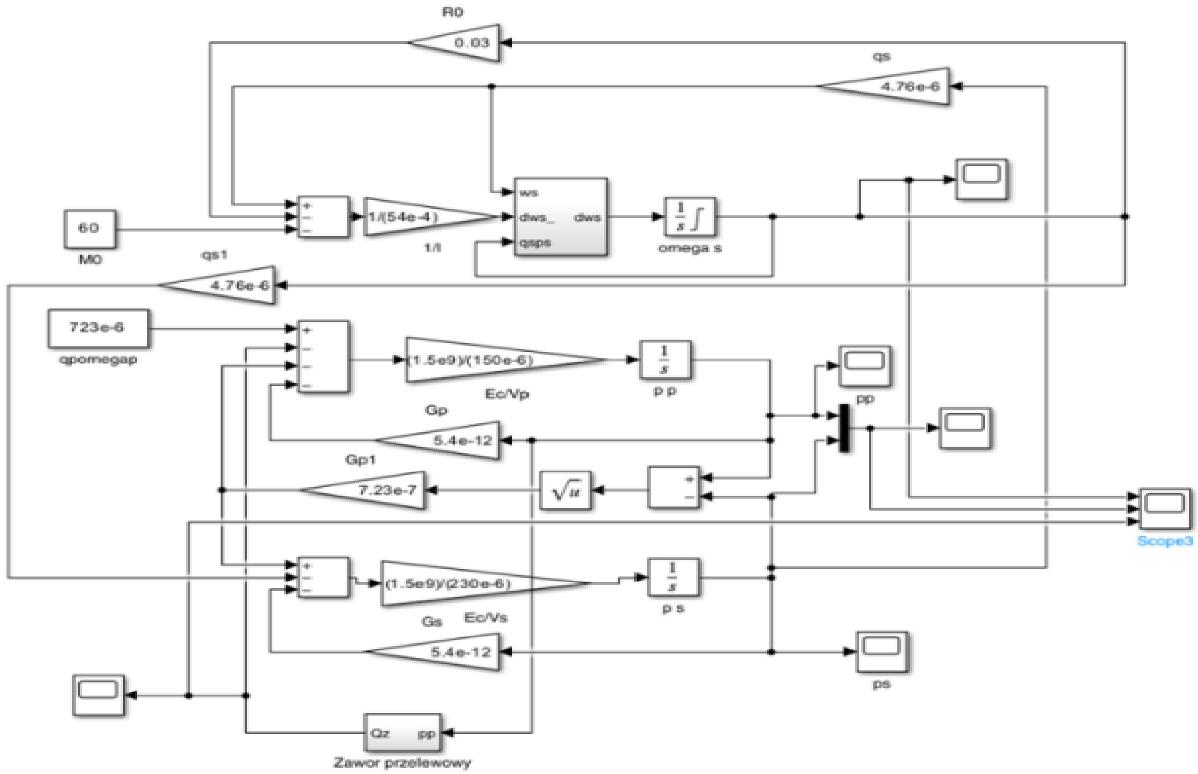

Fig. 4. Schema of simulation model

3. Comparison of simulation and experimental data

Figures 5 and 6 present the results of experimental studies carried out at the HYDRAULICS AND PNEUMATICS RESEARCH INSTITUTE in Bucharest, within the project "Method of effective use of the "digital" hydraulics concept in multi-source hydrostatic drive systems" (50SD/0065/24).

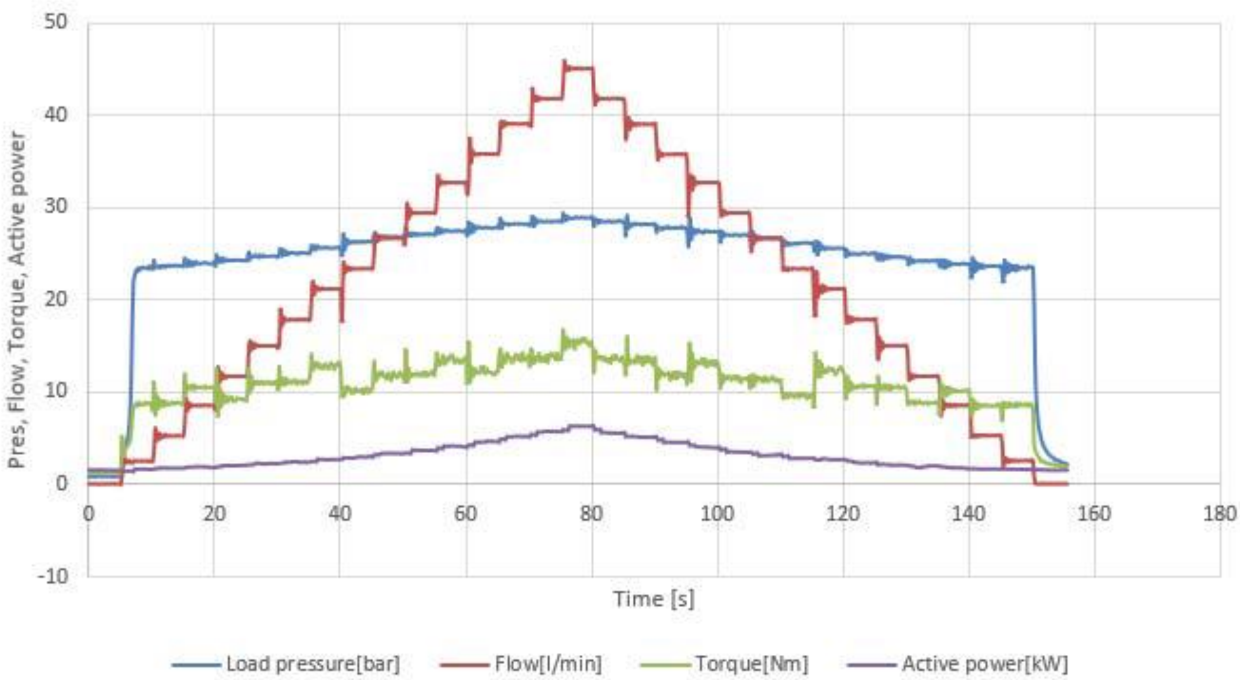

Fig. 5. Experimental research results

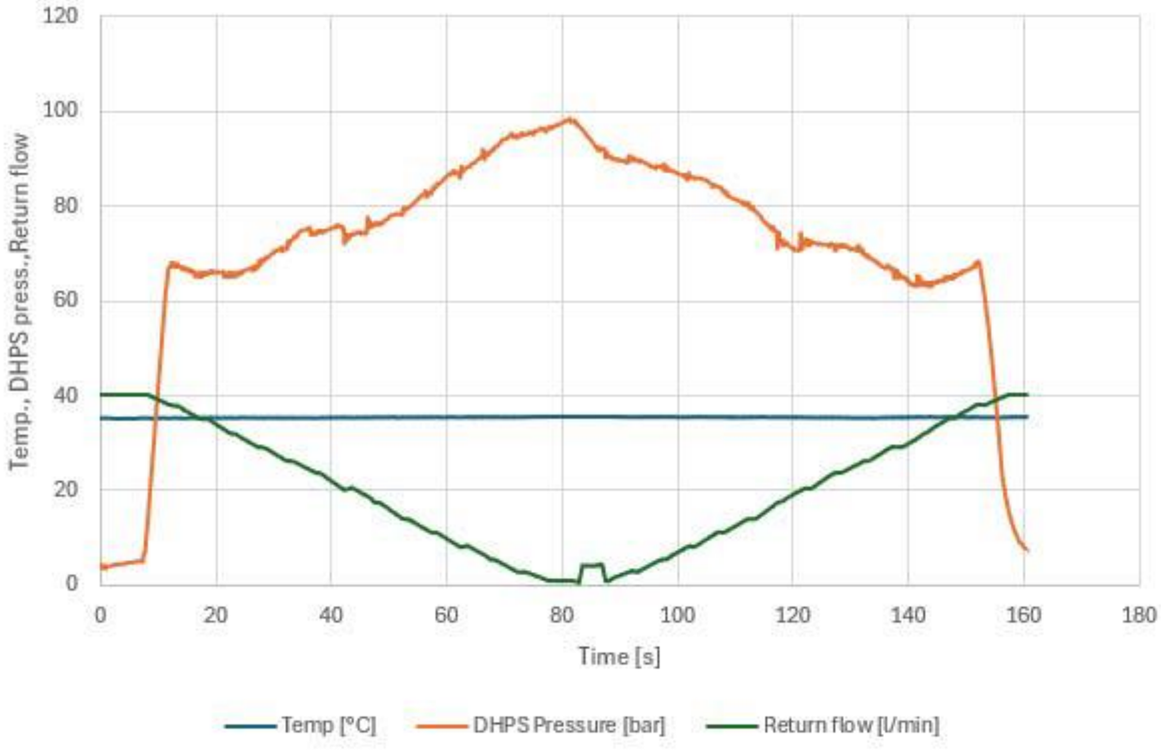

Fig. 6. Experimental research results

The simulation model built and the research results obtained from it initially confirm its correctness (figure 7 and 8). No statistical analysis has been carried out so far to compare the simulation and experimental results. This will be the subject of subsequent publications.

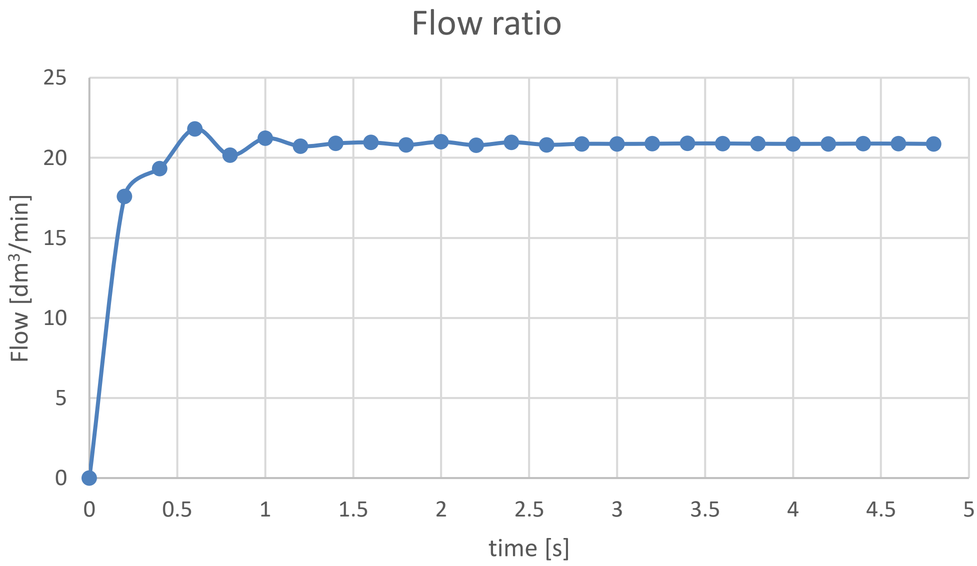

Fig. 7. Experimental research results for 20 dm^3/min flow

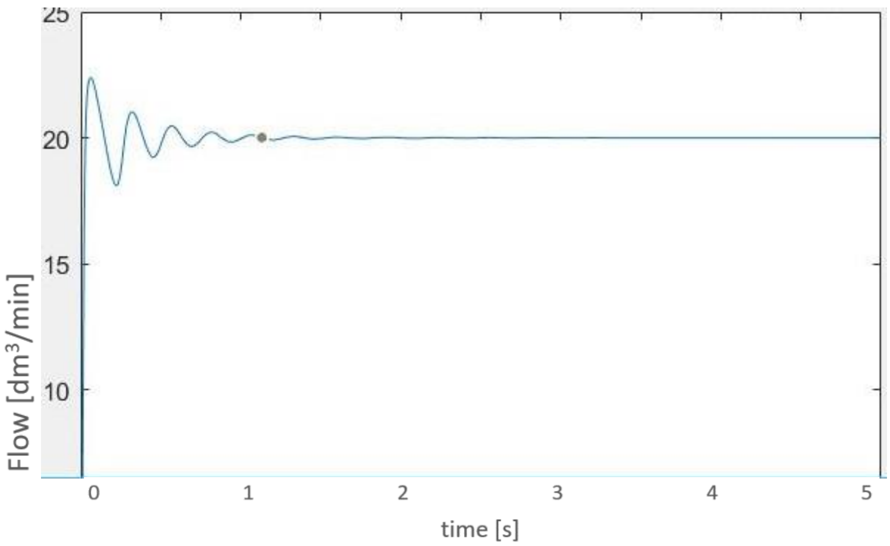

Fig. 8. Simulation research results for 20 dm³/min flow

4. Conclusions

The publication presents the preliminary results of the comparison of experimental studies of the "digital" hydrostatic transmission, conducted at INOE 2000 IHP as part of the grant "Method of effective use of the concept of digital hydraulics in multi-source hydrostatic drive systems" with its simulation model. Due to the too short time between obtaining the results of the experimental studies and the deadline for sending the full text of the paper, only symbolic comparison of the simulation model with the experimental studies is included. An extended comparison of the effectiveness (efficiency) of using different methods of controlling the pump capacity and the hydraulic motor capacity in multi-source, hydrostatic drive systems and a comparison of the experimental results with simulation studies obtained in the Matlab Simulink program will be the subject of future publications.

Acknowledgments

The authors would like to thank the director of INOE 2000- IHP PhD. Eng. Catalin Dumitrescu, as well as chief of Department PhD. Eng. Radu Radoi and Dipl. Eng. Bogdan Tudor for their help, kindness and support in carrying out the experimental studies cited in the article.

References

[1] Seyfferth, W., A.J. Maghzal, and J. Angeles. “Nonlinear modeling and parameter identification of harmonic drive robotic transmissions.” Paper presented at the 1995 IEEE International Conference on Robotics and Automation, Nagoya, Aichi, Japan, May 21-27, 1995.

[2] Tuttle, T. D., and W. P. Seering. “A nonlinear model of a harmonic drive gear transmission.” *IEEE Transactions on Robotics and Automation* 12, no. 3 (June 1996): 368–374.

[3] Kircanski, N.M., and A.A. Goldenberg. “An experimental study of nonlinear stiffness, hysteresis, and friction effects in robot joints with harmonic drives and torque sensors.” *The International Journal of Robotics Research* 16, no. 2 (1997): 214–239.

[4] Kaminaga, H., T. Amari, Y. Niwa, and Y. Nakamura. “Electro-hydrostatic actuators with series dissipative property and their application to power assist devices.” Paper presented at the IEEE/RAS-EMBS International Conference on Biomedical Robotics and Biomechatronics (BioRob 2010), Tokyo, Japan, September 26-29, 2010.

[5] Kaminaga, H., T. Amari, Y. Katayama, J. Ono, Y. Shimoyama, and Y. Nakamura. “Backdrivability analysis of Electro-Hydrostatic Actuator and series dissipative actuation model.” Paper presented at the 2010 IEEE International Conference on Robotics and Automation, Anchorage, AK, USA, May 3-7, 2010.

[6] Jan, A. Z., K. Kędzia, and D. Prostański. “A new approach in hydrostatic drives: "Digital" pumps.” Paper presented at the International Scientific-Technical Conference on Hydraulic and Pneumatic Drives and

Controls, NSHP 2023, Piechowice, Poland, October 11-13, 2023. *Lecture Notes in Mechanical Engineering - Advances in Hydraulic and Pneumatic Drives and Control 2023* (2024): 58-70.

[7] Dąbek, K., P. Osiński, and K. Kędzia. "Preliminary tests for the use of hydrostatic transmission with oscillating energy flow." Paper presented at the International Scientific-Technical Conference on Hydraulic and Pneumatic Drives and Controls, NSHP 2023, Piechowice, Poland, October 11-13, 2023. *Lecture Notes in Mechanical Engineering - Advances in Hydraulic and Pneumatic Drives and Control 2023* (2024): 184-195.

[8] Kędzia, K. *Determinant of load cycle variation of a multi-source hydrostatic drive system*. 2nd edition revised and supplemented / *Wyznacznik zmienności cyklu obciążenia wieloźródłowego hydrostatycznego układu napędowego*. Wydanie II poprawione i uzupełnione. Wrocław, Publishing House of Wrocław University of Science and Technology, 2023.

[9] Jan, A. Z., P. Śliwiński, and K. Kędzia. "Digital hydraulics circuit based on PWM function for controlling hydraulic actuator position." Paper presented at the 26th International Conference on Hydraulics and Pneumatics HERVEX 2022, Băile Govora, Romania, November 9-10, 2022.

[10] Kędzia, K. "A method of determining optimal parameters for the secondary energy source of a multisource hydrostatic drive system in machines working in closed spaces." *Energies* 15, no. 14 (2022): 5132.

[11] Domagała, Z., K. Kędzia, and M. Stosiak. "The use of innovative solutions improving selected energy or environmental indices of hydrostatic drives." Paper presented at the Innovative Mining Technologies: IMTech 2019 Scientific and Technical Conference, Szczyrk, Poland, October 14-16, 2019. *IOP Conference Series: Materials Science and Engineering – Part 2* 679 (2019): 012016.

ISSN 1454 - 8003
Proceedings of 2024 International Conference on Hydraulics and Pneumatics - HERVEX
November 13-15, Băile Govora, Romania

ANALYSIS OF A PNEUMATIC BAND BRAKING SYSTEM FOR INDUSTRIAL WINCHES

Georgiana-Alexandra MOROȘANU[1], George-Ștefan LEOCA[2,3], Doina BOAZU[3], Nicușor BAROIU[4]

[1] Department of Continuous Training and Technological Information, Danubius International University of Galati, Romania, georgianaalexandra.morosanu@univ-danubius.ro

[2] DMT Marine Equipment, Galati, Romania
george.leoca@yahoo.com

[3] Department of Mechanical Engineering, ”Dunarea de Jos” University of Galati, Romania
Doina.Boazu@ugal.ro

[4] Department of Manufacturing Engineering, ”Dunarea de Jos” University of Galati, Romania
Nicusor.Baroiu@ugal.ro

Abstract: *Band braking systems are widely used in industrial and marine mechanisms due to their efficiency in generating braking moment through friction between the brake band and the rotating drum. These systems have a simple construction, consisting of a metal band covered with a friction material (ferodo), which tightens around a drum in order to reduce the rotation speed or to completely stop the mechanism. The analysis of these systems is frequently performed using the finite element method (FEM), which allows the assessment of the distribution of stresses and strains in the structural elements. CAD methods are essential in the accurate modeling of braking components, and the use of CAE-type software for static and dynamic simulation provides a detailed assessment of mechanical performance, including von Mises stress distribution and the safety factor. The paper presents a study on the band braking system from the structure of industrial winches. The design of this system was realized through CAD modeling using Autodesk Inventor software, which allowed the precise creation of the geometry of the system components, such as the brake band, pneumatic cylinders and support elements. Based on this modeling, finite element method (FEM) simulations were performed in Ansys Workbench for both static and dynamic analysis. Static analysis was used to assess the stress and strain distribution in the system components, while dynamic analysis simulated the operating conditions during rapid braking. In addition, the paper includes analytical calculations in order to verify the strength of various components, such as joints and welds, which are used to validate the design and to compare with the results obtained from numerical simulations.*

Keywords: *Band brake, pneumatic cylinder, CAD, resistance calculation, Ansys Workbench, FEM, mesh*

1. Introduction

Mechanisms are provided with braking devices that aim to stop the movement of the load, the mobile part of the mechanism or the entire mechanism and keep them safely in a position of static balance. These braking subassemblies operate on the principle of friction braking and convert mechanical energy into heat energy, which is dissipated into the environment. The construction of the braking devices must be simple and robust, allow easy adjustment and have the smallest possible dimensions. As a rule, the braking elements are installed directly on the shaft connected to the motor, where the external forces generate the smallest moments. In the design of such elements, both kinematic and dynamic parameters must be taken into account, as well as the number of brakings per time unit in which cases the braking moment and the method of exhausting caloric energy must be taken into account in the imposed admissible values. Band brakes have as a specific element a braking band made up of a metal part and a ferodo part, a material with a high friction coefficient. The tape wraps around the brake wheel at an angle of about 250^0 [1, 2, 3].
In the case of the present paper, the braking band consists of two parts, connected at two of the ends by a joint element and connected at the other ends by the rigid body of the brake. In the structure of the brake is a lever directly connected to the band brake, which, once actuated in one

direction, produces the tightening necessary for braking, and in the other direction produces the relaxation of the assembly. It should be noted that the auxiliary element of the drum on which the band brake is placed is called the brake track. This element has a cylindrical shape of small length compared to its diameter, the inner face and the outer face being processed in such a way as to ensure braking under conditions required by operation [4, 5].
By operating conditions it is understood that the brake must provide a maximum braking force imposed in the design, a force which, once defeated, must lead to a decoupling of the braking element. This condition is mandatory to prevent destruction of the braking system.
Braking systems are mounted on the outer surface of the braking track, the inner track being used for couplings that transmit the moment transmitted by the engine to the shaft and from the shaft to the drum [4, 5]. Figure 1 shows the braking path mounted on the drum of a winch [6].

a. b. c.

Fig. 1. Braking systems:
brake track on drum (a); vertical braking system (b); horizontal braking system (c) [6]

From the point of view of the discharge of the forces generated in the brake body, traction and compression brakes are distinguished. These types of brakes are distinguished by the way the cable is wrapped on the drum. Figure 2 shows the forces, moments and reactions occurring within the braking system. It should be noted that reactions occur in the welding area on board brake vessel.

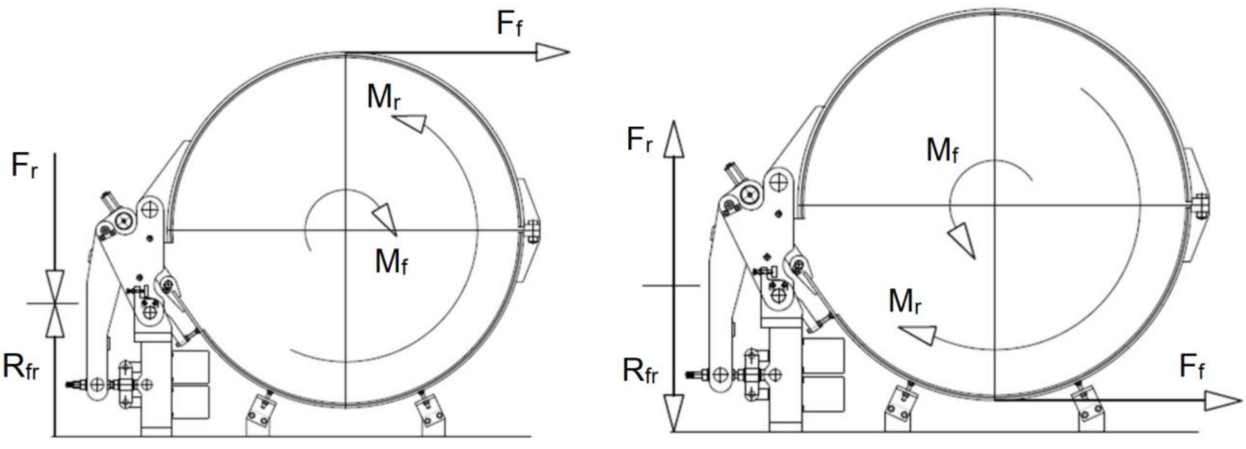

a. b.

Fig. 2. Schematic of a traction (a) and compression (b) brake [6]

It is observed that in the case of the two brakes, the braking force F_f generated in the system is represented, which creates a braking moment M_f. The reaction moment M_r, which opposes the braking moment due to static balance, generates a reaction force F_r, which is equaled by a ground reaction R_{fr}.

Also, the orientation of the R_{fr} reaction gives the name of the brake type: if the reaction is oriented as in Figure 2.a, it generates tensile stresses (hence the traction brake name), and if it is oriented as in Figure 2.b, this generates compression stresses on board the ship, hence the compression brake name.
Figure 3 shows the diagram of a band brake.

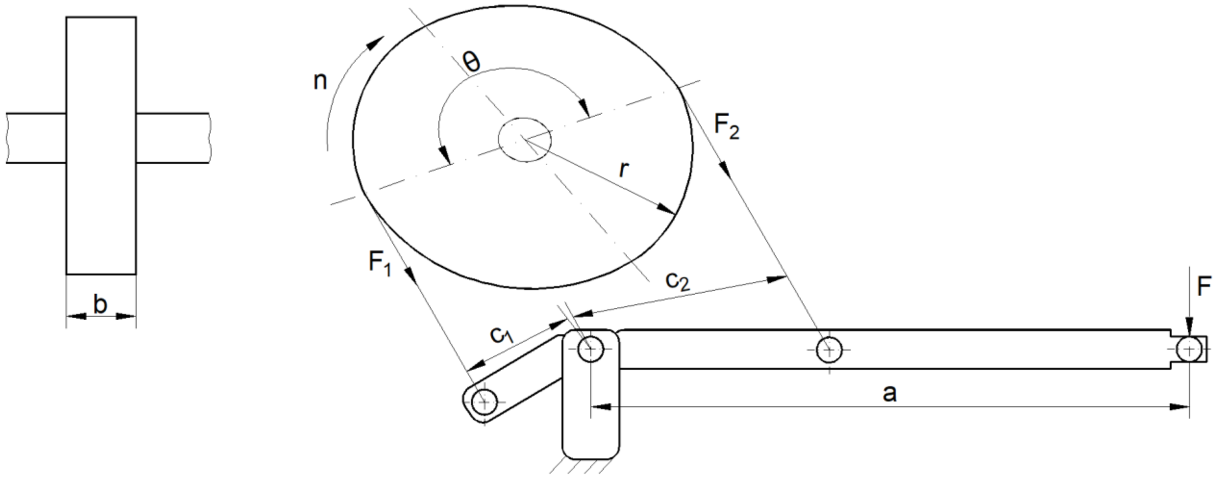

Fig. 3. General case of a band brake - working diagram [6]

Band brakes have in their structure a disc mounted on a shaft, a metal band that enwraps a certain portion of the disc, the metal band that is lined with ferodo in order to increase friction and a lever that can oscillate around a fixed point. The ends of the tape are fixed on the lever. If the lever rotates in a certain direction, the band is pressed against the disc and therefore the brake is tightened. Rotation in the other direction weakens the brake action. The F force required for braking is calculated with relation (1) [6]:

$$F = \frac{F_2 \cdot c_2 - F_1 \cdot c_1}{a} = F_2 \cdot \left(c_2 - c_1 \cdot e^{\mu \cdot \theta}\right)[\mathrm{N}]; \quad F_1 = F_2 \cdot e^{\mu \cdot \theta}\,[\mathrm{N}]\,(\mathrm{Euler}), \tag{1}$$

where: F represents the applied force; n - shaft speed, in rpm; a - operating lever arm, in mm; r - drum radius, in mm; c - the distance from the insertion points of the belt to the joint, in mm; μ - friction coefficient; θ - enwrapping angle, in degrees.

2. Calculation of brake resistance

2.1 Preparation of brake resistance calculation with imposed design requirements

The calculation was divided into sections, such as joint areas of the assembly, connection areas of the band brake and brake body, weld seams or along the band brake. These calculation sections, shown in part, can be identified from the general scheme of the assembly, Figure 4. Table 1 shows the resistance calculation for the band brake drum.
Also, the resulting force at the end of the band of *D-D* section was calculated, Figure 5.a and the dimensioning of the thickness of the metal band was realized, where a higher value was chosen, Table 2. Similarly, the calculation of the tensile stresses found in *E-E* section of the band brake was realized; based on the data, a stress value far below the admisible stress resulted, Figure 5.b and Table 2.

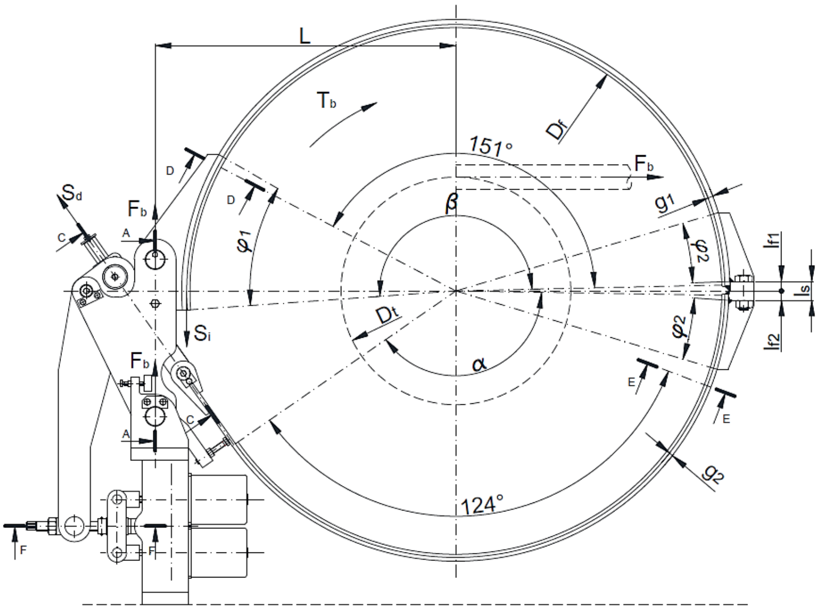

Fig. 4. Loading scheme of the system - 2D representation

Table 1: Calculation of the resistance of the drum on which the brake is placed [6,11,12]

Parameters	Symbol	Result
Cable diameter	Ø	76 mm
Drum diameter after one enwrap of the cable	D_t	726 mm
Braking force for a cable enwrap	F_t	1 000 000 N
Brake diameter	D_f	1.68 m
Brake friction coefficient	μ	0.35
Contact angle of the lower band	α	144°
Contact angle of the upper band	β	173°
Total contact angle	$\varphi = \alpha + \beta \left[{}^{\text{o}} \right]$ (2)	317°
Braking moment	$T = \frac{F_f \cdot D_t}{2} [\mathrm{N \cdot m}]$ (3)	363 000 N·m
The maximum force exerted at the end of the band	$S_i = \frac{2 \cdot T \cdot e^{\mu \cdot \varphi}}{\left(e^{\mu \cdot \varphi} - 1\right) \cdot D_f} [\mathrm{N}]$ (4)	504 967.23 N
The minimum force exerted at the end of the band	$S_d = \frac{2 \cdot T}{\left(e^{\mu \cdot \varphi} - 1\right) \cdot D_f} [\mathrm{N}]$ (5)	72 824.38 N

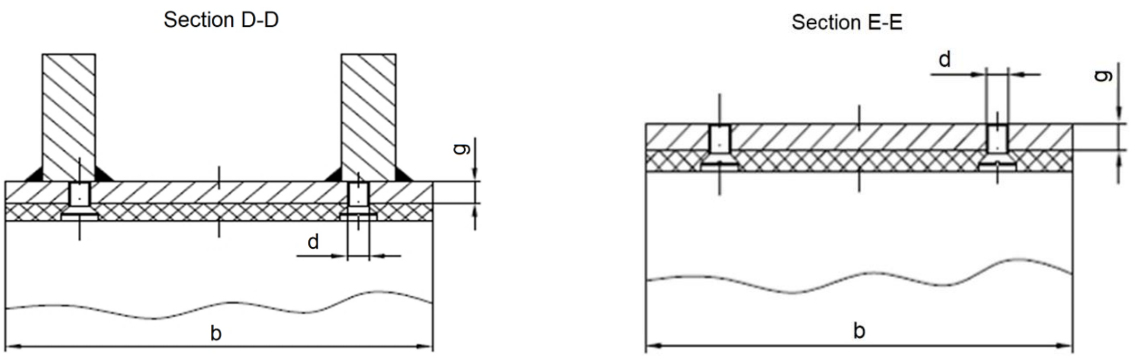

Fig. 5. *D-D* (a) and *E-E* (b) sections of the band brake [6,11,12]

Table 2: Calculation of band stretching in *D-D* and *E-E* sections [6, 11]

D-D section		
Parameters	**Symbol**	**Result**
Contact angle of the band in *D-D* section	$\varphi_x = \alpha + 151^{\circ}\left[{}^{\circ}\right]$ (6)	295°
Band braking force in *D-D* section (Euler)	$S_x = S_d \cdot e^{\mu \cdot \varphi_x}\left[\mathrm{N}\right]$ (7)	441 466.96 N
The number of holes in the band in *D-D* section	i	2
The diameter of the holes in the band	d	10 mm
The width of the metal band	b	200 mm
The yield stress of the band material	$R_{eH(S355J2)}$	345 N/mm²
Tensile safety factor	c	0.8
The thickness of the metal band	$g \geq \dfrac{S_x}{(b - i \cdot d) \cdot c \cdot R_{eH(S355J2)}}\left[\mathrm{mm}\right]$ (8)	8.89 mm
Selected thickness of the band	g	12 mm
E-E section		
Parameters	**Symbol**	**Result**
Contact angle of the band in *E-E* section	φ_{x_1}	124°
Band braking force in *E-E* section (Euler)	$S_{x_1} = S_d \cdot e^{\mu \cdot \varphi_{x_1}}\left[\mathrm{N}\right]$ (9)	155 325.61 N
Area of the *E-E* section	$A = b \cdot g - (i \cdot d)\left[\mathrm{mm}^2\right]$ (10)	2160 mm²
Tensile stress in *E-E* section	$\sigma_t = \dfrac{S_{x_1}}{A}\left[\dfrac{\mathrm{N}}{\mathrm{mm}^2}\right]$ (11)	71.91 N/mm²
Admissible stress	$\sigma_{at} \leq c \cdot R_{eH(S355J2)}\left[\dfrac{\mathrm{N}}{\mathrm{mm}^2}\right]$ (12)	276 N/mm²

A calculation of the welds was made which combines the lugs at the end of the band brake to it. The contact area between the weld and the metal band part of the band brake was defined and the shear stress generated in the weld area was calculated, which stress was compared with the admisible value. From Table 3, it can be seen that the calculated stress value is half of the allowable stress, which indicates a safe operation.

Table 3: Calculation of the weld between the metal band and the lugs of the strip [6, 11]

Parameters	**Symbol**	**Result**
The outer radius of the band	R_b	866 mm
The angle of the weld	φ_s	0.59 mm
Lug thickness	l_s	25 mm
Weld thickness	G_s	7 mm
The contact surface between the weld and the metal band in E-E section	$A = 2 \cdot (R_b \cdot \varphi_s \cdot G_s) + 2 \cdot (l_s \cdot G_s)\left[\mathrm{mm}^2\right]$ (13)	7 544.53 mm²
Calculated shear stress for one lug	$\tau_{t_s} = \dfrac{S_i}{A}\left[\dfrac{\mathrm{N}}{\mathrm{mm}^2}\right]$ (14)	66.93 N/mm²
Shear safety factor	c	0.35
Admisible shear stress	$\tau_{a_s} \leq c \cdot R_{eH(S355J2)}\left[\dfrac{\mathrm{N}}{\mathrm{mm}^2}\right]$ (15)	120.75 N/mm²

The entire brake system assembly has 10 bolts, each part having its established dimensions. In the paper, resistance calculations were performed for two of them. Thus, in Figure 6 and Table 4, bolt 7 is represented with the input data.

Table 4: Dimensioning of the bolt 7 [6, 11]

Parameters	Symbol	Result
Distance between bolt 7 and bolt 8	a	100 mm
Distance between bolt 7 and bolt 9	b	750 mm
Diameter of bolt 7	d_5	40 mm
The thickness of the lug of the stake	S_2	25 mm
Lever lug thickness	S_5	15 mm
The distance between the stake and the lever	δ	1.5 mm
The distance between the lugs of the lever	l_2	55 mm
The yield stress of the bolt material	$R_{eH(X20CrNi\ 17.2)}$	650 N/mm^2
Lever lug material yield stress	$R_{eH(S355J2)}$	345 N/mm^2
Bending safety factor	c	0.8

Calculations for bending, shearing and contact pressure of bolt 7 are shown in Table 5 and verification of the diameter of bolt 7 in bending, shearing and contact is shown in Figure 7. From calculations, values much lower than the admissible ones can be observed, resulting a good bolt sizing. Also, bolt 8 was subjected to bending, shearing and contact pressure stresses, as represented in Figure 8 and Table 6. It is observed that the diameters resulting from the calculations are smaller than the diameter chosen in the design.

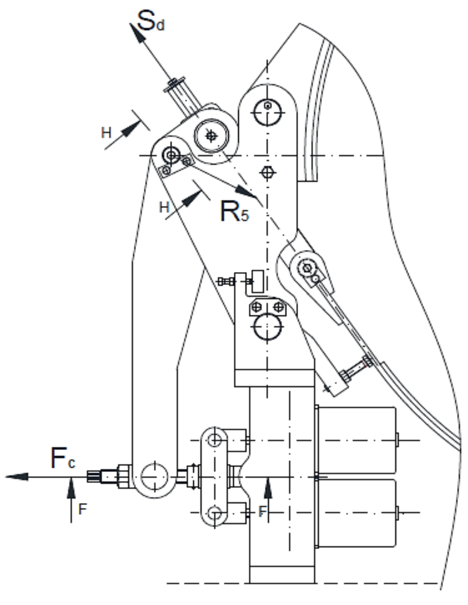

Fig. 6. Graphical representation of input data of bolt 7 [6, 11]

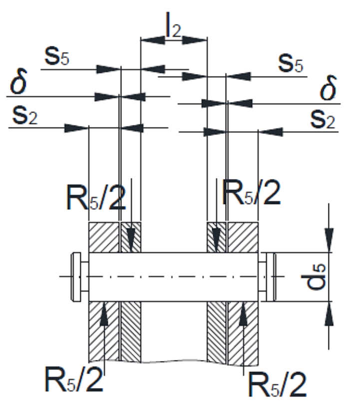

Fig. 7. Verification of diameter of bolt 7 in bending, shearing and contact [6, 11]

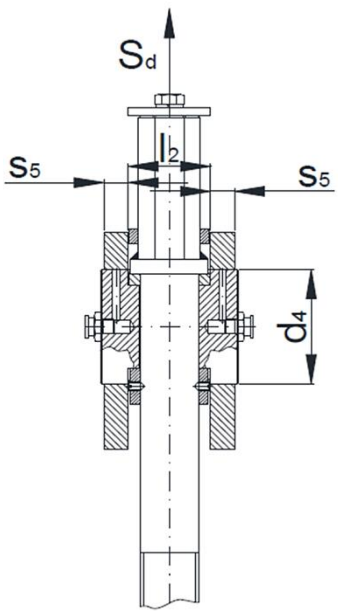

Fig. 8. Verification of diameter of bolt 8 in bending, shearing and contact [6, 11]

Table 5: Calculation of bending, shear and contact pressure of bolt 7 [6, 11]

Parameters	Symbol	Result
The force generated on the rod thread by the pneumatic system	$F_c = \frac{S_d \cdot a}{b} [\mathrm{N}]$ (16)	9 709.92 N
R_5 force felt in the bolt	$R_5 = \frac{F_c \cdot (a+b)}{a} [\mathrm{N}]$ (17)	82 534.29 N

Bolt bending moment	$M_{i_{max}} = \frac{R_5 \cdot (S_2 + S_5 + 2 \cdot \delta)}{4} \left[\frac{\mathrm{N}}{\mathrm{mm}^2}\right]$ (18)	887.24 N/mm²
Polar moment of inertia	W_p	12 566.37 mm³
Moment of inertia	W_z	6 283.19 mm³
Resulting bending stress	$\sigma_i = \frac{M_{i_{max}}}{W_z} \left[\mathrm{N/mm}^2\right]$ (19)	141.21 N/mm²
Admisible bending stress	$\sigma_{at} = c \cdot R_{eH(X\,20CrNi\,17.2)} \left[\frac{\mathrm{N}}{\mathrm{mm}^2}\right]$ (20)	520 N/mm²
Resulting bending stress	$\sigma_{ai} \leq \sigma_{at} = c \cdot R_{eH(X\,20CrNi\,17.2)} \left[\frac{\mathrm{N}}{\mathrm{mm}^2}\right]$ (21)	141.21 N/mm² ≤ 520 N/mm²
Bolt diameter resulting from shear stress	$d_5 \geq \sqrt{\frac{4 \cdot R_5}{\pi \cdot c \cdot R_{eH(X\,20CrNi\,17.2)}}} [\mathrm{mm}]$ (22)	21.49 mm
Diameter of the resulting bolt resulting from the contact pressure	$d_5 \geq \frac{R_5}{2 \cdot S_5 \cdot c \cdot R_{eH(S355J2)}} [\mathrm{mm}]$ (23)	9.97 mm
Minimum outer radius of lugs	$R \geq \frac{R_5}{4 \cdot S_5 \cdot c \cdot R_{eH(S355J2)}} + \frac{d_5}{2} [\mathrm{mm}]$ (24)	24.98 mm
The chosen radius of the lugs	R	45 mm

Table 6: Calculation of bending, shear and contact pressure of bolt 8 [6, 11]

Parameters	Symbol	Result
Lever lug thickness	S_5	15 mm
The distance between the lugs	l_2	55 mm
Bolt material yield stress	$R_{eH(X20CrNi\,17.2)}$	650 N/mm²
Lug material flow stress	$R_{eH(S355J2)}$	345 N/mm²
Bending safety factor	c	0.8
Admisible bending stress	$\sigma_{at} = 0.8 \cdot R_{eH(X\,20CrNi\,17.2)} \left[\frac{\mathrm{N}}{\mathrm{mm}^2}\right]$ (25)	520 N/mm²
Maximum bending moment	$M_{i_{max}} = \frac{S_d \cdot l_2}{4} [\mathrm{N \cdot m}]$ (26)	1 001 335.17 N·m
Dimensioning of the bolt according to the bending moment	$d_4 \geq \sqrt[3]{\frac{32 \cdot M_{i_{max}}}{\pi \cdot c \cdot R_{eH(X\,20CrNi\,17.2)}}} [\mathrm{mm}]$ (27)	26.97 mm
Shear safety factor	c	0.35
Bolt sizing as a function of shear stress	$d_4 \geq \sqrt[3]{\frac{4 \cdot S_d}{\pi \cdot c \cdot R_{eH(X\,20CrNi\,17.2)}}} [\mathrm{mm}]$ (28)	20.19 mm
Existing bolt diameter	d_4	75 mm
Safety factor at contact pressure	c	0.5
Admisible stress at contact pressure between bolt and lever	$\sigma_{at} = c \cdot R_{eH(S355J2)} \left[\frac{\mathrm{N}}{\mathrm{mm}^2}\right]$ (29)	172.5 N/mm²
Lever lug thickness resulting from contact pressure	$S_5 = \frac{S_d}{2 \cdot d_4 \cdot \sigma_{at}} [\mathrm{mm}]$ (30)	2.81 mm

Table 7 shows the calculation of the force generated at the level of the coils of the two M30 screws that join the lower band brake to the upper one in order to form the band brake subassembly.

Table 7: Strength calculation of M30 screws in the metal band joint area [6, 11]

Parameters	Symbol	Result
Contact angle of the upper band	φ_{x_2}	137º
Force between the bands	$S_{x_2} = S_d \cdot e^{\mu \cdot \varphi_{x_2}} [\mathrm{N}]$ (31)	168 163.40 N
Force applied to a screw	$F_{screw} = \frac{S_{x_2}}{2} [\mathrm{N}]$ (32)	84 081.70 N

Also, in table 8, the welds in the joining area of the two bands were calculated. It can be seen that the values resulting from the calculations are much lower than the admissible values, which indicates that the area will resist at the imposed stresses.

Table 8: Calculation of the weld of the joining area of the two bands [6, 11]

Parameters	Symbol	Result
The development angle of a weld	φ_2	15º
The lug thickness of the band joint	s_3	30 mm
Radius of the weld	X	866 mm
Weld thickness	a	7 mm
The contact surface between the weld and the brake bands	$A = 2 \cdot (X \cdot \varphi_2 \cdot a) + (S_3 \cdot a) \left[\mathrm{mm}^2\right]$ (33)	3 384.06 mm²
Shear stress in the weld zone	$\tau_{t_s} = \frac{S_{x_2}}{A} \left[\frac{\mathrm{N}}{\mathrm{mm}^2}\right]$ (34)	49.69 N/mm²
Shear safety factor	c	0.35
The yield stress of thejoint material	$R_{eH(S355J2)}$	345 N/mm²
Permissible shear stress	$\tau_f \le c \cdot R_{eH(S355J2)} \left[\frac{\mathrm{N}}{\mathrm{mm}^2}\right]$ (35)	120.75 N/mm²

2.2 Selection of the pneumatic actuation cylinder

The model of the chosen pneumatic cylinder is R5AHD, 5005 series, Figure 9, with the specifications shown in the table [8].

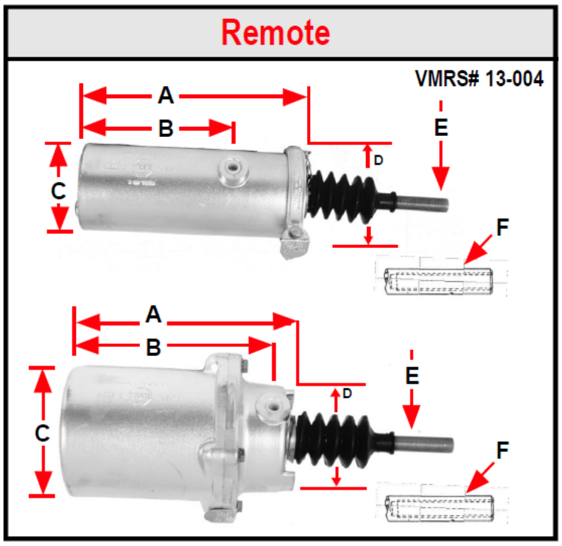

Series/ Model	5005/ R5AHD
Size	4
Stroke [inch]	4.37
20" rod	N/A
15" rod	5005012
7" rod	5005014
A [inches]	10.5
B [inches]	9.38
C [inches]	6.12
D [inches]	5.12
E [inches]	3/4" - 16UNF x 10.75"
F [inches]	1/2" - 20UNF x 3.00"
Inputs	3/8" - NPTF

Fig. 9. R5AHD-5005 pneumatic cylinder gauge dimensions and specifications [8]

The maximum developed force is calculated with the relation [9, 10]:

$$F = \frac{\pi \cdot d_{piston}^2}{4} \cdot p\,[\mathrm{N}]. \tag{2}$$

The pneumatic cylinder develops a maximum pressure, *p*, of *p=85* psi, equivalent to *0.586 Pa.* The diameter of the cylinder piston, d_{piston}, is d_{piston} = *155 mm*. After calculations, it follows:

$$F = \frac{\pi \cdot 155^2}{4} \cdot 0.586 = 11\,057.345\,\mathrm{N}. \tag{3}$$

The band brake is actuated by two cylinders mounted in parallel, the force required for braking being half of the combined load of the two cylinders.

3. FEM analysis of the braking system

Modeling of the band braking system was done using *Autodesk Inventor* software, Figure 10. Based on this modeling, finite element method (*FEM*) simulations were performed in *Ansys Workbench* program for both static and dynamic analysis.
The geometry of the system made in *Autodesk Inventor* was exported as a **.stp* file, followed to be imported into *Ansys Workbench* program [13,14,15,16,17,18].

Fig. 10. Graphical modeling of the pneumatic braking system for industrial winches

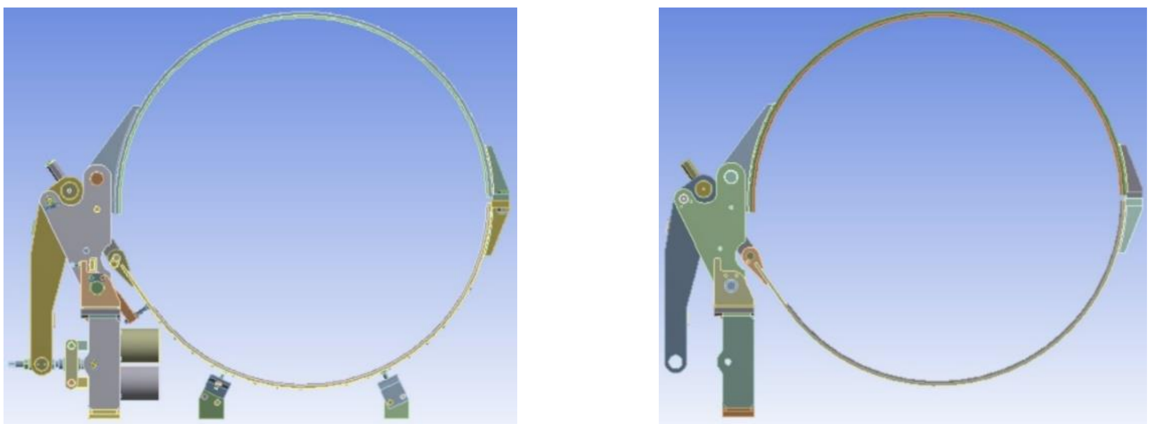

Fig. 11. Braking system imported into *Ansys Workbench*: original model (a) and simplified model (b)

The complex geometry of the band braking system has been simplified to be able to perform a static calculation under the conditions of an acceptable solid finite element discretization, Figure 11. Being a complex structure, the discretization was realized using the *Patch Conforming* method, setting the side of the element to 1 cm. Under these conditions, a network with 438.504 nodes and 259.891 elements was obtained. The *SOLID187* element [17] was used in discretization, Figure 12.

The steel used for the finite element calculation has the following mechanical properties [17]:

- Longitudinal Young's modulus, $E=2.1 \cdot 10^{11}$ [N/m^2];
- Poisson's ratio, $v=0.3$;
- Density, $\rho=7850$ [kg/m^3];
- Yield stress, $\sigma_Y=350$ [MPa].

The boundary conditions imposed on the system are connection type conditions, respectively loads and links type conditions. Due to the specifics of the system addressed, in addition to contact conditions, *Revolute-joint*, *body-body* and *body-ground* conditions were imposed. *Revolute-joint* and *body-body* conditions were applied to the assembly joints and the *body-ground* connection to the inner face of the band brake and simulates the contact between the drum and the band brake. The load is imposed by applying the braking moment in the *revolute body-ground joint*. Fixing the system is done on the lower face of the braking support, indicated by label *A*, Figure 13.

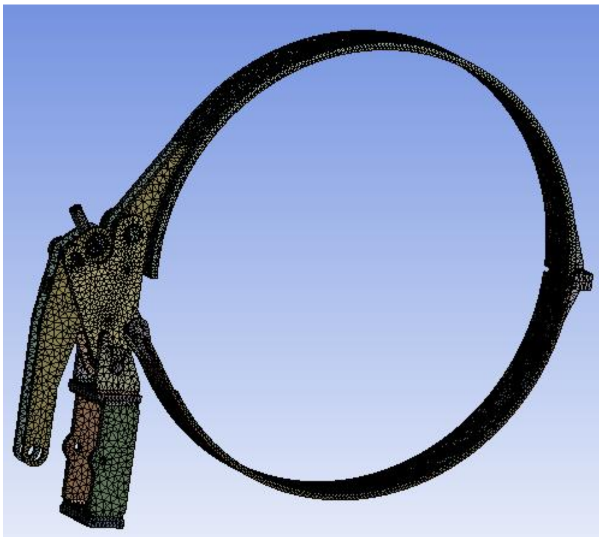

Fig. 12. Mesh of the system

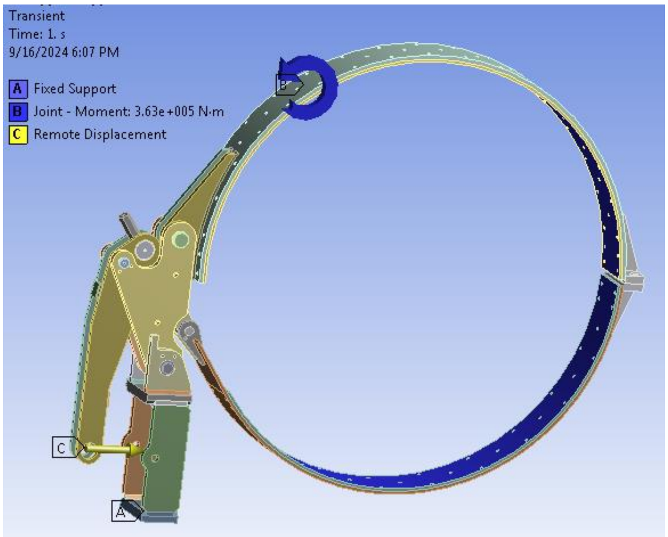

Fig. 13. Boundary conditions imposed to the system

The actuation of the braking lever is achieved by applying the *Remote Displacement* condition, which equates the action of the two pneumatic motors; the reaction in this connection is the very force necessary for the system's stationarity condition. The used material has linear properties and behavior but due to the large displacements and contact conditions as well as the *joint* conditions present, the solution requires a non-linear approach with increasing loading.

Figure 14 shows the von Mises stress distribution for the static analysis, with the maximum value concentrated in the weld seam of the braking support. It should be noted that the maximum stress does not exceed the flow value.

The distribution of the maximum shear stresses occurring in the structure is presented in Figure 15. A distribution similar to the von Mises stresses can be observed, the value being half of the maximum value of the stresses.

The distribution of total displacements is shown in Figure 16. The system is of an organological type, with small displacements and high stresses, the maximum displacement being the imposed one.

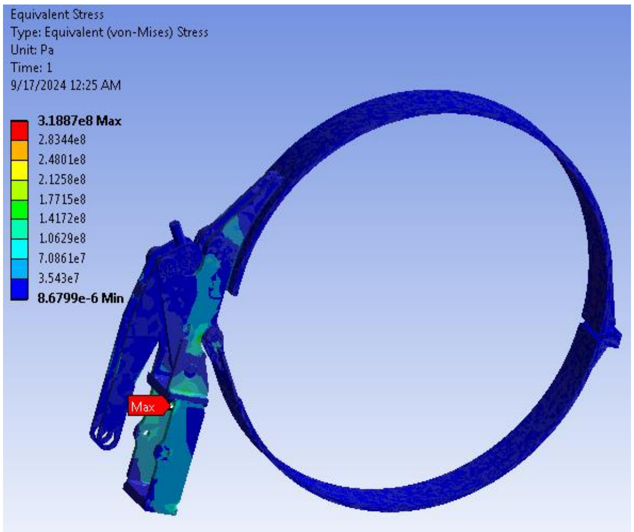

Fig. 14. Equivalent von Mises stress distribution

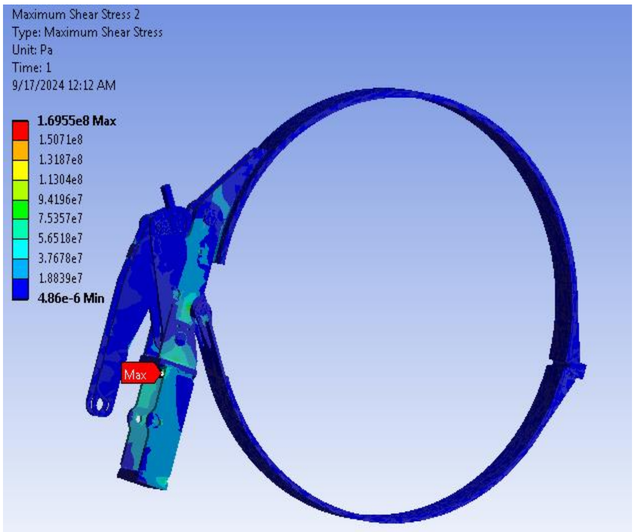

Fig. 15. Maximum shear stress distribution

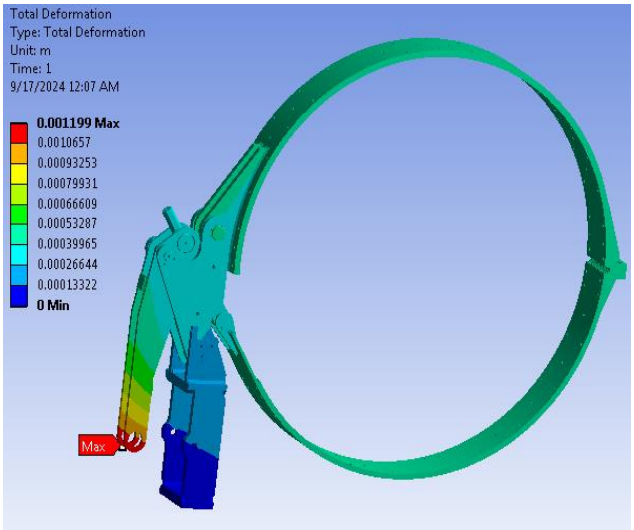

Fig. 16. Total displacement distribution

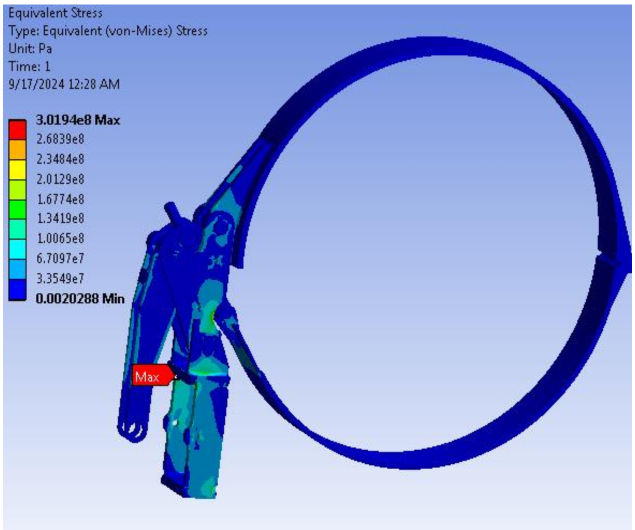

Fig. 17. Equivalent von Mises stress distribution

A global estimate of the stress state in relation to the yield stress of the material is achieved by the distribution of the safety factor over the entire system. The safety factor has values above 1 in the maximum von Mises stress zone, at the dynamic analysis, Figure 17.
The system works in stationary mode. As such, a static calculation is suitable for finite element strength analysis.
In the assumption of a shock actuation, the system is analyzed in dynamic mode, using the *Transient Structural* module of the *Ansys Workbench* program.
In order to make this calculation, a system braking time of 1 second was imposed, a condition that will introduce the phenomenon called ”*shock*” into the system.
The *Transient* module works differently from the *Static Structural* analysis module, the difference being the way to obtain the numerical solution. In the case of the *Static Structural* module, the values of displacements in each node are calculated at the same time, while in the *Transient Structural* module, the values of displacements, velocities and accelerations are calculated and transmitted from node to node, starting with the loading area. The von Mises stress distribution in the system, resulting from the dynamic calculation, is identical to that obtained from the static analysis, Figure 17, the only significant difference being the decrease of the maximum stress by about 20 MPa.

The previously mentioned notion of ”*shock*” is expressed by a sudden increase in the accelerations concentrated in the actuation area of the pneumatic cylinders, followed by a rapid decrease to 0 and a uniform distribution in the system.
Figure 18 shows the distributions of the accelerations at the time of actuation of the pneumatic cylinders (the moment of the shock) and the distribution at the end of the analysis.

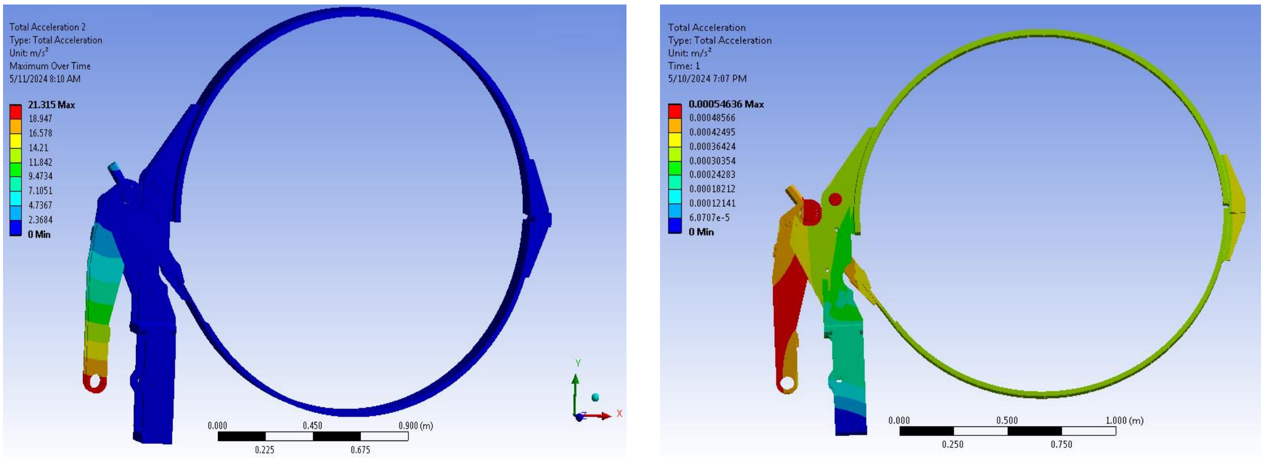

a. b.

Fig. 18. The distribution of accelerations at the time of actuation of the pneumatic cylinders (a) and at the end of the dynamic analysis (b)

The appropriate results of the two types of analysis indicate that a static analysis is sufficient to obtain a suitable solution from the point of view of strength calculation.
The value of the initial accelerations, as shown in Figure 18.a, is about 22 m/s^2, a very high and dangerous value for a long operation of the system. However, the system operates around this value for a short period of time, as previously shown; in the case of long-term operation of the system around this value, a very high wear rate results, leading to a destruction of the braking system in a short period of time.
The von Mises stresses, whose distribution is shown in Figure 14 for static calculation and Figure 17 for dynamic calculation, show values of about 319 MPa and 301 MPa. These values are below the flow level of the material from which the parts are made, which indicates a good exploitation of the entire system. Therefore, these factors lead to high reliability.
It can be seen that the von Mises stress concentration zone is located around the brake support, which is imposed by the designer because this part has a simple and very robust geometry and is also welded directly to the shipboard to allow unloading of the whole system in the ship in order to dissipate the tensions.
From the value of the shear stresses shown in Figure 15 (about 170 MPa), a value that is much lower than that of the von Mises stresses, it is understood that the system does not present danger zones from the point of view of these types of stresses.

4. Conclusions

In the paper, a study was presented regarding the band braking system in the structure of industrial winches. Aspects related to the modeling of the band braking system in *Autodesk Inventor* program were presented, as well as the way to transfer this model to the finite element analysis - *Ansys Workbench* program. The results of the analysis were presented as distributions of displacements and maximum von Mises stresses, maximum shear stresses, including the static safety factor (established in relation to the yield stress of the material).
In addition to the static analysis, a dynamic analysis was also performed when the braking system was actuated for 1s.

The results of this analysis justify performing only a static calculation, because the stress level in the two simulations (static - with *Static Structural* module and dynamic - with the *Transient Structural* module) is the same.
Analytical calculations were also realized for the most important connections in the band brake structure starting from the moment to be overcome at the actuation forces from the pneumatic cylinders. Analysis of the state of stresses and strains in the deterministic approach (with material properties and fixed value loads) for organological structures reveals small displacements and strains, but high stresses, often close to the yield stress of the material. For such systems, static analysis using the finite element method can provide a global assessment of the stress and strain state. The band brake studied in *Ansys Workbench* program, which represents a complex system, includes specific connection elements (*joint* type) and contact conditions that require the calculation with finite elements in large displacements (non-linear calculation, even if the mechanical properties of the material are considered in the linear-elastic domain).

References

[1] Kisiel, M., D. Szpica, J. Czaban, and H. Köten. ”Pneumatic brake valves used in vehicle trailers - A review.” *Eng. Fail. Analysis* 158 (2024): 107942.
[2] Wang, X., D. Geng, L. Zhang, W. Xu, H. Peng, and G. Sun. ”Structure and function experiment of pneumatic ring brake.” Paper presented at the 2021 International Conference on Mechanical Design (2021 ICMD), Changsha, China, August 11-13, 2021. *Mechanisms and Machine Science* 111 - Advances in Mechanical Design (2022): 881-890.
[3] Knott. “Band brake systems & solutions”. Accessed September 17, 2024. https://knottbrake.com/categories/band-brakes.
[4] SEA HydroSystems. “The role of hydraulic brakes in modern heavy machinery”. May 30, 2024. Accessed September 16, 2024. https://seahydrosys.com/heavy-machinery-hydraulic-brakes-guide.
[5] Alterous. “Band brakes”. Accessed September 17, 2024. https://www.alterous.com/products/industrial-applications/brakes/band-brakes.
[6] DMT Marine Equipment. Products. Accessed September 17, 2024. https://www.dmt-winches.com.
[7] EMCÉ Winches. “Winch calculation”. Accessed September 20, 2024. https://emce.com/about-winches/winch%20calculation.
[8] FindItParts. Brake system service. Accessed September 17, 2024. https://www.finditparts.com/products/394230/mgm-5004013.
[9] Baroiu, N., and G.A. Moroșanu. *Hydraulic Drive Systems/Sisteme de acționare hidraulică*. Galati, Academica Publishing House, ISBN 978-606-606-011-0, 2022.
[10] Teodor, V.G., V. Păunoiu, N. Baroiu, and F. Susac. “Optimization of the measurement path for the car body parts inspection” *Measurement* 146 (2019):15-23.
[11] Beznea, E.F. *Material strength. Simple loads. Problems and tests/Rezistența materialelor. Solicitări simple. Probleme și teste*. Galati, Galati University Press, 2018.
[12] Iglesias-Baniela, S., and J.M. Pérez-Canosa. ”Spring-loaded winch band brakes as tools to improve safety during mooring operations on ships.” *The International Journal on Marine Navigation and Safety of Sea Transportation* 14, no. 3: (2020): 711-719.
[13] Autodesk. Products. Accessed September 17, 2024. https://www.autodesk.com.
[14] Moroşanu, G.A., N. Baroiu, V.G. Teodor, V. Păunoiu, and N. Oancea. ”Review on study methods for reciprocally enwrapping surfaces.” *Inventions* 7, no. 1 (2022): 10.
[15] Baroiu, N., G.A. Moroșanu, V.G. Teodor, and N. Oancea. ”Roller profiling for generating the screw of a pump with progressive cavities.” *Inventions* 6, no. 2 (2021): 34.
[16] Teodor, V.G., N. Baroiu, and F. Susac. *The synthesis of new algorithms for CAD profiling of cutting tools*. Saarbrücken, Lambert Academic Publishing, ISBN 978-613-7-08923-1, 2018.
[17] Ansys. Products. Accessed September 17, 2024. https://www.ansys.com/products/ansys-workbench.
[18] Belabend, S., V. Păunoiu, N. Baroiu, R. Khelif, and I. Iacob. ”Static structural analysis analytical and numerical of ball bearings.” Paper presented at the 6th International Conference on Advanced Manufacturing Engineering and Technologies - NEWTECH 2020, Galati, Romania, September 9-11, 2020. *IOP Conference Series: Materials Science and Engineering* 968 (2020): 012026.

ISSN 1454 - 8003
Proceedings of 2024 International Conference on Hydraulics and Pneumatics - HERVEX
November 13-15, Băile Govora, Romania

WATER RUNNING ENGINE

Nicușor NICULAE[1]

[1] National Institute for Research and Development for Land Improvements, Bucharest, Romania (INCDIF-„ISPIF"), bcdispif@gmail.com

Abstract: *The present paper relates to a mechanism which can produce additional mechanical work by recirculation a quantity of water or other heavy and incompressible fluid. The mechanism is similar to the thermal engine because the mechanical work is obtained from the rectilinear - alternative stroke of a floating body with a very low density in relation to the density of water. The mechanism is complex being made up of many mechanical elements of connection and maintenance of the operating cycle. These mechanical elements are: levers, rods, taps, connecting hoses etc. However, its most important components are a water tank with a floating body inside and a water exhaust pump. The exhaust pump is positioned in the immediate vicinity of the tank, below its lower surface and together with the tank are fixed on a general frame of the mechanism. The tank is provided to have from construction, inside, some rollers arranged obliquely on certain generators equidistant at a certain number of degrees between them. The floating body being cylindrical like the tank, will have a spiral on the outer surface, spiral that must be in constant contact with the rollers so that it is imprinted to the floating body and a rotational movement in addition to the movement simple of ascension. This constructive solution was used so that when the water level rises in the tank, the floating body rotates, at the same time, obtaining an additional force from the floating body stroke compared to the simple Archimedes force. In this way the floating body also works as a force multiplier.*
This mechanism has, like the thermal engine, an operating cycle:
Time 1 - filling the tank with water;
Time 2 - emptying the water from the tank into the exhaust pump;
Time 3 - pumping water from inside the exhaust pump outside.
The water engine is not designed to be powered by any external power source (electrical mains) or to be powered by fuel, it operates only the basis of mechanical work obtained from the stroke of the floating body.
Can be used as engine as well as pump, as follows:
1. In case of use as an engine, the ballast or springs equipping the exhaust pump need to be calculated so that drain pump creates a pressure on the water inside the pump body only to pump water to the upper level of the tank, to benefit from a greater mechanical work.
2. When used as a pump, the weight or springs need to develop a maximum force on the water inside the pump, so that the pump can pump water to a height as high as possible.
The benefits of this mechanism can be anticipated, like as:
- zero pollution;
- low production costs compared to the thermal engines, because most of its components can be made of plastic and not metal as in the case of the thermal engine;
- can be a solution to the current and future energy crisis, or the crisis of non-renewable resources.

Keywords: *Cylindrical water tank, floating body, exhaust pump.*

1. Introduction

This paper is aimed to the engineers and physicists whose object of activity is the study of mechanism and devices that work with water or other heavy and incompressible fluids (the name of the field in the university environment being fluid mechanics and hydraulic machines), as well as other persons possessing solid knowledge of mathematic, physics and mechanic.
This paper presents the necessary and sufficient details to be making an engine mechanism what consists as main parts from a cylindrical water tank 20 (Figure 2) with a floating body 21 (Figure 2), also cylindrical, inside and an exhaust pump with flexible membrane 27 (Figure 2), pump situated next to the tank and positioned below its lower surface.
The exhaust pump with flexible membrane, of the water, exhaust carried out after filling the tank with water at the capacity allowed by the floating body inside it, works driven by the elastic force of some

springs 5 (Figure 2) or by a weight/ballast. The connection between the tank with the floating body inside it and the exhaust pump with the flexible membrane located next of the tank, will be assuring by a lever 28 (Figure 2), another component of the mechanism. This mechanism is complex, consisting of many other mechanical elements for connecting and maintaining movement and performing an operating cycle, such as: mechanically controlled taps, tensioning and supporting parts springs, in the tensioning position, parts for printing a rotational movement of the floating body inside the tank etc.
The usefulness of this engine mechanism is only predictable, it being an engine not yet realized and consequently untested. It is expected to be able to operate near all courses and accumulations of water if it is intended to function as a pump for pumping water. In this case, it can convert the hydrostatic pressure, from a certain depth of a water source, into pressure inside the exhaust pump with flexible membrane, pressure necessary to pump water to the exhaust.
If this engine mechanism is to function as an engine, like existing engines known and studied today (the thermal engine and the electric engine), it can produce the mechanical work by recirculating a quantity of water or other heavy and incompressible fluid.
The mechanism works in locations located below the water source and as an operating condition would be that the free surface of the water (FSW) in the water source is at the upper part of the floating body inside the tank, in the relaxed state of the mechanical system (then when the floating body inside the tank is at the bottom).
The mechanism works like the thermal engine based on a stroke and a force.
As is known, a body immersed in a liquid (water) is pushed from the bottom up with an Archimedes force. Suppose we have a cylindrical-shaped body with a determined volume of 1 m^3. If we determine that his height is 2 m, it follows that the radius of his base should be 0,4 m. If we push this body into a water accumulation, up to half, assuming it has a very small weight, it follows that we will perform a mechanical work on it: MW=500 kgfx1m. This fact in physics is called action. If we position this floating body in a water tank located in the immediate vicinity of a water source and located below the level of the free surface of the water in the water source, and we open a tap that connects the water in the water source with the tank, the level the water in the tank increases, the floating body inside the tank is pushed vertically upwards. A floating body race is thus obtained, called in physical reaction (reaction of the opening of the tap and subsequently of the increase of the water level inside the tank). Based on this fact the water engine works.
One might ask a legitimate question: why not push this floating body more or less into water? What would be the problem?
Answer: as long as the mechanism of the water engine exploits the reaction, namely the mechanical work done by the floating body resulting from rising the water level in the tank, if we push the floating body more than half (or completely) into the water, we could not benefit from the stroke of the floating body. If on contrary, we do not push this floating body into the water at all, we would the maximum stroke but not and the force. Therefore, only in the situation of, up to half, the maximum mechanical work can be getting. This will also result in the physical explanation of the process, namely that during the filling of the tank with water it is as we are pushing the floating body into the accumulation of water.
Suppose this floating body also has its own weight of about 10 kgf, it follows that we will perform for his a mechanical work of 490 kgfx1m to push his into the water to the middle of its height, vertically. It is obvious that this stroke and force have nothing to do with the principles of thermodynamics.
We will put this floating body in a water tank, which will have the shape almost identical to the floating body, being both cylindrical, between them being a very small space. The floating body can be made of plastic material and will have from construction practiced on the side surface a helix 37 (Figure 1) surrounding this lateral surface of it, in the form of thread.
The water tank will have inside, on several generators arranged at equal angles to each other on the circumference (for example, for 2 generators they will be arranged 180^o between them and for 3 generators they will be arranged 120^o between them) some rollers 41 (Figure 1) from place to place, at equal distances from each other on height, these rollers will be in contact with the helix made on

the side surface of the cylinder so that, when is moving the floating body inside the tank, will be imprinted it with a rotational movement in around own vertical axis.
The floating body will thus also work as a force multiplier, compared to the simple ascending Archimedes force (of 490 kgf in our case) This will result in an Archimedes force superior to the simple force, the force that will be called in continuation, the complementary Archimedes force (CAF), for abbreviation.
The floating body will have inside positioned in its center, vertically, to be able to be assembled in it a constructive element type: Mechanism of Screw Steering and Ball Oscillating Nut. This mechanism is known at the stage of the technique and is use because it has very small running rubbings in utilization. It will be termed the SDMON (screw drive mechanism and oscillating nut) for abbreviation. The oscillating nut 35 (Figure 1) of this mechanism will be stiff fixed with the floating body at the top of it. The screw of this mechanism (the worm axle 17 (Figure 1)) will have the pitch of the helix inversely to the pitch of the helix surrounding the floating body (if suppose that the pitch of the floating body´s helix is on the right, the pitch of the worm axle will be on left, or vice versa). We have resort to this SDOMN mechanism because by rotating the floating body inside the tank, the amplification and of the stroke to be getting, as will be seen below. This mechanism (SDMON) will work as a stroke multiplier. Since the floating body rotates in operation the axle 17 must be secured against rotation, this condition can be fulfilled by a special construction of the upper extremity of the axle and the right extremity of the lever 28 with which this axle comes into contact (This construction of the two extremities can be seen in Figure 4).
The set of these parts is shown in Figure 1.

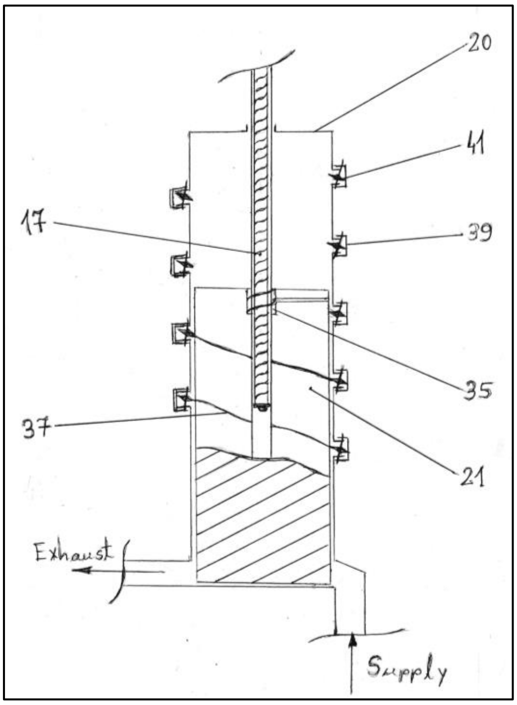

Fig. 1. Ensemble: water tank, floating body

2. Operating cycle times and displacements of parts in relative motion during those times

The engine mechanism components with the three periods of the working times cycle and the mechanical components in the movements at the strokes ends (the cinematic scheme), will be presented below. Let consider that mechanism carries out a full operating cycle during the time T_1-T_2 and the little intervals of times T_1-t_1; t_1-t_2; t_2-T_2. At the initial time, during T_1, the mechanism shows as in Figure 2.

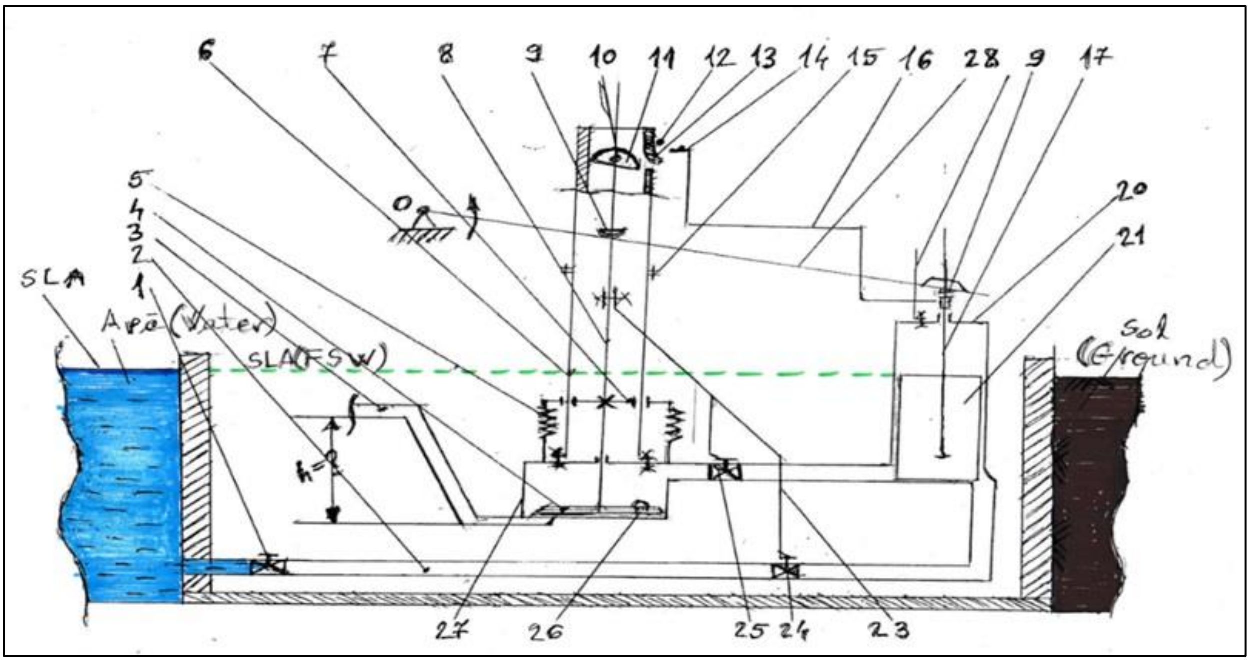

Fig. 2. Position of the component parts at the initial moment T_1

The operating time T_1-t_1 (water tank filling) shown in Figure 3. During this time functioning we have main production of mechanical work, obtained from the stroke of the floating body and therefore will be called during this work, and main active stroke (MAS) for abbreviation. We open the tap 1, supply of the tank, the water from the accumulation, according to the principle of communicating vessels, penetrates into the tank 20 through the supply pipe 2. During this time, the tap 24 is opened and the tap 25 is closed (these taps are mechanically controlled but can also be of another type), thus the water level in the tank, by connecting with the water source, increases. Inside the tank, the floating body 21 is lifting by CAF. This force will act on the right-hand extremity of lever 28, by worm of the axle of the SDMON mechanism, which is assure against rotation to realize its „effect" for which it is assembled there (as in Figure 4). We will therefore, have on this stroke, a mechanical work of the complementary Archimedes force (CAF) on the height of approximately 3m (2m from the stroke of the worm axle inside the floating body, this stroke will depend on the pitch of the worm axle to be in a certain relation to the pitch of the helix that surrounding the floating body+1m from the stroke floating body. Following this floating body stroke will put on moving the following components of the mechanism: lever 28 rotates in a trigonometric sense around the „O" joint, is moving through this lever also the taps control rod 23, the support 7 of the springs, the exhaust pump piston 4 and its rod 8, as well as the lever 16. Lever weight can be reduced by using a counterweight placed on lever, in the side left of the joint „O". The main force needed during this operating time, however, is the tensioning force of the exhaust pump springs or the lifting of the weight (in the case of the use of the exhaust pump with ballast). It also results from this displacement of the floating body: the rod 8 is lifting by means of the nut on it (the nut with hemispherical head to better taking over the arc of the circle described by lever 28 in operation). This springs 5 are tensioning by means of rod 8 and of the support of the springs 7. Also here, the ratchet with symmetrical double end and torsion spring 11, located at the end of the rod 8 and articulated with it by the bolt 10, moves upwards, until it comes out inside the pipe 6 where, after out, due to the spring of torsion (which is not represented in the Figure 3, being in the back) is brought in the horizontal position, to block the return of the rod 8. During this time T_1-t_1 will also occur the liberation of mechanical work, which will be capturing by another type of mechanism compared to the connecting rod-crank mechanism of the thermal engine. During this time, at the upper point, thanks to the ratchet 11 and the rod 8, which is fixing the springs support 7, the springs 5 remains tense. The plunger 4 of the exhaust pump, which is fixing with rod

8, remains at the top of the pump. The control arm 23 of the taps closes the tap 24 after the tank 20 has filled with water, interrupting the connection of the mechanism to the water source, and opens the tap 25, allowing the water in the tank to empty into the exhaust pump.

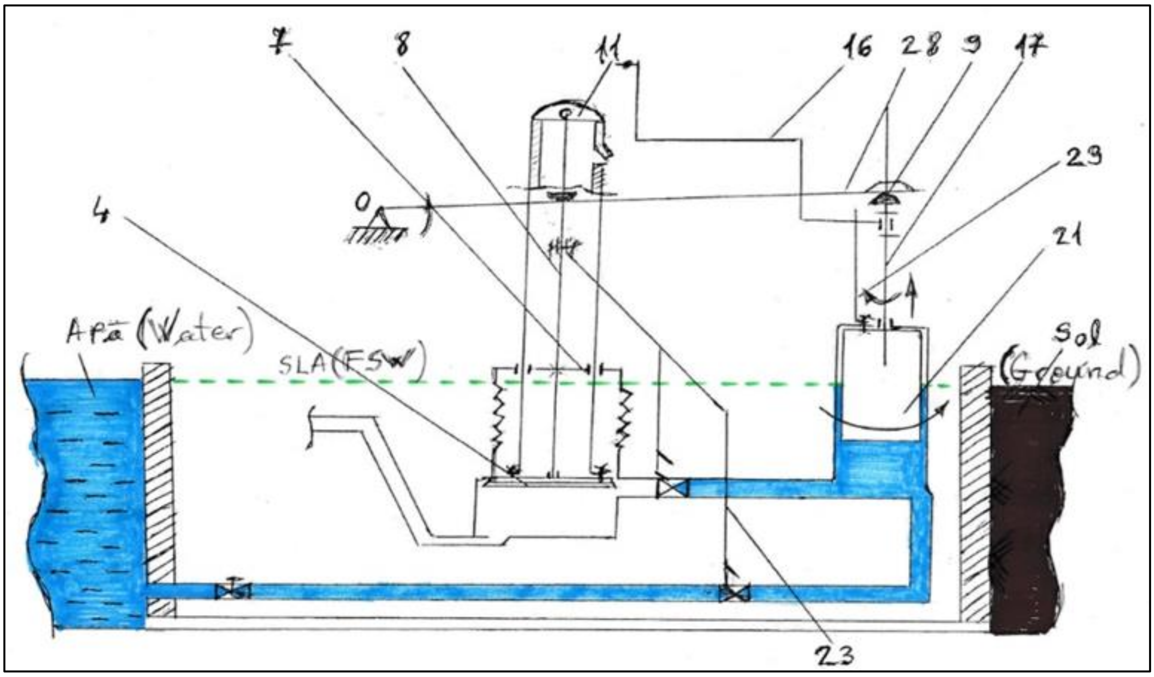

Fig. 3. Water tank filling

The operating time t_1-t_2 (empting water from the tank into the exhaust pump) shown in Figure 5. During this time the water from the tank drains into body of the exhaust pump, the tank is empting. The floating body descends at the same time as the water level in the tank decreases (under the action of its own weight of 10Kgf), the rod 17 also descends (this working time is the only and total inefficient of the water operating cycle).

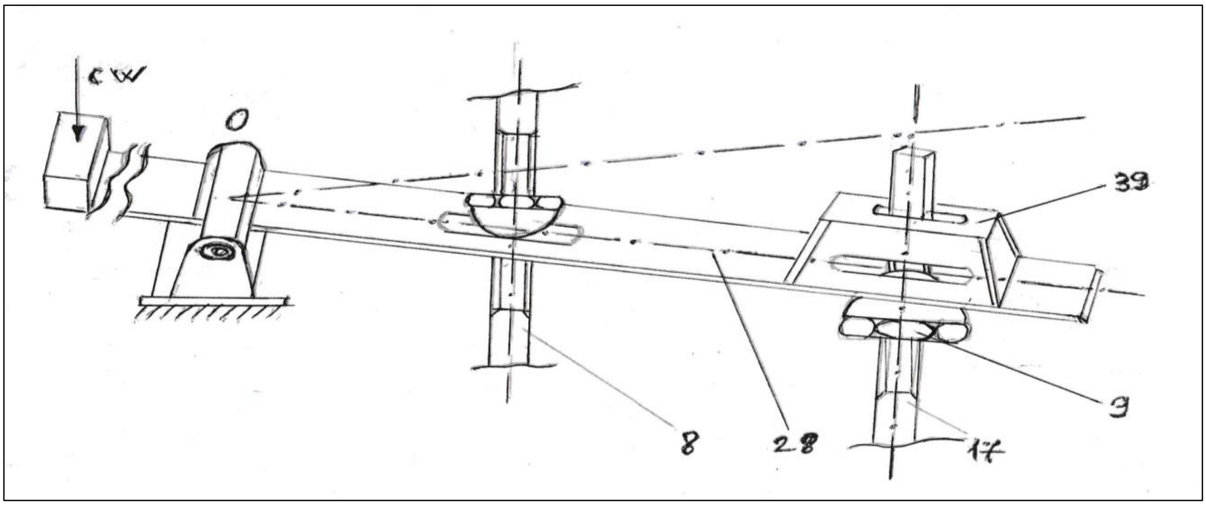

Fig. 4. The lever 28

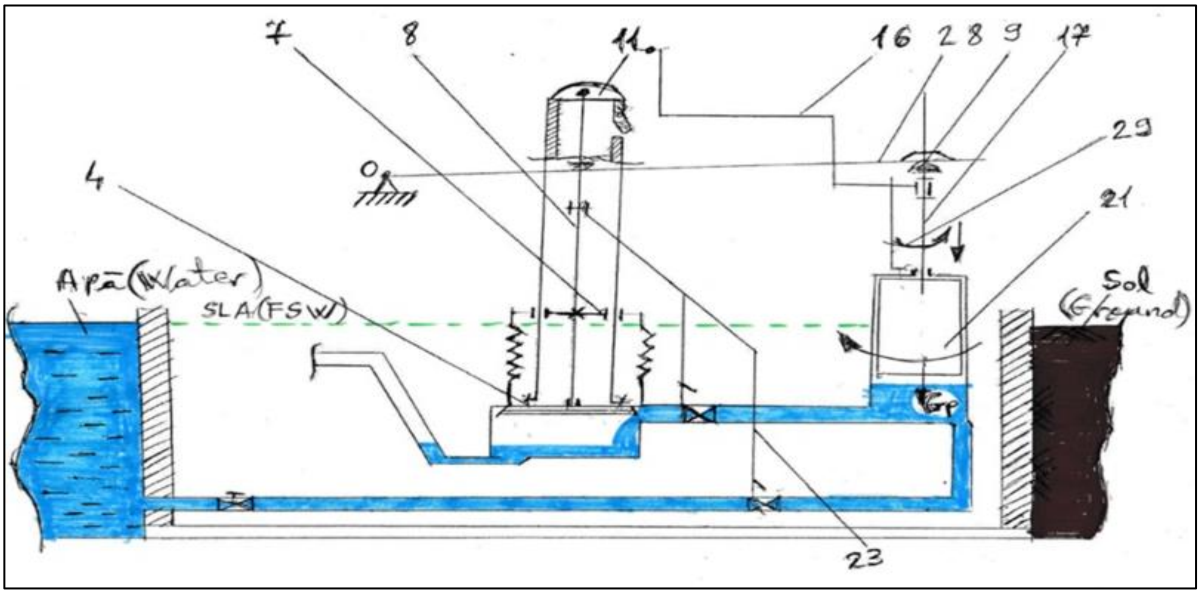

Fig. 5. Empting water from the tank into the exhaust pump

The operating time t_2-T_2 (pumping water from the exhaust pump) shown in Figure 6.
The arm 16 touches at the end of the floating body stroke at the bottom (that descend) the piece 13 that rotate clockwise and unlock the ratchet 11. Unlocking rod 8 release the springs 5 and so resulting the water compressing from the exhaust pump 27, water that is discharged at height „h" (we will see what condition must be imposing to drain it back into the water source) through pipe 3. At the bottom end of rod 8, through the control arm 23, the tap 24 is opening and the tap 25 is closing, thus resuming the operating cycle. It should be noted here that in the drawings in Figures 3, 5, and 6 representing the operating cycle times were numbered only the pieces that are moving during that time, in order to better understand the operation of the mechanism.

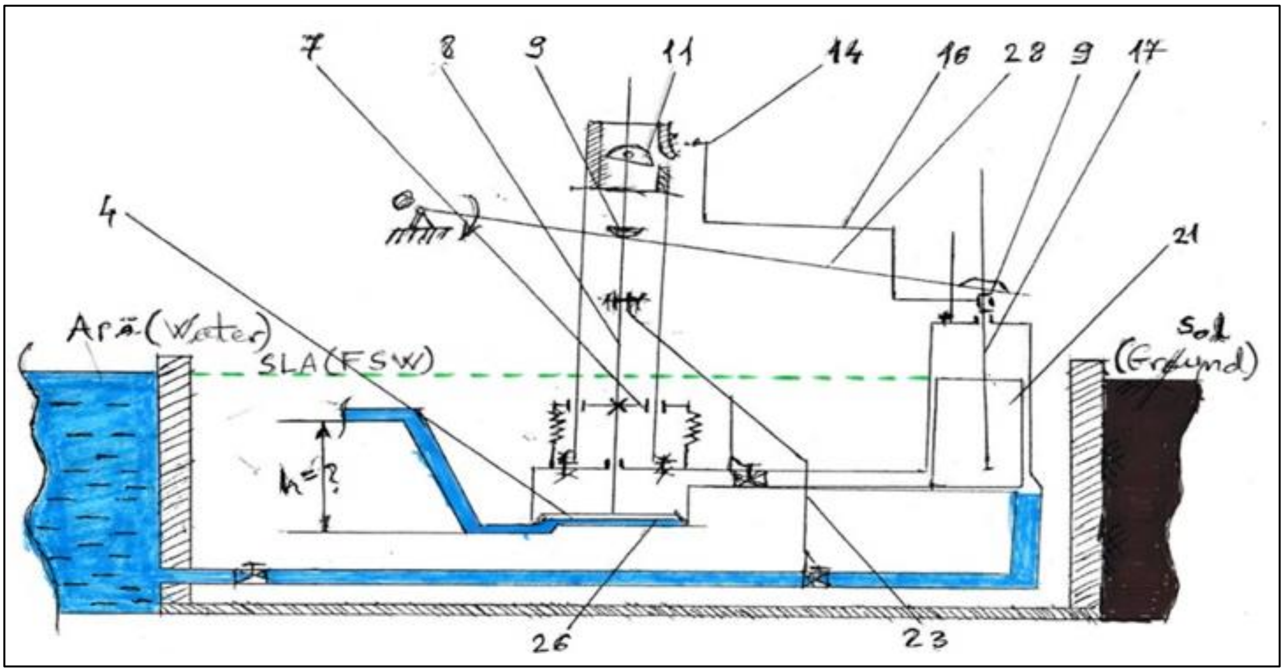

Fig. 6. Pumping water from the exhaust pump

3. Balance of mechanical work during an operating cycle

Because was presented in the description as an engine-mechanism, the following observation shall be required:
The main question is: will he be able to take water back to the water source? (perpetuum mobile function). Let us walk in the different work times, described in the functioning cycle (the three) vertically, with the forces and the strokes we have, comparing them to the free surface of the water (FSW).
- During T_1-t_1 we have the mechanical work obtained: MW=CAFx3m (1m the floating body stroke+2m the floating body axle stroke) above FSW;
- During t_1-t_2 we have a loss of mechanical work of 500kgf (the volume of water dislocated by the floating body, when we push it into the water up into half and which we initially find inside the tank, then inside the exhaust pump) at a depth of about 0,3 or 0,4m (depending on what the exhaust pump will look like)=floating body height of 2m, i.e. 2,3 or 2,4m;
- During t_2-T_2 we will need a mechanical work (performed by the exhaust pump) of 500kgfx2,4m (let take the worst variant) to get water back into the water source.
The resulting inequality will be: the mechanical work during T_2-t_2 time>the mechanical work during t_2-T_2 time, in our case : CAFx3m>500kgfx2,4m.
But CAF cannot be less 500kgf because it is a force multiplier.
It results only the multiplication of the stroke we have the mechanical work necessary to bring/pump water to a high height than FSW, mechanical work available throughout out the length of the lever 28. The CAF will be depending on the pitch of the helix on the lateral surface of the floating body (smaller pitch-higher CAF).
In order to better understand the operation of the mechanism let see a scheme of operation of the taps of the mechanism.
We will use the following symbols:
W.S. – water source;
W.T. – water tank (the tank with the floating body inside);
E.P. – exhaust pump;
T1 – the coupling tap between W.S. and W.T.;
T2 – the coupling tap between W.T. and E.P.
Cycle times:
t_1 – filling water tank (W.T.) with water;
t_2 – exhaust W.T. in E.P.;
t_3 – pumping water out from E.P.
In times t_1, t_2, t_3 we have the position of taps T1, T2:
t_1 – T1 opened, T2 closed;
t_2 – T1 closed, T2 opened;
t_3 – T1 opened, T2 closed = t_1.
This also results in the cycle of the operation of the mechanism.

4. Physical-mathematical calculation model for the sizing of the main components of the mechanism (the exhaust pump respectively the tank with the floating body)

In order for the mechanism to become functional, it is necessary that the design service involved in calculating the dimensions of the component parts takes into account the observance of certain rules, dimensions and formulas in geometry.
Next I will develop this topic, namely what relationships need to be respected between: height h_1 of the floating body (21), radius of the base of the floating body r_1, stroke of the axle (17) of the floating body h_3, stroke of the rod (8) of the exhaust pump h_2, length l of the lever (28) for taking over mechanical work, radius of the base of the cylinder of the exhaust pump r_2, distance from joint „O" to rod (8) of the exhaust pump on the horizontal (quota „b" in Figure 7).
I will use Figure 7 for this example.

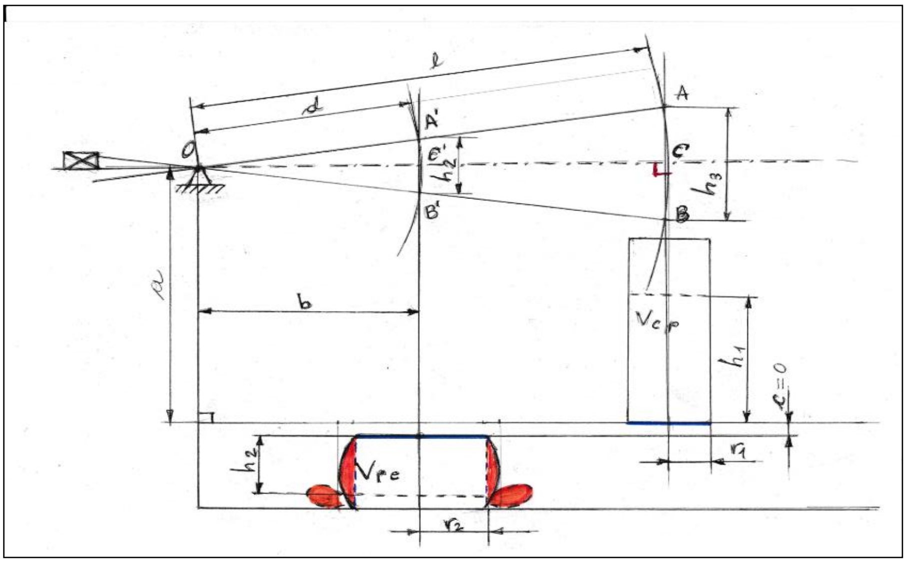

Fig. 7. Geometric model for calculating the dimensions of the main component parts

Figure 7 shows the geometric place of lever (28) in operation as well as where it comes into contact with the axis of the floating body (17) and the piston rod (8) of the exhaust pump.
There needs to be a correlation between the volume of the floating body, the volume of the exhaust pump, the distance between the vertical of joint „O" and the vertical of the center of the exhaust pump (quota „b"). I will continue to provide these relationships with the help of geometry (the only mandatory quota that must be respected regardless of the scale at which the mechanism will be made and the values of the dimensions of the other pieces and quotas (r_1, h_1, r_2, h_2, h_3, l) is the quota „c" that must have the value 0, as seen in Figure 7, if this quota had a numerical value it follows that the exhaust pump should perform a bigger mechanical work.
As we have established from the beginning, an essential condition for the operation of the mechanism is that the volume of the floating body is twice the volume of the exhaust pump.
This result in a first relationship:

$$V_{fb} = V_{ep} \tag{1}$$

These two bodies are cylindrical in shape.
The volume of the cylinder is:

$$V = \pi r^2 h \tag{2}$$

where:

r - radius of the base of the cylinder and
h - is this height.

Let`s note with:

r_1 - radius of the base of the cylinder of the floating body;
h_1 - height of the cylinder of the floating body;
r_2 - radius of the base of the exhaust pump;
h_2 - height of the cylinder of the exhaust pump.

From formula (1) result:

$$\pi r_1^2 h_1 = 2\pi r_2^2 h_2 \tag{3}$$

After simplifying by π the relationship becomes:

$$r_1^2 h_1 = 2 r_2^2 h_2 \tag{4}$$

So results in a first relationship (1) that must be respected.
Figure 7 shows: the lever 28 moves around the „O” joint describing an arc of circle, on the stroke between points A and B of the axis (17) of the floating body. This triangle can be isosceles by adjusting the dimension „a” in Figure 7 (in fact, this quota and many other dimensions can be determined by the adjustment possibilities can you see in the photo with the mock-up that you find at the end of this article).
One solution for this triangle to be isosceles is as follows:

- an h_3 value is chosen for the stroke of the floating body (which is depending on the floating body construction and whether or not a stroke multiplier is chosen - in this case let's assume it is with a stroke multiplier);
- on the axis of the floating body we determine the half of h_3 (point „C");
- from this point „C” we draw a horizontal with a help of a square and determine at what point this horizontal meets the vertical of the joint „O”;
- then adjust the quota „a” according to Figure 7 so that the angle OCB is 90°.

After making this adjustment, so that this OAB triangle is isosceles, we are also interested in positioning the exhaust pump on the right side of the „O” joint (distance between the vertical of the „O” joint and the vertical of the center of the exhaust pump cylinder - „b” quota).
It follows, from Figure 7, points A'B' between the piston rod (8) of the exhaust pump and lever (28).
It will result in alike triangles:
$\Delta OAB \sim \Delta OA'B'$, where:

AB - represents the stroke of the axle 17 of the floating body (noted in Figure 7 by h_3);
A'B' - represents the stroke of the piston rod of the exhaust pump (noted in Figure 7 with h_2).
From the alike of the triangles OAB and OA'B' result:

$$\frac{OA}{OA'} = \frac{OB}{OB'} = \frac{AB}{A'B'} \tag{5}$$

But in the isosceles triangle OAB we have OA=OB - lever length (28).
In the isosceles triangle OA'B' we have OA'=OB' - another equal numerical value, let's note it by d.
It follows like this:

$$\frac{l}{d} = \frac{l}{d} = \frac{h3}{h2} \tag{6}$$

That is:

$$\frac{l}{d} = \frac{h3}{h2} \tag{7}$$

Another relationship to be respected.
In the right triangle OA'C' of the formula of Pythagora results:

$$OA'^2 = A'C'^2 + OC'^2 \rightarrow d^2 = \left(\frac{h_2}{2}\right)^2 + b^2 \tag{8}$$

Results:

$$b^2 = d^2 - \left(\frac{h_2}{2}\right)^2 \tag{9}$$

Substituting formula (2) in formula (3) results:

$$b^2 = \left(l\frac{h_2}{h_3}\right)^2 - \left(\frac{h_2}{2}\right)^2 \tag{10}$$

From where:

$$b = \sqrt{\left(l\frac{h_2}{h_3}\right)^2 - \left(\frac{h_2}{2}\right)^2} \tag{11}$$

How does quota „b" help us?
On r_2 we can choose it by the construction of the upper movable disc 4 (the piston) and lower disc fixed to the frame of the mechanism (see Figure 9). A condition for r_2 is that it must be greater than r_1.
Figure 7 shows an orange volume V_s, V_s being that difference in volume required for the water in the tank to empty completely into the body of the exhaust pump.
With r_2 established from the construction, the „b" dimension helps us determine the distance from the „O" joint to the piston rod of the exhaust pump.
Why physics knowledge is needed?
Knowledges of physics is needed most! There are many questions like: „based on what kind of energy does the mechanism work?" If we made a comparison at the beginning with the thermal engine and the electric engine (almost none), let's first see what kind of energy the thermal engine works? Based on no kind of energy.
The thermal engine works by burning a quantity of fuel inside the cylinder and produces mechanical work through the piston stroke not „an energy".
CAF force depending on the pitch of the whirl on the side surface of the floating body.
Because we will need a mathematical model for future calculations, suppose that the CAF force will double the simple achimedic force of 490Kgf. For this is necessary that the pitch of the whirl on the outer surface of the floating body be executed at a quota such that the CAF force doubles the simple archimedic force. We have thus identified another variable of the mechanism - the multiplication of the CAF force according to the pitch of the whirl on the lateral surface of the floating body.
Through this multiplication we will obtain a CAF force of approximately 1000Kgf which we will take consider below.
With the CAF force setled at 1000Kgf let's return to the situation presented above, these about which I mentioned that knowledges of geometry is needed to understand the operation of the mechanism.
From the rule of using the lever and with the force multiplication coefficient introduced by it, according to Figure 8 and the related formula (l. m. - lever multiplier) below, the situations from the „geometry knowledge chapter" result:

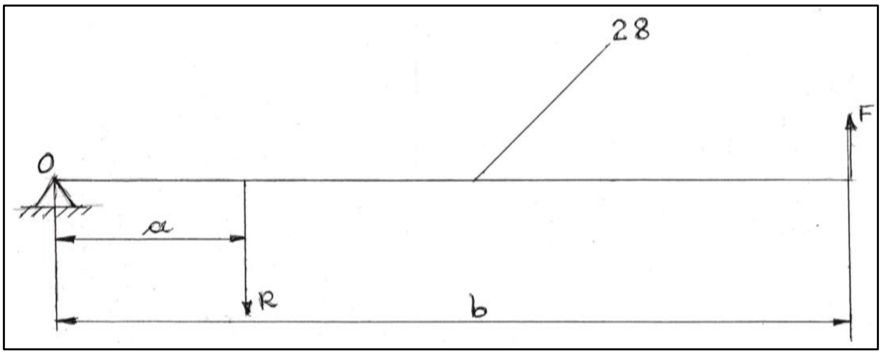

Fig. 8. Lever 28

In Figure 7: $a = b$, $b = l$ and F=CAF:

$$Rxa = Fxb \tag{12}$$

Note: using the lever (28) does not multiply the mechanical work, but only keeps it constant (along the length of the lever from the right extremity to the left „O" joint, the force increases but decreases the stroke, so the mechanical work remains constant.
These values above are important for:
1) Knowledge of the force that is available at the point of contact between the lever (28) and the nut (9) on the rod (8) of the exhaust pump piston. The ratchet with symmetrical double end and torsion spring (11) shall be designed to lock/release this force.

5. Conclusions

By pushing a floating body into a quantity of water (the action) a mechanical work is performed on it. By rising the water level in a tank inside which a floating body is located, the floating body will move upwards resulting reaction (reaction of rising water level in the tank). If the floating body rotates at the same time as the upward movement, an additional mechanical work will be obtained due to this stroke of the floating body, mechanical work exploited by the engine mechanism of the water engine. We cannot talk about „energy" in the case of the water engine because in its case an energy study has not yet been done (mechanical work carried out during an operating cycle). Also, there can be no talk of efficiency. The water engine converts the mechanical work obtained from the stroke of the floating body during T_1-t_1 of the operating cycle into mechanical work performed by a flexible membrane exhaust pump during t_2-T_2 of the operating cycle. From the estimated calculations presented earlier in this article, it follows that this mechanism can have supraunitary efficiency (because it is not dependent on friction like the thermal engine).
For a better understanding of the construction of the mechanism, a photo of a model of the mechanism will be offered in the continuation of this article. Also, those interested I can offer the entire project which totals about 80 pages.

Fig. 9. The experimental model (with a mock-up)

References

[1] Niculae, Nicușor. *Water running engine/Motorul care funcționează cu apă*. Craiova, SITECH Publishing House, 2020, ISBN 978-606-11-7467-6.

ISSN 1454 - 8003
Proceedings of 2024 International Conference on Hydraulics and Pneumatics - HERVEX
November 13-15, Băile Govora, Romania

ASPECTS RELATED TO FLUID VISCOUS DISSIPATION DEVICES USED FOR SEISMIC PROTECTION OF STRUCTURES

Fănel Dorel ȘCHEAUA[1]

[1] “Dunarea de Jos” University of Galati, fanel.scheaua@ugal.ro

Abstract: *A seismic dissipation device working on fluid is presented as a fluid viscous damper (FVD), a constructive type of energy dissipation device used in civil engineering to protect structures (such as buildings and bridges) from the destructive effects of seismic forces. These devices absorb and dissipate energy generated during earthquakes, reducing the forces and deformations transferred to the structure. The seismic dissipation devices convert the kinetic energy from piston translational motion into heat through fluid viscosity enhancing an effective structural damping and seismic response during the earthquake ground motion. The linear fluid viscous device provides a directly proportional damping force to the relative velocity across the damper, being commonly used in structures where a uniform damping response is required, while nonlinear fluid viscous dampers exhibit a damping force that follows a nonlinear behaviour with velocity achieving greater damping at lower velocities being tuned for specific seismic response needs.*
These devices absorb a significant amount of seismic energy, reducing the forces transmitted to the structural elements, limiting the oscillations amplitude and control the structure displacement during an earthquake, reducing the risk of damage to non-structural components like walls, partitions, and equipment.
The fluid viscous devices can be used for existing buildings and bridges retrofit, providing an effective way to upgrade seismic resistance without significant structural alterations, providing a long service life and typically minimal maintenance requirements since they do not rely on other mechanical components. A numerical analysis was conducted based on the NEWMARK-Beta method for highlighting the operational capabilities of a fluid viscous device being presented results for displacement, velocity and acceleration registered and also the force-displacement loop for different velocity coefficient values. The obtained results illustrate the effectiveness of fluid viscous dampers in dissipating energy and reducing seismic-induced responses in structures.

Keywords: *Hydraulic actuation, dissipation device, fluid flow, operational parameters, numerical analysis*

1. Introduction

Fluid viscous dampers rely on the resistance generated by fluid flow through a small orifice or valve within a cylinder. The core components of an FVD are represented by the main cylinder which houses a piston and contains the working fluid. The piston as the movable component inside the cylinder forces fluid to circulate through small orifices made inside the piston head. The orifices or valves maintain control on the fluid flow and generates resistance during fluid movement.
The working fluid is usually silicone or oil, a high-viscosity fluid that resists motion and dissipates energy by generating heat.
During an earthquake or other dynamic event, the structure undergoes oscillatory motion. This motion is transferred to the damper, where it causes relative movement between the damper's piston and cylinder.
As the piston moves within the cylinder, it forces the fluid to flow through specially designed valves or small orifices while further this flow creates resistance to motion. The size of the orifices controls the amount of resistance, and hence, the amount of energy dissipation.
The resistance to fluid flow through the orifice converts kinetic energy (from the earthquake motion) into heat within the fluid. The energy is dissipated through this conversion, reducing the amount of energy transmitted to the structure. The generated heat is harmlessly dissipated to the surrounding environment.
Fluid viscous dampers can be designed to provide non-linear damping, meaning the damping force can be proportional to velocity raised to a power. This gives designers flexibility to adjust the damping properties to match the dynamic behaviour of a structure. For instance, for smaller

vibrations, the damping force may be lower, while for larger, more destructive vibrations, the force increases significantly.
The force exerted by an FVD is proportional to the velocity of motion and this contrasts with other damping devices like friction dampers, where the force is displacement-dependent.
FVDs do not change the stiffness of the structure because the damping force depends on velocity and not displacement. This characteristic makes them suitable for both retrofitting existing buildings and for new structures where altering the stiffness is not desirable.
The performance of FVDs can be easily tuned by changing the orifice size, fluid viscosity, or piston design, allowing engineers to control the level of energy dissipation.
Fluid viscous dampers are commonly installed in both new and existing buildings to mitigate seismic forces. They can be incorporated in the bracing systems of structures, reducing the lateral drift and increasing overall stability during earthquakes.
In bridge structures, FVDs are used to control the displacement and forces on bridge piers during seismic events. They allow controlled movements of bridge decks while dissipating energy.
In tall buildings or slender structures, fluid viscous dampers can be part of a TMD system to reduce oscillations caused by wind or earthquakes.
Advantages are related to high efficiency in operation while FVDs dissipate a significant amount of seismic energy, reducing the demands on the structural members. Since the internal components (fluid and piston) are enclosed, they generally require minimal maintenance and the absence of moving parts prone to wear makes fluid viscous dampers highly reliable for long-term seismic protection, while fluid viscous dampers are able to stabilize the building against both wind and seismic forces.
These hydraulic devices are protecting the structures from earthquake damage by dissipating the kinetic energy induced by ground motion, reducing structural vibrations without increasing stiffness. They are highly effective in both new constructions and retrofits, providing a reliable and low-maintenance solution for seismic protection.
The basic parameters and the operating principle are described in this work for fluid viscous dissipation device. A mathematical model describing the operation is also presented, as well as a numerical approach in order to highlight the operating characteristics.

2. Construction principle and materials used for fluid viscous device

The construction process of fluid viscous damper (FVD) involves several stages and specific materials used in order to achieve energy dissipation through fluid viscosity properties.
The main component of a fluid viscous damper is represented by the cylinder, which houses the piston and the viscous working fluid. It is typically made from high-strength materials, such as steel, to withstand the forces exerted during operation. Inside the cylinder is positioned the piston that divides the fluid in two chambers and generates damping force as it moves back and forth. The piston is designed with orifices or channels through which the working fluid flows, being controlled the fluid flow between the two chambers on either side of the piston. The size and shape of the orifices are critical for determining the damping characteristics.
The fluid inside the cylinder is usually a silicone-based liquid, which provides resistance to the piston's movement. The fluid's viscosity property determines the damping force and needs to remain stable across a range of temperatures.
Special seals and bearings are used to prevent fluid leakage and ensure smooth movement of the piston within the cylinder, while high-quality sealing solutions are essential in order to maintain damper performance over time.
The damper device ends are fitted with connections to attach the device securely to the isolated structure, allowing the damper to be connected to braces, frames, or other structural elements.
Regarding the materials used cylinder and piston are typically made from high-strength steel or stainless steel that handle the stresses during seismic events and prevent deformation [1-7].
The viscous working fluid is usually silicone oil because of its stable viscosity over a wide temperature range, low volatility, and excellent thermal properties.

The sealing is usually made from elastomeric materials, such as VITON (fluoro-elastomers that can retain their flexibility, shape, sealing well even when are exposed to chemical solutions and high temperatures values), or other high-performance rubbers in order to ensure tight sealing and resistance to wear and chemical degradation.
The bearings are often made from low-friction materials like Teflon or bronze, which allow the piston to move smoothly within the cylinder.
FVDs are installed in strategic locations within buildings or bridges where they can most effectively reduce seismic forces. Typical installation locations are within buildings as diagonally braces across structural elements in order to absorb the lateral forces, between floors to reduce inter-story drift by controlling relative motion between floors, or expansion joints within bridges where FVDs are used to limit the movement of expansion joints during seismic events.
During construction, FVDs are subject to strict quality control to ensure consistent performance, especially under varying temperature conditions.
While FVDs are generally low maintenance, periodic inspections are performed to check for fluid leakage, seal integrity and overall structural condition.
The construction of fluid viscous dampers involves precision engineering, high-quality materials, and rigorous testing to ensure effective seismic energy dissipation. By combining a carefully designed piston, a stable viscous fluid and a robust cylinder, FVDs can effectively reduce structural vibrations and protect buildings and bridges from seismic damage. Proper installation activity and periodical maintenance are important in order to maximize the longevity performance efficiency of these protective devices [8-11].

3. Mathematical model for fluid viscous device

The mathematical model for a fluid viscous damper (FVD) is presented in order to describe the device behaviour in dissipating energy during dynamic events such as earthquakes. The damping force generated by fluid viscous damper depends on the relative velocity of the motion across the damper, as well as the properties of the fluid and damper design.
The basic damper mathematical model is given by the generated response force expressed as:

$$F_d = c \cdot v^a \tag{1}$$

where:

F_d - the damping force;
c - the damping coefficient, represents the damper's resistance to motion, determined by the fluid's properties and the damper's configuration;
v - the relative velocity of the damper piston;
a - the velocity exponent, typically between 0.5 and 1, indicating the nonlinearity of the damper's response.
For the device linear model when *a=1*, the damping force is directly proportional to the velocity, while the equation simplifies to:

$$F_d = c \cdot v \tag{2}$$

In this case, the damper is considered linear, and the damping force varies linearly with the velocity.
For the nonlinear model, when *0<a<1*, the damping force varies nonlinearly with velocity and this is commonly used in structural applications because it allows for higher damping forces at lower velocities and can be tuned to achieve specific damping characteristics.
The energy dissipated by the fluid viscous damper is related to the mechanical work done by the damping force over the displacement. The power dissipated at any given time can be calculated as:

$$P_d = F_d \cdot v = c \cdot v^{a+1} \tag{3}$$

where:
P_d - the dissipation power.
The total dissipated energy amount over a time interval can be obtained by integrating the power dissipation over time.
The equivalent viscous damping characteristics for FVD, in structural dynamics is introduced the equivalent viscous damping ratio ς_{vd} as the damping characteristics of the fluid viscous damper in terms of an equivalent linear system. The equivalent damping ratio can be calculated from the damping force characteristics as:

$$\varsigma_{vd} = \frac{c}{2m\omega} \tag{4}$$

where:
m - the equivalent system mass;
ω - the angular vibration frequency.
The damping force in structural system in the context of a dynamic loading such as earthquake motion, the equation of motion for a mass-spring-damper system incorporating a fluid viscous damper can be written as:

$$\begin{gathered} F = m\ddot{x} + c\dot{x} + kx \\ F = m\ddot{x} + c\dot{x}^a + kx \end{gathered} \tag{5}$$

where:

m - system mass;
$\ddot{x}$ - mass acceleration;
c - is the damping coefficient of the fluid viscous damper (linear model);
$\dot{x}$ - velocity (displacement rate of change);
k - the device stiffness;
x - displacement;
F - external force acting on the system.

For nonlinear dampers, the damping term is considered as ($c\dot{x}^a$).
The further modelling considerations are related to temperature dependences while the fluid viscosity changes with temperature, affecting the damping coefficient (c) and the frequency dependence as the damper effectiveness changes with the vibrations frequency, especially for highly nonlinear dampers [1-5, 12].

4. Numerical analysis for fluid viscous device operation

The numerical analysis for a fluid viscous damper (FVD) operation involves simulating of linear and nonlinear behaviour under dynamic conditions in order to predict its effectiveness in dissipating energy in vibrations subjected structures during seismic events. The process typically involves solving the equations of motion that govern the structure's response, incorporating the characteristics of the fluid viscous damper.
Performing a numerical analysis for fluid viscous damper operation implies the proper formulation of the problem necessary to analyze a structural system equipped with a fluid viscous damper and further formulation of the governing equation of motion. For a single-degree-of-freedom (SDOF) system with mass *m*, damping *c*, stiffness *k* and an external force *F,* the equations of motion for the linear and nonlinear model can be written as:

$$F(t) = m\ddot{x}(t) + c\dot{x}(t) + kx(t)$$
$$F(t) = m\ddot{x}(t) + c\left|\dot{x}(t)\right|^{a-1} + kx(t) \tag{6}$$

where:

$x(t)$ - mass displacement as a function of time;

$\dot{x}(t)$, $\ddot{x}(t)$ - velocity and acceleration, respectively;

$F(t)$ - external force applied to the system during earthquake ground motion.

To perform the numerical analysis, the time domain is discretized into small time steps of *Δt*. The time intervals are represented as $t_0, t_1, \ldots, t_n$, where $t_{i+1} = t_i + \Delta t$.
The numerical integration method used to solve the differential equation of motion is represented by NEWMARK-Beta method for solving equations of motion in structural dynamics [1-7, 13].
The selected method makes use of the following iterative relations in order to update displacement and velocity at each time step:

$$x_{i+1} = x_i + \dot{x}_i \cdot \Delta t + \ddot{x} \cdot \frac{\Delta t^2}{2}$$
$$\dot{x}_{i+1} = \dot{x}_i + \ddot{x} \cdot \Delta t \tag{7}$$
$$\ddot{x}_{i+1} = \frac{1}{m}\left[F_{,i+1} - c\left|\dot{x}_{i+1}\right|^{a-1}\dot{x}_{i+1} - k \cdot x_{i+1}\right]$$

The displacement values, velocity and acceleration are updated iteratively for each time step.

Table 1: Fluid viscous device parameters for analysis

Crt. No.	Parameter type	Unit	Values
1.	Mass	(kg)	10000
2.	Stiffness	(N/m)	50000
3.	Damping coefficient	(Ns/m)	10000
4.	Velocity exponent for nonlinear damping	-	0.6/0.7/0.8/0.9
5.	Amplitude of motion	(m)	0.5
6.	Frequency of oscillation	(Hz)	0.5
7.	Total simulation time	(s)	10.0

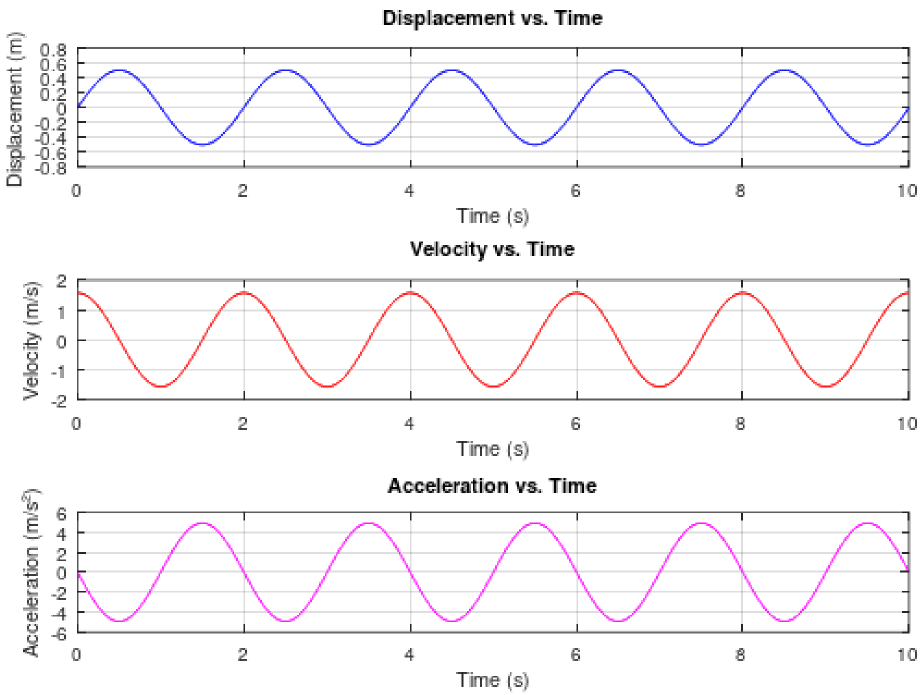

Fig. 1. Diagrams for displacement, velocity and acceleration

The results for displacement, velocity, and acceleration presented in figure 1 show the expected sinusoidal patterns, reflecting harmonic motion. The results indicate that the FVD is effective in controlling both displacement and acceleration, which is crucial for reducing structural responses during seismic events.

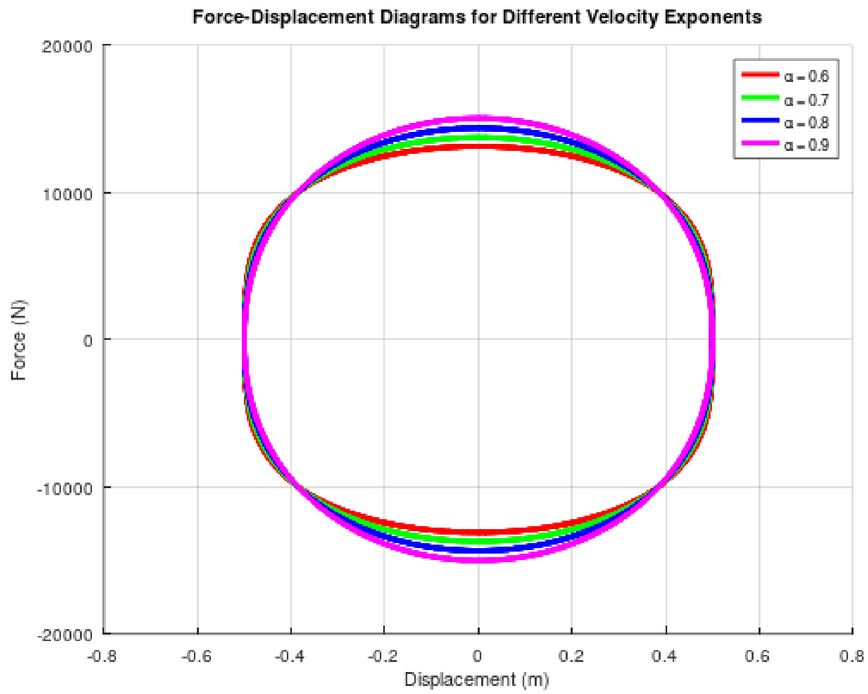

Fig. 2. Force displaments diagram for different velocity exponents values

The force-displacement diagrams demonstrate the characteristic hysteresis loops of devices, indicating energy dissipation during cyclic loading, while the area enclosed by the loops corresponds to the amount of energy dissipated per cycle.
The numerical analysis results confirm that for different velocity exponents, the shape of the force-displacement loops change (figure 2). Lower values (0.6) resulted in flatter hysteresis loops, indicating less force generation for a given velocity. In contrast, higher values (0.9) showed steeper loops, suggesting higher energy dissipation and greater damping forces.
The use of non-linear damping allows a more realistic representation of FVD behaviour under different velocities. The non-linearity helps to model the actual physical characteristics of fluid dampers, where the damping force does not necessarily increase linearly with velocity.
With velocity coefficients less than 1, the device shows a reduced sensitivity to high velocities, which could be beneficial for preventing excessive force transmission in structures during strong seismic events.

5. Conclusions

Based on the simulation results obtained for the fluid viscous damper (FVD) operating under cyclic motion, can be highlighted the device's behaviour and effectiveness in seismic protection of structures where are mounted.
The amount of energy dissipated over time, calculated through numerical integration, confirmed that the device effectively reduces the mechanical energy transmitted to the structure.
The energy dissipation is vital for minimizing the amplitude of structural vibrations and protecting the building from damage.
Fluid viscous dampers, with their ability to provide significant energy dissipation, are well-suited for seismic protection of structures.
The non-linear damping characteristics offer flexibility in design, allowing the improvement of damping behaviour to meet specific performance requirements.
The use of varying damping coefficients and velocity exponents can be adjusted based on the expected ground motion characteristics, ensuring optimal performance in different seismic scenarios.
The numerical analysis using the NEWMARK-Beta method and subsequent obtained results for force-displacement, velocity and acceleration illustrates the effectiveness of fluid viscous dampers in dissipating energy and reducing seismic-induced responses in structures.
The results confirm the value of non-linear damping models in capturing the actual behaviour of FVDs under dynamic loading.
The ability to adjust the damping parameters provides a versatile approach for designing damping systems for mounting in specific structures and meeting the anti-seismic protection demands.

References

[1] El Hankouri, Yousra, and Abdelouafi El Ghoulbzouri. "A Numerical Investigation of the Impact of Non-linear Viscous Damping on Structural Response to Seismic Excitation." *Iranian Journal of Science and Technology, Transactions of Civil Engineering* (2024): under review. https://doi.org/10.21203/rs.3.rs-4934385/v1.
[2] Sabino, Antonio, Antonio Mannella, and Andrea Matteo de Leo. "Seismic Response of a Structure Equipped with an External Viscous Damping System." *Buildings* 10, no. 2 (2020): 19. https://doi.org/10.3390/buildings10020019.
[3] Naranjo-Pérez, Javier, Javier F. Jiménez-Alonso, Iván M. Díaz, Giuseppe Quaranta, and Andrés Sáez. "Motion-Based Design of Passive Damping Systems to Reduce Wind-Induced Vibrations of Stay Cables under Uncertainty Conditions." *Applied Sciences* 10, no. 5 (2020): 1740. https://doi.org/10.3390/app10051740.
[4] Riaz, Raja Dilawar, Umair Jalil Malik, Mati Ullah Shah, Muhammad Usman, and Fawad Ahmed Najam. "Enhancing Seismic Resilience of Existing Reinforced Concrete Building Using Non-Linear Viscous Dampers: A Comparative Study." *Actuators* 12, no. 4 (2023): 175. https://doi.org/10.3390/act12040175.

[5] Michailides, Constantine. "VD-PQ; A Velocity-Dependent Viscous Damping Model for Wave-Structure Interaction Analysis." *Journal of Marine Science and Engineering* 9, no. 2 (2021): 175. https://doi.org/10.3390/jmse9020175.

[6] Tsipianitis, Alexandros, and Yiannis Tsompanakis. "Multi-Objective Optimization of Base-Isolated Tanks with Supplemental Linear Viscous Dampers." *Infrastructures* 7, no. 11 (2022): 157. https://doi.org/10.3390/infrastructures7110157.

[7] Zhang, Yunlong, Weizhi Xu, Shuguang Wang, Dongsheng Du, and Yan Geng. "Mechanical Modeling of Viscous Fluid Damper with Temperature and Pressure Coupling Effects." *Machines* 12, no. 6 (2024): 366. https://doi.org/10.3390/machines12060366.

[8] Sadeghian, Mostafa, Kestutis Pilkauskas, Paulius Palevicius, Jurate Ragulskiene, Giedrius Janusas, Viktoras Dorosevas, and Arvydas Palevicius. "A Nonlinear Damper with Dynamic Load and an Elastic Slit Membrane: Modeling and Interaction Analysis." *Applied Sciences* 14, no. 17 (2024): 7663. https://doi.org/10.3390/app14177663.

[9] Vasile, Ovidiu, and Mihai Bugaru. "A New Modeling Approach for Viscous Dampers Using an Extended Kelvin–Voigt Rheological Model Based on the Identification of the Constitutive Law's Parameters." *Computation* 11, no. 1 (2023): 3. https://doi.org/10.3390/computation11010003.

[10] Chen, Peng, and Xiaobin Wu. "Investigations on the Dynamic Response of Adjacent Buildings Connected by Viscous Dampers." *Buildings* 12, no. 9 (2022): 1480. https://doi.org/10.3390/buildings12091480.

[11] Yip, Chun-Chieh, Jing-Ying Wong, Mugahed Amran, Roman Fediuk, and Nikolai Ivanovich Vatin. "Reliability Analysis of Reinforced Concrete Structure with Shock Absorber Damper under Pseudo-Dynamic Loads." *Materials* 15, no. 7 (2022): 2688. https://doi.org/10.3390/ma15072688.

[12] Conde, Jorge, and Alejandro Bernabeu. "Influence of Maxwell Stiffness in Damage Control and Analysis of Structures with Added Viscous Dampers." *Applied Sciences* 11, no. 7 (2021): 3089. https://doi.org/10.3390/app11073089.

ISSN 1454 - 8003
Proceedings of 2024 International Conference on Hydraulics and Pneumatics - HERVEX
November 13-15, Băile Govora, Romania

THEORETICAL ASPECTS REGARDING THE DEVELOPMENT OF A METHOD FOR INTERNAL VOLUME DETERMINATION OF EXTERNALLY GEARED PUMPS

Ionela-Mihaela POPESCU[1], Mihai AVRAM[1], Victor CONSTANTIN[1], Alexandra-Gabriela VASILESCU[1], Bogdan GRĂMESCU[1]

[1] Department of Mechatronics and Precision Mechanics, Faculty of Mechanical Engineering and Mechatronics, National University of Science and Technology POLITEHNICA Bucharest, 060042 Bucharest, Romania; ionela.baciu@upb.ro; mihai.avram@upb.ro; victor.constantin@upb.ro; avasilescu@upb.ro bogdan.gramescu@upb.ro

Abstract: *The article is focused on the literature study of determining the capacity of an external gear pump by applying Computational Fluid Dynamics (CFD) technology. The solution proposed by the authors involves theoretical research and early numerical simulations on the gear pump to evaluate its performance under various conditions such as suction and discharge. The pump housing was modeled using Autodesk Inventor and the simulation was performed with ANSYS software. The theoretical model proposed by the authors is complemented by CFD simulations, which provide insights into how factors such as suction and discharge affect flow. The obtained results through mathematical modeling correlated with the simulations results allows a comprehensive understanding of the pump's behavior and characteristics, thus validating and refining the flow determination model through empirical data.*

Keywords: *Externally geared pump, computational fluid dynamics, mechatronic system*

1. Introduction

Gear pumps are one of the most common types of pumps and are used in a wide range of applications because of their reliability, compactness, reduced purchasing costs and good efficiency. The two main types of gear pumps are external and internal gears, which can be divided into several categories based on the profile of the teeth. One significant benefit of externally geared pumps is their ability to handle a wide range of fluid viscosities and temperatures, making them suitable for diverse applications across various industries, from automotive to aerospace.
These pumps are often used in hydraulic systems where precise control of fluid flow and pressure is required, such as in heavy machinery, industrial equipment, and hydraulic power units. Overall, externally geared hydraulic pumps are valued for their reliability, efficiency, and versatility, making them a crucial component in many hydraulic systems where consistent fluid power is essential.
High efficiency and overall performance in these systems stands to benefit from a much better understanding and modelling of the pump being used. As such, a clear characterization of the pump’s internal capacity will be the starting point of any model that might allow it to be included in an Industry 4.0 capable system, such as a digital twin or digital shadow. However, given the difficulties encountered in estimating characteristics and mostly incomplete documentation, such a model, especially one that allows for high precision, is usually hard to include. A method for determining key parameters is described in this paper. To this end, a study of current developments in the field has been conducted, with some of the results being listed below.

2. Previous and related works

An external gear pump is a positive displacement device that transfers the fluid from the suction port to the discharge port by means of the gear of the drive and the secondary gear. In the gap between the teeth of the two gears, the fluid is transferred from the suction to the discharge of the pump [1-3]. Several studies have been conducted in the last few years to develop simulation procedures for describing pump fluid dynamics, with numerical methods becoming more prevalent for modeling fluid problems. Current CFD simulations use the finite volume method (FVM) and the finite element method (FEM). They allow the analysis of complex technological processes and the stimulation of various starting and boundary conditions [1,3]. According to Močilan et al. [1], the use of advanced CAD and CFD techniques for product design and simulation has significant applications in the fields of mechanical, automotive and aeronautical engineering. In their paper a strong emphasis was performed on CAD simplification. Their results show that it is possible to predict the dynamic behavior of a pump with an external gear, with good approximation of the phenomena that occur during the operation of these devices such as fluid pressure distribution on, torque in gear movements and many others. A novel approach to capture detailed micron gap information and accurate model of these machines is described in a paper [2], using the commercial CFD tool PumpLinx. Analysis of gear pumps can be integrated into the product design and development process by using PumpLinx simulations in conjunction with test results for system level optimization, including dynamic response and efficiency performance.

Another methodology was adopted in paper [4], where attention was given to structuring the simulation in three iterative calculation phases with great emphasis on the correct characterization of the involute gear tooth profile. To comply with the space requirement and the tooth production constraints, it is designed to ensure proper volumetric displacement. The second calculation step therefore provides the design of the driving shaft and corresponding dimensions for journal bearings based on an analysis pressure load estimation coupled with operating parameters. Lastly, the third part of the procedure will lead to an estimation of clearance for gear tip and housing by means of a power failure approach. The application of this methodology to a case study of a multistage gear pump used in a dry sump lubrication system for an automotive heavy-duty engine illustrates the potential of this methodology. Each calculation step shall be laid down in accordance with the proposal for an analytical formulation and results of parameter calibration shall be disclosed. In this context, a CFD analysis shall be used to assess the procedure. The accuracy of the methodology for the estimation of the required flow rate is highlighted in the results. In addition to being accurate, flexible and reliable, the procedure stands out as an innovative tool in a multistage gear pump system.

The authors in [5] use advanced CFD models of hydraulic gear pumps to study their performance. The focus is put primarily on the numeric aspects, with a view to defining strategies for simulating oil dynamics in gear pumps. Two rotary pumps of fixed displacement type belonging to a family of gear pumps are proposed to be investigated. Three main steps, namely preprocessing, process and post-processing, form part of the study carried out to analyse these pumps as in classical computational fluid dynamics simulations. Another method is presented in paper [6]: a prediction of cavitation at high speed in helical gear pumps, to develop a hydrostatic dynamometer system. The fluid movement is described by means of several stages of fluid transfer from the pump inlet to the outlet, using a variety of meshes and densities.

In [7] the leakage past the tooth flanks of the gears in transition contacts in involute external toothed gear pump is analyzed in detail using CFD in Fluent®. The experimental flow diagrams are supported by analytical results. More rigorous analyses are carried out, considering the actual gear data of the pump and the full cycle of contact, to extend the approach of the earlier investigation.

By using the powerful ANSYS 16 CFX module, the authors of the paper [8] investigate the hydrodynamic behavior of the 8/9 teeth annular gear pump. Until the advent of Ansys immersed solid technology, it was difficult to solve solids that were evolving inside liquids. Reliable results can be obtained by using this technology in very specific areas such as CFD analysis of micro annular gear pumps, which can lead to more detailed studies such as geometrical optimization of functions and existing equipment.

A CFD model of an external gear pump is presented in [9]. One of the commercially available CFD software packages has been chosen to study fluid flow phenomena that occur when external gear pumps are used. To simulate the flow caused by the rotation of the gears, the immersed solid method has been used. The results of simulation studies performed for the different operating

parameters to assess the influence of rotation speed and pressure in the outlet channel on the cavitation intensity, a prepared 2D CFD model has been used.
The current design of external gear fuel pumps shows that flow processes at the meshing zone have an important impact on performance and lifetime, according to analysis provided [10]. In the opening and closing of the cavity in the meshing zone, the incorrect geometry of the truss plate and the compensation system leads to an increase in velocity, which results in intense cavitation. This approach does not give an objective result, although it is possible to determine the true values of pressure and load in relation to angle of rotation. However, as a basis for validation of the flow model, high speed scanning can be applied.
Another effort is described in paper [11] where a moving-deforming grid study was carried out using Fluent®, a commercial CFD solver. The goal was to quantify the level of mixing of a lower viscosity additive (at a mass concentration below 10%) into a higher viscosity process fluid in a big metering device pump configuration, common in plastics manufacturing.
A new method for simulation and evaluation of hybrid external gear pumps using Modelica has been presented [12] and is currently being tested. The authors modeled the entire working process of an external gear pump. The pump chamber is divided into a set of control volumes, the effective volume of which changes with the rotation of the gears. The CVs take in fluid from the inlet port and squeeze fluid out at the outlet port. Flow ripple, pressure distribution, leakage age, meshing conditions and so on are also considered in the overall design of the pump. Details are provided for each com portent of the entire pump. From pressure distribution in the gear tooth space, the radial force on the shaft can be calculated, based on which shaft movement can be simulated.
For fluid power applications, [13] presents a computational fluid dynamics simulation of an external gear pump. The objective of this study shall be to test the model's ability to evaluate pressures within a tooth space for both total shaft revolutions as well as lowest inlet pressure in all filling. The model considers leakage from the internal fluid system and two different configurations of thrust plates have been considered. A proper high dynamic transducer measuring the internal pressure in the tooth space for the entire shaft revolution has been used to validate the simulations in different operating conditions. To determine the drop-in flow rate, due to incomplete filling of tooth spaces when the pressure at the upstream is decreased, stable simulations have also been performed. It was shown that significant results could be obtained despite the need for compromise to overcome limitations on considering fixed axes of gear and thrust plates, which make a CFD approach very suitable for such analysis.
According to [14] it is difficult to obtain an accurate CFD simulation of a component due to its geometric complexity and high-pressure gradients, which characterize the design of flow fields for gears. In general, assumptions are made about the geometrical characteristics and physics to be considered in the analysis. In 3D CFD simulations, due to the intrinsic limitations of dynamic meshing techniques that can hardly effectively cope with a zero or near zero gap point formed during gear rotation, contact between teeth is an essential factor for proper functioning of these pumps. CFD analysis is complex, due to geometric complexity and sharp gradients in the gear pump flow field that characterize it, therefore avoiding contact with gears' teeth is a crucial feature. In [14], a gear pump composed of inlet and outlet pipes was considered, and the contact between the gear’s teeth was modeled in two different ways, one where it is effectively implemented and one where it is avoided using distancing and a proper casing modification.
To achieve energy savings, partial electrification of hydraulic circuits requires increasing the angular velocity of positive displacement pumps with a risk for incomplete filling. In this context, the paper [15] deals with the development of a computational fluid dynamics CFD model using SimericsMP+ for two external gear pumps, namely helical and spur type pumps. The study's objective shall be to analyze phenomena occurring on the Suction side under conditions where the fill is not completed at fast speeds.
A methodology is presented in [16] to predict the motion of a gear pump within its operational range. Complete pump parameterization was done through standard tests, and these parameters were used to create a bond graph model to simulate the unit's behavior. In field tests, this model has been validated on an experimental basis. To do so, experimental data were compared with a

simulation of the volumetric behavior in the same conditions where the pump was used for auxiliary movements on the drilling machine. This paper describes a method for classifying each hydrostatic pump as a black box model predicting its behavior in all operational conditions. The novelty of this method is based on the correspondence between the variation of the parameters and the internal changes of the unit when working in real conditions, that is, outside a test bench.

3. Material and method

Externally geared hydraulic pumps are devices used to generate fluid flow within hydraulic systems. These pumps consist of two gears, an input gear (driven by a motor or engine) and an output gear, enclosed within a housing. The gears mesh together and rotate, creating suction at the inlet side and forcing hydraulic fluid out of the outlet. Starting from the suction phenomenon of the hydraulic fluid, caused by the depression produced by the teeth coming out of the gear, to the discharge phenomenon produced by the gear teeth entering the gear of the pump construction. The aim is to determine the flow supplied by the pump at a speed, n, and the power generated. The pump flow is obtained by taking a quantity of fluid in each impeller tooth space and conveying it from suction to discharge. It is determined by the volume of hydraulic fluid conveyed at one complete rotation of the impellers.
The authors propose the following approach to determine the flow rate of the gear pump by integrating two methods (mathematical modeling and numerical simulation) to obtain more accurate and robust results.

3.1 Analytical method

The flow rate in a gear pump can be determined analytically by a mathematical model that integrates the fundamental principles. Gear pumps belong to the category of positive displacement pumps, which transfer a fixed volume of fluid with each revolution of the gears. Flow rate can be affected by many factors such as: gear dimensions, rotational speed, distance between components and fluid properties. To determine the mathematical model some assumptions are made: fluid incompressibility, that is usually true for most hydraulic oils; steady-state operation conditions; gear imperfections and wear are excluded, if necessary, they can be considered by changing the efficiency parameters.
According to literature the following flow rates are determined analytically: theoretical flow rate, theoretical instantaneous flow rate and theoretical average flow rate. Notation from the theory of fine mechanics mechanisms (fig. 1) will be used to describe the areas of the tooth crowns that contribute to the pump backflow. Using the theory of mechanisms to determine the geometry of the gears in gearing the following expression was obtained:

$$Q_t = b\left\{n_1\pi\left[r_{e_1}^2 - \left(A - r_{e_2}\right)^2\right] + n_2\pi\left[r_{e_2}^2 - \left(A - r_{e_1}\right)^2\right] - n_1 z_1 H\right\} \tag{1}$$

where:
Q_t - theoretical flow; b- the length of the contact line for a pair of teeth; n_1- speed for gear 1; r_{e_1}- radius of the tooth pitch circle (for gear 1); A- gear center distance; r_{e_2}- radius of the tooth pitch circle (for gear 2); n_2 - speed for gear 2; z_1 - teeth number of gear 1; where:
The theoretical instantaneous flow rate is expressed as a function of the angle of rotation, φ, resulting in the following relationship [17]:

$$Q_{ti} = \pi \cdot n \cdot b\left[r_{e_1}^2 + i \cdot r_{e_2}^2 - \frac{i}{i+1}A^2 - (i+1)r_{b_1}^2\varphi_1^2\right] \tag{2}$$

By integrating on a circular arc of length $\frac{\pi}{z}$, we obtain the mean theoretical flow rate with the expression:

$$Q_{tm} = \pi \cdot n \cdot b \left[r_{e_1}^2 + i \cdot r_{e_2}^2 - \frac{i}{i+1} A^2 - (i+1) \frac{\pi^2 m^2 cos^2\alpha}{12} \right] \quad (3)$$

For pumps with gear ratio, $i = 1$, the equation becomes:

$$Q_{tm} = \frac{\pi n b}{2} \left[d_e^2 - A^2 - \frac{\pi^2 m^2}{6} cos^2\alpha \right] \quad (4)$$

where: α – angle of engagement; m – module.

For a unit transmission ratio, the theoretical displacement V_t, the theoretical displacement of the pump can be written as follows:

$$V_t = 2 \cdot z \cdot b \cdot f \quad (5)$$

where: $f = 0{,}5 \cdot p \cdot 2m$ and $p = \pi \cdot m$

From the above relations the equations for theoretical displacement and theoretical flow rate can be written as follows:

$$V_t = 2\pi \cdot m^2 \cdot b \cdot z \quad (6)$$

$$Q = 2\pi \cdot m^2 \cdot b \cdot z \cdot n_0 \quad (7)$$

Through observations made over time by specialists and researchers, it has been found that this type of pump also exhibits a displacement and flow unevenness, which at a unity transmission ratio has the frequency, $v_0 = z \cdot \frac{n_0}{60} [Hz]$

where: $n_0 \left[\frac{rot}{min}\right]$ – instantaneous operating speed; z – number of gear teeth;

Therefore, the non-uniformity coefficient can be expressed as follows:

$$\delta_Q\% = \frac{\pi^2 m^2 cos^2\alpha}{d_e^2 - A^2} \quad (8)$$

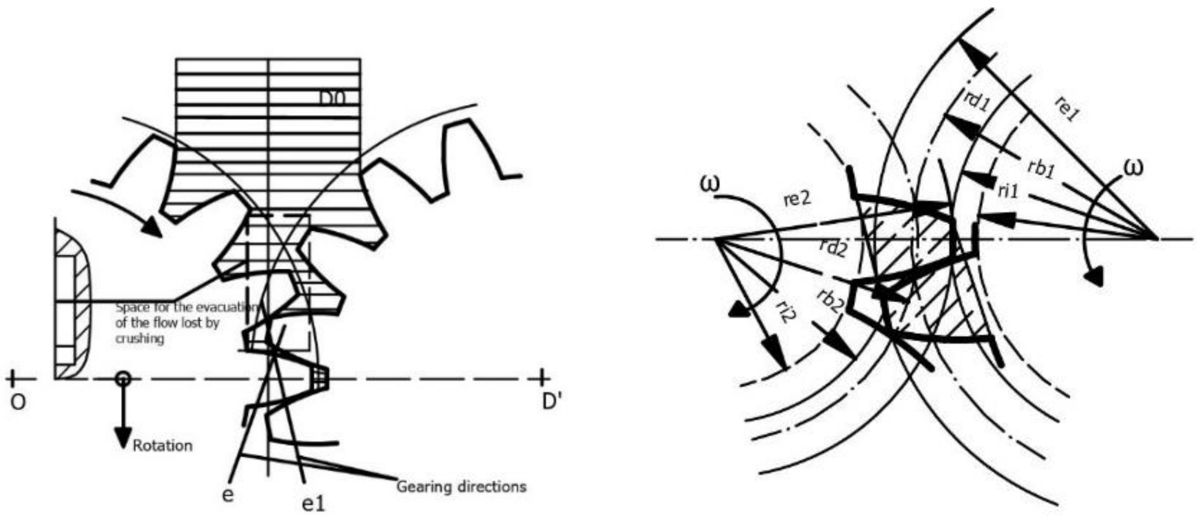

Fig. 1. Gear calculation parameters

3.2 Simulation method

CFD can be used to study and determine the fluid flow behavior inside the gear pump, particularly fluid dynamics influence on performance, efficiency and design. Computational fluid dynamics is based on numerical methods to solve complex equations governing fluid flow. Partial differential equations describe the manner in which momentum, energy and mass transfer occur in the fluid. Precise boundary conditions that define inlet and outlet pressures, flow rates and gear rotation speeds are imposed. Hydraulic fluid properties and thermal effects are taken in consideration in the gear pump model. Gear pump geometry is modeled by dividing the structures into smaller elements. The pump consists of two interlocking gears enclosed in a housing, the hydraulic fluid trapped and pressurized between the gear teeth and the walls. Fig. 2 illustrates a test conducted on a 2D model of a hydraulic gear pump. The geometry of the pump was initially modeled in Autodesk Inventor and then imported into Ansys Fluent. Design Modeler was used to extract the surface of the face and generate the mesh. In the first step, the network was created with default values. In the subsequent stage, element dimensioning was performed and to enhance the mesh quality, the triangle method was employed. Named selections were established for each component of interest, including the two gears, inlet, outlet and fluid. Improvements to the mesh quality in the toothed areas of the gears were achieved through additional element dimensioning in those regions. General simulation settings were configured, specifying the solver type, time and 2D space. Following this, model settings were adjusted in the viscous model sub-menu. The fluid and its composition were selected from the materials database. The cell zone status was set to fluid based on the chosen database entry. Boundary conditions were defined for each pump component in the model. To define the motion of the gears, a User Defined Function (UDF) was created for each gear.

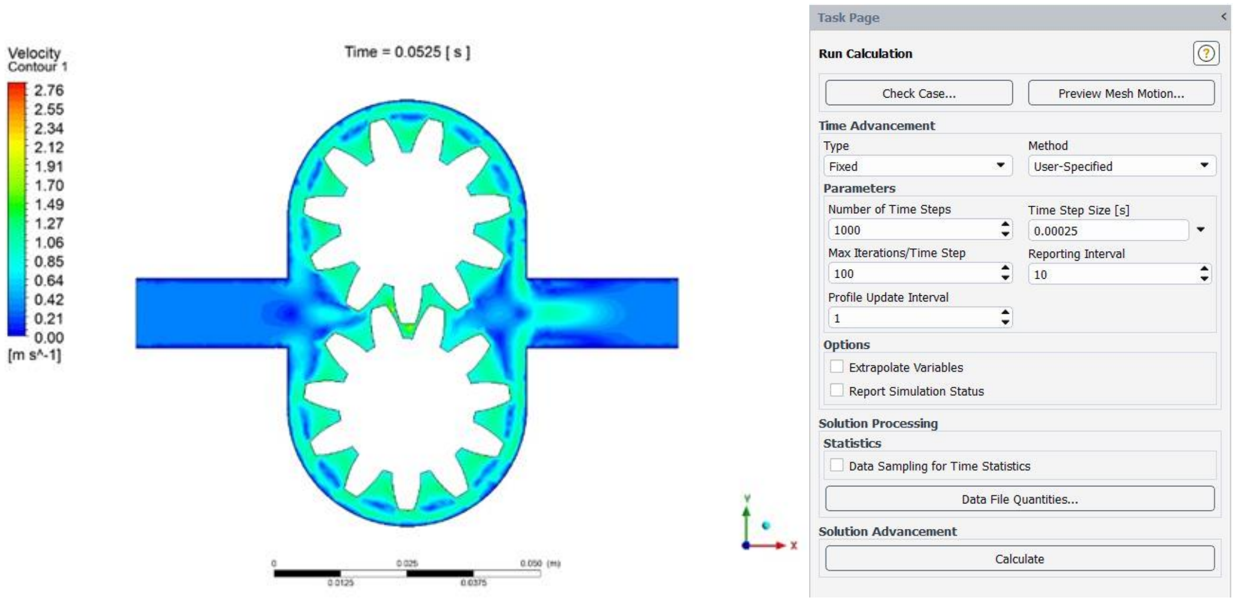

Fig. 2. Simulation parameters

The functions were then loaded into the library from the parameters and customization menu, specifically from the user-defined function section. Mesh methods were selected in the dynamic mesh settings, and the relationships between the UDF functions and the two gears were established. The solution method was chosen for each parameter in the menu. All zones were initialized using the 'Initialize' menu. Simulation parameters, such as the number of time steps, time step size, maximum iterations, and reporting interval, were configured in the 'Run Calculation' submenu, fig. 2. Subsequently, the 'Calculate' option was selected. After simulation, velocity, pressure and residual results were obtained. These simulations are at an early stage, with the phenomena taking place inside the pump to be studied further in more detail.

4. Conclusions

External gear pumps are a tried and tested design in hydraulic systems. However, there are still many aspects of how these mechanisms work that are still either incompletely described or could be improved. Using this aspect as a starting point, the authors tried to propose a methodology that could be applied to better understand and characterize the behavior of this type of pumps, with direct effects on the control of both pressure generation and flow characteristics. By mathematical modeling the flow rate in a gear pump, performance can be predicted under various operating conditions. It is fast, cost-effective and allows designs to be optimized before moving on to more detailed simulations or physical tests. More accurate results can be obtained by using advanced techniques such as CFD for the validation of the model. The fluid interaction with the mechanical components can be better understood with CFD. Valuable information can be revealed about pressure distribution, flow patterns and possible failure causes, such as cavitation or excessive wear. The performance of the gear pump could be optimized before the physical prototype is built by using CFD simulation results correlated with mathematical model result to modify the primary model with improved parameters core. As such, the paper first observes a general survey of how these gear pumps are simulated, with a strong focus on mathematical modeling and CFD simulations being prevalent in the field.

References

[1] Močilan, M., Š. Husár, J. Labaj, and M. Žmindák. "Non-Stationary CFD Simulation of a Gear Pump." *Procedia Engineering* 177 (2017): 532-539. https://doi.org/10.1016/j.proeng.2017.02.257.

[2] Qi, F., S. Dhar, V. Nichani, C. Srinivasan, D. Wang, L. Yang, Z. Bing, and J. Yang. "A CFD Study of an Electronic Hydraulic Power Steering Helical External Gear Pump: Model Development, Validation, and Application." *SAE International Journal of Passenger Cars - Mechanical Systems* 9 (2016): 346-352. https://doi.org/10.4271/2016-01-1376.

[3] Adake, D., N. Dhote, and M. Khond. "Experimentation and 2D Fluid Flow Simulation over an External Gear Pump." *Journal of Physics: Conference Series* 2601 (2023): 012029. https://doi.org/10.1088/1742-6596/2601/1/012029.

[4] Guerra, D., M. Polastri, M. Battarra, A. Suman, E. Mucchi, and M. Pinelli. "Design Multistage External Gear Pumps for Dry Sump Systems: Methodology and Application." *Mathematical Problems in Engineering* (2021): 8888128. https://doi.org/10.1155/2021/8888128.

[5] Houzeaux, G., and R. Codina. *Numerical Simulation of Gear Pumps*. Publication CIMNE Nº-224. Barcelona, International Center for Numerical Methods in Engineering, April 2003.

[6] Heisler, A., J. Moskwa, and F. Fronczak. "Simulated Helical Gear Pump Analysis Using a New CFD Approach." Paper presented at ASME 2009 Fluids Engineering Division Summer Meeting, Vail, Colorado, USA, August 2–6, 2009. https://doi.org/10.1115/FEDSM2009-78472.

[7] Sahoo, V., D. Roy, and R. Maiti. "Analysis of Leakage Flow Through the Flank Contacts in Transition Zone in Involute External Toothed Gear Pump." Paper presented at the ASME/BATH 2017 Symposium on Fluid Power and Motion Control, Sarasota, Forida, USA, October 16–19, 2017. https://doi.org/10.1115/FPMC2017-4287.

[8] Stan, L.C., and I. Călimănescu. "Computer Fluid Dynamics (CFD) Study of a Micro Annular Gear Pump." Paper presented at the 8th Advanced Topics in Optoelectronics, Microelectronics, and Nanotechnologies Conference ATOM-N 2016, Constanta, Romania, August 25-28, 2016. https://doi.org/10.1117/12.2241674.

[9] Szwemin, P., and W. Fiebig. "CFD Model of an External Gear Pump." Paper presented at the 1st Renewable Energy Sources - Research and Business Conference (RESRB-2016), Wrocław, Poland, June 22-24, 2016. *Lecture Notes in Mechanical Engineering* (2017): 221-231. https://doi.org/10.1007/978-3-319-50938-9_23.

[10] Romanenko, I., Y. Martseniuk, and O. Bilohub. "Modeling the Meshing Procedure of the External Gear Fuel Pump Using a CFD Tool." *Computation* 10, no. 7 (2022): 114. https://doi.org/10.3390/computation10070114.

[11] Strasser, W. "CFD Investigation of Gear Pump Mixing Using Deforming/Agglomerating Mesh." *Journal of Fluids Engineering* 129, no. 4 (April 2007): 476-484. https://doi.org/10.1115/1.2436577.

[12] Liping, C., Z. Yan, Z. Fanli, Z. Jianjun, and T. Xianzhao. "Modeling and Simulation of Gear Pumps Based on Modelica/MWorks®." Paper presented at the 8th International Modelica Conference, Dresden, Germany, March 20-22, 2011.
[13] Corvaglia, A., M. Rundo, P. Casoli, and A. Lettini. "Evaluation of Tooth Space Pressure and Incomplete Filling in External Gear Pumps by Means of Three-Dimensional CFD Simulations." *Energies* 14, no. 2 (2021): 342. https://doi.org/10.3390/en14020342.
[14] Orlandi, F., G. Muzzioli, M. Milani, F. Paltrinieri, and L. Montorsi. "Development of a Numerical Approach for the CFD Simulation of a Gear Pump under Actual Operating Conditions." *Fluids* 8, no. 9 (2023): 244. https://doi.org/10.3390/fluids8090244.
[15] Corvaglia, A., M. Rundo, S. Bonati, and M. Rigosi. "Simulation and Experimental Activity for the Evaluation of the Filling Capability in External Gear Pumps." *Fluids* 8, no. 9 (2023): 251. https://doi.org/10.3390/fluids8090251.
[16] Torrent, M., P. J. Gamez-Montero, and E. Codina. "Parameterization, Modeling, and Validation in Real Conditions of an External Gear Pump." *Sustainability* 13, no. 6 (2021): 3089. https://doi.org/10.3390/su13063089.
[17] Ionescu, Florin, Catrina Dumitru, and Dorin Alexandru. *Fluid mechanics and hydraulic and pneumatic drives* / *Mecanica fluidelor si actionari hidraulice si pneumatice*. Bucharest, Didactic and Pedagogical Publishing House, 1980.
[18] Rizescu, C. I., D. Besnea, D. Rizescu, E. Moraru, and V. Constantin. "Mechanical Analysis of Leaf Springs Realized by Additive Technologies." Paper presented at the International Scientific-Technical Conference MANUFACTURING 2019, Poznan, Poland, May 19-22, 2019. *Lecture Notes in Mechanical Engineering - Advances in Manufacturing II. Volume 1 - Solutions for Industry 4.0* (2019): 307-318. https://doi.org/10.1007/978-3-030-18715-6_26.
[19] Besnea, D., D. Rizescu, C. Rizescu, E. Dinu, V. Constantin, and E. Moraru. "Additive Technologies and Materials for Realization of Elastic Elements." Paper presented at the 2nd International Conference of Mechatronics and Cyber-MixMechatronics – 2018, ICOMECYME 2018, Bucharest, Romania, September 6-7, 2018 *Lecture Notes in Networks and Systems* 48 (2019): 62-70. https://doi.org/10.1007/978-3-319-96358-7_7.

ISSN 1454 - 8003
Proceedings of 2024 International Conference on Hydraulics and Pneumatics - HERVEX
November 13-15, Băile Govora, Romania

SOLUTIONS FOR WIND RESOURCE ESTIMATION ON DIFFERENT TERRAIN MODELS

Fănel Dorel ȘCHEAUA[1]

[1] "Dunarea de Jos" University of Galati, fanel.scheaua@ugal.ro

Abstract: *It is known that the growing need for energy has consequences that constitute major demands on the environmental conditions when the classical methods of obtaining are used. This is why this action to develop the capacity to produce energy from renewable sources must be Wind continued, among which wind power occupies a prominent place. Resource estimation is crucial for assessing the viability of wind energy projects. The accuracy of wind resource assessments depends heavily on the terrain over which the wind flows, as different terrains (flat, hill, mountain, coastal) affect wind behaviour in distinct ways. Solutions and methods for estimating wind resources across different terrain models can be developed by computational fluid dynamics (CFD) simulations intended for complex terrains (hill, mountain areas). CFD models simulate the flow of wind over various terrain features by solving the Navier-Stokes equations. The simulations account for the complex interactions between the wind and the terrain, including turbulence, vortex formation, and speed-up effects providing high accuracy for the complex terrains, modelling the local effects such as ridges, valleys, different obstacles and providing further detailed 3D wind flow data. Using numerical analysis methods for wind resource estimation over terrain is feasible, especially for preliminary analysis. It is performed meaningful analyses by processing and visualizing terrain preliminary data, being able to generate further wind profiles using empirical models, applying simple numerical methods in order to estimate wind flow over terrain, permitting the results visualization to gain insights into wind speed distribution and potential energy yield. The method for wind resource estimation depends heavily on the terrain complexity, the scale of the project, the available budget and the required accuracy. A numerical approach is presented in this paper necessary for analyzing the wind resource potential, involving a combination of mathematical models with advanced simulations in order to establish solutions function of terrain complexity type. Starting from specific wind velocity and roughness characteristic values for each terrain type, which can have impact on wind flow, by means of a numerical analysis method the mean wind velocity profile for different heights and terrain types is highlighted. The modelling method used is represented by the logarithmic wind profile method which uses the mathematical model to estimate the wind velocity values at different heights above the ground. This approach provides good estimation results for wind velocity profile over various terrain types.*

Keywords: *Wind resource, air pressure, energy production, terrain model, numerical analysis*

1. Introduction

Wind resource estimation on different terrains represents a critical aspect of planning and optimizing wind energy projects. The availability and characteristics of wind resources can vary significantly depending on the topography and surface features of a specific location.
Terrain influences wind patterns through factors such as elevation changes, surface roughness, and the presence of obstacles like forests or buildings, which affect wind speed, direction, and turbulence levels.
Flat terrain typically allows for more predictable and uniform wind flow, making it easier to estimate wind resources. However, complex terrains, such as mountainous areas, coastal regions, or urban environments, present additional challenges due to the variability in wind speed caused by topographical features. Wind speeds may accelerate over ridges, decelerate in valleys, and experience significant turbulence near abrupt changes in elevation. Similarly, coastal areas exhibit unique wind behaviours due to the interaction between land and sea, while forested and urban terrains introduce roughness elements that disrupt the wind flow.
Accurate wind resource estimation is essential for identifying suitable locations for wind farms, optimizing turbine placement and ensuring efficient energy production. The process involves a

combination of meteorological data collection, computational modelling and the use of specialized software to simulate wind flow across different terrains. Understanding how various terrains influence wind patterns is a key in reducing uncertainty of wind assessments and maximizing the potential of wind energy as a sustainable power source.

2. Wind resource estimation across various terrain models

Estimating wind resources accurately across different terrain models is crucial for optimizing wind energy projects. The complexity of the terrain significantly influences wind flow patterns, requiring tailored approaches and methodologies.

Table 1: The main characteristics of terrain types

Crt. No.	Terrain type	Characteristics	Average wind velocity up to 100 m altitude (m/s)
1.	Flat	Plains - homogeneously gentle terrains	12.5
2.	Complex Terrain	Hills, Valleys, and Ridges	16
3.	Coastal Areas	Sea coast-Sand open space	13
4.	Forested Areas	Forest roughness	18
5.	Urban or Built-Up Areas	Flow separation, turbulence, wind channelling	19
6.	Mountainous Regions	High altitude, steep slopes, temperature gradients	21

For flat terrain the wind flow is generally uniform with fewer disturbances.
Complex terrain can significantly alter wind flow due to topographical features causing speed-ups, turbulence and flow separations.
Coastal terrains pose unique challenges due to land-sea interactions, which create complex wind patterns.
In case of forests significant roughness are created, altering wind speed and turbulence.
Wind estimation in urban environments is complicated by the presence of buildings, which cause flow separation, turbulence, and wind channelling.
Mountainous terrains experience complex wind behaviour due to high altitude, steep slopes, and temperature gradients.
Wind estimation models include some atmospheric stability corrections, as thermal stratification which can significantly affect wind flow, especially in mountainous and coastal areas.
All the specific methods used to establish a wind model help to reduce uncertainties in wind resource assessments, leading to more accurate estimations and better-informed decisions for wind energy projects [1-7].

3. Mathematical model for wind flow potential on different terrain types

In order to establish a start point for modelling the wind flow action the fluid dynamics momentum equation is considered, in a simplified form where the wind action is affected by some factors like pressure gradients, terrain roughness, Coriolis force, or turbulence, that can be modified in accord with the terrain type:

$$\frac{\partial u}{\partial t}+(u\cdot\nabla)\cdot u=-\frac{1}{\rho}\cdot\nabla p+\nu\cdot\nabla^2 u+F_C+F_r \tag{1}$$

For flat terrain the wind velocity profile can be generated as a function of height *(z)* at which is considered the *u(z)* velocity and a constant *(k)* as Karman constant (0.4), using a logarithmic wind profile:

$$u(z) = \frac{u_n}{k} \ln\left(\frac{z}{z_0}\right) \tag{2}$$

For complex terrains, hills, valleys and ridges the wind flow rate is significantly affected from the initial uniform pattern due to topography influence:

$$u(z) = u_f(z) \cdot c_t \tag{3}$$

where:

$u(z)$ -wind velocity at height z;

$u_f(z)$-wind velocity for flat terrain;

c_t - terrain factor dependent on topographic features.

For complex terrains, the Navier-Stokes equations are able to provide an accurate solution by using specific CFD models. This approach considers the non-linear effects from turbulence, flow separation and surface roughness:

$$\frac{\partial u_i}{\partial t} + u_j \frac{\partial u_i}{\partial x_j} = -\frac{1}{\rho}\frac{\partial p}{\partial x_i} + \nu \frac{\partial^2 u_i}{\partial x_j^2} + F_i \tag{4}$$

where:

u_i -velocity components;

x_i -spatial coordinates;

F_i -external forces.

In order to model the wind resources across larger regions with complex terrain features (coastal areas or mountain ranges), meso-scale atmospheric models are used that simulate large-scale wind patterns, while micro-scale models (CFD or linear models) refine the estimates at the local scale. The approach involves for meso-scale the modelling and solving the governing equations for atmospheric flow in order to capture regional wind patterns and meteorological phenomena. Further, for micro-scale modelling the local terrain features, roughness, and obstacles are considered to refine wind velocity predictions [8-10].

If the terrain contains gentle slopes or hills, the velocity can be approximated using simplified models, as an approach is represented by Jackson and Hunt's linear velocity model, which estimates the increase in wind velocity:

$$\Delta u = u_0 \cdot \frac{h}{L} \tag{5}$$

where:

u_0 -undisturbed wind velocity;

h - hill height;

L - hill characteristic length scale.

Regarding the turbulences an important parameter is represented by the turbulence intensity on complex terrain models especially being modelled based on wind velocity standard deviation *(*σ_u*)*, and mean wind velocity *(*u*)* as follows:

$$I = \frac{\sigma_u}{u} \tag{6}$$

4. Numerical approach analysis for wind resource potential on different terrain types

Numerical approach to analyze wind resource potential involves the combination of mathematical models with advanced simulations to account for terrain complexity.
Based on the gathered wind velocity values and direction data from meteorological stations combined with collected terrain data, such as elevation, land use and roughness characteristics, which influence wind flow, using a numerical analysis method is computed the mean wind velocity profile for different heights and terrain types.
The main modelling method used is represented by the logarithmic wind profile method which uses the mathematical model to estimate the wind velocity values at different heights above the ground. This approach provides good estimation results for wind velocity profile over various terrain types. However, this method does not account for complex interactions, such as turbulence and localized effects due to topography [11-13]. Considering the principal terrain types parameters shown in table 2 and based on a different roughness heights characteristic for each terrain type according with their proper surface parameters (case 1 and case2), the wind velocity profile is calculated using the logarithmic wind profile method for each terrain type.
The results are presented in figure 1 and 2, showing the wind velocities for the considered terrain types according the two cases configurations regarding the roughness values.

Table 2: Terrain types parameters for analysis

Crt. No.	Terrain type	Average wind velocity up to 100 m altitude (m/s)	Roughness values (m)	
			Case 1	Case 2
1.	Flat	12.5	0.01	0.02
2.	Complex Terrain	16	0.5	0.6
3.	Coastal Areas	13	0.05	0.06
4.	Forested Areas	18	0.3	0.4
5.	Urban or Built-Up Areas	19	1.5	1.6
6.	Mountainous Regions	21	1.8	2

Based on the obtained results it can be observed that for the flat terrain where the low roughness values are encountered higher wind velocity values are registered near the ground and further this model is adopted also for the coastal areas. For the complex terrain type the roughness value is moderate due to the uneven surface distribution with higher velocity values, the forest areas present a higher roughness because of the trees presence and also an ascendant velocity trend especially beyond a height limit and finally the higher values registered by the urban and mountainous areas due to the high roughness from buildings and rocky mountain surfaces.

Updating the roughness values for each terrain type the obtained results are presented as modification in wind velocity profile with a low increase in the inferior height, but with considerable increase at higher altitude (100 m).

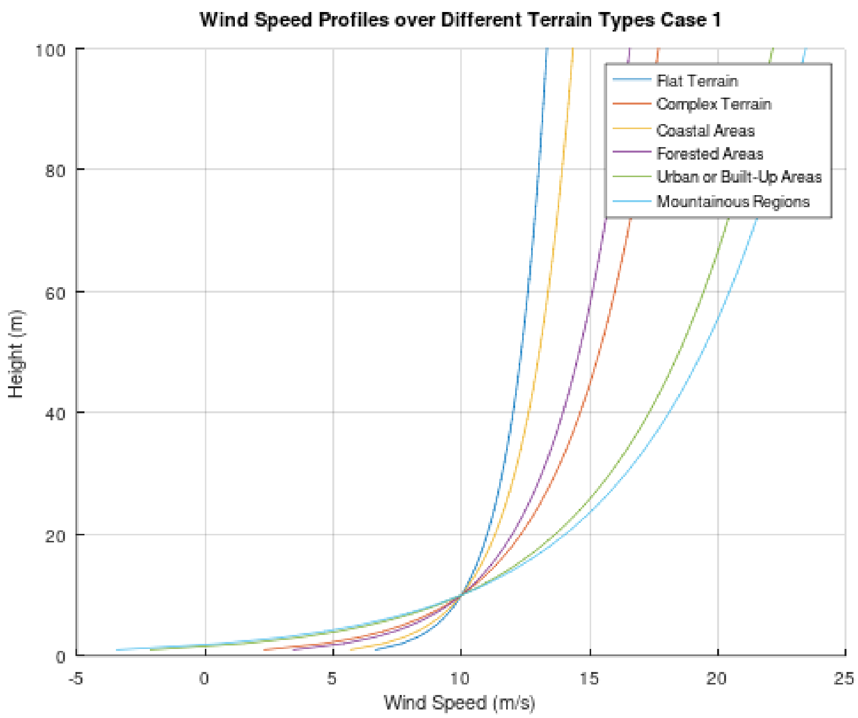

Fig. 1. Wind velocity profile on different terrain types (case 1)

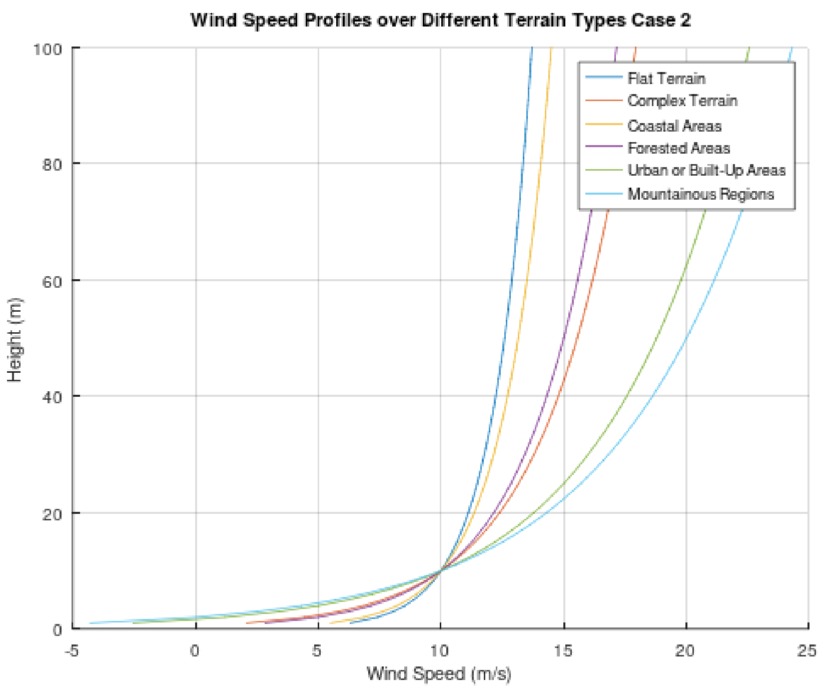

Fig. 2. Wind velocity profile on different terrain types (Case 2)

Based on the obtained results, it is possible to go further to establish the specific wind potential according to the height for the different land types. Considering that horizontal axis wind turbines of low installed power have the rotor positioned at heights between 90-120 m and even lower power vertical axis turbines that are used for residential applications have heights of up to 30 m, an analysis on the potential of wind action is carried out with emphasis on wind velocity function of height and further wind power density function on height values. The obtained results are presented in figure 3.

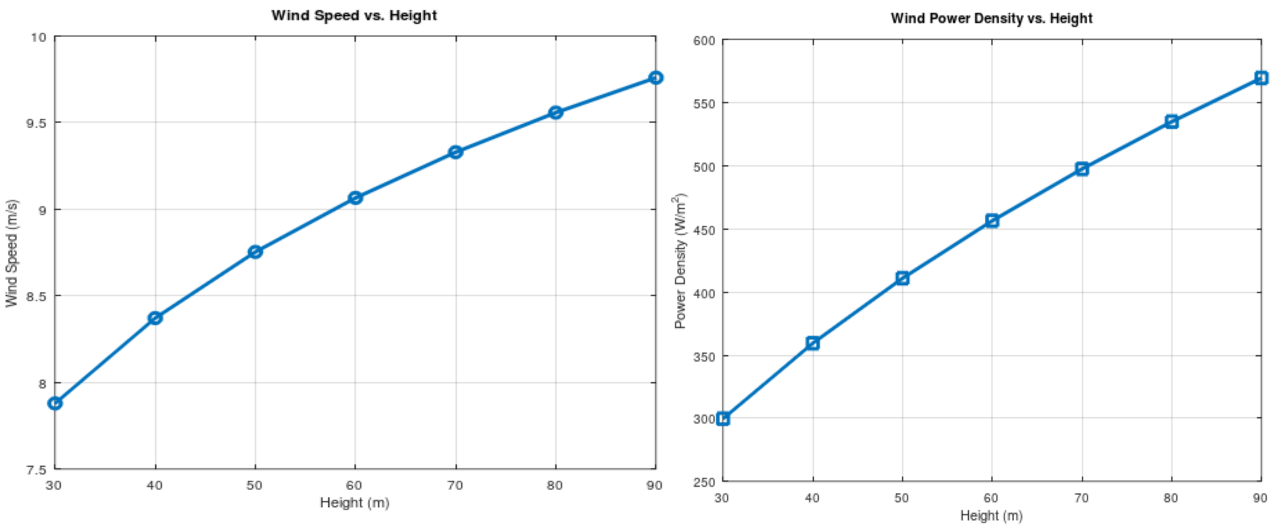

a) Wind velocity function of height values b) Wind power density function on height

Fig. 3. Wind power density and velocity profile on different heights

5. Conclusions

Wind potential varies significantly across different terrain models due to the influence of terrain features on wind speed, turbulence, and flow patterns. Understanding these variations is crucial for accurately assessing wind resources and optimizing wind energy projects. Here are some key conclusions regarding wind potential across various terrain types:
On flat, homogeneous terrain, wind flow is relatively uniform and the logarithmic wind profile method provides a good estimation of wind velocity distribution with height.
Wind potential is generally lower at ground level but increases predictably with height, so flat terrain is suitable for wind turbine installations, especially with taller towers to access the higher wind velocities.
In hilly areas, the topography causes wind speed-up on the windward side of hills and slow-down on the leeward side. The wind potential can be significantly higher in certain locations, like hilltops or ridge lines, compared to valleys.
Mountainous regions experience complex wind patterns with strong turbulence, flow separation, and localized wind accelerations due to steep slopes and valleys, while the potential can be high due to strong wind speed-ups in certain areas, but the variability and turbulence pose challenges for turbine installations and structural integrity.
Coastal terrains often experience steady, strong winds due to the lack of obstacles and proximity to open water. Sea breezes and topographic effects near cliffs or dunes can influence local wind patterns. The coastal regions typically have high wind potential, making them ideal for both onshore and offshore wind farms. The smoother terrain results in lower turbulence levels compared to inland mountainous areas.
Urban areas have high surface roughness due to buildings and other structures, leading to increased turbulence and variability in wind patterns. While wind speeds are generally lower at ground level, tall structures like skyscrapers can access higher winds.
Higher Roughness Length (forests, urban areas) leads to greater wind speed reduction near the surface and higher turbulence.

Lower Roughness Length (open plains, coastal areas) allows reaching higher wind velocities closer to the ground, improving wind turbine efficiency and reducing structural requirements.
The wind potential on different terrain models is shaped by a combination of factors such as surface roughness, topography and local climate conditions. While flat and coastal terrains provide more predictable wind profiles, hilly and mountainous areas can offer higher but more variable wind potential. Accurate wind resource assessment, using a combination of modelling techniques (logarithmic profiles, CFD, meso-scale/micro-scale coupling), is essential for optimizing turbine placement and maximizing energy yield across various terrains.

References

[1] Tabas, Daniel, Jiannong Fang, and Fernando Porté-Agel. "Wind energy prediction in highly complex terrain by computational fluid dynamics." *Energies* 12, no. 7 (2019): 1311.
[2] Gasset, Nicolas, Mathieu Landry, and Yves Gagnon. "A comparison of wind flow models for wind resource assessment in wind energy applications." *Energies* 5, no. 11 (2012): 4288-4322.
[3] Xu, Dong, Feifei Xue, Yuqi Wu, Yangzhou Li, Wei Liu, Chang Xu, and Jing Sun. "Analysis of Wind Resource Characteristics in the Ulanqab Wind Power Base (Wind Farm): Mesoscale Modeling Approach." *Energies* 17, no. 14 (2024): 3540.
[4] Qian, Guo-Wei, and Takeshi Ishihara. "A novel probabilistic power curve model to predict the power production and its uncertainty for a wind farm over complex terrain." *Energy* 261 (2022): 125171.
[5] Cheng, Xu, Bowen Yan, Xuhong Zhou, Qingshan Yang, Guoqing Huang, Yanwen Su, Wei Yang, and Yan Jiang. "Wind resource assessment at mountainous wind farm: Fusion of RANS and vertical multi-point on-site measured wind field data." *Applied Energy* 363 (June 2024): 123116.
[6] Jung, Christopher, and Dirk Schindler. "On the influence of wind speed model resolution on the global technical wind energy potential." *Renewable and Sustainable Energy Reviews* 156 (2022): 112001.
[7] Saadatabadi, Abbas Ranjbar, Nasim Hossein Hamzeh, Dimitris G. Kaskaoutis, Zahra Ghasabi, Mohammadreza Mohammadpour Penchah, Rafaella-Eleni P. Sotiropoulou, and Maral Habibi. "Optimization and evaluation of the Weather Research and Forecasting (WRF) model for wind energy resource assessment and mapping in Iran. " *Applied Sciences* 14, no. 8 (2024): 3304.
[8] Kogaki, Tetsuya, Kenichi Sakurai, Susumu Shimada, Hirokazu Kawabata, Yusuke Otake, Katsutoshi Kondo, and Emi Fujita. "Field measurements of wind characteristics using LiDAR on a wind farm with downwind turbines installed in a complex terrain region." *Energies* 13, no. 19 (2020): 5135.
[9] Zou, Yunfeng, Peng Yue, Qingkuan Liu, Xuhui He, and Zhen Wang. "Wind field characteristics of complex terrain based on experimental and numerical investigation." *Applied Sciences* 12, no. 10 (2022): 5124.
[10] Gottschall, Julia, Alkistis Papetta, Hassan Kassem, Paul Julian Meyer, Linda Schrempf, Christian Wetzel, and Johannes Becker. "Advancing wind resource assessment in complex terrain with scanning lidar measurements." *Energies* 14, no. 11 (2021): 3280.
[11] Quiroga-Novoa, Pedro, Gabriel Cuevas-Figueroa, José Luis Preciado, Rogier Floors, Alfredo Peña, and Oliver Probst. "Towards better wind resource modeling in complex terrain: A k-nearest neighbors approach." *Energies* 14, no. 14 (2021): 4364.
[12] Yamaguchi, Atsushi, Alireza Tavana, and Takeshi Ishihara. "Assessment of Wind over Complex Terrain Considering the Effects of Topography, Atmospheric Stability and Turbine Wakes." *Atmosphere* 15, no. 6 (2024): 723.
[13] Van Ackere, Samuel, Greet Van Eetvelde, David Schillebeeckx, Enrica Papa, Karel Van Wyngene, and Lieven Vandevelde. "Wind resource mapping using landscape roughness and spatial interpolation methods." *Energies* 8, no. 8 (2015): 8682-8703.

ISSN 1454 - 8003
Proceedings of 2024 International Conference on Hydraulics and Pneumatics - HERVEX
November 13-15, Băile Govora, Romania

METHOD AND MEANS OF TESTING LOW-HEAD HYDRAULIC TURBINES

Teodor Costinel POPESCU[1], Alina-Iolanda POPESCU[1], Rareș-Andrei CHIHAIA[2]

[1] National Institute of Research & Development for Optoelectronics / INOE 2000 – Subsidiary Hydraulics and Pneumatics Research Institute / IHP, Bucharest, popescu.ihp@fluidas.ro, alina.ihp@fluidas.ro

[2] National Institute for R&D in Electrical Engineering ICPE-CA Bucharest, rares.chihaia@icpe-ca.ro

Abstract: *Low-head hydraulic turbines, with maximum powers of 5 kW, exploit at low cost, in pico hydroelectric power plants without dams, flowing water courses with low flows and drops. Determining the optimal constructive variant of such a hydropower unit, which exploits with maximum efficiency a constant water drop, specific to a certain real water course, is done in successive loops of mathematical modeling, numerical simulation and experimental identification. Within these loops, experimental testing of the models is decisive; if this is performed in the laboratory, on dedicated stands, for all models, and the "in-situ" testing is done only for the optimal model, the final costs of achieving the optimal turbine constructive variant are significantly reduced. The article presents a constructive variant for such a stand, which reproduces in the laboratory a real and constant water drop, accompanied by the method of testing the hydraulic turbines, mounted at the upper end of the respective drop. A mixed team from two national research and development institutes, led by the main author of the article, is participating in the creation of this stand, for which a patent application has been filed.*

Keywords: *Low-head hydraulic turbine, optimal model, test stand, test method*

1. Introduction

The most common natural hydrological conditions in low-lying areas, prevalent in Central Europe, are characterized by low flows on small and medium-sized watercourses. Such conditions allow the use of the energy of the head of the water drop by means of water wheels, Banki-Mitchell turbines and propeller turbines [1,2,3].

Small hydraulic turbines, a category that also includes low-head hydraulic turbines, are installed at the head of the water drop, at the level of the upper basin, figure 1-left, while large hydraulic turbines require installation below the water table, at the level of the lower basin, figure 1-right. The water drop, denoted by ***H*** in figure 1, is defined as the distance in meters between the water levels in the two basins.

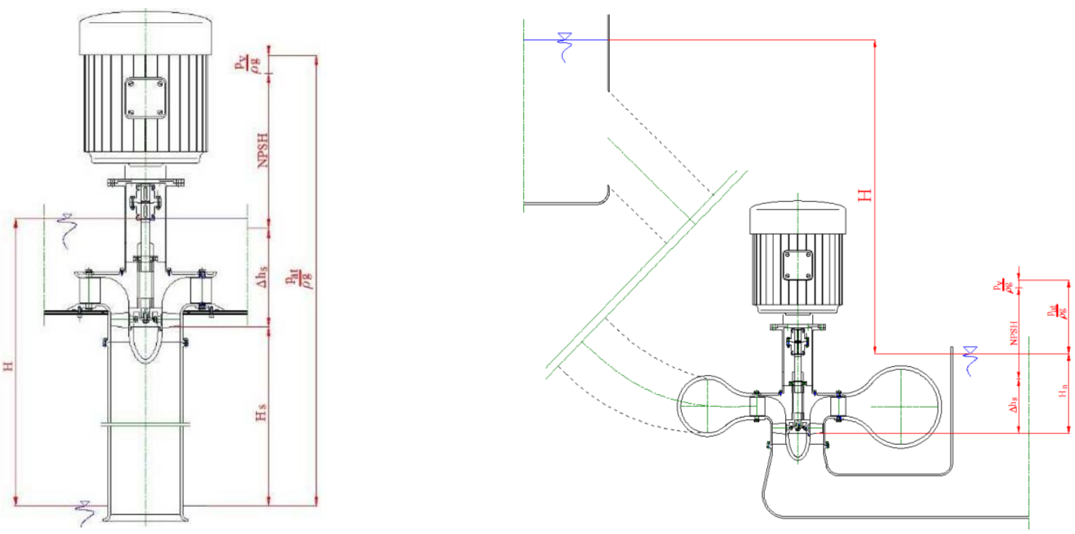

Fig. 1. Installation of hydraulic turbines: left - small turbines; right - large turbines [3]

Mini and pico hydraulic turbines, which operate at a low water drop, of a few meters, have the important advantage that they can work with suction and can be installed at the head of the water drop. This is due to the cavitation reserve of the turbine which, in this case, is much lower than the atmospheric pressure. As a result, a water drop of a few meters allows the turbines to operate practically without an inlet flow, since almost the entire drop takes place in the suction pipe. This construction of the turbine installation significantly reduces the investment cost.

Fig. 2. Installation of low-head hydraulic turbines (at the head of the water drop)

Figure 2 shows the installation of a low-head hydraulic turbine under real operating conditions, with low investment costs, on a small water drop on a river, at the head of the water drop.
Depending on the type of hydraulic energy converted into electrical energy, hydraulic turbines are divided into two categories: *"flow (speed) turbines"*, which harness the kinetic energy, respectively the flow rate $\boldsymbol{Q}$ [m^3/s] or the speed $\boldsymbol{v}$ [m/s] of the water and "*drop turbines*", which exploit the potential energy, respectively the drop $\boldsymbol{H}$ [m] of the water. Therefore, the experimental test stands for hydraulic turbines will be "flow (velocity) stands", with larger horizontal dimensions and "drop stands", with larger vertical dimensions.
A constructive solution for a “drop stand” is presented below, original in the way of achieving a prescribed constant drop $\boldsymbol{H_p}$, [4]. This drop can be adjusted in a range with a length proportional to the vertical dimension of the stand.

2. Vertical stand for testing low-head hydraulic turbines

This stand makes more energy efficient the operation of a constant-level tank [5], located at a height and permanently supplied with an inflow flow rate greater than the useful flow rate (effluent), $\boldsymbol{Q_u}$, required by the consumer (the tested turbine), the excess flow rate $\boldsymbol{Q_e}$ being discharged into a second basin, located on the ground, from where it is taken over by a pumping group with a constant flow rate.
The energy efficiency of the constant-level tank is achieved by automatically regulating the flow rate of a pumping group, $\boldsymbol{Q_p}$, consisting of three adjustable pumps, coupled in parallel. The pumping group sucks from a lower tank, located on the ground and discharges into an upper tank, located at a height and which communicates through a vertical pipe with the first, so that $\boldsymbol{Q_e = Q_p - Q_u = 0}$, and the drop $\boldsymbol{H}$, defined as the distance between the water levels in the two superimposed tanks, remains constant [6].

2.1 Constructive-functional scheme of low-head hydraulic turbine test stand

The construction-functional scheme of the stand in Figure 3 contains the following subassemblies:
1- **adjustable flow pumping group**, consisting of three adjustable centrifugal pumps (**1.1, 1.2, 1.3**), connected in parallel to sum the flow rates, each driven in rotational motion by a 380 V electric motor, equipped with a frequency converter for rotational speed regulation. Each pump, separated from the

suction/discharge manifolds of the group with isolation valves (a check valve is also mounted before the discharge valve) sucks, through the pipe **1.4** from the lower tank and discharges, through the pipe **1.5**, into the upper tank. Elastic sleeves are mounted between these pipes and tanks, which stop the propagation of vibrations of the pumping group to the tanks. For any excess flow, occurring in the event of a possible failure of the automatic flow rate regulation system, the overflow pipe **1.6** was provided.

2-lower tank, equipped with: the partition wall **2.1**, separating the suction and discharge compartments of the pumping group; the cover **2.2** equipped with atmospheric contact; the level glass **2.3**, for viewing the water level;

3-upper tank, equipped with: the spillway threshold **3.1**, which separates the compartment connected to the discharge pipe, from the compartment connected to a transparent tube, through which the water flows into the lower tank; the cover **3.2** equipped with atmospheric contact; the level glass **3.3**, for viewing the water level;

4-vertical and submerged pipe, formed by a transparent plexiglass tube **4.1**, equipped with the flange and gasket **4.2**, above which the model of the low-head turbine to be tested is mounted;

5-model of the low-head turbine to be tested, formed by the stator **5.1** and the rotor **5.2**;

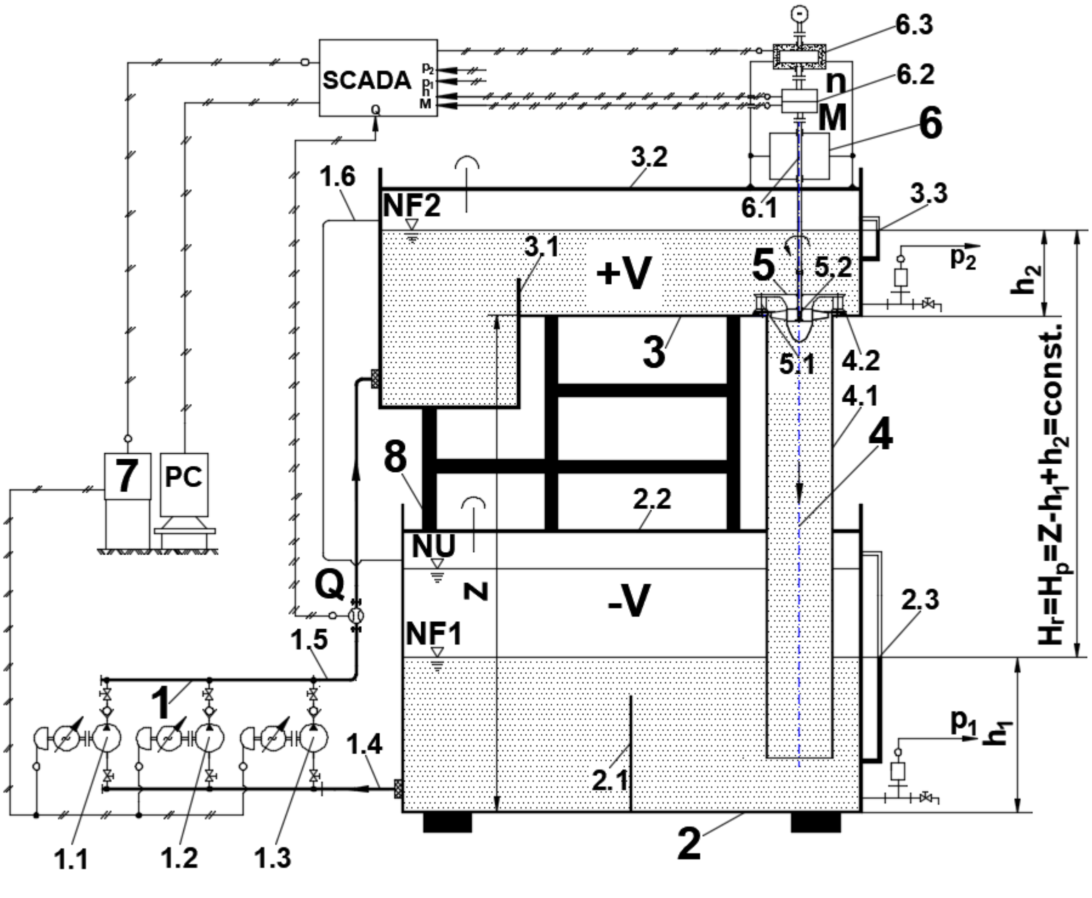

Fig. 3. Constructive-functional scheme of low-head hydraulic turbine test stand

6-adjustable braking system, which is coupled to the turbine shaft and consists of: shaft **6.1**, with two radial-axial bearings; torque and rotational speed transducer **6.2**; magnetic powder brake **6.3**, with adjustable resistive torque depending on the supply current; a 24 V DC electric motor, necessary to drive the brake before starting the tests on the stand, for homogenizing the magnetic powder and determining the value of the friction torque in the bearings;

7-electrical panel for powering the motors of the pumping group and the SCADA system;

8-metal support for the two tanks, equipped with verticality adjustment screws.

The stand is equipped with the following four transducers, respectively: $\boldsymbol{p_1}$, $\boldsymbol{p_2}$ **- hydrostatic pressure transducers**, mounted at the base of the tanks (between the tank and the drain valve), which indirectly measure the water levels in the two tanks:

$$\boldsymbol{h_1 = \frac{p_1}{\rho \cdot g}} \; ; \; \boldsymbol{h_2 = \frac{p_2}{\rho \cdot g}}, \qquad (1)$$

in which: $[\rho] = 1000\ Kg/m^3$, $[g] = 9{,}81\ m/s^2$, $[p_1, p_2] = N/m^2$, $[h_1, h_2] = m$

Q-flow transducer, which is mounted on the **1.5** pipe and measures the flow rate of the pumping group;
M, n-torque and rotational speed transducer, which measures the mechanical parameters of the tested turbine.
The SCADA system of the stand, equipped with a power supply, programmable automation PLC, the four transducers and the magnetic powder brake ensures monitoring of the parameters of the tested turbine, automatic control of the stand and experimental data acquisition.

2.2 The operating principle of the stand

The stand circulates, in a closed circuit, a volume of water between two vertically superimposed tanks; between the lower tank and upper tank the water is forcibly circulated by pumping, and in the opposite direction, the water flows by gravity through the transparent circular tube, at the end of which the tested hydraulic turbine is mounted.

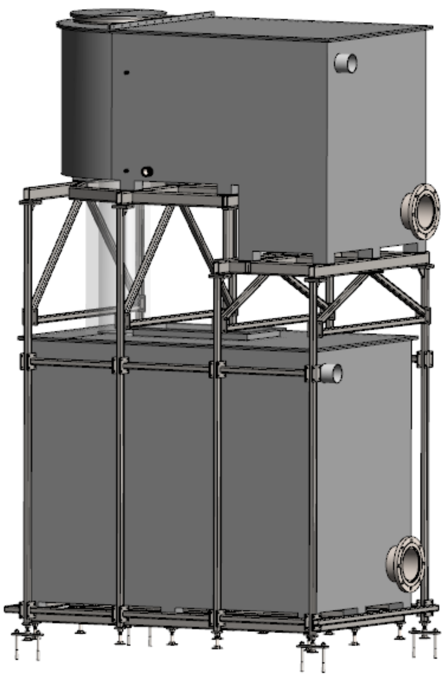

Fig. 4. Subassembly of overlapped tanks

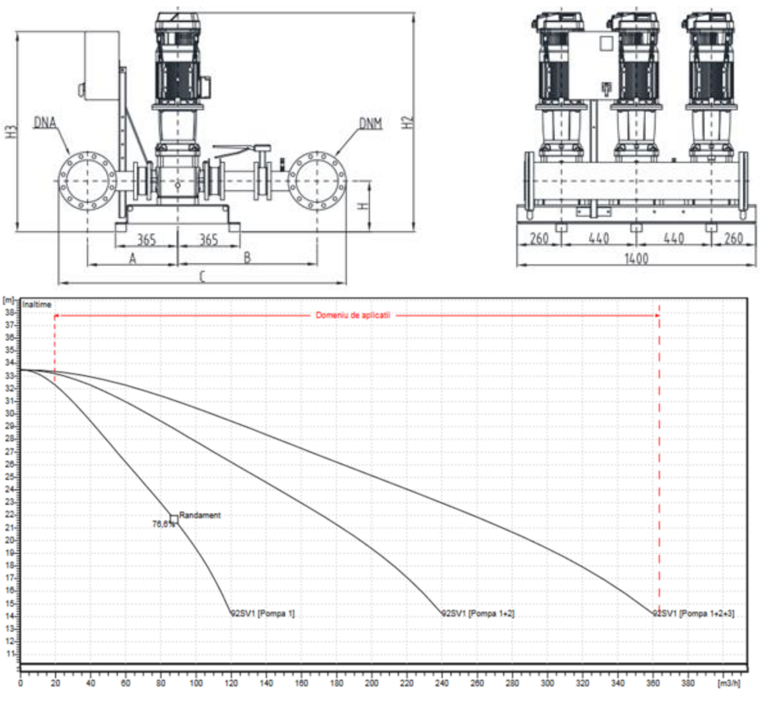

Fig. 5. Pumping group with adjustable flow (3 centrifugal electric pumps model 92SV1N075T-LOWARA)

Before putting the stand into operation, the lower tank is filled with clean water up to the filling level **NU** (Fig.3). Then, the pumping drop that the pumping group $\boldsymbol{H_r}$ must achieve, at which the experimental tests will be performed, is prescribed from the SCADA programmable controller.
+V, -V represent the volume of water sucked (-V) by pumping, from the lower tank, respectively the volume of water discharged (+V) by pumping, into the upper tank, to achieve the water drop $\boldsymbol{H_r}$.

ISSN 1454 - 8003
Proceedings of 2024 International Conference on Hydraulics and Pneumatics - HERVEX
November 13-15, Băile Govora, Romania

The SCADA system, in connection with the transducers p_1 and p_2 (which measure the water levels in the tanks h_1 and h_2), will automatically adjust the flow rate of the pumping group (by modifying the driving rotational speed of the three pumps) so that:

- the forcibly circulated flow rate, by pumping, Q_p, is equal to the useful flow rate, Q_u, necessary for the tests, which flows by gravity;
- after equalizing the flows and achieving the drop H_r, the flow value Q_p should be kept constant.

The equation that highlights the automatic flow regulation for a given reference pumping head is:

$$H_r = H_p = Z - h_1 + h_2 = const. \tag{2}$$

where Z is the distance in meters between the two pressure transducers, mounted in proximity of the bottoms of the overlapping tanks.

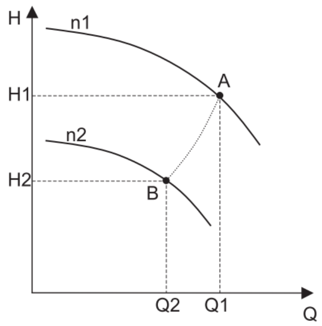

$n_1 > n_2$

n_1 = initial rotational speed; Q_1 = initial flow rate;
H_1 = initial drop; P_1 = initial power;

n_2 = necessary rotational speed; Q_2= necessary flow rate;
H_2 = necessary drop; P_2 = necessary power.

Fig. 6. Modification of pump parameters (Q, H, P) by varying its drive rotational speed

The installation of the frequency converter on each of the three pumps makes it possible to vary their drive rotational speed. The variations of pump rotational speed, figure 6, have the effect of modifying the flow rates Q, the drops H and the powers P according to the following equivalence relations:

$$\frac{Q_1}{Q_2} = \frac{n_1}{n_2} \; ; \; \frac{H_1}{H_2} = \left(\frac{n_1}{n_2}\right)^2 \; ; \; \frac{P_1}{P_2} = \left(\frac{n_1}{n_2}\right)^3 \tag{3}$$

2.3 The main functional characteristics of the stand

Overall dimensions (height x width x length): *4.2 m x 1.5 m x 3 m*;
Volume of the tanks: lower tank *V = 3840 l*; upper tank *V = 2400 l*;
Adjustment range of the water drop (distance between the water levels in the tanks): *H = 2.2-2.4 m*;
Types of low-head hydraulic turbines that can be tested: *Vortex, helical, etc.*;
Measurements and tests that can be performed: *flow rate and pressure* in the turbine suction; *torque* and *rotational speed* at the turbine shaft; stationary curves of *variation of torque and rotational speed* at the turbine shaft, *function of load and flow rate*;
Inner diameter of the vertical transparent plexiglass pipe: $Ø_i$ *= 230 mm*;
Pumping group consisting of 3 pumps connected in parallel: flow rate *Q = 100 l/s* at load *H = 2.4 m*;
Electric motor with frequency converter for pump drive (3 pcs.): power / supply voltage / frequency / rotational speed = *7.5 kW / 3x380-415 V / 50Hz / 2900 rpm*;
Nominal diameter of suction / discharge pipe: *DN 200 mm*;
Overflow pipe diameter: *110 x 3.2 mm*;
Outer diameter of the turbine rotor tested on the stand: $Ø_e$ *= 228 mm*;

Measuring range of the transducers: flow rate transducer $Q = 34\text{-}1131\ m^3/h$; static pressure transducer $p = 0\text{-}0.25\ bar$; torque and rotational speed transducer: $M = 0\text{-}20\ Nm$; $n_{max} = 3000\ rpm$;
Magnetic powder brake: torque $M = 0\text{-}35\ Nm$; rotational speed $n = 60\text{-}3000\ rpm$.

3. The method testing low-head hydraulic turbines

The method of testing low-head hydraulic turbines, on the stand in Fig. 3, contains two types of operations: *stand preparation operations* for experimental testing; *determination of the functional characteristics* of the tested turbine model.

3.1 Stand preparation operations

Check the verticality of the two overlapping tanks as a whole. The verticality of the overlapping tanks will be checked and restored, if it is necessary (by operating the adjustment screws on the tanks support).
Filling the stand with water, adjusting the water level, pumps aeration, mounting the turbine and braking system. The lower tank will be filled, with clean and filtered water from the mains, until the water reaches the filling level **NU**, visualized on the level indicator **2.3**. This level is calculated so that the volume of water from the tank to ensure the filling of the pumping circuit consisting of: suction pipe + pumping group + discharge pipe + upper tank maximum level + transparent vertical pipe***;*** If it is necessary, the drain valve near the transducer $\mathbf{p_1}$ is also used to adjust the filling level. The pumps aeration is done by unscrewing / tightening of the vent caps of each pump. On the flange of the transparent tube, the model **5** of the turbine to be tested will be mounted, to which the adjustable braking system **6** will be connected.
Prescribed drop value $\boldsymbol{H_r = H_p}$***, defined*** by equation (2).
Start the pumping group and initiate the flow adjustment program. The operation will be performed in two steps:
step 1**:** the pumps of the group are started, at ½ of the nominal rotational speed, to fill the hydraulic circuit and the upper tank up to the level of the overflow threshold **3.1**, which separates the tank into two compartments;
step 2*:* when the water reaches the level of the spillway threshold **3.1** and flows by gravity through the transparent tube into the lower tank, the program compares, by analyzing the water levels in the tanks, the flow rate $\boldsymbol{Q_s}$ of the flow through the vertical transparent tube, which depends on the shape of the tested turbine and the vortex formed at the turbine outlet, with the flow rate $\boldsymbol{Q_p}$ of the pumping group. Two situations can occur:
2.1 if $\boldsymbol{Q_s > Q_p}$, because in the upper tank the water stagnates at the level of the spillway threshold for a calculated time interval, in which the hydrostatic pressure transducer $\boldsymbol{p_2}$ does not transmit information of the level increase in the upper tank**,** the **SCADA** system commands the automatic increase of the flow of the pumping group, by increasing the drive rotational speed of the pumps, until the achieved drop $\boldsymbol{H_r}$ equals the prescribed drop $\boldsymbol{H_p}$. From that moment, when the operating levels **NF1** and **NF2** are stabilized in the two tanks, and a volume **V** of water is transferred by pumping from the lower tank **-V** to the upper tank **+V,** the **SCADA** system will provide a closed-loop adjustment of the rotational speed of the pumps, implicitly of the influent flow to the upper reservoir, for the constant maintenance of the drop $\mathbf{H_r=H_p=Z-h_1+h_2}$, implicitly of the effluent flow to the upper reservoir;
2.2 *if* $\boldsymbol{Q_s < Q_p}$*,* the **SCADA** system commands the automatic reduction of the pumps rotational speed, and upon receiving the prescribed value of the drop $\boldsymbol{H_p}$, the system acts to keep it constant, implicitly the effluent flow to the upper tank.

3.2 Determination of functional characteristics of tested turbine model

On the stand, two mechanical parameters (torque $\boldsymbol{M}$ and rotational speed $\boldsymbol{n}$) and two hydraulic parameters (drop $\boldsymbol{H}$ and flow rate $\boldsymbol{Q}$) can be measured. With the measured parameters, three types of functional characteristics of the turbine model installed on the stand can be determined, namely:

characteristic $M = f(Q)$ at M_r = const., respectively the moment at the turbine axis as a function of flow at constant load (the same supply current of the magnetic powder brake) determined experimentally for several constant drops H;
characteristic $n = f(Q)$ at M_r= const., respectively the rotational speed at the turbine shaft as a function of flow at constant load, determined experimentally for several constant drops H;
characteristic $n = f(M_r)$ at Q = const., respectively the rotational speed as a function of load at constant flow rate, determined experimentally for several constant flow rates Q.

4. Conclusions

- The presented stand is intended for testing low-head axial hydraulic turbines with a vertical shaft; these turbines are mounted at the head of the water drop.
- The stand is supplied by a height tank with a constant level, for which the inflow flow, respectively the supply flow of the stand, is equal to the effluent flow, respectively the useful flow of the stand for low-head hydraulic turbine tests.
- The stand regulates the water drop in the vertical section of the turbine test and maintains the adjusted value constant during the experimental tests.
- The water drop from permanent watercourses is simulated in a transparent vertical pipe, made of Plexiglass, supplied by a constant level tank.
- The stand allows the determination of the following functional characteristics of the tested hydraulic turbine: characteristic $M = f(Q)$ at $M_r = const.$, respectively the moment at the turbine shaft as a function of flow at constant load, which can be determined experimentally for several constant drops H; characteristic $n = f(Q)$ at $M_r = const.$, respectively the rotational speed at the turbine shaft, as a function of flow at constant load, which can be determined experimentally for several constant drops H; characteristic $n = f(M_r)$ at $Q = const.$, respectively the rotational speed as a function of load at constant flow, which can be determined experimentally for several constant flow rates Q.

Acknowledgments

The work was carried out through the Core Program within the National Research Development and Innovation Plan 2022-2027, carried out with the support of the Romanian Ministry of Research, Innovation and Digitalization (MCID), project no. PN 23 05.

References

[1] Popescu, Teodor Costinel, Alexandru-Polifron Chiriță, Sergiu Nicolaie, and Rareș-Andrei Chihaia. “Aspects Regarding the Design of a Low-Head Hydraulic Turbine Test Stand.” Paper presented at the 12th International Conference KOD 2024 - Machine and Industrial Design in Mechanical Engineering, Balatonfured, Hungary, May 23-26, 2024.
[2] Peczkis, G., Z. Goryca, and A. Korczak. ”Axial pico turbine – construction and experimental Research”. Paper presented at the 15th International Scientific and Engineering Conference Hermetic Sealing, Vibration Reliability and Ecological Safety of Pump and Compressor Machinery HERVICON+PUMPS-2017, Sumy, Ukraine, September 5–8, 2017. *IOP Conference Series: Material. Science and Engineering* 233 (2017): 012016. DOI: 10.1088/1757-899X/233/1/012016.
[3] Różowicz, Sebastian, Zbigniew Goryca, Grzegorz Peczkis, and Andrzej Korczak. ”Pico hydro generator as an effective source of renewable energy”. *Przegląd Elektrotechniczny* 95, no. 4 (2019): 200-204. DOI: 10.15199/48.2019.04.37.
[4] Popescu, Teodor Costinel, and Alina-Iolanda Popescu. "Considerations on Making Test Stands for Small Hydraulic Turbines." *Hidraulica Magazine*, no. 3 (September 2024): 19-32.
[5] Cazacu, Mircea. “Constant level reservoir” / “Rezervor de nivel constant”. Patent No. RO95193(B1)-16.09.1988, OSIM.
[6] Popescu, Teodor Costinel, Marian Blejan, Alexandru-Polifron Chiriță, Ștefan Mihai Șefu, Sergiu Nicolaie, Rareș-Andrei Chihaia, Gabriela Cîrciumaru, and Florentina Bunea. “Hydraulic turbine test stand fed by means of a constant level reservoir” / “Stand de încercări turbine hidraulice alimentat cu rezervor de nivel constant”. Patent application No. A/00367-26.06.2024, OSIM.

ISSN 1454 - 8003
Proceedings of 2024 International Conference on Hydraulics and Pneumatics - HERVEX
November 13-15, Băile Govora, Romania

USING MODERN CAD-CAE DESIGN METHODS TO DESIGN A SEEDER FOR DIRECT SOWING INTO MEADOW FIELD

Ștefan DUMITRU[1,*], Nicolae-Valentin VLĂDUȚ[1], Eugen MARIN[1], Dragoș MANEA[1], Radu-Iulian RĂDOI[2]

[1] National Institute of Research - Development for Machines and Installations Designed to Agriculture and Food Industry - INMA Bucharest / Romania

[2] National Institute of Research & Development for Optoelectronics / INOE 2000 – Subsidiary Hydraulics and Pneumatics Research Institute / IHP, Bucharest / Romania

Abstract: *The present work presents the constructive description of a technical equipment, which carries out the sowing directly in the stubble of creeping plants (maize, sunflower, etc.), whose execution project used modern CAD-CAE design methods. The reasons that imposed the approach of some modern CAD-CAE methods are the following: - reducing design time and eliminating specialized capabilities by: creating files for CNC machines (stamping, bending, laser cutting, vertical and horizontal machining centers, etc.) or obtaining injection molds for plastic parts; - the ability to design parts in an assembly context; - granting view, search, modification and annotation for project related files; - checking for interference between parts of assemblies, detecting collisions between moving parts, quickly changing a dimension in three dimensions, checking for static load resistance through finite element analysis (FEA) and submitting these changes to the execution drawings. The direct-in-stubble weed planter, which was designed using CAD-CAE design, is intended for the establishment of weed crops on fields with unploughed grass cereal stubble for the second crop or after harvesting other plants (sunflower, soybeans, etc.) on soils not plowed or insufficiently prepared for spring sowing.*

Keywords: *CAD-CAE, direct sown, hoeing plants*

1. Introduction

Continuing to practice conventional agriculture will lead to negative effects on the environment by degrading the main component, the soil, affecting the development of a healthy society [1].
By practicing sustainable agriculture, the aim is to produce agricultural products with positive effects on the environment, while ensuring, at the same time, food for future generations [2].
In the countries of the European Union there is a requirement for the promotion of conservative agriculture, in this sense, the European ecological agreement aims in particular to achieve a fair, healthy and environmentally friendly food system [3].
Conservative systems, which are based on less intensive agricultural land work, represent a viable solution to promote environmental protection, because by storing organic carbon, they lead to a more productive and resistant soil [4].
The evaluation of a tillage system in the conservative category is done by determining the degree of surface coverage with plant residues or protective crops [5].
Direct seeding helps maintain good soil structure by leaving earthworms and plant roots undisturbed, which creates durable drainage channels and pore spaces that remain even after the crop has been harvested [6].
Depending on the degree of coverage of the soil surface with plant residues, the intensity and the method of tillage, the most conservative system is sowing directly in the stubble [7].
Under these conditions, at INMA Bucharest, for the establishment of spring crops by direct sowing in stubble or on land prepared with minimal work, a seeder of creeping plants for direct sowing in stubble was designed as part of a research project financed by the ADER sector program of MADR, whose patent application with the title ”*Tillage equipment and seeding weeds directly into the meadow field*” was registered at OSIM with no. A00562/20.09.2024.
The software SOLIDWORKS® was used for the design [8].

The shift from two-dimensional to three-dimensional design was a very important step in computer-aided design, as designed objects begin to have a shape and thus can be seen from any direction [9].
The reasons that imposed the way of embarking on the execution projects of the performance of technical equipment of direct seeding in stubble and on ridges for leek crops using modern CAD methods through 3D modeling with the parametric design program, were the reduction of design time, the increase of the capacity of designing parts in an assembly context and checking for interference between parts of assemblies, detecting collisions between moving parts, quickly changing a dimension in three dimensions and passing these changes to production drawings [10].

2. Materials and methods

The seeder of creeping plants for sowing directly in stubble (fig. 1) performs the following operations in a single pass:

- uncovering stubble or topsoil by creating a strip 20 centimeters wide and 2 cm deep cleared of plant debris by the two notched discs mounted inclined;
- cutting weeds, plant debris and notching the soil in a vertical plane along the axis of the row to be sown, to a depth of 4...15 cm by the notched straight disc;
- penetrating the soil to a depth of 2...20 cm to create a channel filled with loose soil by breaking and partially driving the soil with the chisel knife;
- the mobilization and loosening of the soil in strips with a width of 20 cm and a depth of 2...8 cm by the pair of spherical discs;
- the sown hoeing plants.

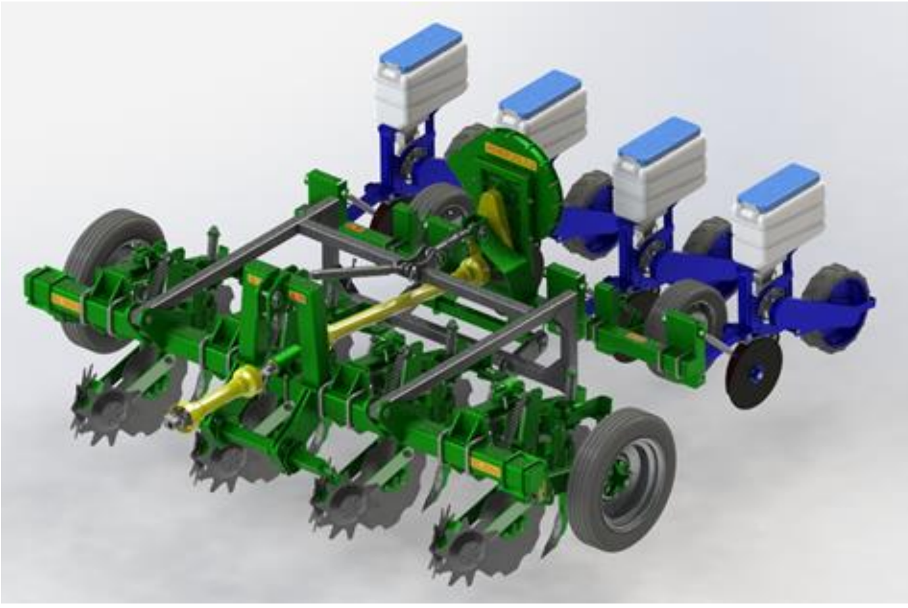

Fig. 1. Cultivator seeder for sowing directly into stubble

A constructive optimization method of a subassembly was used in the work ”Seeder support” from the structure ”Tillage equipment and seeding weeds directly into the meadow field”, by using static analysis with finite elements.
In the first stage of this study, the three-dimensional geometric model of the subassembly was made ”Seeder support” (fig. 2). For this purpose was used a Workstation 22H2, Intel(R) Xeon(R) W-2123 CPU @ 3.60GHz. The 3D modeling was done with the parameterized design program SOLIDWORKS® Premium 2018.

Three-dimensional modeling of the subassembly ”Seeder support” was made in the module „Parts” from the design program, in figure 3 two different views of the obtained model are presented, as well as the program interface SOLIDWORKS® Premium 2018.
After completing this step, the next step was to enter the 3D geometric model of the subassembly ”Seeder support”, in the module „Simulation” of the design program.
In the construction of welded metal constructions, different metal materials are used, which mitigate the negative influence of disturbing factors that occur directly during work, such as: shocks, vibrations, uneven terrain, the appearance of rigid obstacles, etc. [11].

Fig. 2. The three-dimensional geometric model of the subassembly ”Seeder support”- isometric view

a.

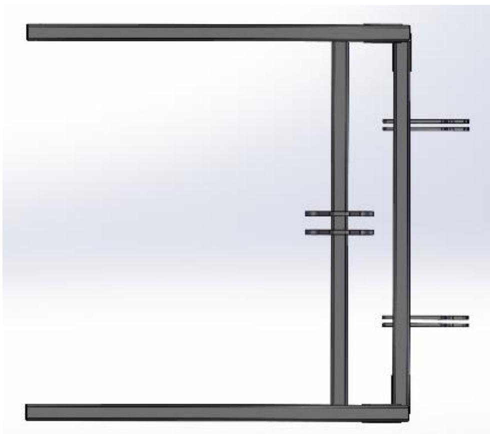

b.

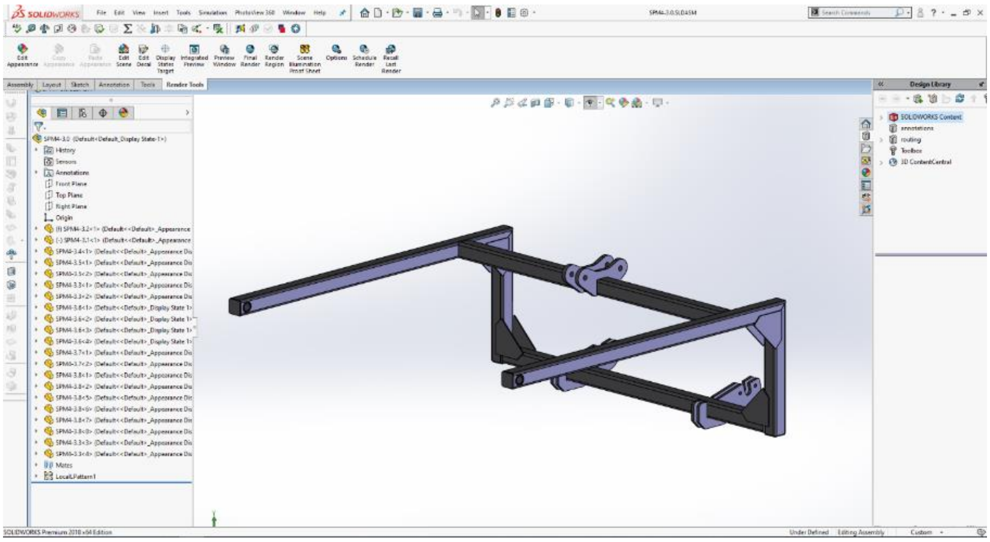

c.

Fig. 3. Subassembly views " Seeder support"
a. side view, b. top view, c. the interface of the software used

Table 1 shows the characteristics of the materials used in the design of the subassembly "Seeder support".

Table 1: Characteristics of the materials used

Mechanical property	Value		Unit of measurement
	S235JR	**E335**	
Elastic Modulus	**2.1e+11**	**2.1e+11**	N/m^2
Poisson's Ratio	**0.28**	**0.28**	-
Shear Modulus	**7.9e+10**	**7.9e+10**	N/m^2
Mass Density	7800	**7800**	kg/m^3
Tensile Strength	**3.6e+08**	**5.5e+08**	N/m^2
Yield Strength	**2.35e+08**	**2.75e+08**	N/m^2
Thermal Expansion Coefficient	**.1e-05**	**1e-05**	Kelvin

The total force acting on the subassembly "Seeder support" was determined taking into account the mass of the seeder in the general assembly "Cultivator seeder for sowing directly into stubble". Thus, the total force corresponds to the value of 3600N.
The value of this force was applied for the two static studies corresponding to the materials S235JR and E335, with the help of the Simulation module in the software SOLIDWORKS® Premium 2018 (fig. 4).

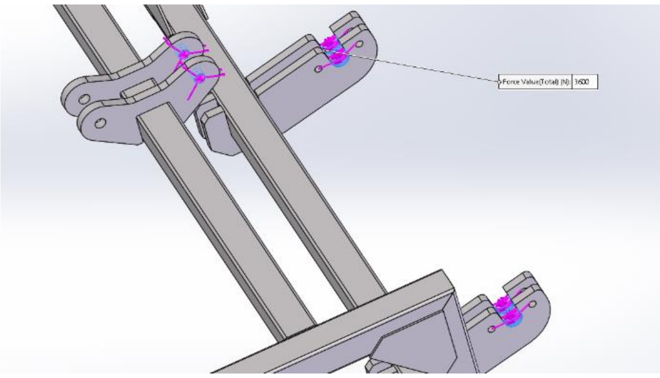

Fig. 4. Applying the force of 3600 N

The discretized finite element model of the subassembly ”Seeder support” is presented in fig. 5.

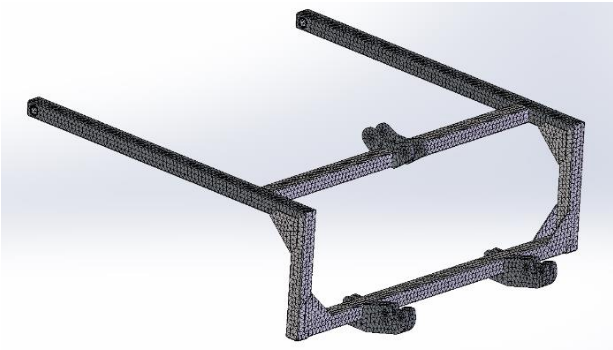

Fig. 5. Finite element discretization of the geometric model

After discretizing the mesh with finite elements, the simulation was performed, the results of which are presented below.
After the simulation, the design program provided the obtained results in graphical form; the geometric pattern is divided into areas of a certain color, each area comprising the region of the geometric pattern where the analyzed dimension has the value specified in the color legend on the right side of the screen.

3. Results

For the subassembly model ”Seeder support”, modeled and analyzed are presented below the results obtained from the simulation in SOLIDWORKS® the Simulation module.
Thus, table 2 shows the values of equivalent von Mises stresses, equivalent displacements and deformations in the welded metal construction resulting during the defined stresses, which are the same in both working regimes.

Table 2: Values of equivalent von Mises stresses, equivalent displacements and strains

Name	Type	Min	Max
Displacement 1	URES: Resultant Displacement	0.000e+00 m Node: 53	2.218e-03 m Node: 77472
Stress 1	VON: von Mises Stress	1.599e+03 N/m^2 Node: 81546	1.687e+08 N/m^2 Node: 72169
Strain1	ESTRN: Equivalent Strain	5.238e-09 Element: 38215	3.197e-04 Element: 34863

Analyzing this data, it can be seen that the largest displacements of nodes in the subassembly structure ”Seeder support”, appear on the peak of the torques in both working regimes (as expected), its maximum value being of 2.218×10^{-3} (fig. 6).

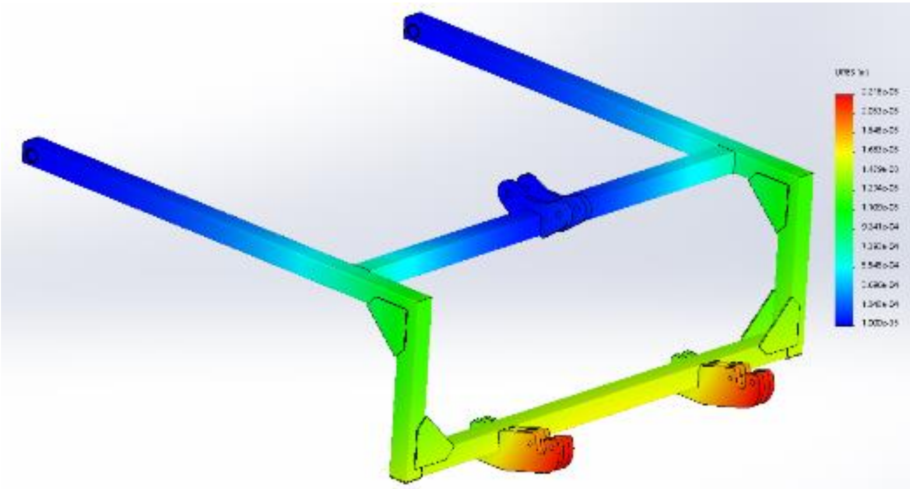

Fig. 6. The values of the displacements occurring in the structure during the two working regimes

Fig. 7 shows the values of the equivalent stresses in the structure of the subassembly ”Seeder support”, stresses calculated according to the von Mises criterion.

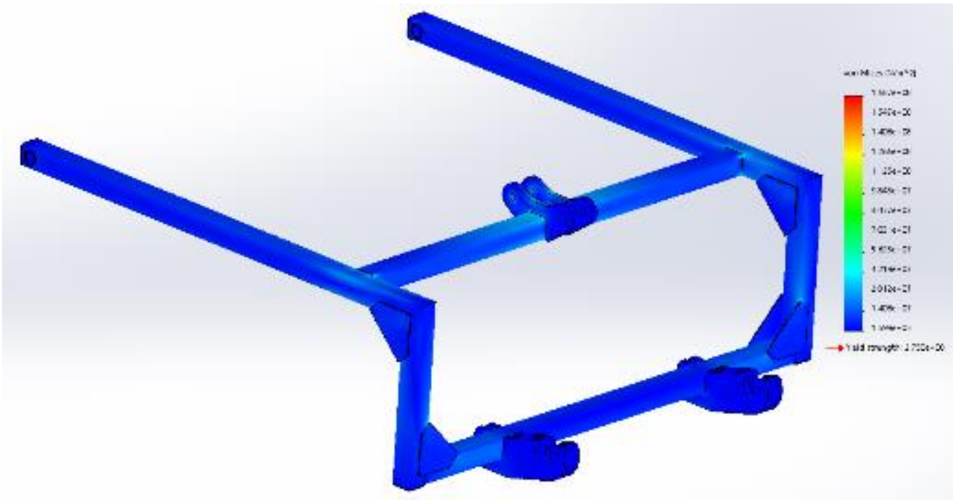

Fig. 7. The values of the von Mises equivalent stresses appearing in the structure during the two working regimes

Analyzing table 2 it can be seen that in the structure of the sub-assembly ”Seeder support”, stress concentration points appear, located in the upper area of the lugs for the tie rods at the joint with the metal mounting pipe. The values of the equivalent von Mises stresses created at these points are 1.687×10^{8} Pa in the case of the first working regime and the second working regime.
The values of the equivalent deformations that appear in the structure as a result of the stress to which the subassembly ”Seeder support” is subjected. So, the maximum equivalent strain occurs at the same points of stress concentration, the value of the strain being of 3.197×10-4 in the case of the first working regime and the second working regime (fig. 8).

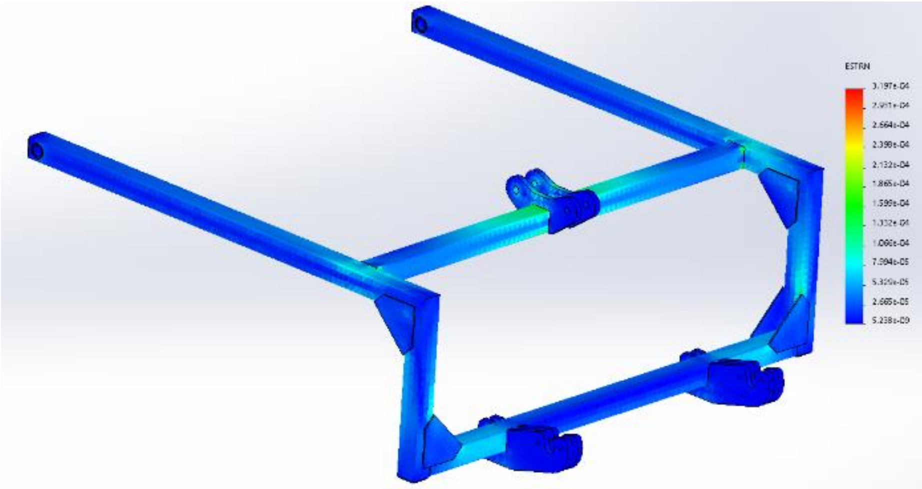

Fig. 8. The values of the equivalent deformations appearing in the structure, during the two working regimes

Table 3 shows the values of the safety coefficient appearing in the subassembly ”Seeder support”, during the demands defined for the two working regimes.

Table 3: Safety factor

Name	**Type**	**Min**	**Max**
Factor of Safety 1	Automatic	1.393e+00 Node: 72169	1.470e+05 Node: 81546
Factor of Safety 2	Automatic	1.630e+00 Node: 72169	1.720e+05 Node: 81546

4. Conclusions

The minimum value of the safety coefficient had values of 1.393 and 1.630, respectively. For supporting metal structures, the safety factor must have values between 1.0 and 1.8.
Thus, it can be said that the subassembly ”Seeder support” it is oversized, but the decision was made that in the physical execution, a metal pipe with a thickness of 4 mm instead of 3 mm should be used, to increase the resistance to dynamic stresses during work.
The results of this work are primarily aimed at designers of agricultural machines for tillage, but not only.

Acknowledgments

The results presented in this article were obtained with the support of MADR through the "Sectoral Plan - ADER 2026", financing contract no. 25.1.2 / 14.07.2023, ADER project 25.1.2. Tehnologie inovativă de prelucrare minimă a terenului agricol adaptată la schimbările climatice actuale – TEHCONS.

References

[1] Cárceles Rodríguez, B., V.H. Durán-Zuazo, M. Soriano Rodríguez, I.F. García-Tejero, B. Gálvez Ruiz, and S. Cuadros Tavira. “Conservation agriculture as a sustainable system for soil health: A review.” *Soil Systems* 6, no. 4 (2022): 87.
[2] Sharma, P., P. Sharma, and N. Thakur. “Sustainable farming practices and soil health: a pathway to achieving SDGs and future prospects.” *Discover Sustainability* 5 (2024): 250.
[3] Guyomard, H., L.G. Soler, C. Détang-Dessendre, and V. Réquillart. “The European Green Deal improves the sustainability of food systems but has uneven economic impacts on consumers and farmers.” *Communications Earth & Environment* 4 (2023): 358.

[4] Cavalieri-Polizeli, K.M.V., O. Guedes Filho, V.S. Romanoski, B.E.S. Ruthes, Z.P. Calábria, and L.B. de Oliveira. "Conservative farming systems and their effects on soil organic carbon and structural quality." *Soil and Tillage Research* 242 (2024): 106143.
[5] Marin, E., M. Mateescu, and C. Bălțatu. "Advanced method of managing soil conservation works in Smart Farms." Paper presented at 10th International Conference on Thermal Equipments, Renewable Energy and Rural Development (TE-RE-RD 2021), online, June 10-12, 2021.
[6] Mateescu, M. *Equipment for directly sowing straw cereals on unploughed soil* / *Echipamente de semănat cereale păioase în teren nearat*. Iasi, "Terra Nostra" Publishing House, 2009.
[7] Marin, E., C. Sorică, D. Manea, and Z. Vezirov. 2010. "Technical equipment for innovative technology of soil preparation and establish hoeing crops, basic promoting sustainable agriculture." *INMATEH – Agricultural Engineering* 31, no. 2 (2010): 87-92.
[8] *** https://www.solidworks.com/
[9] Constantin, G. A., Gh. Voicu, B. Olac, F. Ilie, and G. Paraschiv. "Structural analysis with finite elements of a subsoiler working part." Paper presented at the International Symposium ISB-INMA-TEH, Agricultural and Mechanical Engineering, Bucharest, Romania, October 31 - November 1, 2019.
[10] Cristea, O.D., M.G. Matache, M. Mateescu, and E. Marin. "Use of an innovative method for structural analysis of the distribution device used in pneumatic machines for weeding plant sowing." *Annals of the University of Craiova-Agriculture, Montanology, Cadastre Series* 49, no. 2 (2020): 361-366.
[11] Gheorghe, G., C. Persu, E. Marin, and D. Manea. "Structural analysis of technical equipment for setting up row crops and applying degradable film." Paper presented at the 16th International Scientific Conference "Engineering for rural development", Jelgava, Latvia, May 24-26, 2017.

ISSN 1454 - 8003
Proceedings of 2024 International Conference on Hydraulics and Pneumatics - HERVEX
November 13-15, Băile Govora, Romania

PRACTICAL ASPECTS REGARDING IMPLEMENTATION OF PID CONTROLLER ON A PROGRAMMABLE LOGIC CONTROLLER

Marian BLEJAN[1,*], Robert BLEJAN[1]

[1] National Institute of Research & Development for Optoelectronics – Subsidiary Hydraulics and Pneumatics Research Institute (INOE 2000 – IHP); * blejan.ihp@fluidas.ro

Abstract: *The accessibility of programmable logic controller, abbreviated as PLC, with real-time signal processing performance for the control of fast systems (such as hydraulic drives), allows the implementation of high-performance control algorithms that are executed in real time. The paper presents the software and hardware considerations for the implementation in a common PLC of a Proportional-Integral-Derivative PID controller.*

Keywords: *PID controller, PLC, servo hydraulics, servo valve driver*

1. Preliminary

PID algorithm, mathematical form

$$u(t) = A(e(t) + \frac{1}{T_i}\int_0^t e(\tau)d\tau + T_d\frac{de(t)}{dt}) \tag{1}$$

where $u(t)$ is the command value of the actuator, $e(t)$ is error value, the difference between desired target value and actual value of the process variable, A is then gain value, T_i is the integration time value and T_d is the derivation time value.

PID algorithm, numerical implementation using the trapezoidal method

$$u_k = A\left[e_k + \frac{T_s}{2T_i}\sum_{n=1}^{k}(e_n + e_{n-1}) + \frac{T_d}{T_s}(e_k - e_{k-1})\right] \tag{2}$$

where u_k is the command value of the actuator, e_k is error value, the difference between desired target value and actual value of the process variable and T_s is the sampling period value.

PID algorithm, form of FIR (*Finite Impulse Response*) filter

$$u_k = u_{k-1} + A\left[\left(1 + \frac{T_s}{2T_i} + \frac{T_d}{T_s}\right)e_k - \left(1 - \frac{T_s}{2T_i} + 2\frac{T_d}{T_s}\right)e_{k-1} + \frac{T_d}{T_s}e_{k-2}\right] \tag{3}$$

The PID algorithm with the derivative of the process signal, eliminates the derivative kick

$$u_k = A\left[e_k + \frac{T_s}{2T_i}\sum_{n=1}^{k}(e_n + e_{n-1}) - \frac{T_d}{T_s}(y_k - y_{k-1})\right] \tag{4}$$

where y_k is the process variable.

The relation (4) can also be written like this

$$u_k = u_{k-1} + A\left[\left(1 + \frac{T_s}{2T_i}\right)e_k - \left(1 - \frac{T_s}{2T_i}\right)e_{k-1} + \frac{T_d}{T_s}(y_k - 2y_{k-1} + y_{k-2})\right] \quad (5)$$

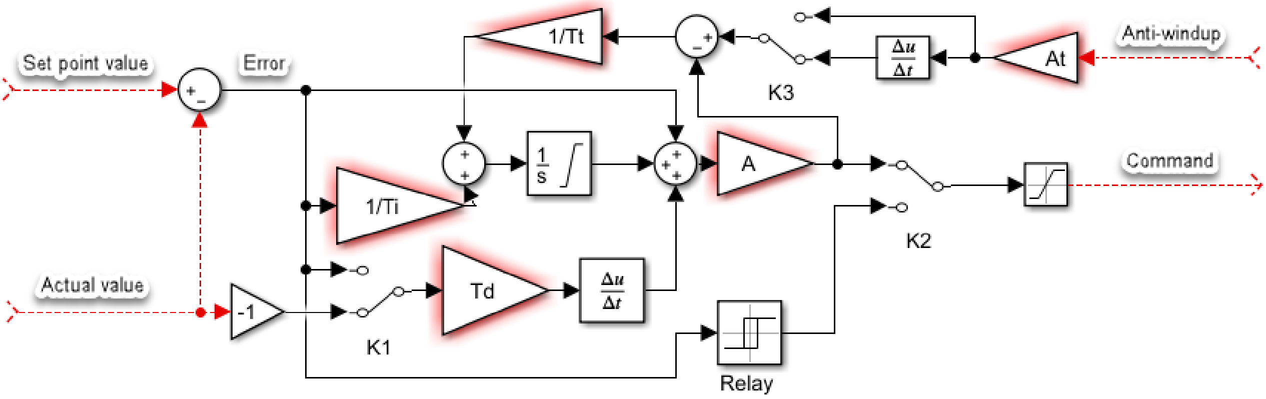

Fig. 1. PID algorithm diagram implemented on PLC

Switch K1 selects the mode of calculus of the derivative component. Thus, its value can be the derivative of the error value e or the derivative of opposite actual value y. The second choice cancels the variation disturbance of the reference point x, the derivative kick, see fig. 1 [1].
Switch K2 is used to adjust the controller parameters, A the gain, T_i the time constant of the integrator, T_d the time constant of the derivative, in the sense of obtaining a stable operation of the controlled process. K2 selects the operating mode of the controller, respectively the normal operation in the closed loop with the PID regulator or the operation in the closed loop through the relay, bringing the regulation process to the stability limit with small amplitude oscillations, known as the Åström-Hägglund tuning method [2]. In the relay closed-loop mode, it is possible, by determining the values of the amplitude and frequency of the process oscillations, to calculate the value of the controller parameters in such a way as to avoid the unstable operation of the automatic regulator [3].
To avoid integral windup, when integral term of a PID controller accumulates a significant error during periods when the process is saturated, is necessary to implement anti-windup scheme based on back-calculation [4]. For this purpose, the *[t]* entry, the command execution input or its derived value, selected from K3, is required.
Parameters of the PID regulator with the phase margin value of 45^0 is

$$A = 0.9K_u \quad (6)$$

$$T_d = 0.1816T_u \quad (7)$$

$$T_i = 6.25T_d \quad (8)$$

where K_u is the inverse of the gain in the closed loop through the relay, and T_u is the oscillation period.

2. Simulation

In fig. 3 shows the simulation model for a hydraulic servo cylinder [5] with the proposed PID controller. A servo valve Rexroth 4WSE2EM10 actuates the hydraulic cylinder. The stroke of the cylinder is *200mm*. The servo valve is driven by with a current of *-30…30mA* and has a flow rate of *-60...60l/min*. The speed of the hydraulic cylinder rod varies in the range *-0.6...0.6m/s* corresponding to a flow rate of *-60...60l/min*.

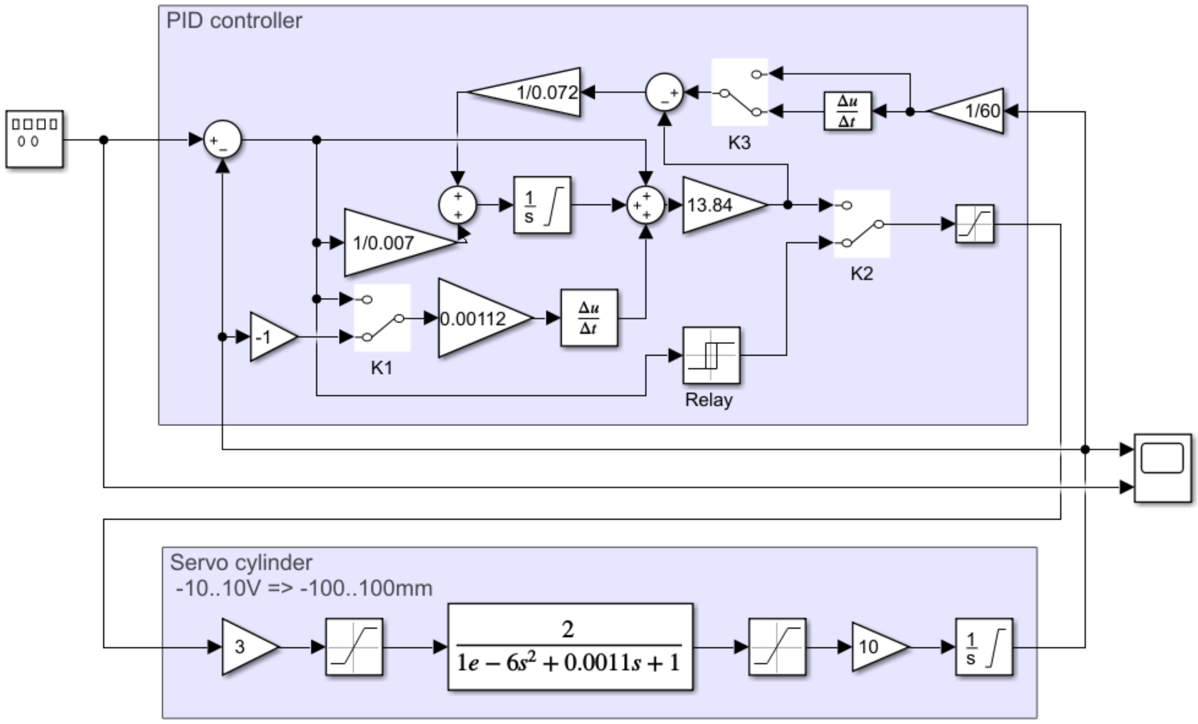

Fig. 2. Matlab model of the automation system

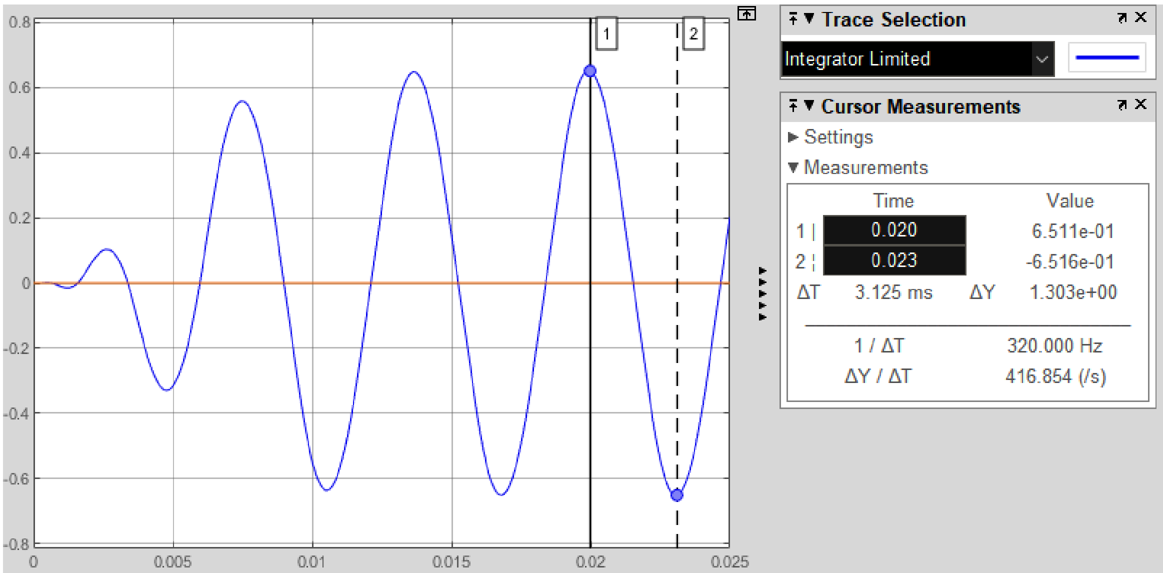

Fig. 3. Closed loop response with relay for *-10mm* and *10mm* saturation limits

For $K_u = \frac{20}{1.3} = 15.38$ and $T_u = 2 * 3.125 = 6.25ms$ the result is

$$A = 13.84\,;\ T_d = 1.12ms\,;\ T_i = 7ms \tag{9}$$

see fig. 2 and (6), (7) and (8).

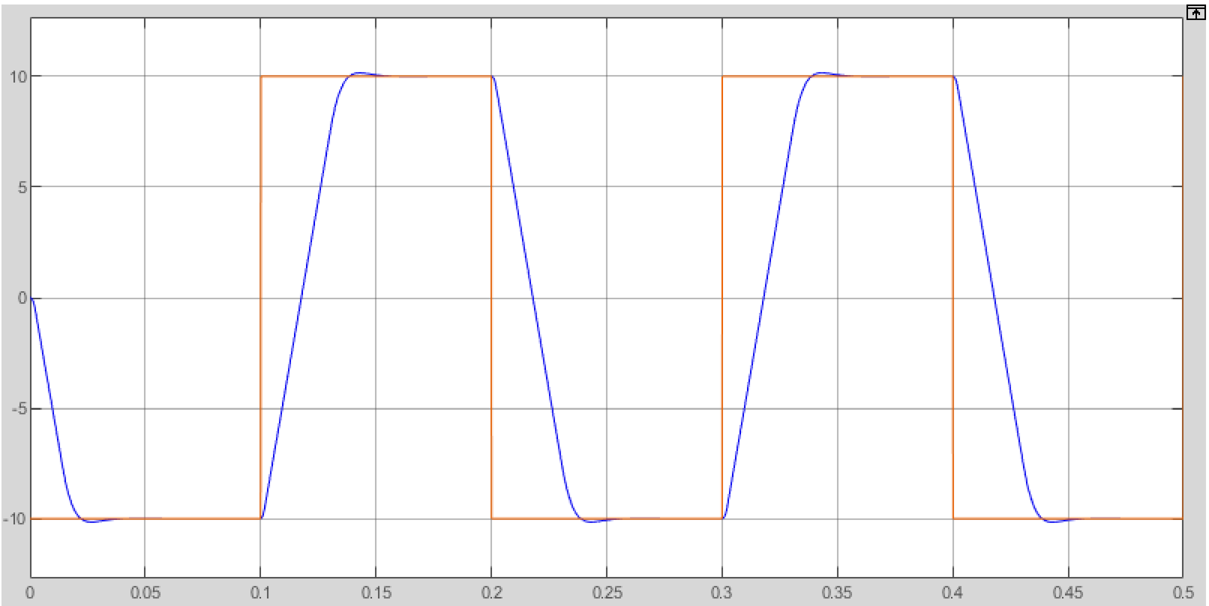

Fig. 4. Response for ±*10mm, 5Hz* input signal - red trace and hydraulic actuator position - blue trace

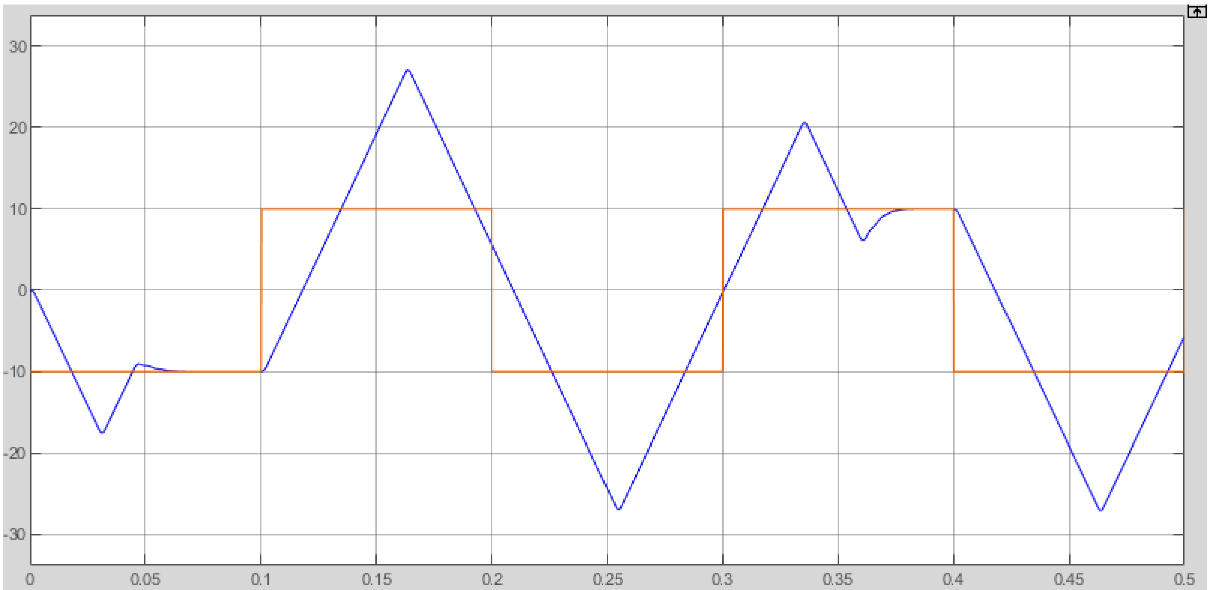

Fig. 5. Response for ±*10mm, 5Hz* input signal, with integral windup

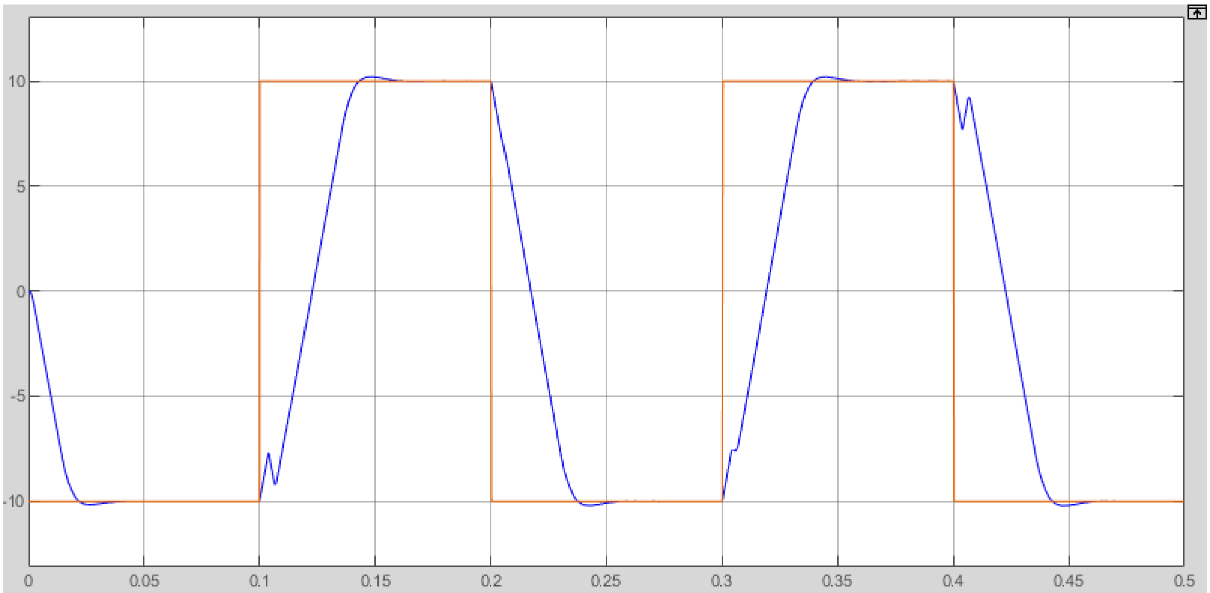

Fig. 6. Response for ±*10mm, 5Hz* input signal, with derivative kick

3. Servo valve driver

Usually PLC has analog input/output modules with unified current *4..20mA* or voltage ±*10V* signals. On the other hand, automation systems with PLC are powered by 24V DC power supplies. To control the servo valve, a voltage to current converter is required. This servo valve driver, see fig. 7, has the role of interfacing the analog voltage signal generated by the PLC with the analog current signal required by the hydraulic device. The driver is powered by the same power supply as the PLC, 24 VDC.

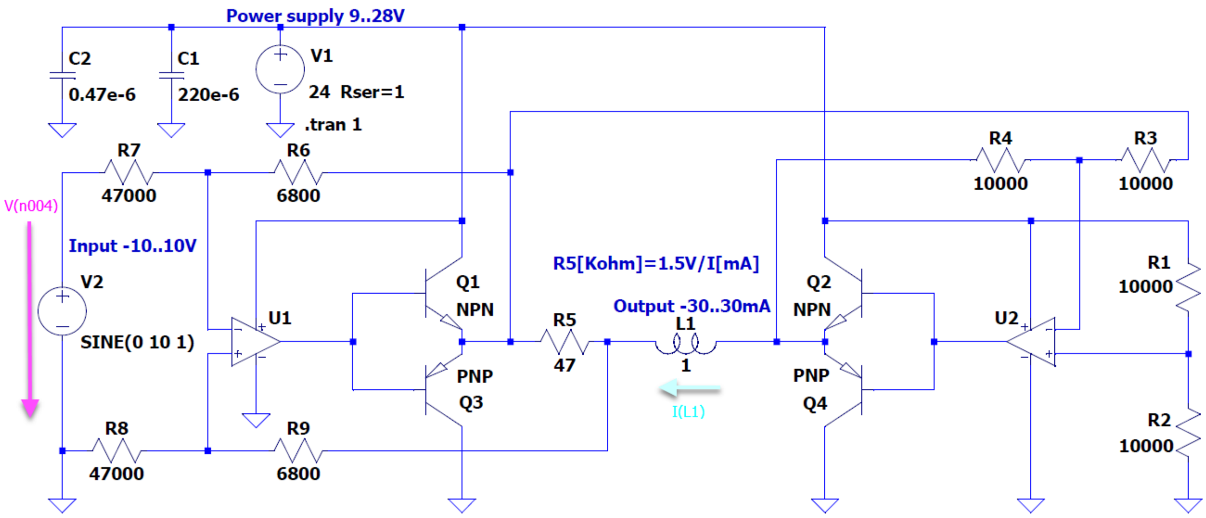

Fig. 7. Electronic schematic of servo valve driver

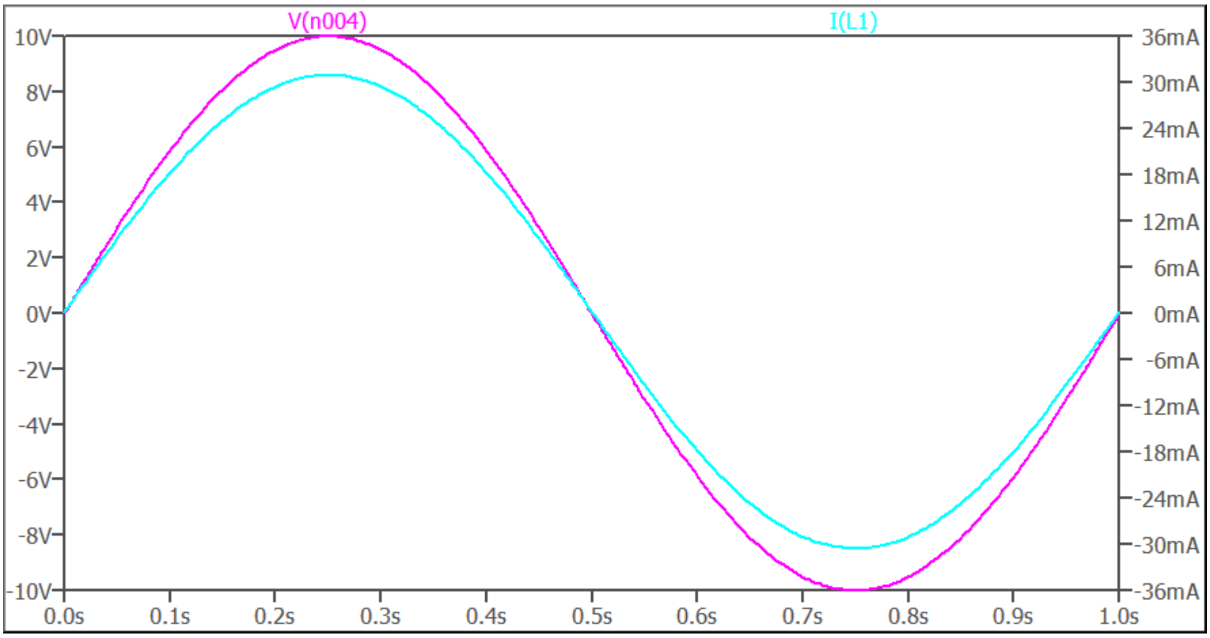

Fig. 8. Transfer function of servo valve driver, input *V(n004)* – fuchsia and output *I(L1)* – aqua

4. Conclusion

This paper presents formulas for implementing software for a PID controller, (2), (3), (4), (5) and fig. 1. The controller has advanced features such as anti-windup, derivative kick cancellation and closed loop regulation with relay. The control algorithm is tested by simulating a hydraulic servo cylinder consisting of a servo valve and a bilateral rod cylinder.
The paper also presents the original electronic diagram of the servo valve driver. The driver is built from a Howland voltage controlled current source adapted for H-bridge output. The circuit is simulated in the LTspice® simulator software.

Acknowledgement

This work was carried out through the Core Program within the National Research Development and Innovation Plan 2022-2027, carried out with the support of MCID, project no. PN 23 05.

References

[1] National Instruments. "The PID Controller & Theory Explained". September 9, 2024. Accessed September 30, 2024. https://www.ni.com/en/shop/labview/pid-theory-explained.html.
[2] Åström, K.J., T. Hägglund, C.C. Hang, and W.K. Ho. "Automatic Tuning and Adaptation for PID Controllers - A Survey." *IFAC Proceedings Volumes* 25, no. 14 (July 1992): 371-376. https://doi.org/10.1016/S1474-6670(17)50762-4.
[3] van der Zalm, G.M. *Tuning of PID-type controllers: literature overview*. DCT rapporten; Vol. 2004.054. Technische Universiteit Eindhoven, 2004.
[4] Åström, K.J., and L. Rundqwist. "Integrator Windup and How to Avoid It." Paper presented at the 1989 American Control Conference, Pittsburgh, PA, USA, June 21-23, 1989, pp. 1693-1698, doi: 10.23919/ACC.1989.4790464.
[5] Thayler, W.J. "Transfer functions for Moog servovalves." Technical bulletin 103, Moog Inc. Controls Division, East Aurora, N.Y. 14052, 1958 (Revision in 1965)].
[*] https://www.mathworks.com/products/matlab.html. Accessed September 30, 2024.
[*] https://www.analog.com/en/resources/design-tools-and-calculators/ltspice-simulator.html. Accessed September 30, 2024.

ISSN 1454 - 8003
Proceedings of 2024 International Conference on Hydraulics and Pneumatics - HERVEX
November 13-15, Băile Govora, Romania

ANALYSIS OF THE DYNAMIC BEHAVIOR OF THE HYDRAULIC VIBRATION SYSTEM OF THE COMPACTOR EQUIPMENT, UNDER DIFFERENT OPERATING CONDITIONS

Daniel Sorin MIRON[1], Carmen Nicoleta DEBELEAC[1]

[1] "Dunarea de Jos" University of Galati, Engineering and Agronomy Faculty in Braila, Research Center for Mechanics of Machines and Technological Equipments, Braila, Romania

Abstract: *This paper addresses the design and operation of the hydraulic vibration generating system of a compactor, focusing on some operational aspects with significant impact. A major problem is the inability of the system to adequately regulate the hydraulic flow, especially during sudden changes in the working regime, which leads to sudden pressure fluctuations and hydraulic shocks. These shocks negatively influence the stability, efficiency and lifetime of the hydraulic actuation system of the roller drum. The paper presents the solutions adopted by the manufacturers for operational performance improvement of these systems.*

Keywords: *Dynamic behavior, hydraulic vibration system, compactor equipment, working regime, analysis*

1. Introduction

The analysis of the dynamic behavior of the hydraulic vibration system in compactor equipment under various operating conditions is critical for understanding the system's performance, reliability, and efficiency. Hydraulic vibration systems in compactors are responsible for generating the vibrations necessary for soil and material compaction, which makes their stability and dynamic response essential in achieving the desired compaction results while ensuring the longevity of the equipment. The hydraulic vibration system of a compactor consists of a hydraulic pump, control valves, hydraulic motors or cylinders, and vibratory drums. All these components work together to generate and control the mechanical vibrations transmitted to the compactor drum. The roller's ability to efficiently transfer these vibrations to the terrain depends largely on the system's dynamic behavior, including how it responds to changes in pressure, flow, load, and external forces.

2. Operational aspects of vibratory rollers

Operating conditions that affecting the hydraulic system dynamics of the compactor equipment are:

a) Load fluctuations, particularly during transitions between compacting different types of soil or material, cause sudden changes in hydraulic pressure and flow. These variations can result in unstable operation, pressure surges, and hydraulic shocks, leading to potential damage to the system components.
b) Pressure and flow control are very important because the effective regulation of hydraulic flow and pressure is necessary to maintain constantly vibration frequencies and amplitudes, which are determinant for an adequate compaction. A challenge is preventing hydraulic shocks during sudden pressure changes, which can occur due to load shifts or rapid changes in the operating regime.
c) The viscoelastic properties of the soil significantly impact the dynamic response of the compactor's hydraulic vibration system. Softer, more elastic soils absorb more vibration energy, requiring adjustments in system settings to maintain the compaction process efficiency. Conversely, denser, more compact soils may cause increased hydraulic pressure, further influencing the hydraulic system's behavior.
d) The frequency and amplitude of the hydraulic vibration system need to be carefully controlled to match the operational requirements. Higher frequencies may be necessary for compacting finer materials, while lower frequencies are more effective for coarser soils. Studies show that improper

control of these parameters can result in inefficient compaction and increased wear on the hydraulic components.

e) Hydraulic fluid properties, as viscosity, density, and temperature sensitivity of hydraulic fluids directly influence the system's dynamic behavior. Thus, the high-viscosity fluids can cause increased resistance in the hydraulic system, reducing flow and efficiency, while lower-viscosity fluids may not provide adequate damping, leading to excessive vibrations and shocks.

The impact of these operational factors on the dynamics of hydraulic actuation systems in vibratory compactors has been a subject of global research. The most significant results are outlined below.

3. Simulation of dynamic behavior of hydraulic system

To better understand the dynamic behavior of the hydraulic vibration system, dedicated simulation environments such as AMESim, Matlab or other dynamic modeling tools are often used. The results of these simulations allow engineers to predict how the system will behave under various operating conditions, including changes in load, pressure, and fluid properties. For example, Wang Haifei (2003) studied the mechanisms of hydraulic impact and recommends measures to prevent hydraulic shocks, highlighting the importance of control systems in improving system resistance under different working conditions [1]. Ma and Yang (2016) use the AMESim environment to model the roller hydraulic vibration system and understand how changes in the system parameters influence the overall performance and reliability of the construction machine [2]. Figure 1 shows some examples of developed schemes for simulating the behavior of the hydraulic system that drives the movement of the compactor or the vibration generator of the drum [1-3].

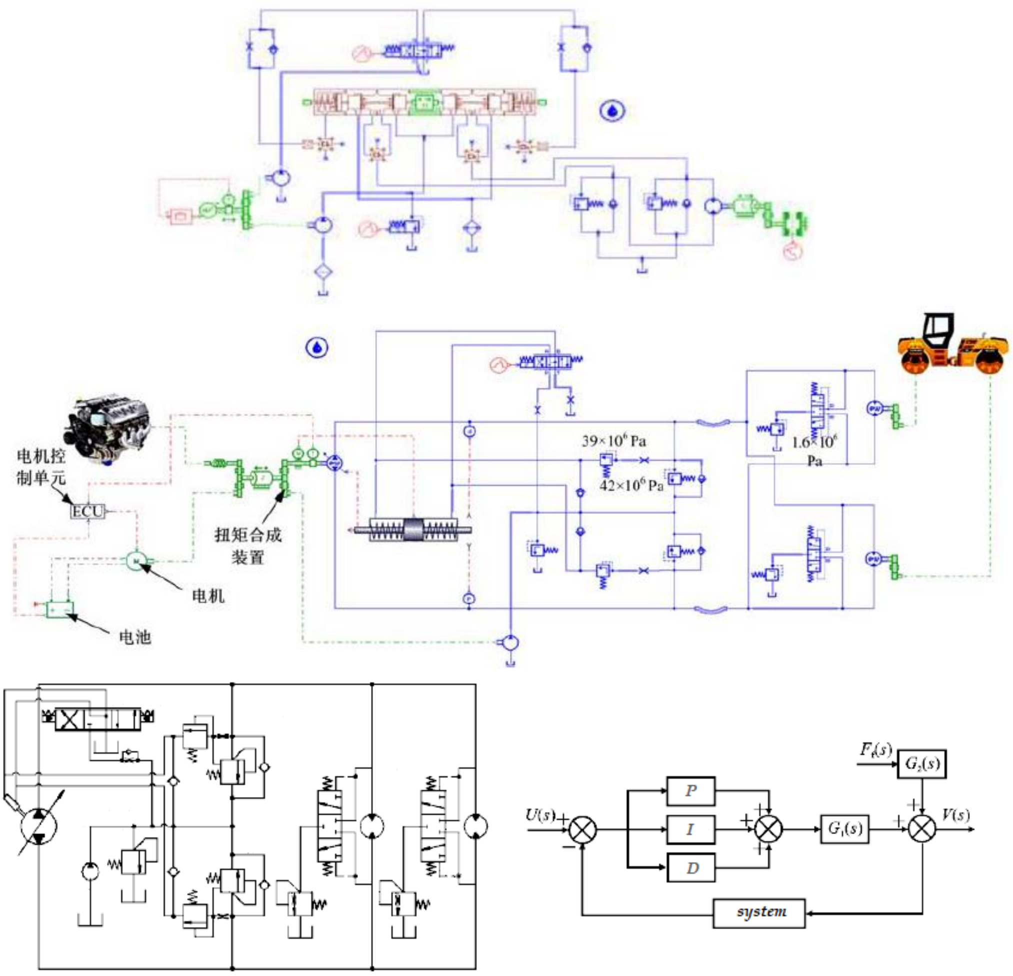

Fig. 1. Scheme for AMESim and Matlab environment simulation

Studies such as those by Debeleac et al. (2019) emphasize the nonlinear dynamic behavior of the system when compacting different construction materials [4]. Simulation tools like Matlab are often used to model and predict how the system responds under different loading conditions.
The dynamic response of the vibrating compactor roller is influenced by several factors, including the viscoelastic properties of the soil being compacted. Studies have shown that these material properties significantly affect the system's stability and its ability to absorb and dampen the vibrations generated during operation [5]. To alleviate these issues, this paper proposes incorporating control elements into the hydraulic actuation scheme to improve flow regulation. Additionally, the authors employ Matlab simulation software to model the dynamic behavior of the hydraulic system under varying conditions such as different loads, pressure variations, and the use of various hydraulic fluids.
This approach is in line with other studies that have modeled the rheological interaction between the working tool and the ground during vibratory compaction. Such modeling helps in understanding the material deformation and energy dissipation processes that occur during compaction, which are critical for optimizing the hydraulic system's design [6].
The results obtained from these simulations show that large load fluctuations can cause rapid changes in hydraulic flow, resulting in pressure spikes that produce hydraulic shocks. These sudden pressure increases can lead to significant system damage, including premature wear of components and potential system failure. Similar findings have been reported by other researchers, particularly in the computational assessment of vibratory compaction processes for different terrains. These studies emphasize that improper regulation of hydraulic flow can result in system breakdowns and reduced performance, especially in harsh construction environments [7].
An additional phenomenon observed in hydraulic systems is "pressure resonance," which occurs when the system's natural frequency aligns with the excitation frequency from the hydraulic motor. This resonance can lead to severe pressure spikes and damage the hydraulic system. Such phenomena further underscore the importance of effective control mechanisms and damping solutions to prevent resonance and other harmful effects in vibratory systems [8].
In order to prevent hydraulic shocks and enhance system reliability, various control strategies are explored in this paper, including the use of accumulators, pressure-relief valves, and advanced control algorithms. Similar methods have been proposed in the literature, where accumulators act as buffers to absorb excess pressure surges, mitigating the impact of sudden pressure changes [2, 9]. Similar results have been observed in studies focusing on hydraulic systems in construction machinery, where sudden flow or load changes can induce system shocks, increasing maintenance demands and operational inefficiencies [10,11]. The paper offers solutions aimed at preventing these shocks, particularly during start-up, by reinforcing the hydraulic system, which is especially crucial for heavy rollers used in construction.
For example, the inclusion of accumulator systems or pressure-relief valves has been proposed to absorb excess pressure surges, reducing the risk of system failure [12]. Ultimately, the proposed measures are aimed at improving the performance of hydraulic systems, minimizing maintenance costs, and increasing the reliability of construction equipment in demanding environments. The approach aligns with other research highlighting the importance of shock prevention and flow regulation in hydraulic systems used in industrial applications [13].
The selection of hydraulic fluids also plays a significant role in system performance. Fluid viscosity and temperature dependence have a direct impact on hydraulic flow and pressure regulation. Research has demonstrated that optimizing fluid properties for specific operating conditions can reduce the risk of hydraulic shocks and improve the overall efficiency of the system [8, 14]. For instance, the density and viscosity of the working fluid significantly influence the system’s ability to maintain stable operation under varying loads and temperatures. Addressing these factors can enhance the compactor's performance and extend its operational life [15].
In order to improve the aspects produced by the factors presented previously, the manufacturers of compactors have implemented various solutions to improve the dynamic stability of the hydraulic vibration system, presented in detail in Table 1.

Table 1: The main control strategies for dynamic stability of the hydraulic system

Control strategies	Description
Feedback Control Systems	To uses the real-time feedback from sensors to adjust hydraulic pressure and flow in response to changes in load and terrain conditions
Pressure-Relief Valves	To mitigate the effects of sudden pressure surges, pressure-relief valves can be installed to release excess pressure and prevent hydraulic shocks
Accumulators	These devices absorb pressure fluctuations and act as buffers to smooth out rapid changes in hydraulic flow, reducing the likelihood of system damage
Variable Displacement Pumps	Adjusting the flow rate in response to operational requirements it can help maintain consistent vibration characteristics, regardless of external conditions

Simulation-based analyses help identify potential instabilities, failures, and inefficiencies that could occur under real construction machine operating conditions. By virtually testing different case scenarios and control strategies, engineers come up with solutions to optimize hydraulic system design, control mechanisms and functional parameters to improve the reliability and performance of compactors. This approach brings great benefits especially when analysing the complex interactions between the hydraulic components of the actuation circuit, the vibration system and the external environment.

4. Conclusions

The dynamic behavior of the hydraulic vibration system in compactor equipment is influenced by a variety of operating conditions, including load changes, soil properties, fluid characteristics, and system configuration. Understanding and controlling these factors is essential for optimizing system performance, preventing hydraulic shocks, and ensuring the longevity of the equipment. Through advanced simulation tools and effective control strategies, engineers can design more robust hydraulic systems capable of performing reliably under a wide range of working conditions.

Acknowledgments

This research was funded by “Dunarea de Jos” University of Galati, Romania, Intern Grant,” Research on the performance estimation of the construction material compaction process in the context of digitization – CompactInfo”, grant number RF 2476/31.05.2024.

References

[1] Wang, Haifei. *Study on vibration hydraulic impact mechanism and prevention measures of vibratory rollers [D]*. Master Thesis. Chang'an University, 2003.
[2] Ma, Ting-Ting, and Guo-Ping Yang. "Study on hydraulic vibration system of roller based on AMESIM." *International Journal of Research in Engineering and Science* 4, no. 7 (July 2016): 28-37.
[3] Zhu, W.-W., Y. Li, Z.-X. Feng, X.-B. Zhang, and Y.-S. Yao. "Improvement of roller running system based on closed-loop control.” *China Journal of Highway and Transport* 30, no. 5 (May 2017): 152-158.
[4] Debeleac, C., S. Nastac, and A. Buraga. "On Nonlinear Dynamics of Vibrating Compaction Process of Construction Materials." Paper presented at the 26th International Congress on Sound and Vibration, ICSV 2019, Montreal, Canada, July 7-11, 2019.
[5] Dobrescu, Cornelia. "The Dynamic Response of the Vibrating Compactor Roller, Depending on the Viscoelastic Properties of the Soil." *Applied System Innovation* 3, no. 2 (2020): 25.
[6] Năstac, S., G. Căpățână, and C. Debeleac. ”On Rheological Schematization of Working Tool - Ground Interaction for Vibratory Compaction”. Paper presented at the Annual Symposium of the Institute of Solid Mechanics - SISOM 2012 and Session of the Commission of Acoustics, Bucharest, Romania, May 30-31, 2012.

[7] Căpățână, G., and C. Debeleac. ”Computational assessments regarding operational ultimate state of vibrating compaction process for different terrains.” Paper presented at the Annual Symposium of the Institute of Solid Mechanics SISOM 2015 and Symposium of Acoustics, Romanian Academy, Department of Technical Sciences, Academy of Technical Sciences, Commission of Acoustics of Romanian Academy, Bucharest, Romania, May 21-22, 2015.
[8] Axinti, G., S. Năstac, C. Debeleac, and A. Axinti. "About the “pressure resonance” phenomenon in the hydraulic driving systems with rotative motor." *Romanian Journal of Acoustics and Vibration* 2, no. 1 (March 2005): 27-32.
[9] Bair, S., and P. Michael. "Modelling the pressure and temperature dependence of viscosity and volume for hydraulic fluids." *International Journal of Fluid Power* 11, no. 2 (2010): 37-42.
[10] Smith, J., and R. Johnson. "Hydraulic systems in construction machinery: Challenges and innovations." *Journal of Construction Engineering* 23, no. 2 (2015): 123-135.
[11] Zhao, Q., H. Liu, and Y. Wang. "Dynamic behavior of hydraulic systems under fluctuating loads: A simulation approach." *International Journal of Fluid Power Engineering* 45, no. 3 (2017): 234-240.
[12] Kumar, P., and A. Singh. "Pressure regulation and shock absorption in hydraulic systems: A comprehensive review." *Journal of Mechanical and Industrial Engineering* 32, no. 4 (2018): 411-427.
[13] Lee, M., J. Park, and S. Choi. "Improving reliability in hydraulic systems for construction equipment through advanced control mechanisms." *Construction Equipment and Maintenance Journal* 40, no. 1 (2019): 101-115.
[14] Borș, Adriana Mariana, Liliana Dumitrescu, Ștefan-Mihai Șefu, and Marin Șenilă. "Analysis of the Behavior of Fluids Specific to Electrohydraulic Systems and the Performance of Industrial Machine Tools." *Hidraulica Magazine*, no. 3 (September 2023): 64-70.
[15] Șcheaua, Fănel. "Density and Viscosity Effects of Hydraulic System Working Fluid." *Hidraulica Magazine*, no. 1 (March 2024): 34-39.

ISSN 1454 - 8003
Proceedings of 2024 International Conference on Hydraulics and Pneumatics - HERVEX
November 13-15, Băile Govora, Romania

HYDROGEN PRODUCTION VIA STEAM REFORMING OF NATURAL GAS WITH INTEGRATED CARBON CAPTURE: A BRIEF OVERVIEW

Mihaela Ionela BIAN[1], Paula Veronica UNGUREȘAN[1], Dan OPRUȚA[1]

[1] Technical University of Cluj-Napoca, Romania, email: mihaela.ileni@campus.utcluj.ro; paula.unguresan@termo.utcluj.ro; dan.opruta@termo.utcluj.ro

Abstract: *This article presents a succinct analysis of hydrogen as a critical component of the future energy landscape. Hydrogen produces three times as much heat as gasoline but has a 50% lower lifecycle carbon footprint than traditional fossil fuels. The benefits and characteristics of hydrogen, as well as the methods for producing it, will be discussed. With 96% of global hydrogen production currently dependent on fossil fuels, it is becoming increasingly clear that both traditional and pilot hydrogen production technologies must be investigated in order to contribute to the goal of reducing greenhouse gas emissions.*

While hydrogen is classified as a zero-emission fuel at the end of use, its environmental impact is determined by its manufacturing process. Thus, the provenance of hydrogen is critical in determining whether it can truly be classified as 'clean' energy.

An overview of hydrogen availability, properties, and potential sources is provided, as well as an analysis of hydrogen production methods. Furthermore, the relationship between hydrogen and renewable energy, as well as its environmental and climate benefits, are thoroughly discussed. Currently, the vast majority of industrial hydrogen production relies on fossil fuels, primarily natural gas and coal, either directly or indirectly through electricity generation. According to projections, this trend will persist for the foreseeable future unless significant changes are made to the energy system. As a result, hydrogen generators continue to be a significant source of CO_2 *emissions, contributing to climate change and threatening ecological stability. In light of these challenges, there is an urgent need to reduce or eliminate* CO_2 *emissions from fossil fuel-based hydrogen production in order to fully realize hydrogen's potential as a sustainable fuel.*

The main methods for reducing CO_2 *emissions in hydrogen production from fossil fuels fall into three categories: (1) coupling hydrogen plants with carbon capture and storage (CCS) technologies; (2) hydrocarbon dissociation to separate hydrogen and carbon; and (3) combining hydrogen production with carbon-free energy sources such as nuclear or solar. This article reviews and analyzes the current state of these technological approaches, offering insights into how they can significantly reduce emissions. A short- and medium-term outlook is also provided, outlining how new technological advancements could lead to a shift to low- or zero-emission hydrogen production from fossil fuels.*

Finally, the future of hydrogen as a clean energy source is heavily dependent on overcoming current technological and economic barriers. Hydrogen adoption will necessitate advancements in production technologies, improvements in storage, transportation, and quality of hydrogen as fuel, and the development of a robust infrastructure. Furthermore, because hydrogen has a fast flame speed and a short ignition delay, combustion systems must be closely monitored to avoid problems such as pre-ignition and backfiring.

Policy incentives, such as renewable hydrogen subsidies and carbon pricing, will be required to accelerate the transition to a hydrogen-based energy economy. When combined with renewable energy sources, hydrogen has the potential to significantly reduce carbon emissions and contribute to global climate goals.

Keywords: *Hydrogen, carbon capture, natural gas, steam reforming*

1. Introduction

The continued growth of the global population and economy, combined with rapid urbanization, has resulted in a significant increase in energy consumption. Traditionally, energy supply has relied on hydrocarbon (fossil fuel) resources, which are limited by geological distribution and the feasibility of extraction [1]. The use of fossil fuels as the primary energy source since the advent of mechanical transformation has contributed to a significant rise in carbon dioxide (CO_2) and other greenhouse gases (GHGs) in the atmosphere, which is the main cause of global warming. As a result, decarbonizing the energy supply requires a shift to cleaner, more cost-effective, and renewable energy sources in order to ensure future energy sustainability and global security.

Hydrogen, as a carbon-free energy carrier, is most likely to play an important role in a world with severe constraints on greenhouse gas emissions. Free hydrogen is rarely found in its pure form within the Earth's crust, as it is typically bound to other elements. However, it can be synthesized from compounds found in natural or industrial sources. Hydrogen is the most abundant element in the universe, accounting for roughly 75% of total matter; in the Earth's crust, it is the tenth most common element.[2] Hydrogen is not found in Earth's atmosphere since the Earth's gravitational pull is not strong enough (unlike Jupiter and Saturn) to retain the light-weight H_2 molecules.
Three isotopes of hydrogen are available: protium, deuterium, and tritium. Consisting of one proton and one electron, protium is the main component of hydrogen, the simplest element. Although it is the lightest element, hydrogen has the highest energy content per unit mass among all fuels. A brief presentation of its properties is given in Table 1 below.

Table 1: Hydrogen properties

Properties	U.M. (S.I.)	Reference
Date of discovery/Author/Formula	1766/Henry Cavendish/H_2	[3]
Isotopes	^1H (99.98%). ^2H. ^3H. (^4H-7H Instable)	[3]
Equivalences: Hydrogen in solid. liquid. and gaseous states at p = 981 mbar and T = 20 °C	1 kg = 14.104 l = 12.126 m^3	[4]
Molecular mass	1.00794	[5]
Vapor pressure at (-252.8 °C)	101.283 kPa	[5]
Gas density at the boiling point and pressure of 1 atm	1.331 kg/m^3	[5]
Specific gravity of the gas at 0°C and 1 atm. (air = 1)	0.0696	[5]
Specific volume of the gas at 21.1°C and 1 atm	11.99 m^3/kg	[5]
Specific gravity of the liquid at the boiling point and 1 atm	0.0710	[5]
Specific volume of the liquid at the boiling point and 1 atm	67.76 kg/m^3	[5]
Boiling point at (101.283 kPa)	-252.8℃	[5]
Freezing/Melting point at (101.283 kPa)	-259.2℃	[5]
Critical temperature	-239.9℃	[5]
Critical pressure	1296.212 kPa. abs	[5]
Critical density	30.12 kg/m^3	[5]
Triple point	-259.3℃ la 7.042 kPa. abs	[5]
Latent heat of fusion at the triple point	58.09 kJ/kg	[5]
Latent heat of vaporization at the boiling point	445.6 kJ/kg	[5]
Solubility in water (vol/vol) at 15.6°C	0.019	[5]
Viscosity of the dilute gas at 26°C (299 K)	9×10^{-6} Pa s	[5]
Molecular diffusivity in air	6.1×10^{-5} m^2/s	[5]
CP	14.34 kJ/kg (℃)	[5]
Cv	10.12 kJ/kg (℃)	[5]
Ratio of specific heats (CP/Cv)	1.42	
Lower heating value. based on weight	120 MJ/kg	[6]
Higher heating value. based on weight	141.8 MJ/kg	[6]
Lower heating value. based on volume at 1 atm	11 MJ/m^3	[6]
Higher heating value. based on volume at 1 atm	13 MJ/m^3	[6]
Stoichiometric air-fuel ratio at 27°C and 1 atm	34.2 kg/kg	[6]

Flammable limits in air	4%-75%	[6]
Explosive limits	18.2 to 58.9% vol.	[6]
Maximum burning rate in air	2.7/3.46 (m s-1)	[6]
Maximum flame temperature	1526.85 ℃	[6]
Autoignition temperature / in air	400℃ /571℃	[6]

Hydrogen can be produced from renewable energy sources such as solar, wind, and nuclear power through processes such as direct thermal conversion or electrolysis. However, in the short term, a more practical approach involves producing hydrogen from conventional fossil fuels, utilizing conversion technologies that incorporate CO2 sequestration to mitigate environmental impacts [7].
Understanding the characteristics and parameters associated with various types of hydrogen is critical for assessing their environmental impact, economic viability, and overall potential in the transition to a low – carbon energy economy.
The following table presents a concise classification of the various types of hydrogen based on their energy source.

Table 2: Hydrogen color classification

<table>
<tr><th colspan="2">Nomenclature</th><th>Technology</th><th>Electricity source</th><th>Green gas emissions</th></tr>
<tr><td rowspan="7">Hydrogen through electric energy</td><td rowspan="5">Green Hydrogen</td><td rowspan="7">Electrolysis</td><td>Wind</td><td rowspan="6">Minimal</td></tr>
<tr><td>Solar</td></tr>
<tr><td>Hydro</td></tr>
<tr><td>Geothermal</td></tr>
<tr><td>Tidal</td></tr>
<tr><td>Purple/Pink Hydrogen</td><td>Nuclear</td></tr>
<tr><td>Yellow Hydrogen</td><td>Mixed-source grid energy</td><td>Medium</td></tr>
<tr><td rowspan="6">Hydrogen production through fossil fuels</td><td rowspan="2">Blue Hydrogen</td><td>Natural gas reforming and CCUS</td><td>Natural Gas</td><td rowspan="2">Low</td></tr>
<tr><td>Gasification and CCUS</td><td>Coal</td></tr>
<tr><td>Turquoise Hydrogen</td><td>Pyrolysis</td><td rowspan="2">Natural Gas</td><td>Solid carbon (by product)</td></tr>
<tr><td>Grey Hydrogen</td><td>Natural gas reforming</td><td rowspan="2">Medium</td></tr>
<tr><td>Brown Hydrogen</td><td rowspan="2">Gasification</td><td>Brawn coal (lignite)</td></tr>
<tr><td>Black Hydrogen</td><td>Black coal</td><td>High</td></tr>
</table>

Hydrogen is extensively used in industries like oil refining, ammonia and methanol production, and iron and steel manufacturing. Between 1975 and 2018, hydrogen production quadrupled, reaching 115 million tons per year globally. Currently, fossil fuels account for more than 95% of hydrogen production, resulting in the emission of approximately 830 million tons of CO_2 per year [8].
48% of hydrogen is produced through steam reforming of natural gas (SR), 30% from petroleum fractions, 18% via combustion activation, and only 4% through electrolysis due to its higher production costs (ranging from €0.61 to €1.30 per liter of gasoline equivalent, compared to €0.33 to €0.57 for SR). Additionally, electrolysis requires electricity, which remains largely dependent on fossil fuel combustion for the foreseeable future [8].
Other renewable-based hydrogen production methods, such as aqueous phase reforming, photo electrolysis, and thermochemical water splitting, are still in the experimental stage. Biomass

fermentation has reached commercial scale, but it remains more expensive than steam reforming, with production costs of up to €0.86 per liter of gasoline equivalent [8].

2. CO_2 capture from hydrogen plant process streams

CO_2 capture is the first stage of the carbon capture and storage (CCS) chain, and it is typically the most energy-intensive and costly process. In many cases, carbon capture, especially from flue gases, along with its purification and compression (usually to pressures between 100 and 135 atm for economical transport) accounts for the majority of the overall costs associated with CCS [9].
Currently, significant research and development efforts are underway worldwide to improve the efficiency and cost-effectiveness of the CO_2 capture process. While many of these initiatives focus on capturing CO_2 from coal-fired power plants, which are the largest stationary source of CO_2 emissions, it is worth noting that existing carbon capture technologies can also be used in hydrogen production facilities.
In recent decades, significant research has focused on finding efficient and cost-effective CO_2 sorbents. A wide range of materials are now commercially available for CO_2 capture via various technological processes, including activated carbons, zeolites, alkali and alkaline earth metal oxides, ionic liquids, polymeric membranes, and metal-organic frameworks (MOFs).

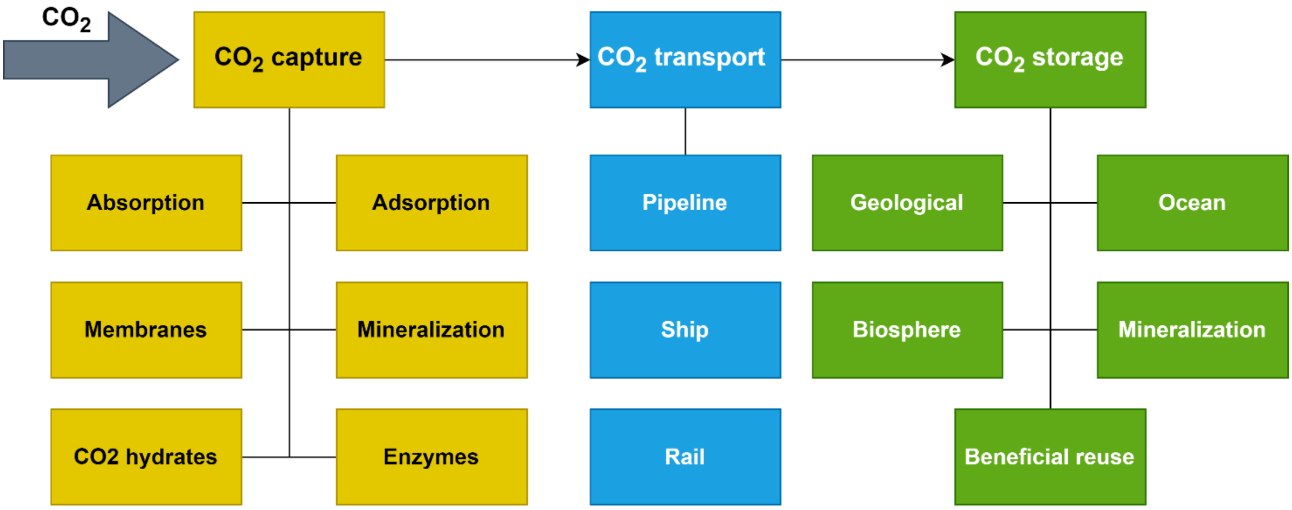

Fig. 1. Overview of Current and Emerging CO_2 Capture and Storage Technologies [9]

3. Integration of Steam Methane Reforming with Carbon Capture and Storage

The steam methane reforming (SMR) process is the most common industrial method for hydrogen production, having been used for decades to produce hydrogen efficiently. As a mature technology, natural gas SMR operates at or near the theoretical efficiency limits and is responsible for producing nearly all of the hydrogen (in the form of a mixture of hydrogen and carbon monoxide) used in the chemical industry, as well as supplemental hydrogen for refineries.
Tessie du Motay and Marechal were the first to document the process of converting hydrocarbons into hydrogen in the presence of steam in 1868, and SMR was first used in industry in 1930 [10]. This process uses methane, naphtha, and fuel oil as feedstocks.
The SMR process is catalytic in nature and involves multiple steps and harsh reaction conditions. It is a reaction between natural gas or other light hydrocarbons and steam that produces a mixture of hydrogen, carbon monoxide, carbon dioxide, and water through a series of three reactions. In the conventional SMR process, as shown in Figure 2, the first reforming step is a catalytic reaction of methane with steam introduced into the reformer furnace, which produces hydrogen and carbon monoxide via an endothermic reaction.

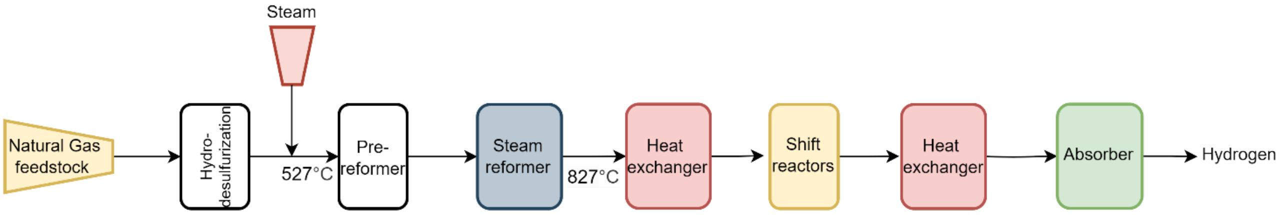

Fig. 2 Overview of Current and Emerging CO2 Capture and Storage Technologies [11]

PSA is a commonly used technique for removing CO_2, water, methane, and CO from off-gas streams. The traditional steam methane reforming (SMR) process requires multiple complex reaction steps to purify hydrogen (H_2), resulting in high capital investment and reduced efficiency. According to Myers et al.,[12] the combined costs of the water-gas shift reaction and PSA account for approximately 30% of the total expenditure on hydrogen production.

4. Conclusions

Hydrogen is emerging as a key energy carrier to facilitate the decarbonization of global energy and industrial sectors; thus, the production of hydrogen from renewable energy sources has garnered significant interest in recent years. Extensive research is underway to advance hydrogen (H_2) generation technologies. Hydrocarbon reforming is currently the most advanced and widely used technology. To reduce reliance on fossil fuels, considerable efforts are being directed toward the development of alternative hydrogen generation methods utilizing renewable resources, such as biomass and water.
To diminish dependence on fossil fuels, considerable efforts are underway to devise alternative hydrogen production techniques utilizing renewable resources like biomass and water. Despite the potential of these technologies, the most efficient way to produce green hydrogen—namely, steam methane reforming combined with carbon capture – is still up to seven times more expensive than producing conventional fossil fuels.
To address these economic challenges, various governments and institutions are increasingly providing subsidies and financial incentives for hydrogen generation. These subsidies aim to reduce production costs, stimulate research and development, and accelerate the adoption of hydrogen technologies. These initiatives are vital for a sustainable energy future and promoting the global shift away from fossil fuels by facilitating the transition to hydrogen as a clean energy carrier.

References

[1] Dawood, Furat, A. Martin, and G. M. Shafiullah. “Hydrogen production for energy: An overview.” *International Journal of Hydrogen Energy* 45, no. 7 (2020): 3847-3869. https://doi.org/10.1016/j.ijhydene.2019.12.059.
[2] Baykara, S. Z. “Hydrogen: A brief overview on its sources, production and environmental impact.” *International Journal of Hydrogen Energy* 43, no. 23 (2018): 10605–10614. https://doi.org/10.1016/j.ijhydene.2018.02.022
[3] Blumenthal, G. “Kuhn and the Chemical Revolution: A re-assessment.” *Foundations of Chemistry* 15, no.1 (2013): 93–101. DOI:10.1007/s10698-011-9129-6.
[4] Huertas, Gaja P., Maria del Mar Llompart Jaume, Raed Kouta, Jean Marc Le Canut, and Xavier Francois. *Standards, codes and regulations of Hydrogen Refueling Stations and Hydrogen Fuel Cell Vehicles*. Final Degree Project (2014), IMSI Department-Fuel cell, UTBM University.
[5] Rivkin, C., R. Burgess, and W. Buttner. “Hydrogen Technologies Safety Guide,” 2015. www.nrel.gov/publications; https://www.nrel.gov/docs/fy15osti/60948.pdf.
[6] Tabkhi, F., C. Azzaro-Pantel, L. Pibouleau, and S. Domenech. “A mathematical framework for modelling and evaluating natural gas pipeline networks under hydrogen injection.” *International Journal Hydrogen Energy* 33, no. 21 (2008): 6222–6231. https://doi.org/10.1016/j.ijhydene.2008.07.103.
[7] Saeidi, Samrand, András Sápi, Asif Hussain Khoja, Sara Najari, Mariam Ayesha, Zoltán Kónya, Bernard Baffour Asare-Bediako, Adam Tatarczuk, Volker Hessel, Frerich J. Keil, and Alírio E. Rodrigues. “Evolution

paths from gray to turquoise hydrogen via catalytic steam methane reforming: Current challenges and future developments." *Renewable and Sustainable Energy Reviews* 183 (September 2023): 113392. https://doi.org/10.1016/j.rser.2023.113392.

[8] International Energy Agency. "Global Hydrogen Review 2024." 2024. www.iea.org.

[9] Muradov, N. "Low to near-zero CO_2 production of hydrogen from fossil fuels: Status and perspectives." *International Journal of Hydrogen Energy* 42, no. 20 (2017): 14058-14088. https://doi.org/10.1016/j.ijhydene.2017.04.101.

[10] Barelli, L., G. Bidini, F. Gallorini, and S. Servili. "Hydrogen production through sorption-enhanced steam methane reforming and membrane technology: A review." *Energy* 33, no. 4 (2008): 554-570. https://doi.org/10.1016/j.energy.2007.10.018.

[11] Go, K. S., S. R. Son, S. D. Kim, K. S. Kang, and C. S. Park. "Hydrogen production from two-step steam methane reforming in a fluidized bed reactor." *International Journal of Hydrogen Energy* 34, no. 3 (2009): 1301–1309. https://doi.org/10.1016/j.ijhydene.2008.11.062.

[12] Myers, D. B., G. D. Ariff, B. D. James, J. S. Lettow, C. E. Thomas, and R. C. Kuhn. "Cost and Performance Comparison Of Stationary Hydrogen Fueling Appliances." Engineering, Environmental Science, Report (2002), Corpus ID: 30167057. https://www.nrel.gov/docs/fy02osti/32405b2.pdf.

ISSN 1454 - 8003
Proceedings of 2024 International Conference on Hydraulics and Pneumatics - HERVEX
November 13-15, Băile Govora, Romania

EFFICIENCY OF LED BULBS COMPARED TO CONVENTIONAL BULBS - ENERGY CONSUMPTION STUDY

Emina PAŠIĆ[1], Nusret IMAMOVIĆ[1]

[1] University of Zenica, Faculty of Mechanical engineering, Bosnia and Herzegovina,
emina.kadusic@unze.ba, nusret.imamovic@unze.ba

Abstract: *This study examines the energy efficiency of LED bulbs in comparison to more traditional lighting technologies, specifically focusing on incandescent and compact fluorescent lamps (CFLs). In today's world, where there is an increasing emphasis on environmental conservation and sustainable energy practices, the need for energy-efficient lighting has become more prominent. This paper aims to provide a detailed analysis of the energy consumption, light output, and overall operational performance of these three lighting technologies. By doing so, it offers deeper insights into their long-term sustainability, economic feasibility, and potential environmental impact. This research evaluates how LEDs, incandescent bulbs, and CFLs compare in terms of energy consumption and the amount of visible light they produce, measured in lumens. The primary objective of the study is to provide a quantitative comparison between these lighting options, enabling consumers and industries to make informed decisions based on their lighting requirements. The experimental design includes a range of wattages to ensure a comprehensive analysis. For incandescent bulbs, the study focuses on three common wattages: 60W, 75W, and 100W. These incandescent bulbs will be compared to equivalent LED and CFL counterparts, matched in terms of lumen output. This approach allows the research to assess not only how energy efficiency varies between different bulb types but also how wattage impacts performance within each lighting technology. By examining multiple wattages, the study provides insight into how various lighting sources perform under different conditions and lighting demands. For a detailed comparison, energy consumption will be carefully measured alongside light output at varying distances from the light source. This ensures that the analysis is not based solely on power consumption but also on the practical usability of the light produced. These findings are expected to support the global transition toward more energy-efficient and environmentally sustainable lighting systems, contributing to the broader objective of sustainable development.*

Keywords: *LED bulbs, energy consumption study, energy efficiency, green transition*

1. Introduction

Lighting efficiency plays a crucial role in global efforts to reduce energy consumption and conserve resources. In recent decades, LED bulbs have become a popular alternative to conventional incandescent bulbs and fluorescents bulbs due to their higher energy efficiency and longer lifespan. Among all the electric consumers, lighting has one of the highest shares in the residential and commercial sector. Lighting accounts for approximately 20% to 30% of the electricity consumption worldwide [1]. The first LED lamps that could replace traditional incandescent lamps appeared on the market as early as the late 1990s, but their light did not yet provide adequate visual comfort. Satisfactory results were obtained only at the beginning of the current century. At present, most of the lamps produced achieve luminous efficacy from 70 even to 205 lm/W [2]. Although the initial costs of LED bulbs are higher, the potential energy savings and lower operational costs make them an attractive choice for households and commercial spaces. In general, energy efficiency is defined as the consumption of less energy in the process of guaranteeing the same energy service. Figure 1 shows the energy efficiencies of selected major lamp technologies. Incandescent lamps have efficiencies ranging between 1.5% and 2.2%, while LEDs are much more efficient, with efficiencies varying between 19% and 29.2%. These differences in efficiency are related to the conversion efficiency of electricity into luminous flux in each technology, based on the different physical principles used. From Figure 1, the conversion efficiency is close to 30% for LED technology. [3]

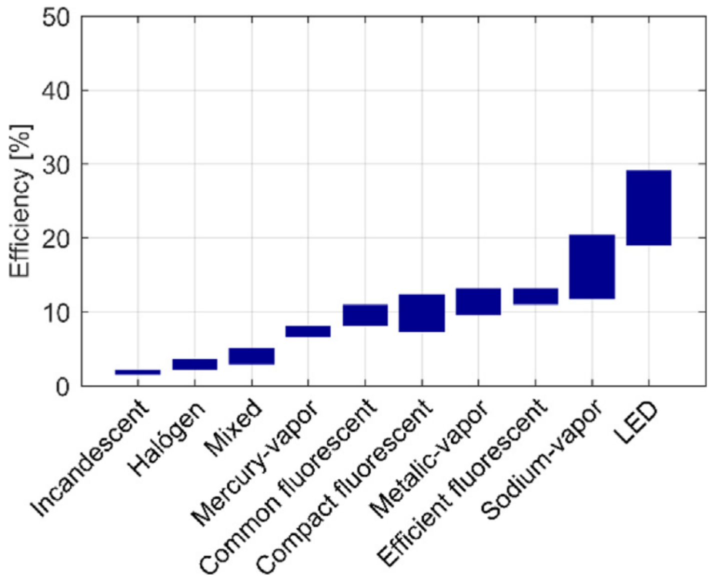

Fig. 1. Lamp technology efficiencies [1]

While LED lamps are generally regarded as the most energy-efficient choice for lighting projects, followed by CFLs, the actual effectiveness of electrical energy usage can vary. This is because energy efficiency depends not only on the power rating of the lamps but also on their power factor. As a result, even with lower energy consumption, the desired level of illumination might not be achieved. To reach the necessary brightness, additional lamps of the same power might be required, leading to an overall increase in energy consumption, which contradicts initial estimates. In this study the main effort was to analyze the energy consumption of each type of light bulbs compared to their change of power factors. The power factor significantly affects the amount of energy required to deliver effective power at the point of consumption and indicates how much actual energy consumption exceeds the nominally declared amount [3].
This research was initiated following multiple case studies and energy audits which consistently highlighted significant reductions in electricity consumption after the installation of LED light bulbs. These findings demonstrated the potential for LED lighting to enhance energy efficiency, motivating a deeper investigation into the relationship between light intensity, energy usage, and bulb type across different environments [4,5].

2. Methodology

In this study, three different types of light bulbs were used: incandescent, fluorescent, and LED, with three tested lumens emitted. The experimental design includes a range of lumens to ensure a comprehensive analysis. By examining multiple wattages, the study provides insights into how various lighting sources perform under different conditions and lighting demands. For a detailed comparison, energy consumption will be carefully measured alongside light output at varying distances from the light source. Measurements were conducted at three different distances from the light source. This ensures that the analysis is not based solely on power consumption but also on the practical usability of the light produced. The goal is to determine how efficiently each lighting technology converts electrical energy into light and whether it provides sufficient illumination for different applications. This is particularly important in identifying which lighting technology is most suitable for residential, commercial, and industrial settings.

2.1. The experimental setup

The experiment was conducted under controlled conditions, where all other light sources were eliminated, and a constant room temperature was maintained. The light bulbs were positioned at a fixed height of 2m meters above the floor, while the measuring device i.e. lux meter was placed at three fixed distances (0.5, 1m, and 1.5m) from the light source. An energy meter was placed between the light bulb and the power source to accurately record energy consumption. Each type of light bulb was tested at three power levels: 60W, 75W, and 100W for the incandescent bulbs, while lumen equivalents were used for the LED and fluorescent bulbs, specifically 800 lm, 1000 lm, and 1500 lm. This means that for LED, bulbs which was used were 8W, 10W and 14W, while for fluorescent bulbs 15, 20, 25W. Each light bulb was placed in a controlled environment, without additional light sources. Measurements began after 15min, i.e. when the light bulb had been operating long enough to reach a stable state. The illustration of experimental setup can be seen in Figure 2, where H represents the distance of light body from the ground and h represents distance of working plane.

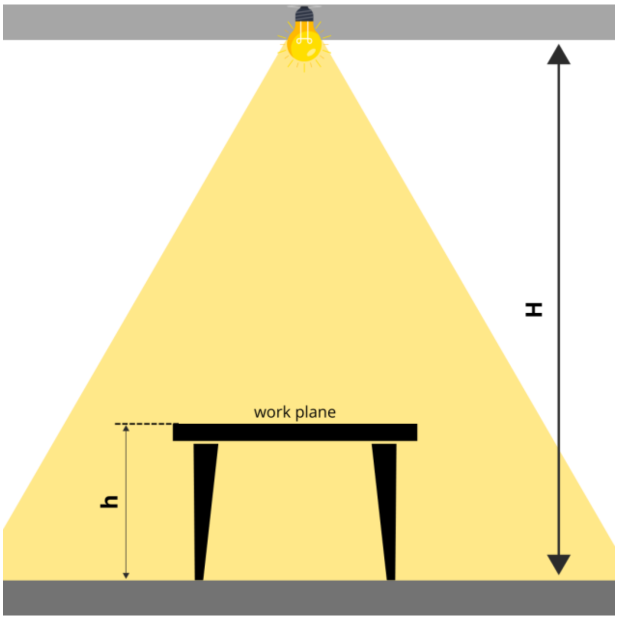

Fig. 2. Illustration of experimental setup

For maintaining the controlled conditions (room temperature and humidity) as well as measuring light intensity in lumens, it was used the device PCE-222 - digital thermometer shown in Figure 3a, while for measuring the energy consumption the smart plug which was connected to the mobile app Smart Life in order to measure real time energy consumption while the lights bulbs were working, as shown in Figure 3b. By using all input parameters, the experiment was conducted using a 3x3x3 factorial design (3 types of lights bulbs x 3 x power levels x 3 distances) which means total of 27 measurements combinations were performed. For each combination (type of bulb, power, and distance), measurements were repeated three times to obtain average values. Measurements were conducted sequentially for all three distances, starting from the closest. In Table 1. is shown a plan of experiment.

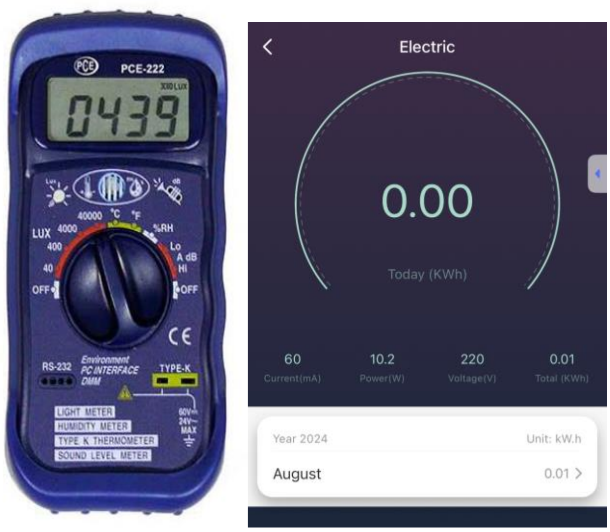

Fig. 3. Instruments used for the experiment; 3a. PCE-222 3b. Smart life app for energy consumption measurements

Table 1: Plan of experiment

Type of light bulb	Lumen value [lm]	Lux [lm/m^2]			Energy Consumption
		Distance 0,5m	Distance 1m	Distance 1,5m	
Incandescent	800	Measurement 1	Measurement 2	Measurement 3	Measurement X1
Incandescent	1000	Measurement 4	Measurement 5	Measurement 6	Measurement X2
Incandescent	1500	Measurement 7	Measurement 8	Measurement 9	Measurement X3
Fluorescent	800	Measurement 10	Measurement 11	Measurement 12	Measurement X4
Fluorescent	1000	Measurement 13	Measurement 14	Measurement 15	Measurement X5
Fluorescent	1500	Measurement 16	Measurement 17	Measurement 18	Measurement X6
LED	800	Measurement 19	Measurement 20	Measurement 21	Measurement X7
LED	1000	Measurement 22	Measurement 23	Measurement 24	Measurement X8
LED	1500	Measurement 25	Measurement 26	Measurement 27	Measurement X9

3. Results and data processing

The main goal of this experiment was to compare the performance of three different types of bulbs across various power levels and distances. Key parameters such as light intensity and energy consumption were measured to evaluate the efficiency and effectiveness of each bulb type. The collected data provides valuable insights into how different lighting technologies perform under specific conditions, allowing for a detailed analysis of their practical applications. The following section presents the results of the measurements and outlines the steps taken in data processing to ensure accurate and reliable finding.

3.1. Results

After conducting measurements for all combinations of bulb types, power, and distances, the collected data includes values for light intensity and energy consumption is shown in Table 2. The experiment was conducted under controlled conditions (room temperature 20^{o}C and humidity 46%).

Table 2: Results of experiment

Type of light bulb	Lumen value [lm]	Lux (lm/m^2)			Energy Consumption [W]
		Distance 0.5m	Distance 1m	Distance 1.5m	
Incandescent	800	524	125	52	62.1
Incandescent	1000	657	223	87	78.1
Incandescent	1500	1001	337	129	93.4
Fluorescent	800	543	153	37	9
Fluorescent	1000	688	306	68	10.3
Fluorescent	1500	841	431	103	16.2
LED	800	643	213	98	8.3
LED	1000	887	435	124	10.2
LED	1500	1020	520	179	11.8

3.2. Data processing

To address the research objectives, a detailed statistical analysis was conducted to evaluate the differences in light output (lux) between different types of light bulbs (incandescent, fluorescent, and LED), to assess the effect of distance on light intensity, and to analyse the energy efficiency of each bulb type. The analysis involved four major components:

- Comparison between light bulbs types: Using a one-way ANOVA to compare the lux values between incandescent, fluorescent and LED bulbs across different distances;
- Effect of distance on lux: Perform a linear regression analysis to see how distance affects lux values for each type of bulb and visualize the trend.
- Energy efficiency comparison: Compute the ratio of lux to energy consumption (lux per watt) for each type of bulb to measure their energy efficiency.
- Comparison of measured vs. specified power levels.

4. Results discussion

A one-way analysis of variance (ANOVA) was performed to compare the lux values produced by incandescent, fluorescent, and LED bulbs at different distances. This statistical test was chosen to determine whether there were significant differences in the brightness levels (lux) emitted by the three types of bulbs. The null hypothesis for this test was that there is no significant difference in lux output between the bulb types, while the alternative hypothesis posited that at least one group had a significantly different mean lux value. The results indicated that at all distances, the p-values were greater than 0.05, suggesting that the differences in lux values between the bulb types were not statistically significant. Therefore, it can be concluded that incandescent, fluorescent, and LED bulbs produce similar levels of brightness at these measured distances. To further investigate the impact of distance on the intensity of light (lux), a linear regression analysis was performed for each type of bulb. The regression analysis aimed to quantify the relationship between the lux values at three measured distances and to determine how distance affects the light intensity for each bulb type. For all three bulb types, the results showed a clear negative slope, indicating that lux values decrease as the distance from the light source increases. LED bulbs exhibited the steepest decline in lux levels with distance, followed by incandescent and fluorescent bulbs, as shown in Figure 4.

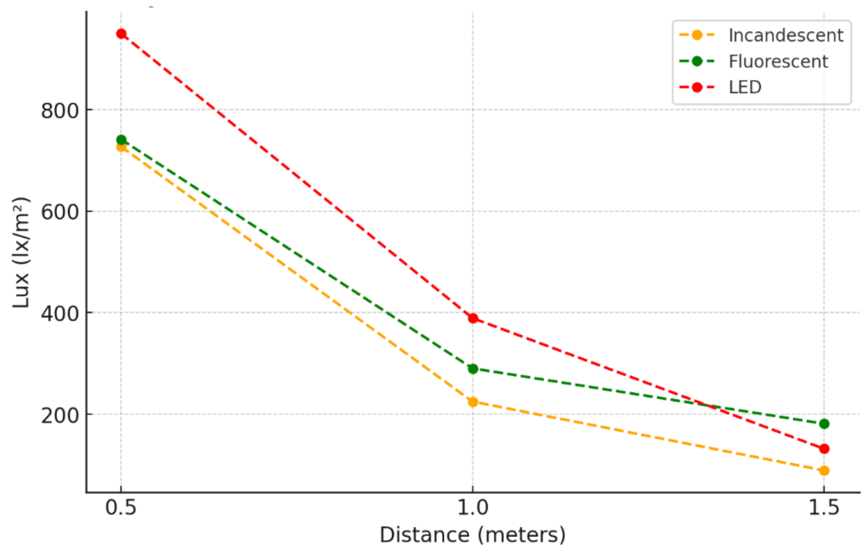

Fig. 4. Effect of Distance on Lux for Different Bulb Types

Energy efficiency is a critical factor when evaluating lighting systems. To measure the energy efficiency of each type of bulb, the ratio of lux per watt (lux divided by energy consumption) was calculated at all three distances. This metric provides a standardized way to compare how much light (lux) each bulb produces per unit of energy consumed, as shown in Table 3. The analysis revealed that LED bulbs were the most energy-efficient, producing the highest lux per watt across all distances. Fluorescent bulbs were moderately efficient, while incandescent bulbs had the lowest energy efficiency, consuming significantly more power to produce the same level of brightness. This finding is consistent with the well-documented superiority of LED and fluorescent technology in terms of energy savings compared to traditional incandescent bulbs.

Table 3: Energy efficiency of light bulbs

Type of light bulb	Lux per Watt		
	Distance 0.5m	**Distance 1m**	**Distance 1.5m**
Incandescent	9.189213	2.825444	1.110823
Fluorescent	59.681010	24.437892	5.690359
LED	83.623780	37.459168	13.044527

To assess the accuracy of manufacturer-reported power levels, the measured energy consumption of each bulb type was compared to the specified (nominal) consumption provided by the manufacturer. This analysis aimed to quantify any discrepancies between the actual energy consumption and the expected values, providing insights into how closely each type of bulb adheres to its nominal specifications**.** Table 4 shows the average measured energy consumption, expected energy consumption, and the difference (discrepancy) between the two for each type of light bulb.

Table 4: Comparison of measured energy consumption vs. producer specified

Type of light bulb	Measured consumption [Wh]	Expected Consumption [Wh]	Difference [Wh]
Incandescent	11.83	20.00	-8.17
Fluorescent	77.87	78.33	-0.47
LED	10.10	10.67	-0.57

The results indicate that fluorescent bulbs exhibit the largest discrepancy, with an average measured consumption of 11.83Wh, which is 8.17Wh lower than the expected 20Wh. This substantial deviation suggests that the actual energy use of fluorescent bulbs in the tested conditions is considerably more efficient than specified by the manufacturer. In contrast, incandescent bulbs demonstrated a much smaller deviation, with a measured consumption of 77.87Wh, only 0.47Wh lower than the expected average of 78.33Wh. This near-perfect alignment suggests that incandescent bulbs perform as expected in terms of energy consumption. Similarly, LED bulbs showed only a slight deviation from their specified power levels, consuming 10.10Wh on average, 0.57Wh lower than the expected value of 10.67Wh. The close match between the measured and expected values for LED bulbs reinforces their reliability and energy efficiency. The lower-than-expected consumption of fluorescent bulbs could be attributed to variations in testing conditions or improvements in the energy efficiency of modern fluorescent technologies. However, this differences can vary from different producers.

5. Conclusions

This study aimed to evaluate and compare the performance of three different types of light bulbs—incandescent, fluorescent, and LED—across various power levels and distances. The primary goal was to assess the light output (lux), energy consumption, and energy efficiency of each bulb type, while also examining any discrepancies between measured energy consumption and manufacturer-reported power levels. The analysis revealed several key insights:

- Lux Output and Distance: A one-way ANOVA showed no statistically significant differences in lux output between the bulb types at various distances. While the lux values decreased with increasing distance for all bulb types, the rate of decline was most pronounced for LED bulbs, followed by incandescent and fluorescent bulbs. This indicates that distance significantly impacts the effectiveness of each lighting technology, particularly for LED bulbs.
- Energy Efficiency: LED bulbs were found to be the most energy-efficient, producing the highest lux per watt across all distances. Fluorescent bulbs were moderately efficient, while incandescent bulbs were the least efficient, consuming significantly more energy to produce the same level of brightness. These findings align with previous studies, highlighting the energy-saving potential of LED and fluorescent technologies compared to traditional incandescent lighting.
- Measured vs. Specified Power Levels: The comparison between measured and specified power levels revealed some discrepancies, particularly for fluorescent bulbs, which consumed 8,17Wh less on average than the manufacturer-specified 20Wh. This suggests that fluorescent bulbs may be more energy-efficient in real-world applications than reported. In contrast, incandescent and LED bulbs showed minimal deviations from their specified power levels, reinforcing the reliability of their reported energy consumption.

In conclusion, LED bulbs offer the greatest energy efficiency and light output per watt, making them an ideal choice for both residential and commercial lighting applications. Fluorescent bulbs provide a moderate level of efficiency but may offer unexpected energy savings in certain conditions. Incandescent bulbs, while performing close to their expected power levels, remain the least energy-efficient option. As the global emphasis on energy conservation and sustainability continues to grow, this study reinforces the importance of selecting appropriate lighting technologies to reduce energy consumption and operational costs. Further research could explore how these findings translate to larger-scale lighting systems and different usage.

References

[1] Wantuch, A., and M. Olesiak. "Effect of LED Lighting on Selected Quality Parameters of Electricity." *Sensors* 23, no. 3 (2023): 1582. https://doi.org/10.3390/s23031582.

[2] Ferreira de Souza, D., P. Fernandes da Silva, L. Almeida Fontanele, G. Barbosa, and M. Jesus. "Efficiency, Quality, and Environmental Impacts: A Comparative Study of Residential Artificial Lighting." *Energy Reports* 5 (November 2019): 409-424. https://doi.org/10.1016/j.egyr.2019.03.009.

[3] Jayaweera, A. *Energy Analysis & Effects on Power Utility of LED's Compared to Conventional Bulbs*. Master's thesis. Royal Institute of Technology, Sweden, 2014.

[4] Fawkes, S., K. Oung, and D. Thorpe (Imamović, N., and S. Mujičić, trans.). *Best Practices and Case Studies for Industrial Energy Efficiency Improvement - An Introduction for Policy Makers* / *Najbolje prakse i studije slučaja za poboljšanje energijske efikasnosti u industriji - Uvodne smjernice za kreatore politika*. Zenica, Institute for Economic Engineering, 2023, ISBN 978-9926-543-00-6.

[5] Imamović, N., E. Kadušić, D. Eminović, and L. Mešeljević. *Detailed Energy Audit for the Building "Mettalon Plast" d.o.o., Zenica* / *Izrada detaljng energijskog audita za objekat „Mettalon Plast" d.o.o., Zenica.* Center for Energy Efficiency, Faculty of Mechanical Engineering, University of Zenica / Centar za energetsku efikasnost Mašinskog fakulteta Univerziteta u Zenici.

ISSN 1454 - 8003
Proceedings of 2024 International Conference on Hydraulics and Pneumatics - HERVEX
November 13-15, Băile Govora, Romania

SYSTEM FOR RECOVERING AND CONVERTING POTENTIAL ENERGY INTO ELECTRICAL ENERGY FROM A DIGITAL HYDRAULIC CYLINDER

Ioan PAVEL[1], Radu- Iulian RĂDOI[1], Gabriela MATACHE[1], Ștefan-Mihai ȘEFU[1]

[1] National Institute of Research & Development for Optoelectronics/INOE 2000, Subsidiary Hydraulics and Pneumatics Research Institute/IHP, Romania

Abstract: *Energy recovery in hydraulic systems is becoming increasingly important for reducing energy consumption and carbon emissions. This article presents a solution for recovering and converting potential energy into electrical energy from a digital hydraulic cylinder. The solution was studied on a test stand for digital hydraulic cylinders. During the retraction of the cylinder rod under simulated potential energy load, the flow discharged from the three chambers of the digital cylinder is used to rotate a hydraulic motor/electric generator unit. The generated electrical energy was measured and stored in a battery. The results are promising, especially for mobile machinery that can store the recovered energy directly in a battery.*

Keywords: *Potential energy recovery, Digital hydraulic cylinders*

1. Introduction

The concept of digital hydraulics for hydraulic cylinders is based on discretizing the working surface, with each discretized size having two on/off states. By combining sections and states, active control of speed or force can be achieved at the actuator.

The studied solution for the digital cylinder involves discretizing the active surface into three concentric sections for extension and one for retraction. The result is a digital servocylinder, which operates with constant flow and pressure while providing seven selectable levels of force or speed.

The digital hydraulic cylinder can be used as an actuator in any hydraulic system that requires force and speed adjustments. For example, it can be applied to stamping presses that need high speed for idle strokes and high force for pressing. Traditional solutions use variable flow pumps and sophisticated multi-stage pressure valves, resulting in high initial costs and low energy efficiency.

Despite the good efficiency of hydraulic components, the overall efficiency of hydraulic systems is generally low. Hydraulic load-sensing systems with potential energy recovery, widely used in mobile applications, can offer an efficiency improvement of up to 4% [1].

The potential to reduce losses by over 33% in multi-actuator systems has been studied through simulations on a loader, replacing the traditional LS system with a digital hydraulic valve system (DVS) [2].

Another solution to minimize or eliminate the need for proportional valves involves the use of hydraulic transformers. These are powered by a pressure line that drives both the working mechanisms and the rotary drive system of a front loader [3,4].

A simulation was also conducted to obtain multiple speed levels at the rod of the digital hydraulic cylinder by using a signal source configured with five steps [5].

Energy recovery in hydraulic systems is becoming increasingly important for reducing energy consumption and carbon emissions. Recent studies focus on recovering potential energy in lifting-lowering equipment equipped with hydraulic cylinders, using hydraulic accumulators to offset consumption peaks.

An extremely efficient hybrid hydraulic system was also developed for an excavator, utilizing a multi-chamber cylinder and secondary control. A detailed energy analysis was performed, explaining energy flow in the hybrid system [6].

A solution for converting potential energy into electrical energy was evaluated through simulations on a digital hydraulic cylinder test bench [7].

In conclusion, the trend in modern hydraulic research is to minimize losses by investigating energy recovery methods [8,9,10,11].

2. Test results on an experimental model of a digital cylinder

The test results were obtained using an experimental model of a digital cylinder with three extension chambers, mounted on a specialized test stand developed by the authors at INOE 2000 IHP.
The test stand (Figure 1) comprises: two electro-pumps, SP1 and SP2, a distribution block (BD) with four distributors, a motor-generator (MG) unit, a data acquisition board and virtual instrument software programmed in LabVIEW with embedded control logic for supplying the chambers of the digital hydraulic cylinder (CD) and the data acquisition system for the measured signals (force, displacement, pressure, flow rate).

Fig. 1. Test stand

The digital hydraulic cylinder (CD) tested in the laboratory (Figure 2) features a piston surface divided into three functionally independent annular zones. The cylinder was supplied with constant pressure, and by selecting combinations of active zones, seven force levels were achieved. These force levels can be controlled by commanding the distribution block via dedicated software.

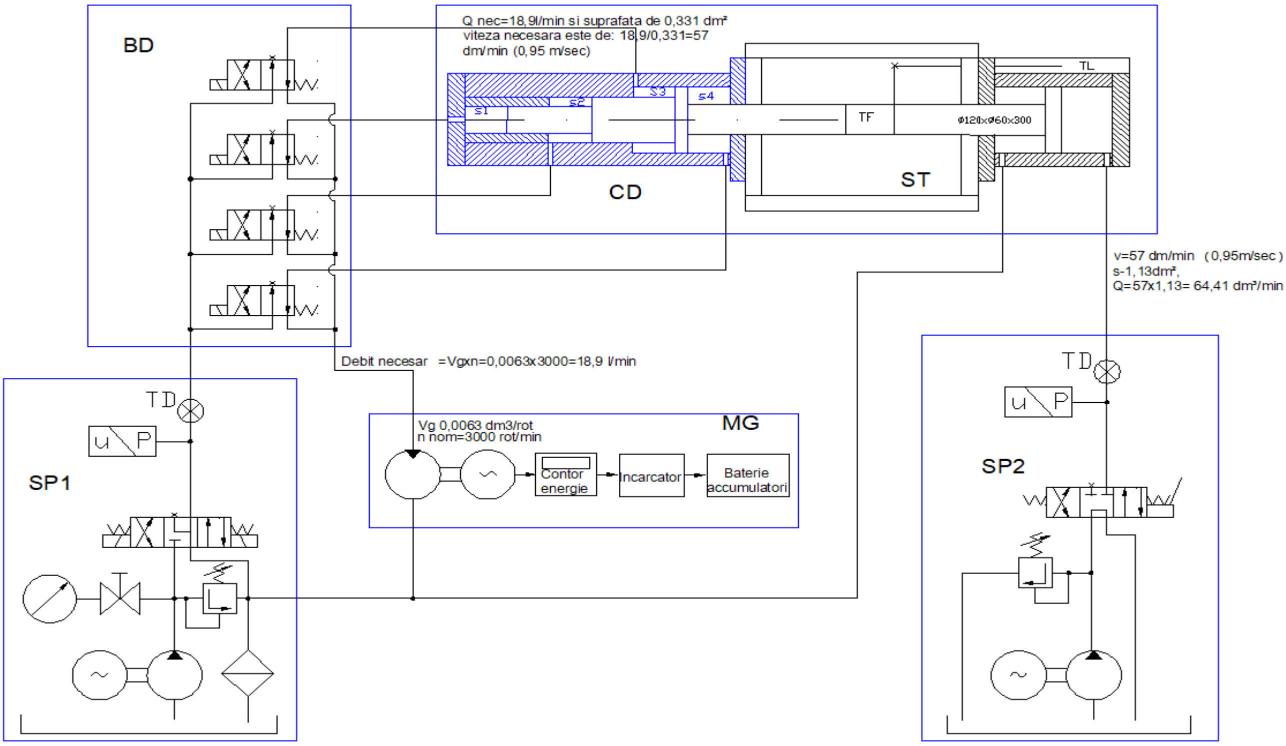

Fig. 2. Hydraulic diagram of the stand for converting potential energy into electrical energy

For energy recovery, a return of the digital cylinder under a load representing the potential energy targeted for recovery and transformation into electrical energy was simulated.

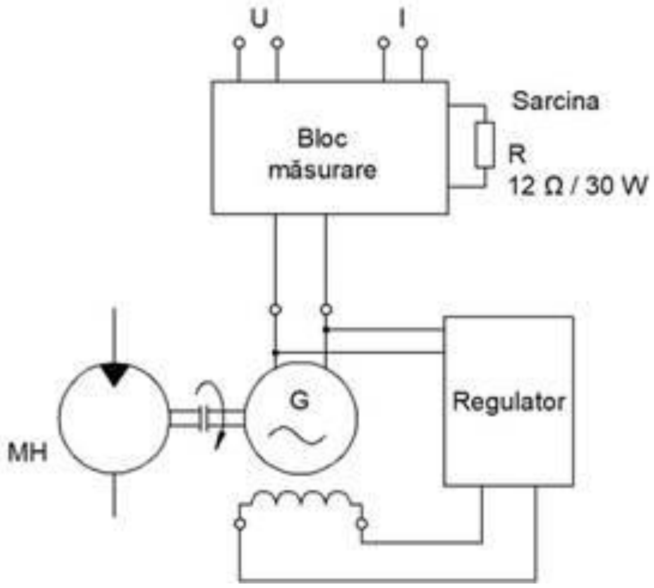

Fig. 3. Electrical diagram of the block measuring the recovered energy

The energy of the pressurized hydraulic fluid expelled from the hydraulic cylinder at retraction is recovered by driving a rotary hydraulic motor coupled with a synchronous electric generator (Figure 3). The generator contains an internal regulator that adjusts the excitation coil to provide a constant voltage. To measure the voltage and current delivered by the generator, a measuring block and a load resistor are used. The measuring block contains a bridge rectifier and a 0.3 ohm shunt for measuring the current, and a resistive divider is used for the voltage at the load resistor terminals, so that the measured voltage does not exceed the input level in the data acquisition board.
The tests were carried out in two stages:
1. In the first stage, the data acquisition was carried out for the advance of the digital cylinder in which the seven combinations of aligned chambers are ordered and the seven force stages are obtained (Figure 4).

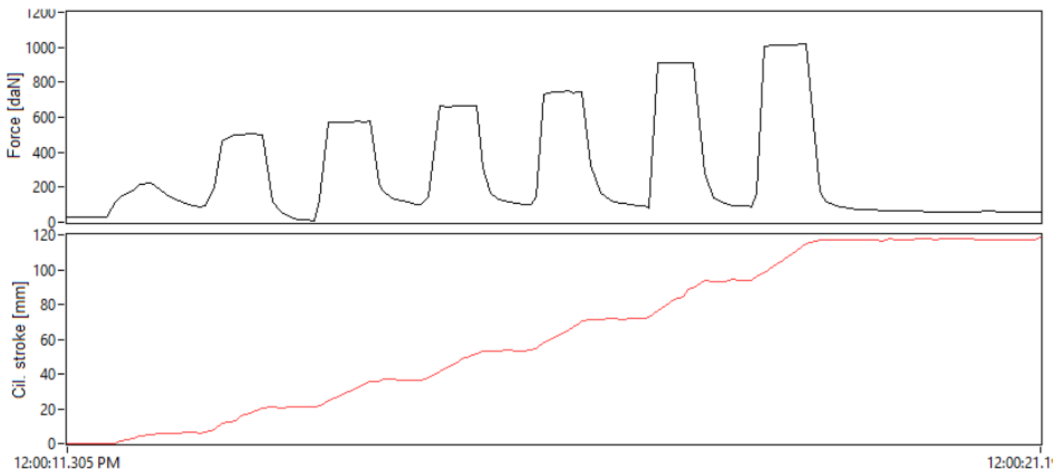

Fig. 4. Power steps obtained from powered chamber combinations

2. In the second stage, data acquisition was performed for the withdrawal of the digital cylinder (Figure 5) and the recovery of the simulated potential energy by using the flow discharged by the three chambers of the digital cylinder when rotating a hydraulic motor-electric generator unit. The

ISSN 1454 - 8003
Proceedings of 2024 International Conference on Hydraulics and Pneumatics - HERVEX
November 13-15, Băile Govora, Romania

electricity obtained was measured (Figure 6) and stored in a battery. The sudden acceleration of the simulated load to approximately 2000 daN develops an initial measured force of almost 5000 daN after which it stabilizes at the set value throughout the rest of the stroke.

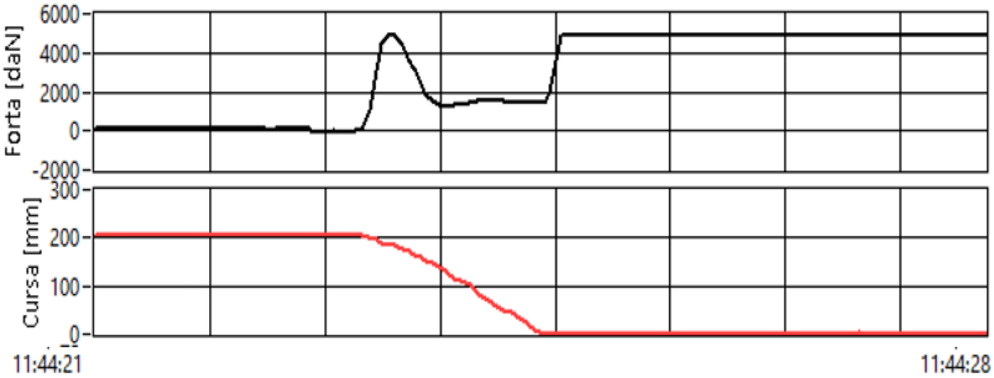

Fig. 5. Evolution of the force along the entire stroke of the digital cylinder at the rebound stroke with energy recovery

In order to measure the recovered energy, the values of current, voltage and power were acquired (Figure 6).

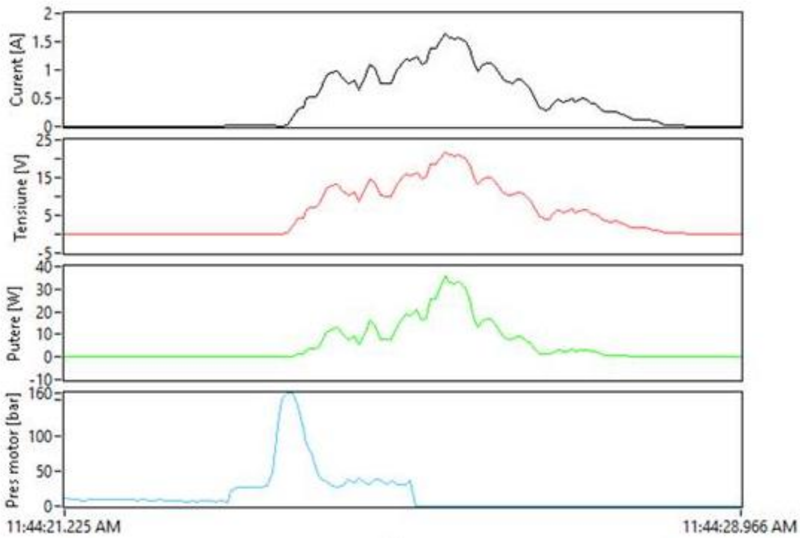

Fig. 6. Evolution of current, voltage, power and pressure at the hydraulic-electric generator motor unit during a rod retraction stroke

The current obtained from the recovery of the simulated potential energy was 1.5 A and the voltage was 15 V. The resulting power was approx. 20 W. The overload created at the initial acceleration of the simulated load created a pressure peak at the initial rotation of the hydraulic motor-electric generator set of 160 bar after which it decreased and stabilized at 40 bar.

4. Conclusions

The hydraulic cylinder is the most widely used piece of equipment in hydraulic drives and is an essential starting point in plant design. Digital cylinders allow the variation of the working area, and implicitly of the operating force and speed, offering innovative solutions for hydraulically driven equipment. The introduction of digital technologies in this field can pave the way for new, more efficient applications in modernized or newly designed facilities. It was found on this stand configuration (Figure 2), that in order to reach the nominal speed of the electric generator of 3000 rpm, a cylinder rod retraction speed of 57 dm/min (approx. 1m/sec) is required, thus ensuring a flow rate discharged from chambers C1, C2 and C3 of 18.9 l/min. To achieve this withdrawal speed, the SP2 pumping station must deliver a flow rate of 64.4 l/min. Even in these conditions, due to the short time in which the stroke is carried out and the pressure drops on the routes of the connecting pipes, although the hydraulic engine is accelerated, it does not reach the nominal speed. The voltage obtained under normal test conditions was 15 v and the current was 1.5 A, which means that the application is very well suited to mobile machines for recharging the battery. Even if at first glance the values of the recovered energy are small, if a lifting/lowering machine works continuously then the idea of recovery becomes interesting.

The energy savings resulting from the application of the right energy recovery solutions with digital cylinders can improve the technical-economic performance of production lines, mobile machinery, thus contributing to cost reduction and support for sustainable development.

Acknowledgments

This work was carried out through the Core Program within the National Research Development and Innovation Plan 2022-2027, carried out with the support of the Romanian Ministry of Research, Innovation and Digitalization (MCID), project no. PN 23 05.

References

[1] Garbacik, A., and J. Stecki (eds.). *Developments in Fluid Power Control of Machinery and Manipulators*. Virvalo, T., and M. Vilenius. “The Influence of Pumps and Valves on the Efficiency of a Hydraulic Boom.” Cracow, Fluid Power Net Publication, 2000.
[2] Huova, M., M. Karvonen, V. Ahola, M. Linjama, and M. Vilenius. “Energy Efficient Control of Multiactuator Digital Hydraulic Mobile Machine.” Paper presented at the 7th International Fluid Power Conference (7th IFK), Aachen, Germany, March 22-24, 2010.
[3] Heybroek, K., G.E.M. Vael, and J.-O. Palmberg. (2012). “Towards resistance-free hydraulics in construction machinery.” Paper presented at the 8th International Fluid Power Conference (8th IFK), Dresden, Germany, March 26-28, 2012.
[4] Mäkelä, J. (2020). *Energy efficiency of a digital hydraulic multi-pressure actuator for use in load-lifting applications*. Master Thesis. Aalto University School of Engineering, 2020.
[5] Rădoi, Radu, Ionel Pavel, Polifron Chiriță, Bogdan Tudor, and Vasilica Ștefan. “Energy efficient drive system with digital hydraulic cylinder for construction and agricultural machinery.” *INMATEH - Agricultural Engineering* 68, no. 3 (2022): 13-20.
[6] Heybroek, K., and M. Sahlman. (2018). “A hydraulic hybrid excavator based on multi-chamber cylinders and secondary control – design and experimental validation.” *International Journal of Fluid Power* 19, no. 2 (March 2018): 91-105.
[7] Pavel, Ioan, Gabriela Matache, and Ștefan-Mihai Șefu. “Recovery of potential energy by using a digital hydraulic cylinder.” *Hidraulica Magazine*, no. 3 (September 2024): 74-79.
[8] Bishop, E. “Digital Hydraulic Transformer - Approaching Theoretical Perfection in Hydraulic Drive Efficiency.” Paper presented at the 11th Scandinavian International Conference on Fluid Power, SICFP’09, Linköping, Sweden, June 2-4, 2009.
[9 Kogler, H., R. Scheidl, M. Ehrentraut, E. Guglielmino, C. Semini, and D. A. Caldwell. “Compact Hydraulic Switching Converter for Robotic Applications.” Paper presented at the Bath/ASME Symposium on Fluid Power and Motion Control (FPMC 2010), Bath, UK, September 15-17, 2010.
[10] Juhala, J., J. Kajaste, and M. Pietola. “Improving Energy Efficiency of Hydraulic Accumulator.” Paper presented at the Twelfth Scandinavian International Conference on Fluid Power, SICFP’11, Tampere, Finland, May 18-20, 2011.
[11] Linjama, M., H-P. Vihtanen, A. Sipola, and M. Vilenius. “Secondary Controlled Multi-Chamber Cylinder.” Paper presented at the 11th Scandinavian International Conference on Fluid Power, SICFP’09, Linköping, Sweden, June 2-4, 2009.

ISSN 1454 - 8003
Proceedings of 2024 International Conference on Hydraulics and Pneumatics - HERVEX
November 13-15, Băile Govora, Romania

USING A NEW CAD-CAE DESIGN METHOD FOR DESIGNING A MICROHYDROPOWER SYSTEM FOR HYDRO ENERGY RECOVERY

Eugen MARIN[1,]*, Dragoș MANEA[1], Iulian-Florin VOICEA[1], Liliana DUMITRESCU[2]

[1] National Institute of Research - Development for Machines and Installations Designed to Agriculture and Food Industry - INMA Bucharest / Romania

[2] National Institute of Research & Development for Optoelectronics / INOE 2000 – Subsidiary Hydraulics and Pneumatics Research Institute / IHP, Bucharest / Romania

Abstract: *This paper presents a CAD-CAE design method of a welded metal sub-assembly that is a main component of a microhydropower system, which will recover hydro energy and transform it into electrical energy needed to operate aeration systems in fish ponds, under the conditions of efficient use of exploitable resources in animal husbandry. This research proposes a new approach to 3D modeling and advocates for the promotion of the role of microhydropower systems to minimize* CO_2 *emissions in Romania's economy.*

Keywords: *CAD-CAE design, microhydropower system, renewable energy*

1. Introduction

Climate change is a danger to future generations in the modern world because it causes great damage to economic growth and industrialization [1]. Fossil fuels are considered the main source of global warming and environmental degradation that has occurred with the growth of the global population and the economies of industrially developed countries [2]. Many countries around the world have policy initiatives to switch from conventional fossil fuel-based energy systems to cleaner and more sustainable alternatives [3]. In the world, policy makers leading developed economies can promote sustainable development, mitigate climate change and ensure long-term sustainable electricity production [4]. Internationally, renewable energy is becoming more and more promoted because it is cheaper, cleaner and more efficient than traditional forms of energy. The most important is hydropower, as a source of renewable energy, considered green energy because it is produced in a way that is beneficial to the environment [5].

In the context of the corresponding global need to increase the share of renewable generation in the energy mix, small-scale hydropower systems offer a significant opportunity to move closer to this goal [6].

The design of a micro hydropower system using CAD-CAE concepts and tools based on the application of parameterization methods that are technically and economically viable is very important to ensure sustainable operation [7]. In the design of hydropower generators, which bear multiple forces from various sources during operation, finite element analysis is used for three-dimensional (3D) modeling, with the aim of studying their performance and static properties [8].

Modern design methods are used, for example, for one-way simulation of three-dimensional fluid-structure interaction to analyze the performance of a static Savonius hydrokinetic turbine at different rotor positions [9].

In practical applications, in engineering, methods of analyzing deformable mechanical systems are used, which are based on numerical techniques related to the finite element method (FEM) as well as on the application of classical methods used in analytical mechanics [10].

2. Materials and methods

In the framework of a research project, a microhydropower system was designed, which will recover hydro energy and transform it into electricity necessary for the operation of aeration systems in fish ponds, under the conditions of efficient use of exploitable resources from animal husbandry. Aeration

brings numerous benefits to aquatic ecosystems. In addition to improving fish habitat, water quality, reducing algae and phosphorus, aeration kills unwanted bacteria, solves the mosquito problem and removes unpleasant odors, all by recirculating water and adding dissolved oxygen.
The main elements that make up the microhydropower system are the following:

- the collection and transfer circuit that includes the system of pipes, valves, the exhaust channel, the water outlet;
- frame, rotor with paddle type blades, transmission guard;
- the speed multiplier, the belt for transmitting the movement to an electrical generator with permanent magnets;
- the electric cables, the controller, the electric energy storage batteries and the inverter for the transformation of the direct voltage electric energy into the 220V alternating voltage electric energy needed to supply the ventilation systems.

Figure 1 shows the 3D geometric model of the microhydropower system, which was CAD designed using SolidWorks software.

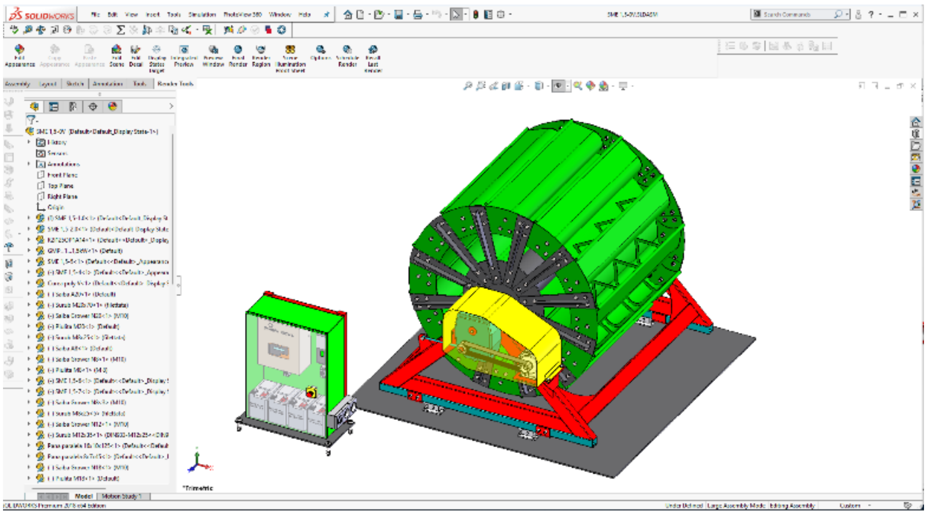

Fig. 1. The 3D geometric model of the microhydropower system

The rotor with paddle-type blades (fig. 2) is the main working organ of a microhydropower system and is intended for the conversion of the kinetic energy of the water flow and its transmission through the kinematic chain to the aggregates producing electricity (multiplier+generator).

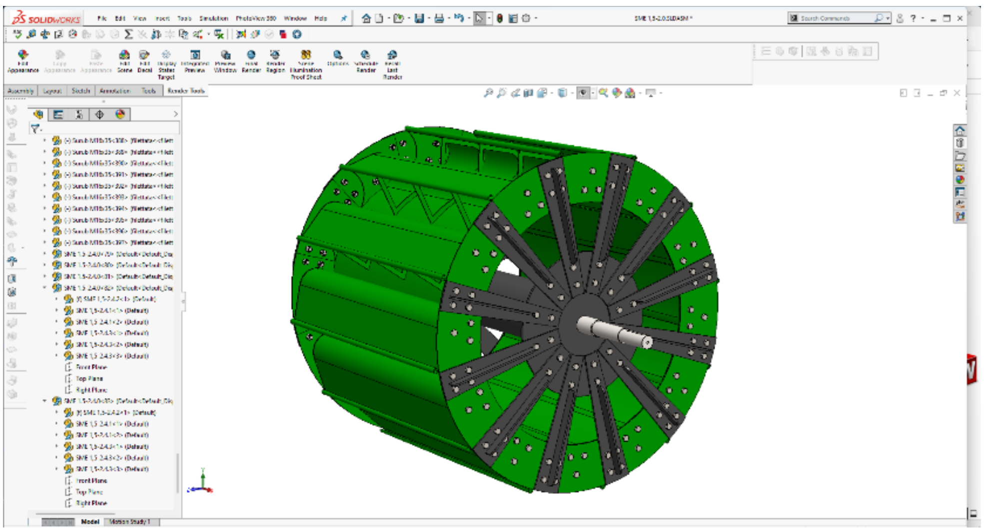

Fig. 2. The rotor with paddle-type blades from the microhydropower system

The blade (fig. 3), a component of the rotor, was designed by assembling from previously defined landmarks, a method called bottom-up design. First, the 3D geometric model was created for each individual component, after which they were assembled using the *Assemblies* module.

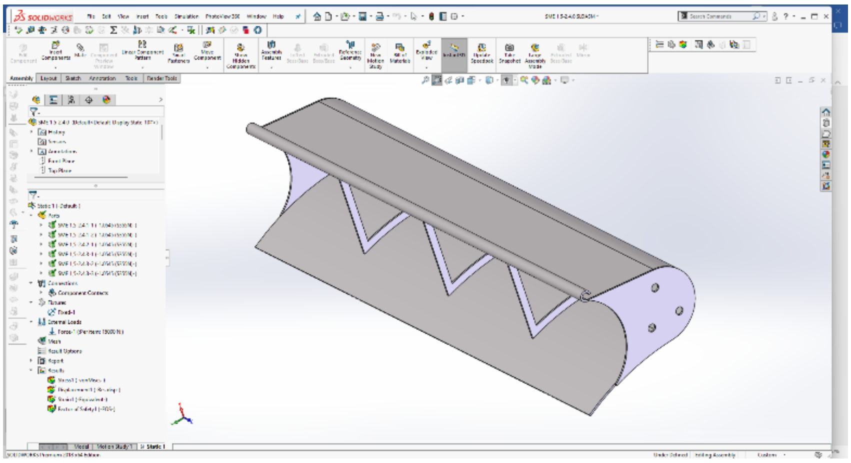

Fig. 3. Component blade of the rotor of the microhydropower system

3. Results

When designing the blade, the static or dynamic loads that will require the microhydropower system were taken into account. When checking the resistance to static stresses, in order to identify the more stressed areas and remove the excess material, the Simulation module was used, which is fully integrated in SolidWorks, which involved importing the geometry of the 3D model made, defining the material, defining the appropriate restrictions for the discretizations, running the program for analysis calculation of Von Mises stress, displacement, relative elongation, safety factor and visualization of the results in the form of diagrams.
The structural analysis with the CAD-CAE method involved the following operations [11, 12]:

- selecting static as the analysis type, solid for the discretization type and the FFEPlus solver (fig. 4).

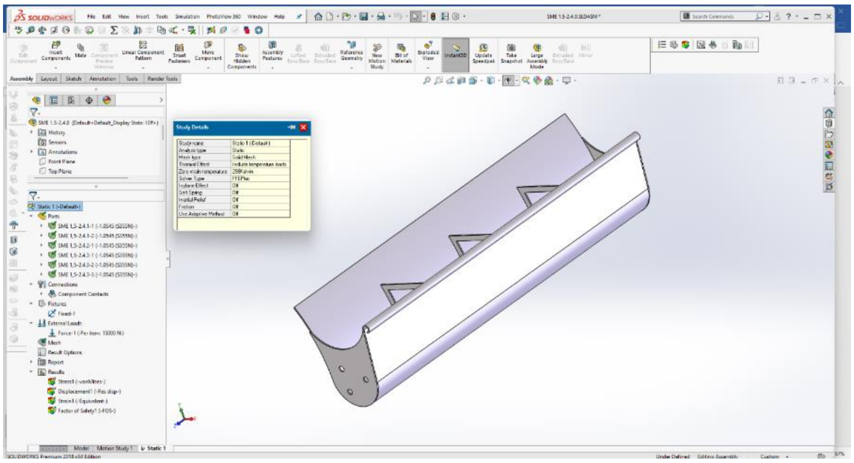

Fig. 4. Static option as analysis type, solid for discretization type and FFEPlus solver

- selecting the material from the SolidWorks library and automatically assigning these properties to each component reference (as shown in Table 1).

Table 1: Properties of selected materials

Material name:	1.0545 (S355N)	**1.0503 (C45)**	**AISI 4340 Steel, normalized**
Model type:	Linear Elastic Isotropic	**Linear Elastic Isotropic**	**Linear Elastic Isotropic**
Default failure criterion:	Max von Mises Stress	**Max von Mises Stress**	**Max von Mises Stress**
Yield strength:	2.75e+08 N/m^2	**5.8e+08 N/m^2**	**7.1e+08 N/m^2**
Tensile strength:	4.5e+08 N/m^2	**7.5e+08 N/m^2**	**1.11e+09 N/m^2**
Elastic modulus:	2.1e+11 N/m^2	**2.1e+11 N/m^2**	**2.05e+11 N/m^2**
Poisson's ratio:	0.28	**0.28**	**0.32**
Mass density:	7800 kg/m^3	**7800 kg/m^3**	**7850 kg/m^3**
Shear modulus:	7.9e+10 N/m^2	**7.9e+10 N/m^2**	**8e+10 N/m^2**
Thermal expansion coefficient:	1.1e-05 /Kelvin	**1.1e-05 /Kelvin**	**1.23e-05 /Kelvin**

- applying the appropriate load. In accordance with the real mode of operation (operational), the simulation scenario was adapted accordingly. The load was applied at the points corresponding to the mode of operation shown in table 2.

Table 2: Applying the appropriate load

<table>
<tr><td>Fixture name</td><td>Fixture Image</td><td>Fixture Details</td></tr>
<tr><td>Fixed-1</td><td>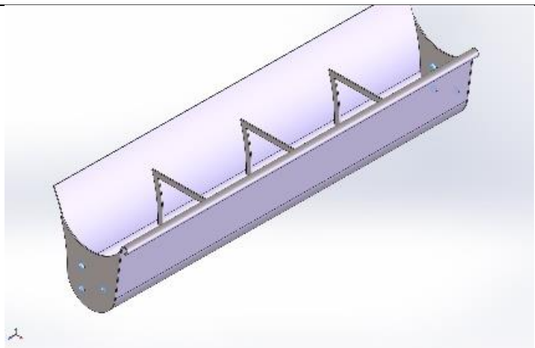</td><td><table><tr><td>Entities:</td><td>6 face(s)</td></tr><tr><td>Type:</td><td>Fixed Geometry</td></tr></table></td></tr>
<tr><td colspan="3">Resultant Forces<table><tr><td>Components</td><td>X</td><td>Y</td><td>Z</td><td>Resultant</td></tr><tr><td>Reaction force (N)</td><td>14867.3</td><td>-1990.7</td><td>-0.00219727</td><td>15000</td></tr><tr><td>Reaction Moment (N.m)</td><td>0</td><td>0</td><td>0</td><td>0</td></tr></table></td></tr>
<tr><td>Load name</td><td>Load Image</td><td>Load Details</td></tr>
<tr><td>Force-1</td><td>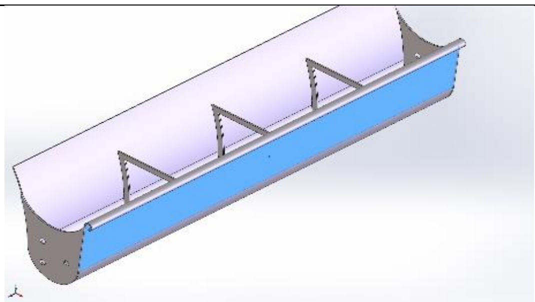</td><td><table><tr><td>Entities:</td><td>1 face(s)</td></tr><tr><td>Type:</td><td>Apply normal force</td></tr><tr><td>Value:</td><td>15000 N</td></tr></table></td></tr>
</table>

- using the "*meshing procedure*" to break down the model into discrete elements (table 3). In general, a finite element model is defined by a mesh, which is completely made of a geometric arrangement of elements and nodes. Nodes represent points, where features such as displacements are calculated.

Table 3: Break down the model into discrete elements

Total Nodes	10651
Total Elements	30708
Maximum Aspect Ratio	19.68
% of elements with Aspect Ratio < 3	2.95
% of elements with Aspect Ratio > 10	0.466
Time to complete mesh(hh;mm;ss):	00:00:11

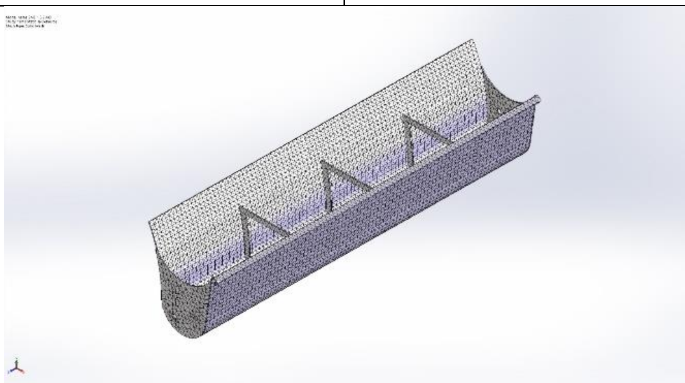

- running the analysis study to calculate stress, factor of safety and displacement, which is based on geometry, material, load, constraint conditions and discretization type. The results can be viewed in table 4.

Table 4: Results of analysis study 1 (material S355N)

Name	Type	Min	Max
Stress1	VON: von Mises Stress	0.000e+00 N/m^2 Node: 9944	2.271e+08 N/m^2 Node: 23
Displacement1	URES: Resultant Displacement	0.000e+00 mm Node: 1	2.568e+00 mm Node: 1012
Strain1	ESTRN: Equivalent Strain	0.000e+00 Element: 29255	1.216e-03 Element: 1716
Factor of Safety1	Automatic	1.211e+00 Node: 23	1.000e+16 Node: 9944

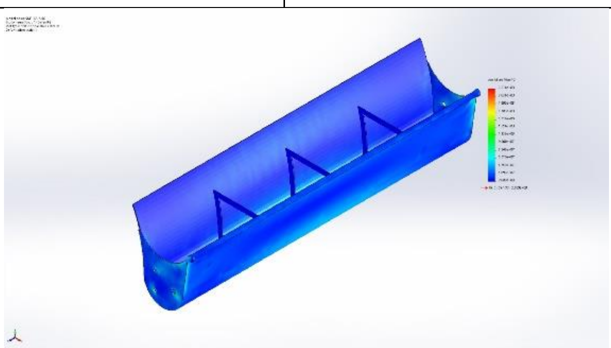

Static 1-Stress-Stress1

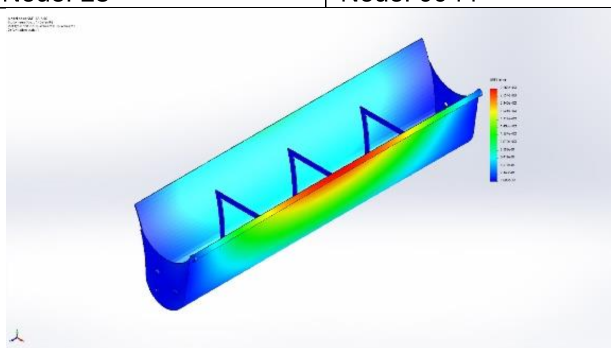

Static 1-Displacement-Displacement1

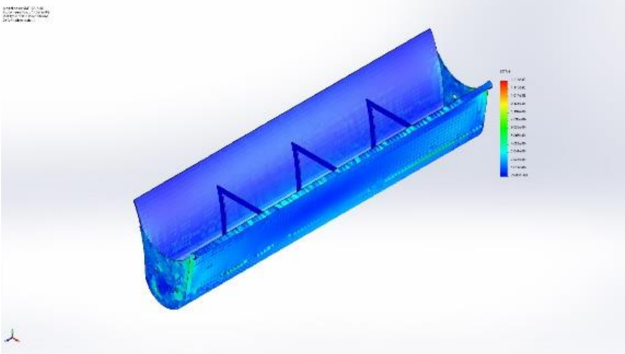

Static 1-Strain-Strain1

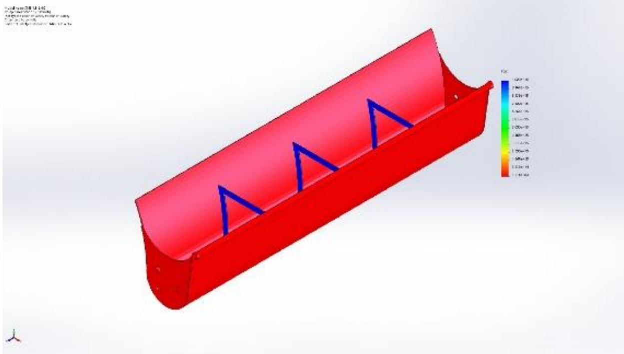

Static 1-Factor of Safety-Factor of Safety1

After running Analysis Study 2, the results can be viewed in Table 5.

Table 5: Results of analysis study 2 (material C45)

Name	Type	Min	Max
Stress1	VON: von Mises Stress	0.000e+00 N/m^2 Node: 9944	2.271e+08 N/m^2 Node: 23
Displacement1	URES: Resultant Displacement	0.000e+00 mm Node: 1	2.568e+00 mm Node: 1012
Strain1	ESTRN: Equivalent Strain	0.000e+00 Element: 29255	1.216e-03 Element: 1716
Factor of Safety1	Automatic	2.554e+00 Node: 23	1.000e+16 Node: 9944

Static 2-Stress-Stress1

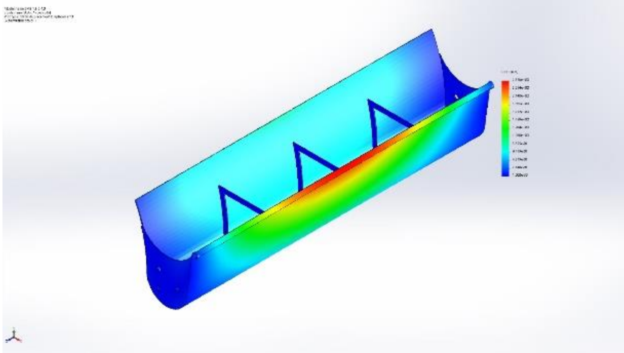

Static 2-Displacement-Displacement1

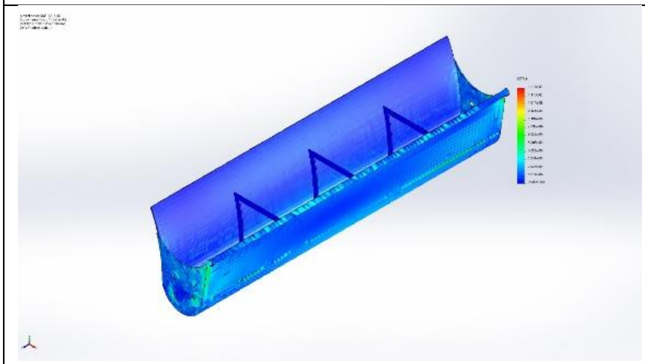

Static 2-Strain-Strain1

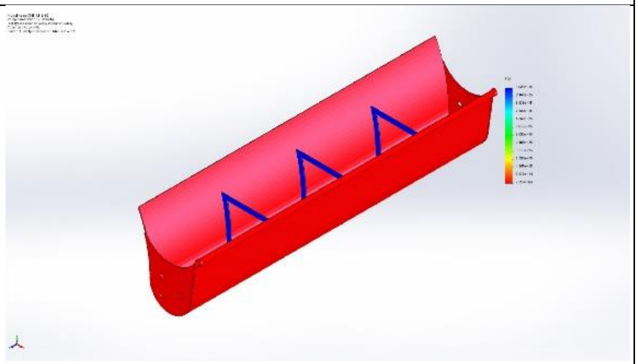

Static 2-Factor of Safety-Factor of Safety1

After running Analysis Study 3, the results can be viewed in Table 6.

Table 6: Results of analysis study 3 (material AISI 4340)

Name	**Type**	**Min**	**Max**
Stress1	VON: von Mises Stress	0.000e+00 N/m^2 Node: 9944	2.199e+08 N/m^2 Node: 23
Displacement1	URES: Resultant Displacement	0.000e+00 Element: 29255	1.269e-03 Element: 1716
Strain1	ESTRN: Equivalent Strain	0.000e+00 Element: 29255	1.269e-03 Element: 1716
Factor of Safety1	Automatic	3.228e+00 Node: 23	1.000e+16 Node: 9944

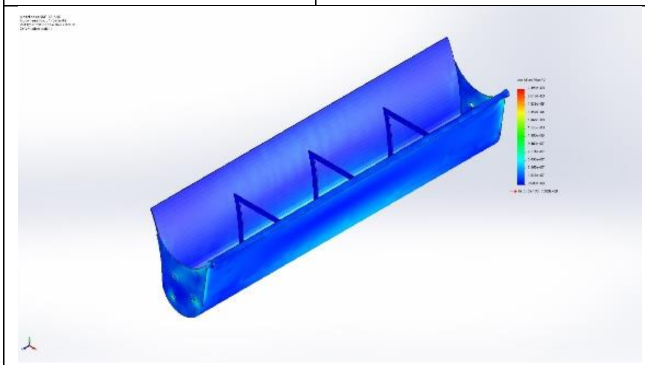

Static 3-Stress-Stress1

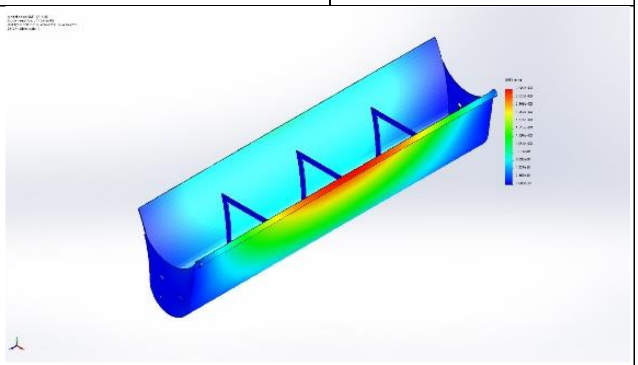

Static 3-Displacement-Displacement1

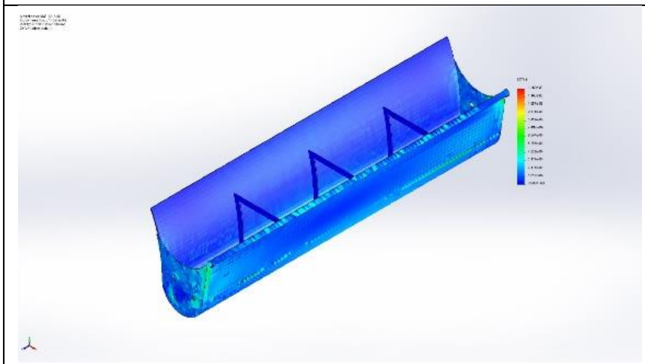

Static 3-Strain-Strain1

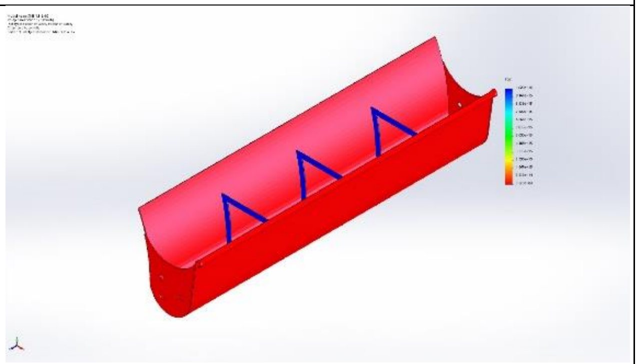

Static 3-Factor of Safety-Factor of Safety1

The results of the analysis on technical-economic criteria in the choice of the metal material from which the blade is made are presented in table 7.

Table 7: The results of the analysis on technical-economic criteria

Name	**Measure unit**	**Value**		
		Material 1 **1.0545 (S355N)**	**Material 2** **1.0503 (C45)**	**Material 2** **AISI 4340 Steel. normalized**
Safety factor	-	1.21	2.55	3.22
Mass	kg	28.55	28.55	28.55
Cost price	lei/kg	4.98	25.57	33.01
Cost price / Safety factor	-	117.41	286.30	292.70

The cost price was obtained by averaging the prices of at least three offers (print screen from specialized websites, offers received by email, photos of offers identified on the shelf, etc.).
In figure 5, the indicators obtained for the choice of the metal material from which the blade of the microhydropower system is made are graphically represented.

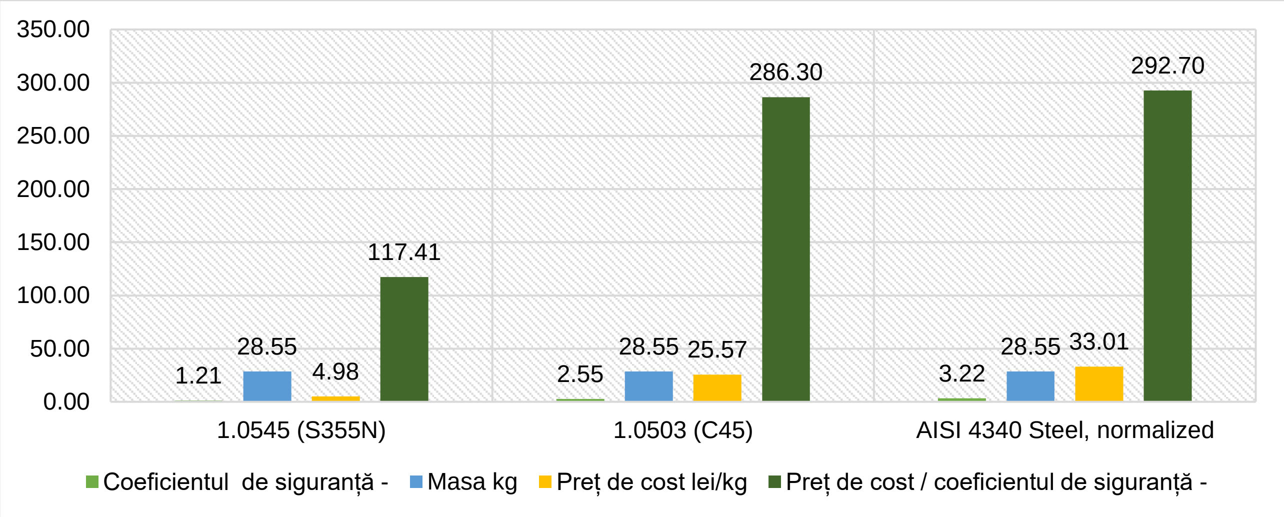

Fig. 5. Graphic representation of the indicator obtained for the choice of the metal material from which the blade of the microhydropower system is made

The comparison of the indicators in figure 5 led to the choice of the optimal variant (the material S355N was chosen, which has the lowest "Price-cost / Safety coefficient" ratio, which was 117.41). Table 8 shows the chemical properties of the chosen material.

Table 8: Chemical composition % of steel S355NL (1.0546): EN 10025-3-2004

C %	**Si %**	**Mn %**	**P %**	**S %**	**Al %**	**Cr %**	**Cu %**	**Mo %**	**N %**	**Nb %**	**Ni %**	**Ti %**	**V %**
max 0.18	max 0.50	0.90 - 1.65	max 0.025	max 0.020	mind. 0.0200	max 0.30	max 0.55	max 0.10	max 0.015	max 0.050	max 0.50	max 0.05	max 0.12

EN10025-3 S355NL grade is a normalized weldable and a fine grain structural steel. It has greater yielding strength at a room temperature of about 355 MPA at 16mm and falling temperature at 250 mm to 250 MPA. Knowledge of the chemical properties of the chosen material helped in the choice of corrosion protection by using an epoxy primer rich in activated zinc and a polyurethane paint which are designed for the protection of steel in highly corrosive atmospheric conditions in full compliance with Directive 2004/42/EC.

4. Conclusions

- Analysis by the finite element method, represents a modern method for the study of metallic structures, allowing the determination of Von Mises stress, displacement, relative elongation and safety factor;
- The technical-economic indicator (manufacturing cost per unit of safety coefficient) proposed by the authors for the analysis of the choice of the optimal variant, contributes to the reduction of the design validation time and to the reduction of manufacturing costs;
- The CAD-CAE design method of a welded metal subassembly of the microhydropower system advocates for the promotion of the role of microhydropower systems in order to minimize CO_2 emissions in the Romanian economy.

Acknowledgments

The results presented in this article were obtained with the support of MADR through the "Sectoral Plan - ADER 2026", financing contract no. 13.1.1 / 17.07.2023, ADER project 13.1.1. *Research on increasing profitability in aquaculture farms by introducing valuable species with the implementation of specific aquaculture, animal husbandry and agricultural technologies - the realization of the integrated aquaculture farm*, managed by the The Research and Development Institute for Aquatic Ecology, Fishing and Aquaculture – Galati.

References

[1] Magraw, D. and M. Siemes. “The right to a healthy environment, the rights of future generations, and climate change.” *The Fletcher Forum of World Affairs* 47, no. 1 (2023): 87-96.

[2] Wang, J. and W. Azam. “Natural resource scarcity, fossil fuel energy consumption, and total greenhouse gas emissions in top emitting countries.” *Geoscience Frontiers* 15, no. 2 (2024): 101757.

[3] Adelekan, O.A., B.S. Ilugbusi, O. Adisa, O.C. Obi, K.F. Awonuga, O.F. Asuzu, and N.L. Ndubuisi. “Energy transition policies: a global review of shifts towards renewable sources.” *Engineering Science & Technology Journal* 5, no. 2 (2024): 272-287.

[4] Gayen, D., R. Chatterjee, and S. Roy. “A review on environmental impacts of renewable energy for sustainable development.” *International Journal of Environmental Science and Technology* 21, no. 5 (2024): 5285-5310.

[5] Mohsin, M., D. Orynbassarov, M.K. Anser, and Y. Oskenbayev. “Does hydropower energy help to reduce CO2 emissions in European Union countries? evidence from quantile estimation.” *Environmental Development* 45 (2023): p.100794.

[6] Alapfy, B., N.F. Gamarra, and N. Rüther. “Towards Hydraulic Design Optimization of Shaft Hydropower Plants: A 3D-CFD Application Based on Physical Models.” *Water* 16, no. 19 (2024): 2790.

[7] Dolmatov, S., V. Tsubiks, O. Zhadan, A. Scherbakov, A. Sayfutdinova, and R. Sakhapov. “Increasing the efficiency of design in CAD CAE systems based on the application of parametrization methods.” Paper presented at the IV International Conference on Agricultural Engineering and Green Infrastructure Solutions (AEGIS-IV 2024), Tashkent, Uzbekistan, March 28-30, 2024. *BIO Web of Conferences* 105 (2024): 05010.

[8] Rondon, D., S. Pääjärvi, J.O. Aidanpää, R. Gustavsson, and P. Jeppsson. “Three-Dimensional Modeling for Mechanical Analysis of Hydropower Generators with Floating Rotor Rim.” *Machines* 12, no. 4 (2024): 268.

[9] Yazik, M.H.M., M.H. Zawawi, A.N. Ahmed, L.M. Sidek, H. Basri, and F. Ismail. “One-way fluid structure interaction analysis of a static savonius hydrokinetic turbine under different velocity and surface roughness with different blade materials.” *Ocean Engineering* 291 (2024): 116373.

[10] Vlase, S., M. Marin, and I. Negrean. “Finite element method-based elastic analysis of multibody systems: A review.” *Mathematics* 10, no. 2 (2022): 257.

[11] Cârdei, P. “Applications of finite element structural analysis in the microstructures field and their specific issues.” Paper presented at the 16th SGEM 2016 Vienna Green International Scientific Conference, Vienna, Austria, November 2-5, 2016.

[12] Cristea, O.D., M.G. Matache, M. Mateescu, and E. Marin. “Use of an innovative method for structural analysis of the distribution device used in pneumatic machines for weeding plant sowing. ” *Annals of the University of Craiova-Agriculture, Montanology, Cadastre Series* 49, no. 2 (2020): 361-366.

ISSN 1454 - 8003
Proceedings of 2024 International Conference on Hydraulics and Pneumatics - HERVEX
November 13-15, Băile Govora, Romania

THE ARCHITECTURE OF INTELLIGENT MECHATRONIC SYSTEM USED FOR INCREASING THE NEUROMUSCULAR CONTROL

Cristian Radu BADEA[1], Sorin Ionuț BADEA[1], Florentina BADEA[1], Tudor Cătălin APOSTOLESCU[2], Dana Mirela VĂLEANU[3]

[1] The National Institute of Research and Development in Mechatronics and Measurement Technique (INCDMTM), adresacontact@gmail.com, sorin_ib@yahoo.com, mihaiflori@yahoo.com

[2] Titu Maiorescu University, Faculty of Informatics, catalin.apostolescu@prof.utm.ro

[3] National University of Science and Technology Politehnica Bucharest, Department of Mechanisms and Robots Theory, valeanu_dana@yahoo.com

Abstract: *The paper presents intelligent and complex mechatronic system which can perform predefined sequential motion cycles used for increasing neuromuscular control of athlete performance. The equipment comprises two parts: an automation panel and a pneumatic assembly. The Master Control Unit of the automation panel is programmed to run a specific software application that ensures the proper fulfilment of the motion cycles. The MCU is connected to a Radio Frequency transceiver and could be easily connected to IoT and/or LAN using a wired net controller. The input data has the following sources: the remote RF sensors' data, the position of the proximity sensors (placed on the pneumatic cylinders), the numerical codes transmitted by the IR remote control and/or by IoT connection and the current motion cycle's settings. The output data consists of digital output signals (send both to the solenoid valves through relays and to the status lamps) and text messages written onto a LCD display.*

Keywords: *Mechatronic system, neuromuscular control, Biomechanics.*

1. Introduction

In the training of athlete, due to the competitive specificity, in addition to the development of motor skills (speed, strength and endurance), a very important aspect is the development of motor skills balance and coordination. The development of these two elements in fact involves the execution of physical exercises aimed at increasing the neuromuscular control of the athlete performance. To perform specific exercises, such as counter-procedures used against the design techniques of the opponent on the ground, there is currently no dedicated equipment, which is why they are performed with the help of a partner. In the development activity of the athlete, the first stage is the formation of conditioned reflexes stimulated by performing repetitive movements of low intensity, ie by performing at low speed some movement cyclograms. In order to develop coordination, it is necessary to dynamically change the parameters of the movement, namely: speed and direction of movement. It is very important that, with the development of neuromuscular control, the endurance of the athlete in question can be developed, thus eliminating the obstacle created by the appearance of fatigue.
This endurance development is achieved by increasing the execution time of the cyclogram, by adding additional movements within it. Also, the development of the speed of execution and / or reaction of the athlete can be achieved by imposing an increasingly fast pace in the execution of the exercise cycle or by dynamically changing the direction of travel imposed on the athlete in question. Another very important aspect in the development of balance in the case of athlete is the mobility of their coxo-femoral joints, as an important part of the opponent's ground design procedures is based on manipulating one of the opponent's legs, over the mobility of the coxo-femoral joints. his femurs. The main problem with using a human partner in these exercises is that he cannot perform the required cyclograms correctly due to lack of experience, fatigue and last but not least due to the subjectivism in making the necessary decisions. Therefore, there is a need for well-trained human partners, or for the use of systems that allow the correct implementation of the necessary

cyclograms. As these well-trained partners are generally athlete or coach, it is often inefficient to use them, as they are short of their own training time and / or not enough to cover as many people as possible. trainers simultaneously.

2. The requirements that the intelligent mechatronic system must meet

Starting from the aspects mentioned above, it was necessary to design an intelligent mechatronic system, which would allow the implementation of such movement cyclograms, necessary for the development of the neuromuscular system of strength and endurance of the lower limbs and mobility of coxo-femoral joints of athlete. The proposed mechatronic system will replace a human partner in the execution of the movements required to train the athlete against the ground design procedures of the opponent and not only. This will be called the handling system (abbreviated - SM). The main requirements that such a system must meet are:
- enable the movement and posture to be performed with a high degree of precision and repeatability, which facilitates symmetrical development in terms of neuromuscular control / dynamic and static balance, strength and endurance in the lower limbs, and from the point of view of the mobility of the coxo-femoral joints, of the athlete;
- to allow the level of intensity of the physical stress to be adjusted according to the specific needs of each athlete;
- allow for easy and risk-free operation;
- be able to be used, under certain conditions, by athletes who are injured or in the recovery phase after exercise, whether it is training or competitive;
- to allow all these goals to be achieved without the help of a third party;
- be able to be placed in a regular training room.

3. Description of the manipulation system (MS), designed to be used in the training of athletes, for the development of neuromuscular control

The purpose of any training session is for the athlete to overcome his limits, consciously and voluntarily, by adapting the neuromuscular to the demands to which he is subjected. The level and types of demands are determined by the coach through the training plan, based on the latter's experience, as well as on the information gained during the relationship established between the latter and the athlete, which allows the coach to estimate in objectively the level of training of the athlete and to know his anatomo-physiological specificities.
The designed handling system replaces the actions that usually need to be performed by a partner / coach to help train an athlete (referred to in this case as the user). This system allows the user to perform certain exercises whose purpose is to develop neuromuscular control / dynamic and static balance, strength and endurance of the lower limbs of athlete, as well as to maintain and / or develop the mobility of their coxo-femoral joints. Specifically, the manipulation system will allow the user to perform in the best conditions training for the development of neuromuscular control / dynamic and static balance, strength and endurance of his lower limbs, allowing him to perform exercises such as those that form the basis of counter-procedures. used against the design techniques of the opponent on the ground. to correct the biomechanics of movements and reduce the risk of injury during training.
Also, the manipulation system will allow the user to perform in the best conditions training to maintain and / or develop the mobility of his coxo-femoral joints. During these trainings, the manipulation system will supplement the actions of the athlete's human partner.
One of the most complete exercises, which allows the development of neuromuscular control / dynamic and static balance, strength and endurance of the lower limbs of the athlete, is to move in one leg of the latter, in the direction and speed imposed by a human partner. [1,6,7,8]. The athlete's moving leg is called the support leg, and the other leg is called the manipulated leg, as the human partner dictates to him the direction and speed of movement by manipulating the latter limb. The role of the human partner is to keep the athlete in a constant state of imbalance, constantly changing the

direction of travel, and the role of the athlete is to adapt to the demands imposed, trying to move and even intuit the direction of movement. to be able to maintain balance. As an example in this sense, if the human partner finds that the athlete has the center of gravity [2] backwards, then he will push him backwards, by means of the manipulated leg. The correct reaction from the athlete will be for him to move (hopping in one leg) in the required direction (backwards), simultaneously with the movement of the center of gravity towards the face (i.e. bending his torso towards the face). The disadvantage in this case is that the full control over the determination of the position of the athlete's center of gravity and also the speed of change of direction of travel is left to the discretion of the human partner. Therefore, any mistake of his can have a negative impact on the health of the athlete. This type of exercise is the foundation of the counter-procedures used against the design techniques of the opponent on the ground, allowing the simultaneous development of both motor skills and motor skills, as well as reducing the risk of injury in the training of athletes.
Regarding the exercises that allow the maintenance and / or development of the mobility of the coxo-femoral joints, of the athletes, they are performed in two ways:
- using specially built devices [3] [4]. Their major disadvantage is related to the fact that the training of the mobility of the coxo-femoral joints is done with both feet on the ground, or on the device in question, thus eliminating the balance component of the exercise;
- with the help of a human partner. This exercise is performed by supporting one of the legs on the partner, who has the role of opening the angle between the two limbs as much as possible. In this situation, the disadvantage is that the human partner must be very well prepared to be able to respond quickly and correctly to the requests of the athlete in question, otherwise the risk of injury is imminent. The advantage in this case is given by the presence of the balance component during the exercise, the athlete having only one foot on the ground and having to maintain a correct posture [5].
The role of the designed handling system is to supplement the presence of the human partner in performing the exercises described above, eliminating the disadvantages mentioned in each situation, to correct the biomechanics of movements and reduce the risk of injury during training.

3.1 The architecture of the manipulation system designed for its use in athletes' training, for the development of neuromuscular control

Starting from the requirements that are to be fulfilled by the designed handling system, the main elements / subassemblies that are part of it, are (see fig.1):

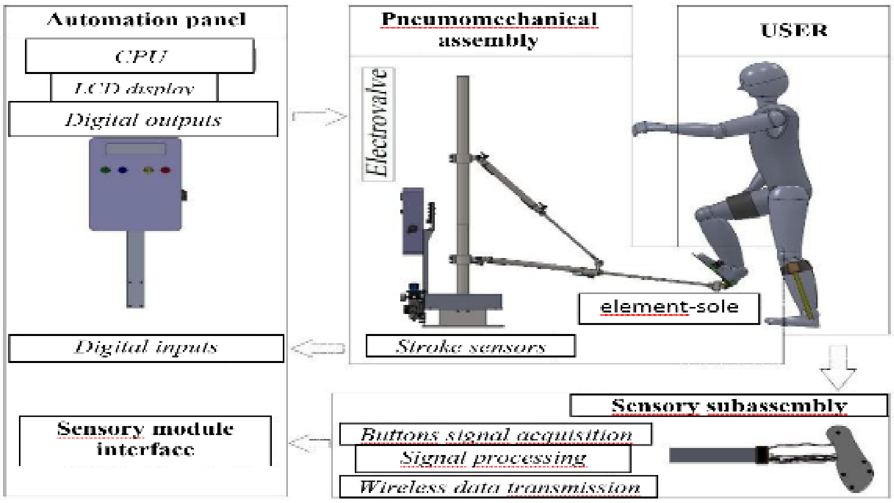

Fig. 1. Schematic representation of the architecture of the handling system

a) A pneumomechanical assembly consisting of:
a.1) The lower subassembly, used to perform the horizontal rotational movements of the assembly, these having the role of causing the user to move to the left or to the right, thus supplementing the

movement actions imposed on the athlete by a partner / coach, in accordance with the requirements of the exercise in question.

The main features of this subassembly are:

- allows to change the direction of travel, to the left or to the right, depending on the changes of the user's center of gravity, detected by means of a sensory system mounted on the support leg of the athlete concerned. If the center of gravity is positioned toward the inside of the athlete's support foot, the subassembly will rotate counterclockwise, unbalancing the user and thus causing him to try to rebalance dynamically, and if the center of gravity is positioned towards the outside of the foot of its support leg, the subassembly will rotate to the right, causing the user to become unbalanced and thus causing the user to try to rebalance dynamically again;
- allows to change the speed of movement / rotation, depending on the needs of the user.

a.2) The upper subassembly, used to perform the vertical displacement movements of the device, these having the role of causing the user to move forward or backward, thus supplementing the actions of forced displacement to one of the aforementioned directions, imposed the athlete by a partner / coach, in accordance with the requirements of the exercise in question. The main features of this subassembly are:

- allows the direction of travel to change, up or down, depending on changes in the user's center of gravity, detected by a sensory system mounted on the support leg of the athlete concerned. If the center of gravity is positioned towards the tip of the athlete's support foot, the subassembly will move in front of the user, the manipulated foot support, unbalancing him and thus causing him to try to rebalance dynamically. , and if the center of gravity is positioned towards the heel of the athlete's support leg, the subassembly will move towards the user's back, the manipulated foot support, causing the user to become unbalanced and thus causing the user to react again;
- allows to change the speed of movement / rotation, depending on the needs of the user;
- allows the start / end of the action at the user's command, so that he has control at all times.

b) A sensory subassembly, which contains a portable electronic module and a sensitive module containing a set of five return micro-buttons located on a shoe insole. The sensitive module is used to determine the position of the support at the level of the user's support foot. This position of support is in fact an approximation of the position of the user's center of gravity during the movement imposed on him by the handling system. If the user is with one of the feet suspended in the air, he can achieve a state of balance when his center of gravity is positioned inside the triangle formed by his thumb, toe and the heel of his supporting leg. In the case of displacement imposed by a partner / handling system, the position of the user's center of gravity can be approximated as follows:

- if the support is made predominantly at the user's toe, the center of gravity is positioned outside the foot of the foot in question, on its proximal-frontal side;
- if the support is made predominantly at the user's toe, the center of gravity is positioned outside the foot of the foot in question, on its distal-frontal side;
- if the support is made predominantly at the heel of the user's foot, then the center of gravity is positioned outside the foot of the foot in question, on its back;

The main advantages of the sensory subassembly are:

- small size;
- portability and energy autonomy during each working session;
- wireless data transmission - this allows the unrestricted performance of movements performed by the human user in order to rebalance.

c) A subassembly of the central electronic unit, called an automation panel, used for the management and implementation of all the functions of the system concerned, as well as their related actions, either on the basis of a predefined cyclogram, which can be dynamically modified to the information provided by the sensory subassembly is also taken into account, either on the basis of orders received directly from the human user. Thus, this subassembly will control the solenoid valves responsible for actuating the pneumatic cylinders, which implement the necessary movements of the system in question.

The data flow between the sensory subassembly and the automation panel ensures the dynamic configuration of the movement cycle that the human subject will perform. The entire manipulation

system is designed in such a way that, depending on how the sensitive subassembly, the sensory subassembly micro-buttons are pressed, the control software, which manages the entire activity of the manipulation system, will send to the drive system. pneumatic of the mechano-pneumatic subassembly, those commands that will keep the human subject in a continuous state of imbalance, forcing him to continuously adjust his posture to maintain balance.
The designed handling system allows the implementation of individualized movement cycles, whose movement parameters are adapted according to the needs of each individual.

4. The description of the mechanical structure of the manipulation system designed for the use in atheletes' training for the development of neuromuscular control

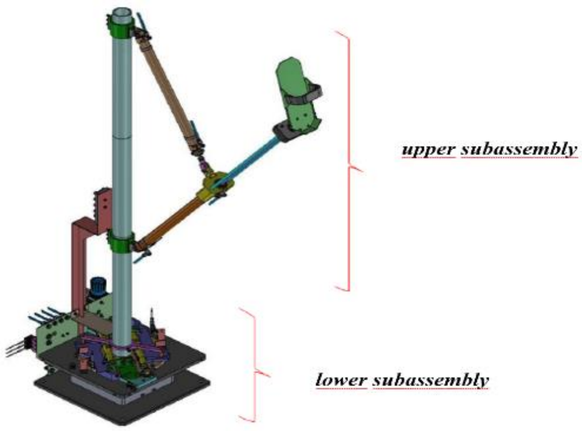

Fig. 2. The perspective view of the handling system

The manipulation system designed to be used in performance training in athletes, in order to allow the development of neuromuscular control / dynamic and static balance, strength and endurance of the lower limbs and mobility of the coxo-femoral joints of athletes, represented in fig. 2, consists of the following subassemblies and basic elements:

a) The lower subassembly

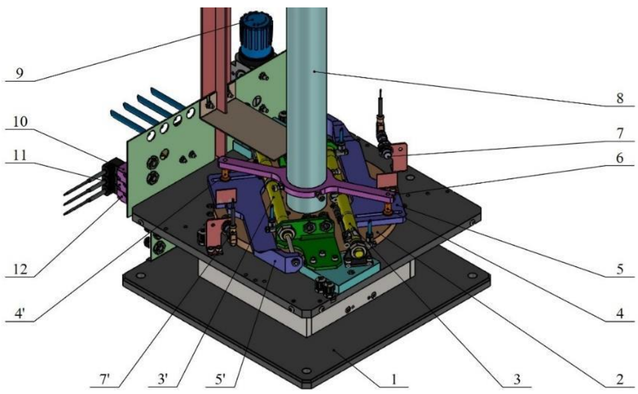

Fig. 3. The perspective view of the handling system highlighting the elements of the lower subassembly

The lower subassembly consists of a housing 1, a disc 2, a pair of rotating pneumatic cylinders (3, 3 ') two spacers 4 and 4', respectively, a pair of connecting rods (5, 5 '), a stabilizing element 6, a pair of inductive sensors (7, 7') a support column 8, a pressure regulator 9, a group of solenoid valves (10, 11, 12) , a pair of inductive limit switches (13, 13 ') and a pair of throttles (14, 14') , located on the cylinder pneumatic 3, a pair of throttles (15, 15 ') and a pair of inductive limit switches (16, 16') , located on the pneumatic cylinder 3 '(see fig. 3), a central shaft 17, a pair of radial-axial bearings

(18, 18 ') , a pair of sliding washers (19, 19'), a protection cap 20 (see fig.4.5) and a pair of limiting pins (21, 21 '), see fig.6. The inductive sensors 7 and 7 'have the role of detecting the touching of the stroke ends of the rotating pneumatic cylinder rods 3 and 3', respectively, in case the stroke end sensors 13, 13 ', 14, 14' show defects.

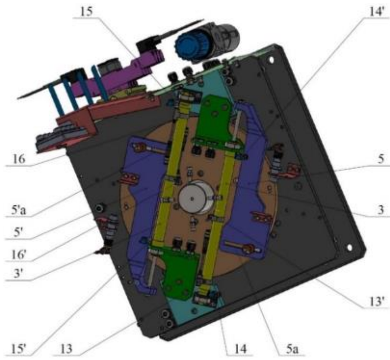

Fig. 4. Top view, in perspective, of the handling system, highlighting the elements of the lower subassembly

The rods of the two rotating pneumatic cylinders 3 and 3 ', have the free ends fixed on the connecting rods 5 and 5' respectively, the bodies of the pneumatic cylinders being fixed on the housing 1 (see fig.4.4). The support column 8 is welded to the disc 2, which is fixed, with screws, to the central axis 17, the latter being rotatably mounted on the housing 1, by means of the pair of radial-axial bearings (18, 18 '), see fig .4.5. The two connecting rods 5 and 5 'have two transverse channels 5a and 5'a respectively (see fig.4.4), which have the role of allowing the transmission of the movement from the disc 2 to the stabilizing element 6 and therefore the transmission of the movement from the pair of pneumatic cylinders. (3, 3 '), in support column 8. In this way, by means of the two connecting rods 5 and 5', the translational movement from the two pneumatic cylinders 3 and 3 ', which act simultaneously (i.e. the rods of both pneumatic cylinders advances and retracts, respectively), is transformed into a rotational movement at the level of the support column 8.
The two pairs of throttles, (14, 14 ') located on the rotating pneumatic cylinder 3 and (15, 15') located on the rotating pneumatic cylinder 3 ', respectively, have the role of allowing the adjustment of the speeds of movement of the rods of the two pneumatic cylinders. remember, which must be equal to each other on both the forward and the reverse stroke, but also equal between the forward stroke and the retraction stroke. The two rotating pneumatic cylinders, 3 and 3 ', respectively, are actuated by the same solenoid valve 10. This translates into the simultaneous action of the rods of the two rotating pneumatic cylinders, 3 and 3', respectively, on the two connecting rods 5 and 5 ', respectively.

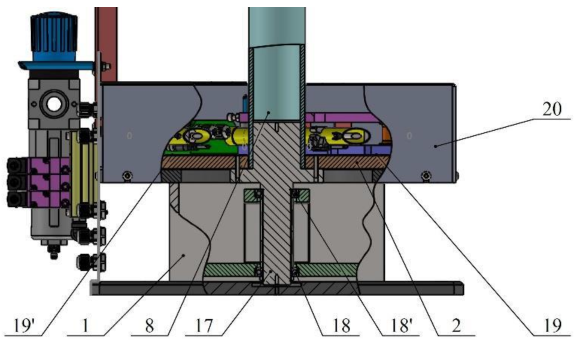

Fig. 5. Side view of the handling system, with rupture at the lower subassembly

The two spacers 4 and 4 'respectively (see fig.4), in addition to the role of fixing the stabilizing element 6 on the disc 2 and transmitting the movement from said disk to the element in question and that of maintaining the coplanarity between the lower faces of 5 and 5 'connecting rods also have the role of keeping the distance between these connecting rods and the disc 2 fixed (this distance is determined by the thickness of the sliding washers 19 and 19'). In this sense, the stabilizing element 6, which is fixed by means of the screws on the support column 8, prevents the vertical movement of the two spacers mentioned above (see fig.5).

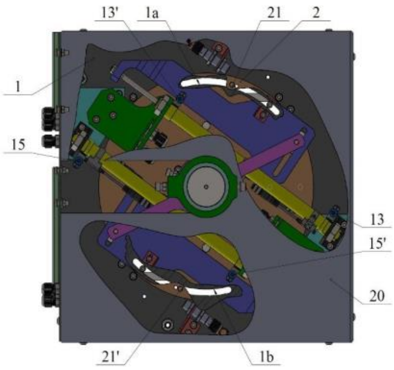

Fig. 6. Top view of the handling system, with rupture at the lower subassembly, to highlight the mechanism of transformation of the translational movement, printed by the two rotating pneumatic cylinders 3 and 3 ', in rotational motion, at the level of the support column 8

On the disc 2 are mounted two limiting pins 21 and 21 'respectively, which have the role of preventing the seizure of the mechanism of transformation of the translational movement into rotational movement, previously mentioned, in case of a failure at the limit sensors 13, 13 ', 14, 14' and / or at the level of the inductive sensors 7 and 7 ', situation in which the movement of the rods of the rotating pneumatic cylinders 3 and 3' respectively, is blocked by the forced contact between the aforementioned pins and the ends of the two circular channels 1a and 1b , made in housing 1 (see fig.4.6). These two channels are coradial and have the center of rotation coinciding with the center of the disk 2. Also, the axis of rotation of the support column 8 coincides with that of the disk 2, and the two circular channels 1a and 1b are equal, respectively, their length being the same as the maximum permissible stroke length of the rotating pneumatic cylinder rods 3 and 3 'respectively.

b) The upper subassembly

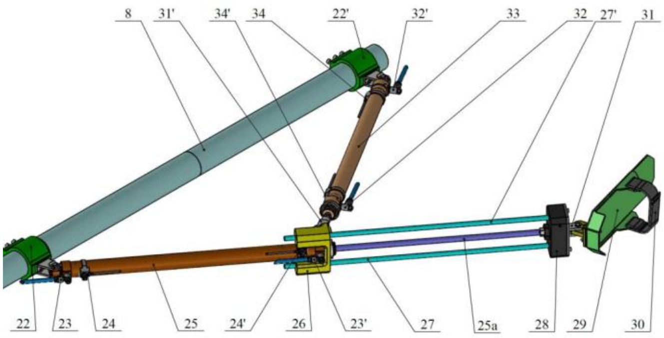

Fig. 7. Perspective view of the handling system, highlighting the elements of the upper subassembly

The upper subassembly consists of an advancing pneumatic cylinder 25, with the free end mounted articulated on a collar 22, placed in a row or on the support column 8 (mentioned in the description of the lower subassembly), a pair of inductive sensors (24, 24 '), mounted on the aforesaid pneumatic cylinder, a pair of rods (27, 27'), which slide freely through a guide piece 26, a sleigh element 28, fixed on the upper ends of the rods 27 and 27 ', a sole element 29 or sole element 29' (see fig.4.9.a and fig.4.9.b), on which a fastening system 30 is placed, of "VELCRO" type, two hinge elements 31 and 31 'respectively, a pneumatic tilting cylinder 33 having the free end mounted articulated on a collar 22', fixed in turn or on the support column 8, a pair of throttles (32, 32 ') and a pair of end-of-stroke inductive sensors (34, 34') , mounted on the tilting pneumatic cylinder 33. The forward pneumatic cylinders 25 and the tilting cylinders 33, respectively, articulated to the clamp 22 and the clamp 22 ', respectively, can rotate in the median transverse plane of the system in question. The free end of the rod 25a, of the pneumatic feed cylinder 25, is fixed to the sleigh element 28.

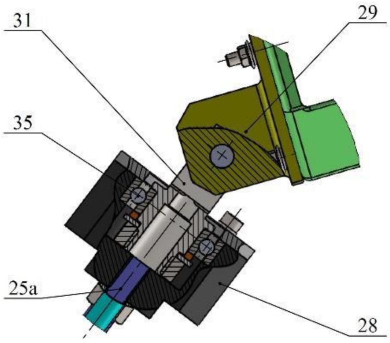

Fig. 8. Section view at the level of the lower subassembly, highlighting the elements that contribute to the transmission of movements from the handling system to the manipulated leg of the user

The hinge member 31 is fixed to the inner ring of a radial bearing 35 , the outer ring of which is mounted inside the sleigh member 28, which allows the hinge member 29, mounted articulated on the hinge member 31, to rotate. both in the frontal plane and in the plane containing the upper face 29a, of the sole-element 29 (see fig.4.8 and fig.4.9.a), this being extremely important to avoid injuring the user, his manipulated leg being able to achieve natural movements in the joints involved.

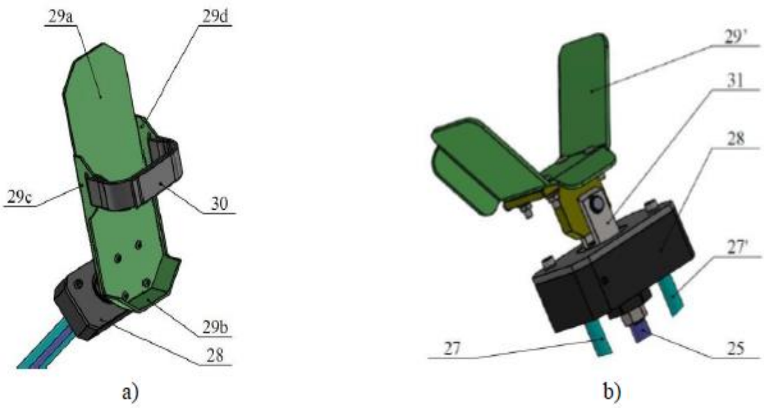

Fig. 9. Perspective view of the sole-element of the handling system, with the highlighting of its two constructive variants: a) the sole-element 29 - in the variant with fixing elements of the manipulated foot, of the user; b) sole element 29 '- in the version without fasteners of the manipulated foot, of the user

The free end of the rod 33a, of the tilting pneumatic cylinder 33, is mounted articulated on the hinge element 31 ', rotatably fixed, in turn, on the body of the guide piece 26. The latter element is fixed on the end from the rod of the advancing pneumatic cylinder 25 so that advancing or retracting the rod 33a of the tilting pneumatic cylinder 33 raises or lowers the base member 29. Advancing or retracting the rod 25a of the advancing cylinder 25 causes the base member 29 to move closer or further away from the support column 8. combining the movements of the two pneumatic cylinders mentioned above, the two-dimensional displacement of the sole element 25 is obtained.
The role of the sole element 29 is to support and fix the manipulated foot of the human subject (user), subject to analysis, during the imposed cycle of movement. Accidental movement of the user's manipulated foot to the left, right, or back is impeded by the shape of the sole member 29, which has a dorsal wall 29b and two side walls 29c and 29d, respectively (see Fig. 8). Accidental movement of the user's manipulated foot to the front, or detachment of it from the sole-element 29, is prevented

by the fastening system 30, located on the element in question (see fig.4.8). The choice of a "Velcro" fastening system was also determined by the need to untie it relatively quickly, in case of force majeure (for example, if the user is suddenly affected by a severe muscle cramp, at the foot of support or manipulated, which may cause him to stop moving urgently). The pair of rods (27, 27 ') has the role of taking over some of the stresses exerted on the rod 25a, the pneumatic cylinder 25, during the three-dimensional movement of the sole element 29, by the user, in response to the changes of direction imposed by the handling system in question. The two pairs of throttles, (23, 23 ') located on the advancing pneumatic cylinder 25 and (32, 32') respectively located on the tilting pneumatic cylinder 33, have the role of allowing the adjustment of the speeds of movement of the rods of the two pneumatic cylinders previously mentioned, which are actuated by solenoid valves 11 and 12 respectively.
By properly positioning the two clamps 22 and 22 ', respectively, on the support column 8, it is possible to move the sole element 29 in such a way that it reaches closer or farther to the ground, the ceiling, or the column of support 8.

5. Conclusions

The paper presents a mechatronic system that can perform motion cycles based on a predefined cyclogram. By means of a remote control, the user can control the vertical movement of the subassembly which ensures the support of its manipulated foot, to the desired height and then its controlled descent, so as to allow it to change its maximum angle between the lower limbs. as required by the exercises dedicated to obtaining the positions but at the same time to provide him with an element of support in case he becomes unbalanced or tired.
The system can be easily embedded into other much complex equipment, such as those used in neuromuscular control training, biomechanics, medicine and physical therapy.

Acknowledgments

This work was carried out through the NUCLEU Program, conducted with the support of MCID (Ministry of Research, Innovation and Digitalization of Romania), project number: PN 23 43 03 01 -17N/2023.

References

[1] Badea, C.R, O. Dontu, and I.G. Gheorghe. “Using the method of determining the variation of the length of the stretched chord, as a means of monitoring the postural changes of the athletes spine.” *U.P.B. Scientific Bulletin, Series D* 83, no. 3 (2021): 55-70.
[2] Freyler, K., A. Gollhofer, R. Colin, U. Brüderlin, and R. Ritzmann. “Reactive Balance Control in Response to Perturbation in Unilateral Stance: Interaction Effects of Direction, Displacement and Velocity on Compensatory Neuromuscular and Kinematic Response.” *PLoS One* 10, no. 12 (December 2015): e0144529.
[3] Bryan, L., and S. Randy. “The relationship between various modes of single leg postural control assessment.” *The International Journal of Sports Physical Therapy* 7, no. 3 (June 2012): 257-266.
[4] Badea, C.R. “Device used for maintaining and / or improving the mobility of coxo-femoral joints”. Patent no. RO 125003 B1, published on 30/08/2012.
[5] Gheorghe, I. G., A. Constantin, and I. Ilie. “Mechatronics and Cyber Mechatronics in Intelligent Applications from Industry and Society.” Paper presented at the International Conference on Aerospace, Robotics, Manufacturing Systems, Mechatronics and Neurorehabilitation OPTIROB 2016, Jupiter, Romania, June 29-July 2, 2016.
[6] Badea, Cristian Radu. “Researches on inertial mechatronic motion analysis systems, based on mems.” *The Scientific Bulletin of Valahia University, section – Materials and Mechanics* 16, no. 15 (2018): 44-50.
[7] Badea, Cristian Radu, and Sorin Ionuț Badea. “The positioning errors generated by Xsens MVN inertial system during the analysis of Push-ups exercise, using the Single Level scenario, before and after the calling of REPROCESS function.” *International Journal of Mechatronics and Applied Mechanics – IJOMAM*, no. 4 (2018): 120-133.
[8] Badea, Cristian Radu. ‘’Study on the influence of contact points, scenarios and graphical reference elements on the motion analysis process, carried out using the inertial mechatronic system MVN Analyze.’’ *International Journal of Mechatronics and Applied Mechanics* 2, no. 6 (2019): 74-81.

ISSN 1454 - 8003
Proceedings of 2024 International Conference on Hydraulics and Pneumatics - HERVEX
November 13-15, Băile Govora, Romania

ENVIRONMENTAL ASSESSMENT OF FLOATING PHOTOVOLTAIC SYSTEMS USED IN IRRIGATION IN DOBROGEA REGION

Gabriela Larisa MARAVELA[1], Sanda BUDEA[2]

[1] National University of Science and Technology Politehnica Bucharest – Doctoral School of Energy Engineering, gabrielamaravela@icloud.com

[2] National University of Science and Technology Politehnica Bucharest – Doctoral School of Energy Engineering, sanda.budea@upb.ro

Abstract: *The rising necessity of energy production with low to zero carbon emissions has challenged researchers to develop new technologies to meet population's requirement of reliable and continuous energy sources and have a minimum environmental impact. This led to exploring possibilities of energy production using renewable sources, such as wind, sun and water, used individually or sometimes combined.*
In order to achieve the European goal of zero emissions by 2050, the International Energy Agency reported in a study from 2021 that there has to be an increase in solar energy production by 24% yearly [1]. Photovoltaic panels are now widely spread across the globe due to their lower cost of energy production and low maintenance. Some countries have also governmental programs that encourage households and small businesses by covering partially or totally the cost for PVs and most recently, storage solutions. These projects represented a success in the past and encouraged people to make use of green energies with minimum investment.
A new technology that has become more popular in the last years are floating photovoltaic systems. It has been observed that they have increased energy efficiency, 5-10% higher than on-ground photovoltaic systems and they help to reduce evaporation in water-scarce regions. They help to reduce global water crisis, especially when used in agriculture or irrigation systems assuring efficient water management. Such systems of energy resolve farmers' dependence on fossil fuels, such as diesel for diesel generators used for water pumps and allow them to provide sustainable farming with low carbon emissions.
Floating photovoltaics (FPV) have also multiple benefits in reducing the land occupation as they are installed over irrigation canals, irrigation reservoirs, and ponds. While conventional photovoltaic systems are in continuous increase, they become more accessible for farmers and households. However, the major inconvenience is that they require large areas of land, which is often hard to find and very expensive. To obtain 1MW from photovoltaic panels, it is necessary around of15000 m2 of land [2][4].
This research aims to present various floating photovoltaic systems and explore the environmental and social impact and energy efficiency of these technologies. The purpose of this study is to provide a comparison between on-ground and floating photovoltaic systems by calculating the potential energy production in Dobrogea region.
Site suitability for the installation of floating photovoltaic technologies require the following environmental aspects: low precipitation and limited periods of fog, no shadowing from mountains or existing buildings, compact soil for anchoring and bodies of water low salinity, low hardness and lower waves [3]. Environmental and geographical characteristics make Dobrogea the most suitable site for such, due to its multiple bodies of water: lakes, rivers, irrigation canals and sea. However, installation at sea might be challenging as Black Sea is unpredictable in the cold season and higher waves, between 6 to 9 meters height, have been reported in the last couple of years.
The study will cover the correlation between floating photovoltaics and irrigation following technical aspects of floating photovoltaics (FPVs) in irrigation, environmental and economic assessment, current challenges and limitations, case studies and further discussions.

Keywords: *Renewable energy, photovoltaic systems, solar energy, floating photovoltaic, energy efficiency, irrigation, agriculture*

1. Introduction

Renewable energy sources have been a hot topic for energy engineering in the last few years, being extensively researched. With the growth of the population, the rising necessity of more power

sources has become the main subject of discussion in the research community. It has been agreed worldwide that there is a need to transition from fossil fuels to reduce greenhouse gases, such as CO_2. Solar energy is currently preferred over other renewable sources of energy due to its global availability, sun energy is available in every part of the world, and to its limited amount of maintenance and gas emissions during its operability lifecycle. The main issue with current technology is land occupation, solar systems require a large area of land for power generation. This challenged the researchers to develop technologies that can be installed wherever there is a piece of land that cannot be used otherwise. In the past few years, floating photovoltaic systems have been researched and finally brought to life in water-scarce regions, such as Brasil. This technology has overcome its experimental phase and it has been demonstrated that it is efficient.
The main purpose of this study is to highlight the environmental benefits of floating photovoltaic systems in Dobrogea region for irrigation purposes.
Dobrogea hosts the largest wind farms available in Romania due to its landforms and wind, which promote the production of wind energy.

2. Study area

Dobrogea region is located in South-East of Romania and it is adjacent on the east by Black Sea, in the South by Bulgaria, in the North by Danube Delta and Ukraine and in the West by Danube River.

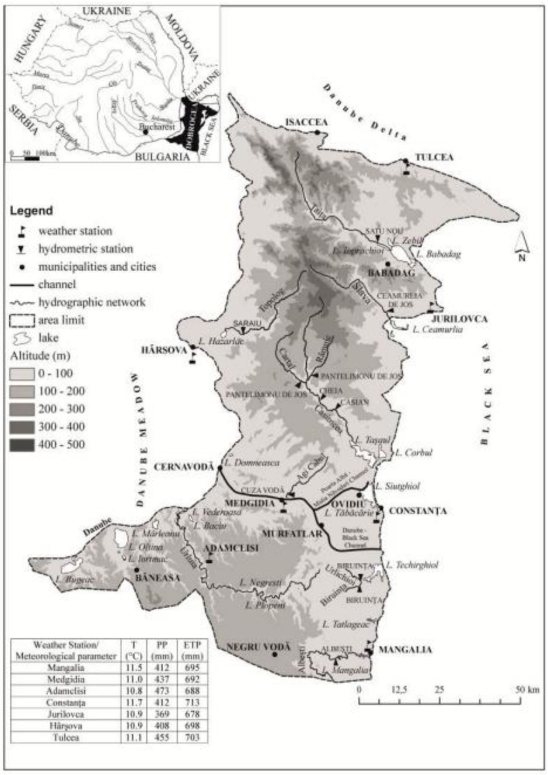

Fig. 1. Hydrographic map in Dobrogea and mean values of meteorological parameters [6]

Dobrogea is characterized by a continental climate with yearly mean air temperature between 10.8° C and 11.8° C, -1.2° C and 2° C in winter and 19° C – 22.5° C in summer. For precipitations, higher values are being recorded in the rainy months of May, June and November, when precipitations recorded are higher than 41 mm. Lower amounts are registered in January, February and October where values are lower than 27 mm. Yearly values recorded are comprised between 369 mm and 473 mm.
Evapotranspiration values recorded for Dobrogea region have yearly values between 678 mm and 713 mm, lowest values being recorded in winter and higher in summer, with mean values of 10 mm in winter and 110 mm in summer.

Dobrogea land is covered mostly by arable land, about 66.7% and 8.7% by temperate deciduous forests, rest of the land being covered mostly by urban and rural settlements [7].

2.1 Irrigation needs

Multiple studies conducted for precipitation regimes in Dobrogea confirm that there is a high need of irrigation, this being the most arid region of Romania. A study conducted by the Euro-Atlantic Resilience Centre (E-ARC) highlights that the lack of watering equipment and electricity infrastructure, along with gaps in the legislative system for the management of agricultural needs, resulted in an inefficient irrigation system in Romania. The study also shows that in 2022 only 32% of the planned land has been irrigated while in 2023 38% of the planned area has been irrigated [8]. Below table from Land Improvement National Agency (ANIF) summarizes all irrigation sources available in Dobrogea.

Table 1: Land surface and irrigation sources available in Constanta region [9]

Name	Land surface		Irrigation Source
	Gross (ha)	Net (ha)	
Constanta North			
Carasu – Nicolae Balcescu	29602	29172	CDMN – PAMN
Terasa Seimeni	22999	22819	Danube
Terasa Topalu	18885	18832	Danube
Carasu – Mihail Kogalniceanu	26914	26492	CDMN – PAMN
Terasa Sinoe	53096	52789	Golovita Lake
Terasa Harsova	31955	31749	Danube
Ciobanu – Girliciu	2689	2489	Danube
Orezaria – Harsova	3063	2954	Danube
Carasu – CDMN/PAMN North	3154	3108	CDMN – PAMN
Daeni – Ostrov - Peceneaga	5908	5904	Danube
Total	**198265**	**196308**	
Constanta South			
Carasu – Basarabi	5993	5907	CDMN - PAMN
Carasu – Galesu	4818	4750	CDMN - PAMN
Carasu – Poarta Alba	3694	3641	CDMN - PAMN
Carasu – Valea Seaca	7171	7067	CDMN - PAMN
Carasu – Faclia	8766	8640	CDMN - PAMN
Carasu – Topraisar	4624	4557	CDMN - CMNV
Carasu - Amzacea	2275	2242	CDMN - CMNV
Carasu – Biruinta	14854	14329	CDMN - CMNV
Carasu – Movilita	8172	8054	CDMN - CMNV
Carasu – Baaraganu	14794	14578	CDMN - CMNV
Carasu – Potirnichea	2304	2272	CDMN - CMNV
Carasu – Lanurile	7153	7049	CDMN - CMNV
Carasu – Mangalia North	805	793	CDMN - CMNV
Carasu – Mangalia South	9932	9788	CDMN - CMNV
Carasu – Tatara	11812	11640	CDMN - CMNV
Carasu – Mosneni	31603	31150	CDMN - CMNV
Rasova - Vederoasa	2297	1673	CDMN - CMNV
Oltina West	84136	80584	Danube
Carasu – CDMN/PAMN South	2452	2440	Danube
Carasu – Canal Negru Voda	1464	1443	CDMN - PAMN
Cochirleni	2695	2651	CDMN - PAMN
Total	**232565**	**225988**	
Total North & South	**430830**	**422296**	

2.2 Floating Photovoltaic Systems in Irrigation

Despite low quantities of precipitation, Dobrogea has multiple sources of water which allow the installation of floating photovoltaic systems. These have benefits for land owners as they assure independence from national regulations, energy sources and fossil fuels. Floating photovoltaic systems (FPVs) ensure the energy necessity for irrigation even in remote areas and prevent evaporation from irrigation ponds or canals. FPVs reduce costs for irrigation.

3. Calculation of the Energy Generation

For the calculation made further in this study, the land area of Sinoe has been considered. Sinoe is located in the northern part of Constanta County, right at the border with Tulcea county. Arable land is being irrigated using water from Lake Golivita. The lake is 7.2 km long and 18 km wide, covering a surface of 7500 hectares.

Using the standard equation for the power generation it can be determined the energy generation of a photovoltaic installation on a determined area.

$$P = A \times G \times \eta \tag{1}$$

, where P represents the energy generated in kW, A is the area covered by panels (m^2), G is solar irradiation in $kWh/m^2/day$ and η is the efficiency of the system, usually ranging between 15-20% [10]. Lake area considered for this is study is 1 hectare, equivalent to 10000 m^2.
Solar irradiation has been obtained utilizing online calculators which have collected solar data for 20 or more years and it has been calculated for panels facing directly south, positioned horizontally on a flat surface [11]. Values obtained have been summarized below table for $\eta = 18\%$.

Table 2: Average monthly solar irradiation for Constanta County and energy generation for floating photovoltaic systems

Month	**Solar Irradiation G** ($kWh/m^2/day$)	**Energy Generation** (kW)
January	1.47	2646
February	2.23	4014
March	3.20	5760
April	4.37	7866
May	5.53	9954
June	6.05	10890
July	6.24	11232
August	5.38	9684
September	4.09	7362
October	2.63	4734
November	1.57	2826
December	1.15	2070
Yearly mean value		6586.5

Usually, photovoltaic panels lose their efficiency when they reach temperatures above 25° C. For each degree over 25, panels lose 0.5% of their efficiency. Considering the above information and assuming on-ground photovoltaic panels do not have any cooling systems, data has been summarized in the below table.

Table 3: Average monthly solar irradiation for Constanta County, mean temperatures and energy generation for on-ground photovoltaic systems

Month	**Solar Irradiation G** (kWh/m²/day)	**Higher mean monthly temperature** (° C)	***η*** (%)	**Energy Generation** (kW)
Jan	1.47	4	18	2646
Feb	2.23	6	18	4014
Mar	3.20	10	18	5760
Apr	4.37	15	18	7866
May	5.53	21	18	9954
Jun	6.05	26	17.5	10587.5
Jul	6.24	29	16	9984
Aug	5.38	29	16	8608
Sep	4.09	24	18	7362
Oct	2.63	18	18	4734
Nov	1.57	12	18	2826
Dec	1.15	6	18	2070
Yearly mean value				6367.63

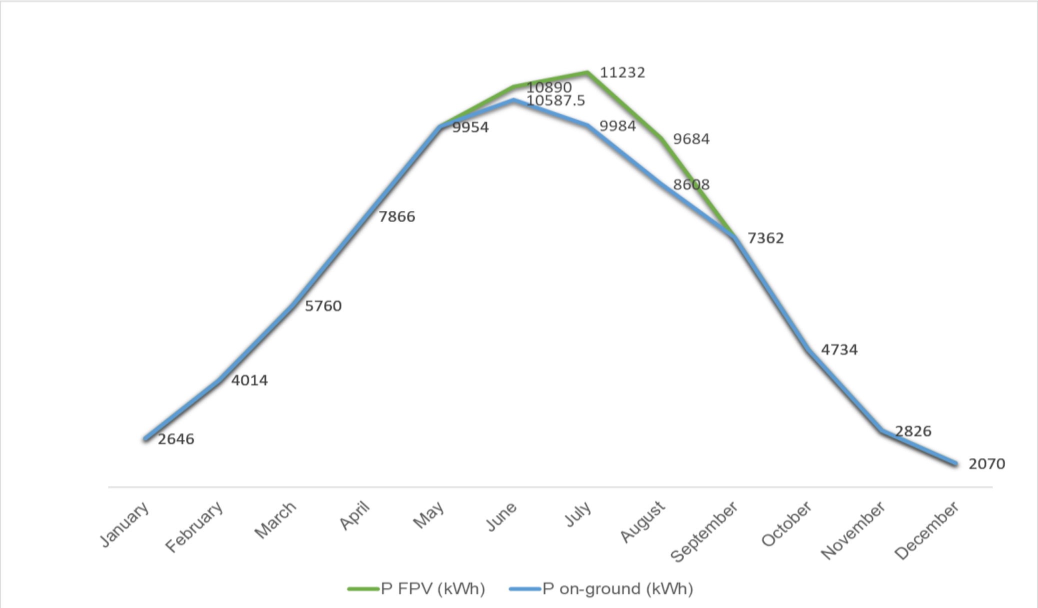

Fig. 2. Monthly Energy Generation for on-ground PVs and FPVs.

4. Efficiency gains

Efficiency gains between on-ground PVs and FPVs is calculated with the following formula:

$$\Delta\eta = \eta_{FPV} - \eta_{on-gound} \tag{2}$$

$$\eta = \frac{P}{A \times G} \tag{3}$$

$$\eta_{FPV} = \frac{6586{,}5 \text{ kW}}{10000\ m^2 \times 3{,}66\text{kWh/m2/day}} = 18\% \tag{4}$$

$$\eta_{on-ground} = \frac{6363{,}63 \text{ kW}}{10000\ m^2 \times 3{,}66\text{kWh/m2/day}} = 17\% \tag{5}$$

Therefore $\Delta\eta = 1\%$ the efficiency gains yearly.

5. Water conservation from evaporation

One of the benefits FVPs installed over irrigation ponds or canals is the reduction of water evaporation. The panels act as a barrier between the water body of the irrigation source and direct sunlight. Since evaporation is strictly linked to heat, the barrier acts as a heat protectant for the body of water. The physical panel barrier acts as a shield from winds that carry away water particles and promote the transportation and evaporation of water. Studies have shown that evaporation is reduced by 30 to 60% by using floating photovoltaic systems [12, 13]. Water savings can be calculated with the formula

$$Water\ saving = E_{baseline} \times A_{FPV} \times C \tag{6}$$

, where $E_{baseline}$ represents baseline evaporation yearly evaporation rate expressed in meters, A_{FPV} is the area covered by FPVs and C is the percentage of reduced evaporation by FPVs covering. This percentage is an empirical value which ranges from 30 to 60%. For this study, C is assumed to be 40% and a higher evaporation rate has been considered for Dobrogea region (7,13m).

$$Water\ savings = 7{,}13\ m \times 10000\ m^2 \times 40\% \tag{7}$$

$$Water\ savings = 28520\ m^3$$

In conclusion, 1 hectare of water covered by FPVs in Dobrogea region would save 28520 m^3 of water yearly.

6. Limitations and uncertainties

All data used for conducting this study has been collected from other studies or public reports from Romanian national agencies and it refers to Dobrogea region. In reality, values might differ from north to south. So, in order to have accurate results, in situ measurements over long period of time have to be carried out.

7. Conclusions

Floating photovoltaic panels represent an alternative to traditional on-ground photovoltaic panels. Both types of systems carry advantages and disadvantages. In terms of energy efficiency, floating photovoltaic systems resulted might generate more power as they do not require cooling systems, water acting as coolant and keeping a constant temperature. In reality, their efficiency depends on multiple factor such as their position, cleaning and maintenance.

For the environmental aspects, studies carried on the topic shown that FPVs have a lower impact due to water conservation and no need for land occupation. However, an environmental assessment has to be carried to ensure marine life is not disturbed during the installation of these systems.

In terms of costs, compared to on-ground solutions, floating photovoltaic systems are not very popular. However, with the increasing necessity of energy production and lower cost of operability, floating photovoltaic systems start to gain more popularity which might result into lower cost for the panels and installation. The energy source for the pumping system is in the immediate vicinity, eliminating additional energy losses during transport.

Other challenges might be related to regulatory and permitting. Currently Romanian laws for offshore green energy production are not complete and permits for installation of floating photovoltaic systems over water surface might be difficult to obtain.

In conclusion, floating photovoltaic systems are representing a promising technology for energy production in arid and water-scarce regions.

References

[1] IEA. "Solar, P.V. Technical Report". IEA: Paris, France, 2021. Accessed September 22, 2024. https://www.iea.org/reports/clean-energy-transitions-programme-2020.

[2] Cuce, E., P.M. Cuce, S. Saboor, A. Ghosh, and Y. Sheikhnejad. "Floating PVs in Terms of Power Generation, Environmental Aspects, Market Potential, and Challenges." *Sustainability* 14, no. 5, (2022): 2626.

[3] Solar Energy Institute of Singapore. "Where Sun Meets Water: Floating Solar Market Report. Technical report". World Bank: Washington, DC, USA, 2019.

[4] Essak, Laura, and Aritra Ghosh. "Floating Photovoltaics: A Review." *Clean Technol.* 4, no. 3 (2022): 752–769. https://doi.org/10.3390/cleantechnol4030046.

[5] Yousuf, Hasnain, Muhammad Quddamah Khokhar, Muhammad Aleem Zahid, Jaeun Kim, Youngkuk Kim, Eun-Chel Cho, Young Hyun Cho, and Junsin Yi. "A Review on Floating Photovoltaic Technology (FPVT)." *Current Photovoltaic Research* 8, no. 3 (2020): 67-78.

[6] Telteu, Camelia-Eliza, F. I. Stan, and O. Oprean. "Runoff characteristics in Dobrogea." Paper presented at Air and Water Components of the Environment International Conference, Cluj-Napoca, Romania, March 17-19, 2023.

[7] Telteu, Camelia-Eliza, and Liliana Zaharia. "Morphometrical and dynamical features of the South Dobrogea lakes, Romania." *Procedia Environmental Sciences* 14 (2012): 164-176.

[8] Ciobotaru, Miruna-Ecaterina. "The ongoing challenge. Why doesn't Romania irrigate to its potential?" *Euro-Atlantic Resilience Centre / Centrul Euro-Atlantic pentru Reziliență - E-ARC*, August 15, 2023. Accessed October 10, 2024. https://e-arc.ro/en/2023/08/15/the-ongoing-challenge-why-doesnt-romania-irrigate-to-its-potential-2/.

[9] Romanian Land Improvements National Agency (ANIF). Annex II6e. "Irrigation systems administrated by Land Improvements National Agency (ANIF) – Territorial Region of Dobrogea / Sisteme de irigații administrate de Agenția Națională de Îmbunătățiri Funciare (ANIF) – Regiunea Teritorială Dobrogea". Accessed October 10, 2024.

[10] Masters, Gilbert M. *Renewable and Efficient Electric Power Systems*. Chapter 7 - The Solar Resource. 2nd Edition, IEEE Press, 2013.

[11] Boxwell, Michael. *Solar Electricity Handbook: A Simple, Practical Guide to Solar Energy - Designing and Installing Photovoltaic Solar Electric Systems*. Greenstream Publishing, 2010.

[12] Paul, D., D. Devaprakasam, S. Patil, and A. Agrawal. "Floating solar: A review on the comparison of efficiency, issues, and projections with ground-mounted solar photovoltaics." *International Journal of Sustainable Development and Planning* 18, no. 10 (October 2023): 3213-3228. https://doi.org/10.18280/ijsdp.181021.

[13] Perez, M., R. Perez, C.R. Ferguson, and J. Schlemmer. "Deploying effectively dispatchable PV on reservoirs: Comparing Floating PV to other renewable technologies." *Solar Energy* 174 (November 2018): 837-847. https://doi.org/10.1016/J.SOLENER.2018.08.088.

ISSN 1454 - 8003
Proceedings of 2024 International Conference on Hydraulics and Pneumatics - HERVEX
November 13-15, Băile Govora, Romania

DEVELOPMENT AND LABORATORY TESTING OF A DIGITAL FLOW CONTROL UNIT

Bogdan TUDOR[1], Radu RĂDOI[1], Robert BLEJAN[1], Ioana ILIE[1], Ștefan DUMITRU[2]

[1] National Institute of Research & Development for Optoelectronics – Subsidiary Hydraulics and Pneumatics Research Institute (INOE 2000 – IHP)

[2] National Institute of Research – Development for Machines and Installations Designed for Agriculture and Food Industry – INMA Bucharest

Abstract: *Industrial and mobile equipment uses proportional hydraulics to perform precise movements such as positioning of machined parts or movement of the tools. In recent years, digital hydraulics has developed a lot in terms of control schemes and equipment such as digital valves (parallel hydraulic valves, high speed switching hydraulic valves and stepping hydraulic valves) or digital hydraulic pumps (switching and parallel digital hydraulic pumps etc.). By using digital hydraulics, proportional hydraulic valves, which are expensive and demanding in terms of hydraulic oil filtration conditions can be replaced. This paper presents the development and laboratory testing of a digital flow control unit that can be used to step-change the speed of a hydraulic motor.*

Keywords: *Digital hydraulics, DFCU, PCM, control software*

1. Introduction

Digital Flow Control Units (DFCU) can be used in industries (construction, manufacturing, agriculture) due to their efficiency, reliability, and precision. In industrial machinery, particularly in sectors like pulp and paper, they are applied to achieve precise flow and pressure control. By replacing traditional proportional valves with durable on/off valves, DFCU enhance system reliability, can reduce downtime, and lower operational costs [1,2].
In hydraulic drives and actuators, DFCU systems facilitate intelligent and independent metering control. This capability allows for improved tracking of velocity and pressure, even at low flow rates, making them ideal for applications requiring high precision.
Energy efficiency is another significant advantage of systems containing DFCU. These units help reduce energy consumption by eliminating the need for pumps to run continuously during steady states [3].
In heavy machinery and construction equipment, DFCU systems can play a role in managing the precise movement of large and heavy components [4,5]. DFCU systems can be used in research and experimental rigs where hydraulic control is crucial. Their versatility and precise control make them ideal for laboratory environments and custom industrial applications.
In the case of the parallel digital hydraulic system in present paper is used the Pulse Code Modulation (PCM) method with the 2^n series, i.e. 1, 2, 4, 8, 16, ..., depending on the value of n, where n is the number of solenoid valves and is the most common coding method in the implementation of such systems. Calculation of the number of flow rate adjustment points using the PCM method with binary series is done using the formula 2^n-1, where n is the number of valves.
In the case of the present work, the developed DFCU unit uses 5 binary coded throttle valves and 5 normally closed 2/2 solenoid valves, obtaining $2^5 - 1 = 31$ flow rate adjustment points [6,7].

2. Physical realisation of the DFCU

The hydraulic diagram of the system It is found in figure 1. For its construction, in-line hydraulic devices connected with hydraulic pipes were used. Normally such a parallel flow control system would have been made up of binary-coded solenoid valves of different sizes.

The solution of using adjusting throttle valves was chosen to enable future research using different methods of encoding the throttle opening, so that several types of research on parallel digital hydraulic systems can be carried out on this unit.

The DFCU system is composed of a group of ON/OFF 2/2 cartridge type solenoid valves, a group of throttle valves, the elements for measuring the system parameters and the electrical command and control system with programmable logic controller (PLC).

The hydraulic diagram of the DFCU is made up of the following components:

- the group of ON/OFF 2/2 cartridge type solenoid valves marked with DH1,...,DH5;
- the group of throttles DR1,...,DR5 adjusted so that the flow rate passing through each throttle is coded using the binary series, i.e. 2, 4, 8, 16, 32 l/min;
- pressure transducers TP;
- throttle valve for pressure load DS;
- temperature transducer TT;
- flowmeter DM.

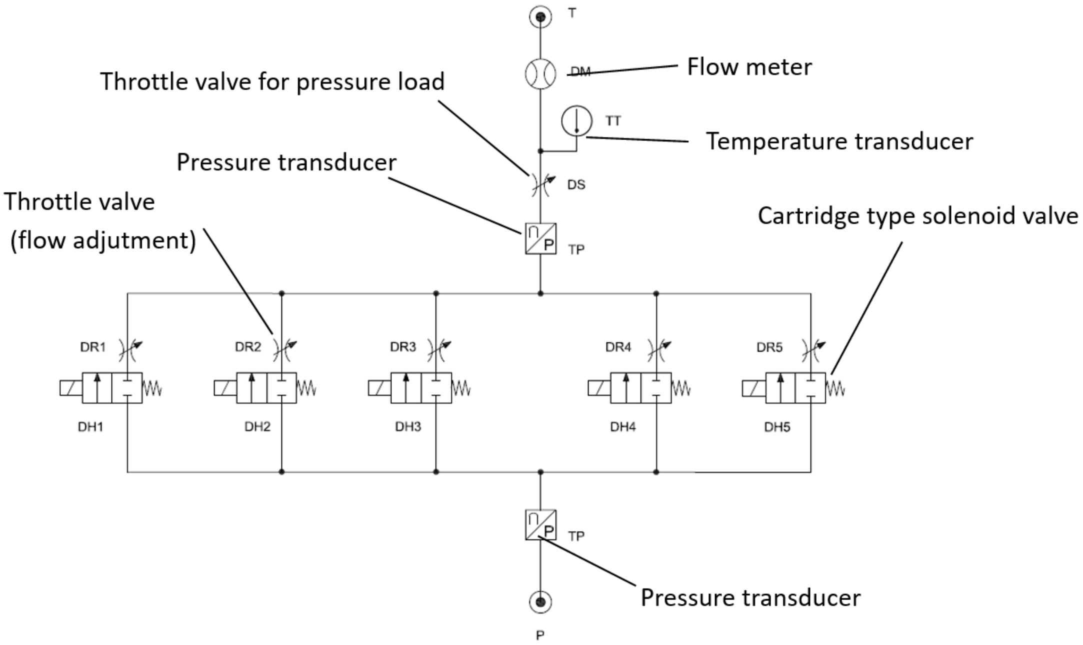

Fig. 1. Hydraulic diagram of the DFCU

Fig. 2. The assembled DFCU

Figure 2 shows an image of the assembled DFCU system, which contains the following elements:
- the group of 2/2 ON/OFF cartridge type solenoid valves, which are electrically operated by means of solenoids located on them;
- the group of throttles valves consists of 5 throttles valves, of which 2 with an inlet size of ½ inches and 3 with an inlet size of ¾ inches;
- two pressure transducers (0…250 bar), one located at the entrance to the system and the other at the exit from the system;
- a flow transducer with the measuring range: 1…75 l/min;
- a temperature transducer with the measuring range: 0…100 °C.

3. Electric system and control software

For the laboratory testing of the digital hydraulic unit, an electrical cabinet (figure 3) was created that contains a 10A, 24V power supply for powering the solenoids, an automatic circuit breaker, 5 relays for controlling the solenoids of the hydraulic valves and a programmable logic controller equipped with an analog input module for the transducers included in the digital hydraulic unit. The PLC has implemented software for controlling the solenoids through digital outputs (discrete output coils) and monitoring the signals from the transducers through analog inputs (analog registers). The PLC communicates discrete or analog data through the Modbus TCP/IP protocol. Thus, a computer with the corresponding software connected to the same local network as the PLC can access the data.

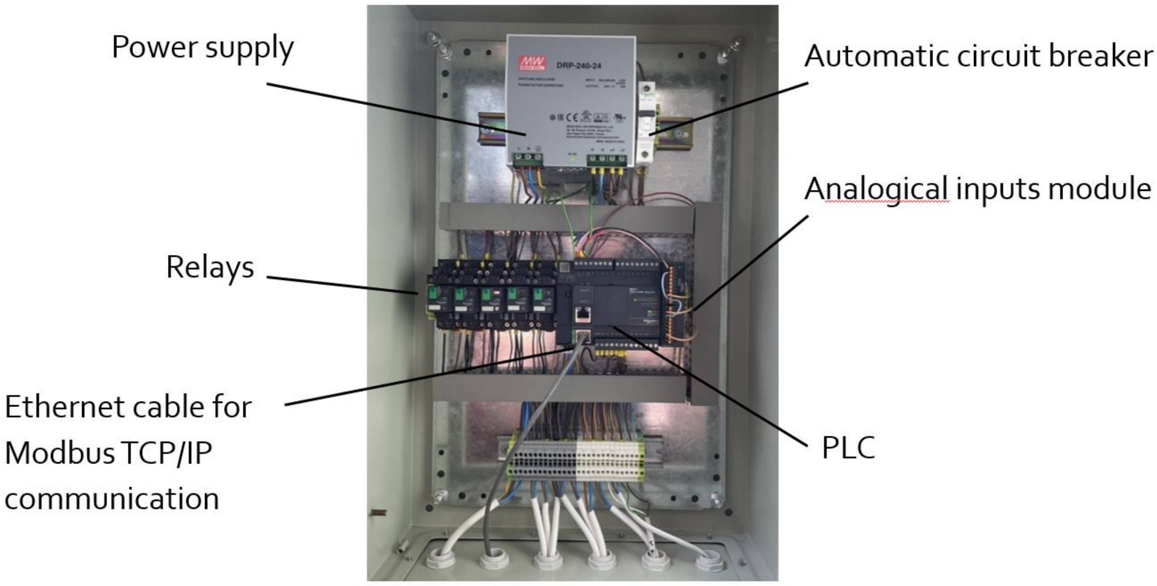

Fig. 3. The electrical cabinet for command and control of the digital hydraulic unit

In order to be able to perform tests for DFCU a control interface is made in the form of an application installed on a computer (figure 4). The application is designed in such a way that it is possible to perform tests in which the operator can manually select the command of each solenoid valve, but also automatic tests that perform system testing using a previously defined action table in an excel file (Table 1). In the application's control window, there is also a section for numerical visualization of the system parameters (flow, pressure at the entrance to the system, pressure at the exit from the system, temperature at the exit from the system), but also a section for graphical visualization of the parameters, with the possibility of viewing both the graphic curve of each parameter and the curves of all parameters on the same graph [8].

Table 1: Command steps to obtain increasing flow rate

Step	Step time [s]	Valve 1	Valve 2	Valve 3	Valve 4	Valve 5	Flow [l/min]
0	0	0	0	0	0	0	0
1	5	1	0	0	0	0	2
2	10	0	1	0	0	0	4
3	15	1	1	0	0	0	6
4	20	0	0	1	0	0	8
5	25	1	0	1	0	0	10
6	30	0	1	1	0	0	12
7	35	1	1	1	0	0	14
8	40	0	0	0	1	0	16
9	45	1	0	0	1	0	18
10	50	0	1	0	1	0	20
. .	. .	. .	. .	. .	. .	. .	. .
25	125	1	0	0	1	1	50
26	130	0	1	0	1	1	52
27	135	1	1	0	1	1	54
28	140	0	0	1	1	1	56
29	145	1	0	1	1	1	58
30	150	0	1	1	1	1	60
31	155	1	1	1	1	1	62

In order to process the data obtained from the experiment, the application generates an Excel file at the end of the test with all the system parameters acquired at a sampling interval that can be set between 50...200 milliseconds.

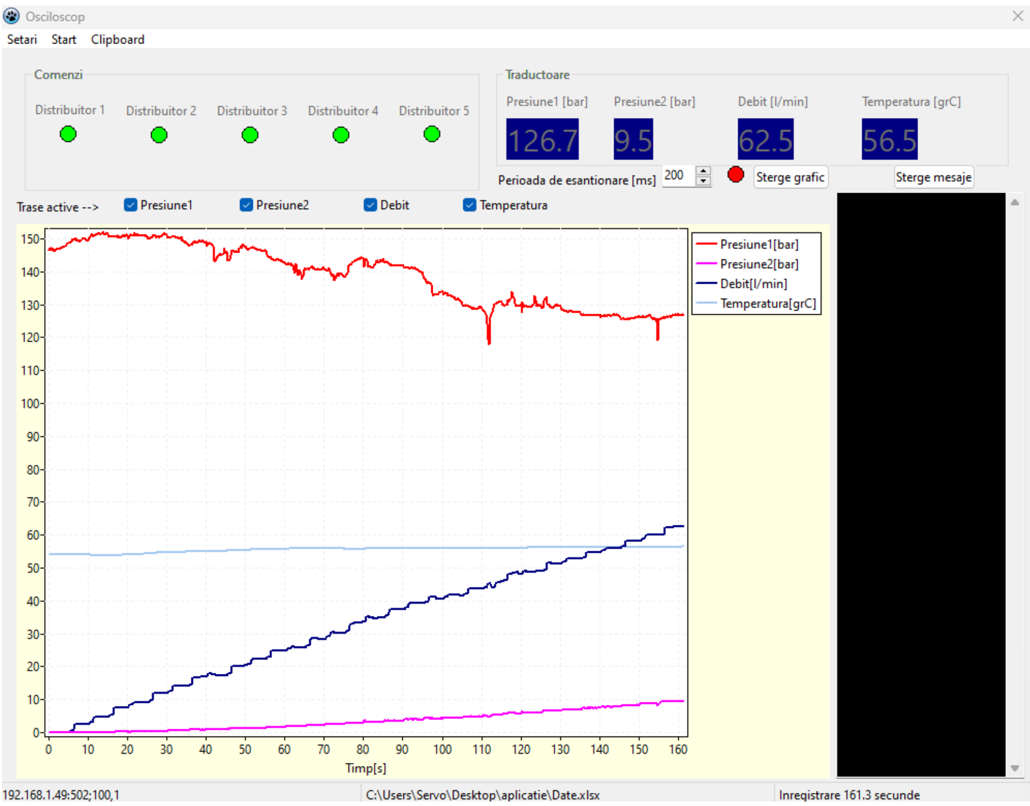

Fig. 4 The software interface with the recording of the increasing flow of the DFCU

In Figure 5 can be seen the decreasing variation of the DFCU flow rate.
A similar control system for a DFCU can be implemented in the PLC of mobile or industrial machines for custom applications.
A disadvantage of this digital flow control unit may be the pressure peak phenomenon that occurs when switching hydraulic circuits with valves, and some authors are studying their minimization [9,10].

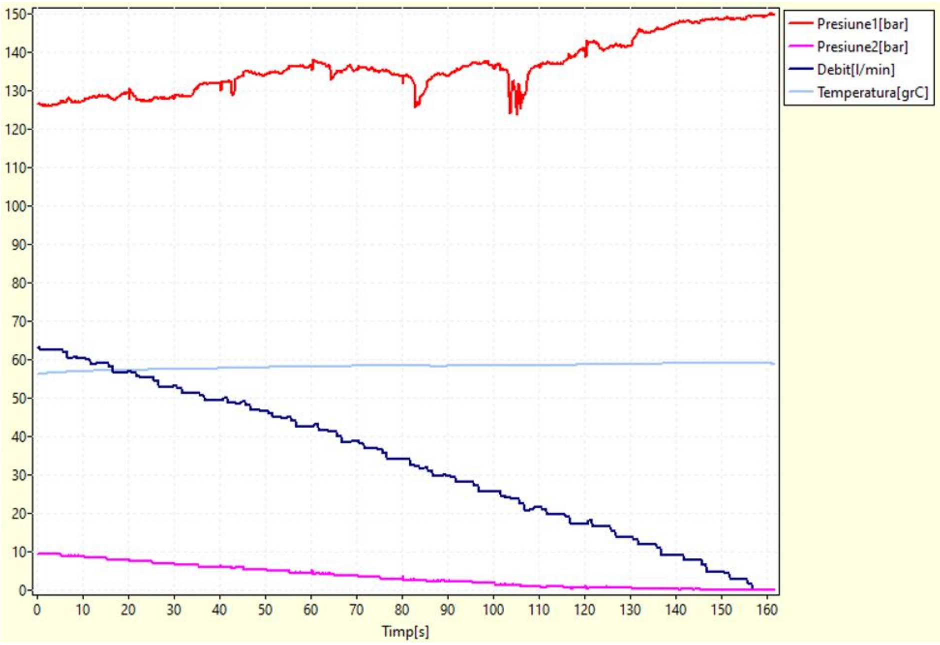

Fig. 5 Decreasing variation of the DFCU flow rate

4. Conclusions

The flow control unit developed for experimental purposes works well, achieving 31 flow values, and by increasing the number of valves, very good resolution can be obtained.
The developed software allows testing of the DFCU with recording of supply pressure, load pressure, flow rate and temperature at the hydraulic fluid discharge.
DFCU allow precise control of flow rates through a combination of multiple on/off valves operating in parallel.
By assigning discrete flow rates to each valve, DFCU effectively acts as a hydraulic digital-to-analog converter.
Overall, DFCU technology represents an advancement in hydraulic systems, enabling more efficient, precise, and reliable operations while presenting opportunities for optimization in control methods and manufacturing.
In the future, our team aims to develop a compact DFCU version in the form of a hydraulic block containing solenoid valves and sensors for measuring operating parameters.

Acknowledgments

The work was carried out through the Core Program within the National Research Development and Innovation Plan 2022-2027, carried out with the support of the Romanian Ministry of research, innovation and Digitalization (MCID),project no. PN 23 05.

References

[1] Valmet. “Digital Hydraulics, Technical Paper Series”, March 25, 2016. Accessed October 22, 2024. https://www.valmet.com/globalassets/media/downloads/white-papers/process-improvements-and-parts/wpp_digihydraulics.pdf.

[2] Sciatti, F., P. Tamburrano, E. Distaso, and R. Amirante. “Digital hydraulic valves: Advancements in research.” *Heliyon* 10, no. 5 (2024): e27264. https://doi.org/10.1016/j.heliyon.2024.e27264.
[3] Laamanen, A., L. Siivonen, M. Linjama, and M. Vilenius. “Digital Flow Control Unit-An Alternative for a Proportional Valve.” Paper presented at Bath Workshop on Power Transmission and Motion Control (PTMC 2004), Bath, United Kingdom, January 1, 2004.
[4] Donkov, V. H., T. Andersen, M. Linjama, and M. Ebbesen. “Digital hydraulic technology for linear actuation: A state of the art review.” *International Journal of Fluid Power* 21, no. 2 (2020): 263–304.
[5] Ketonen, M., and M. Linjama. “High flowrate digital hydraulic valve system.” Paper presented at the 9th Workshop on Digital Fluid Power, Aalborg, Denmark, September 7-8, 2017.
[6] Laamanen, A., M. Linjama, and M. Vilenius. “Characteristics of a digital flow control unit with PCM control.” Paper presented at the 7th Triennial International Symposium on Fluid Control, Measurement and Visualization, Sorrento, Italy, August 25-28, 2003.
[7] Rong, L., W. Xuanyin, T. Guoliang, and D. Fan. “Theoretical and experimental study on hydraulic servo position control system with generalization pulse code modulation control.” Paper presented at the Fifth International Conference on Fluid Power Transmission and Control (ICFP'2001), Hangzhou, China, April 3-5, 2001.
[8] Elsaed, E., and M. Linjama. “Development and simulation of a test system for analyzing high flow rate digital flow control units.” Paper presented at The Twelfth Workshop on Digital Fluid Power, Tampere, Finland, June 6-7, 2024.
[9] Laamanen, A., M. Linjama, and M. Vilenius, “Pressure peak phenomenon in digital hydraulic systems - A theoretical study.” Paper presented at Bath Workshop on Power Transmission and Motion Control (PTMC 2005), Bath, United Kingdom, September 7-9, 2005.
[10] Laamanen, A., M. Linjama, and M. Vilenius. “On the pressure peak minimization in digital hydraulics.” Paper presented at The Tenth Scandinavian International Conference on Fluid Power SICFP'07, Tampere, Finland, May 21-23, 2007.

ISSN 1454 - 8003
Proceedings of 2024 International Conference on Hydraulics and Pneumatics - HERVEX
November 13-15, Băile Govora, Romania

ELECTRIC PLATFORM FOR TRANSPORTING SMALL OBJECTS ON SUSTAINABLE CONSTRUCTION SITES

Cătălin FRÂNCU[1], Mihail SAVANIU[1], Oana TONCIU[1]

[1] UTCB – Faculty of Mechanical Engineering and Robotics in Constructions

catalin.francu@utcb.ro; mihai.savaniu@utcb.ro; oana.tonciu@utcb.ro

Abstract: *The paper presents the development of an electric platform for the transportation of small objects in the logistic activities of supplying various components for electrical and plumbing works in a sustainable construction site. The transportation platform was developed, in the first stage, in the laboratory at the concept level and the results were used in the design of the electrical transportation platform presented in this paper. The use of stand-alone electric transportation systems on construction sites is a necessity at the present time when the reduction of greenhouse gas emissions is desired. The mobile platform is powered from renewable sources and allows use in both outdoor and indoor areas of construction sites. A pair of rubber tracks was used as a propulsion system to ensure easy moving in difficult terrain specific to construction sites. The test results recommend this type of transportation for the construction sites of the future to be as environmentally friendly as possible.*

Keywords: *Electric transportation, construction logistics, sustainable construction site*

1. Introduction

The field of construction has introduced innovative automated electric platforms for the transportation of small objects in the transportation of various objects, addressing the efficiency, safety and sustainability of these solutions to ensure logistics.
One solution for the integration of modular electric platforms for the transportation of objects is the modular integrated construction (MiC) technology. In paper [1], the integration of electrically powered transportation systems with digital tools such as Building Information Modeling (BIM) and IoT sensors is highlighted. These systems enable just-in-time component delivery and real-time monitoring, increasing construction site efficiency and operator safety. Another solution for the transportation of small objects on construction sites is the use of drones and artificial intelligence: drones, combined with artificial intelligence, are increasingly being used for material transportation and site monitoring. Although mainly used for surveillance, these platforms represent a step towards automating the transportation of objects on construction sites [2,3].
Electric transportation platforms equipped with sensors and AI algorithms help to safely move materials in a construction site, reducing the risk of accidents. These technologies help to proactively identify and mitigate risks in dynamic work environments [2]. Semi-autonomous electric-powered platforms are being adopted to help move materials, with an evolution towards fully autonomous systems for controlled environments such as warehouses and prefabricated construction sites. However, on typical construction sites, semi-automated systems currently dominate due to the variability and complexity of these environments. Advances in artificial intelligence and remote control systems are paving the way for wider deployment [4,5]. Automated platforms are part of broader trends in smart construction, driven by digitization and automation specific to sustainable construction sites.
The solutions proposed by developers of platforms for material transportation on construction sites can be: the WestonRobot platform that can transport 60 kg for logistic transportation on construction sites with a power of 120 W [6]; Robotnik Automation has developed RB-VOGUI, a modular, autonomous and collaborative ground robot designed for autonomous material transportation in the industrial and construction sectors. The platform consists of a modular, all-terrain mobile base suitable for transporting loads up to 200 kg [7]. The Cross-country XC-30 crawler transporter is a heavy-duty transporter that combines power and versatility. With a carrying capacity of up to 2200

kg on flat surfaces, this compact, electric-powered equipment can be used for transporting objects on construction sites [8].

2. Implementation

Construction sites require efficient logistics for moving tools, materials and equipment. With the increasing importance of sustainability goals, traditional fuel-based transportation systems are being replaced by environmentally friendly alternatives. This study presents the development of an electric transport platform to streamline logistics on construction sites while minimizing environmental impacts. The study pursues the efficient conversion of transportation equipment equipped with heat engine to autonomous electric equipment. In developing a small object transportation platform we aimed to: Reducing carbon emissions and noise pollution; increasing worker safety and ergonomics; Integrating renewable energy systems for charging; compactness and maneuverability average payload capacity 100-300 kg, sufficient for tools, small equipment or materials; use of lithium-ion batteries for energy density or lithium-iron-phosphate for safety and longevity; renewable charging options (solar panels) and fast-charging compatibility; high-efficiency brushless DC motors; options for remote control or autonomous navigation ; use of weatherproof and dust-resistant materials.
The development of an electric platform for transporting small objects on sustainable construction sites is an innovative approach to improving efficiency while maintaining environmentally friendly practices. The considerations and features considered in the development of the electric platform for small object transportation were as follows:

- Compact dimensions optimized for movement in narrow spaces on construction sites.
- Electric undercarriage use of zero-emission electric motors powered by rechargeable batteries.
- Durable construction use of materials that can withstand harsh conditions such as dust, water.
- Configurable, modular compartments or adjustable shelves to carry tools, materials or small equipment.
- Renewable charging use of solar panels or compatibility with on-site renewable energy sources.
- Recycled materials use of recycled or low-impact materials.
- Energy efficiency: intelligent systems to optimize battery use.
- Autonomous or semi-autonomous capabilities: GPS-guided navigation or remote control options.
- Optimized charging capacity: Designed to carry loads efficiently without excessive energy consumption.
- Safety Sensors: Equipped with obstacle detection sensors, anti-collision systems and emergency stop functions.
- Smart connectivity: Integration with site management software to track usage, optimize routes and monitor battery status.
- Reduced noise level by using electric motors.
- Tool transportation use: moving small hand tools or power tools to large sites; material delivery: transporting small quantities of materials such as bricks, screws or pipes; collecting recyclable waste from different areas of the site.

The development of the electric transportation platform was aimed at converting an existing thermal engine powered equipment into an equipment usable in the sustainable construction sites of the future. To this end we converted the GeoPorter 330 D [10] motorized platform with a useful transport capacity of 330 kg. Its transportation system is powered by a Briggs and Stratton 6.5 HP [11] gasoline engine with a capacity of 280 cm3 with a maximum power of 6.5 hp and a maximum torque of 2800 rpm coupled, through a belt transmission, to a gearbox with three forward and one reverse gear. The GeoPorter 330 D platform is equipped with a travel system with two rubber tracks with a width of 190

ISSN 1454 - 8003
Proceedings of 2024 International Conference on Hydraulics and Pneumatics - HERVEX
November 13-15, Băile Govora, Romania

mm and a diameter of the drive stellate wheel of 150 mm, as in fig 2. The design of the platform consisted of the survey and subsequent modeling of the GeoPorter 330 D motorized platform in the 3D SolidWorks virtual environment, see Fig 1. The modeler was made in order to implement modifications to the transmission and actuation to ensure the initial transport performance.

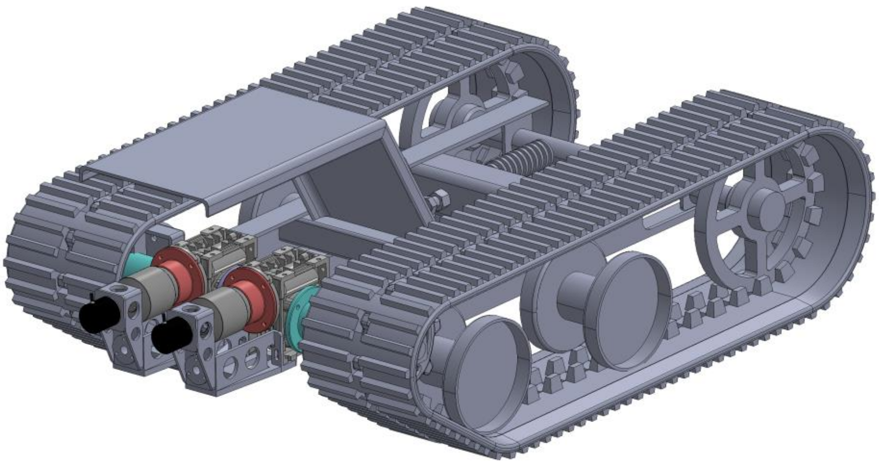

Fig. 1. 3D model of the electric powered transportation platform

The modification of the platform travel system has taken into account the following parameters of the kinematic chain for thermal engine and speed reducer actuation: maximum moment speed of the thermal engine 2600 rpm; total transmission ratio in first gear is 70. 95; in gear II it is 36.55; in gear III it is 30.10 in reverse R 94.6. The travel speed of the heat engine driven platform is 0.091 m/sec in gear I; 0.177 m/sec in gear II; 0.215 m/sec in gear III; 0.073 m/sec in gear R.

Fig. 2. Actual model of the electric powered transportation platform

The kinematic chain of the electric transportation platform, fig.3, consists of the following components: brushless electric motor 6374 170 kV [12] with a maximum power of 2800 W, a maximum power of 1700 W, a speed range of 4080 - 7920 rpm; a gearbox with a transmission ratio of 100. Under these conditions the speed at the level of the stellate wheel driving the track is between 41 - 79.2 rpm which corresponds to a speed range of 0.102 - 0.198 m/sec. The practical realization of the modified kinematic chain of the electric transportation platform is shown in fig.4.

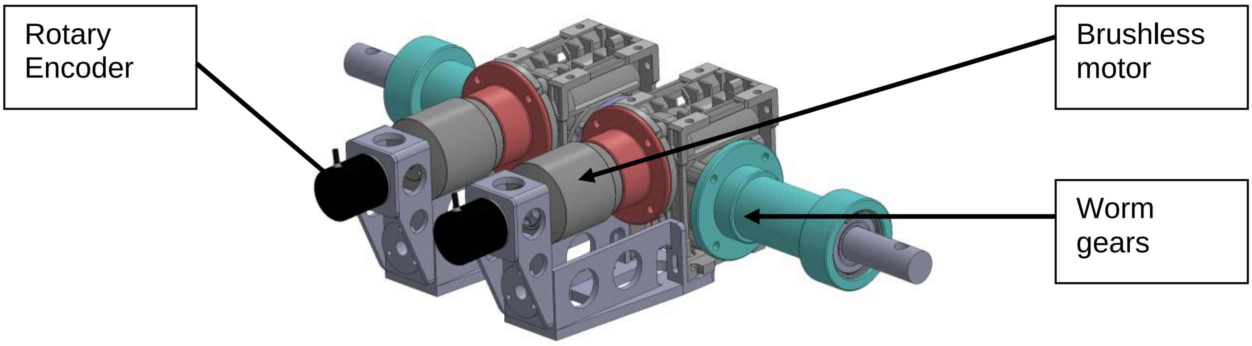

Fig. 3. 3D modeled mechanical transmission of electrically powered transport platform

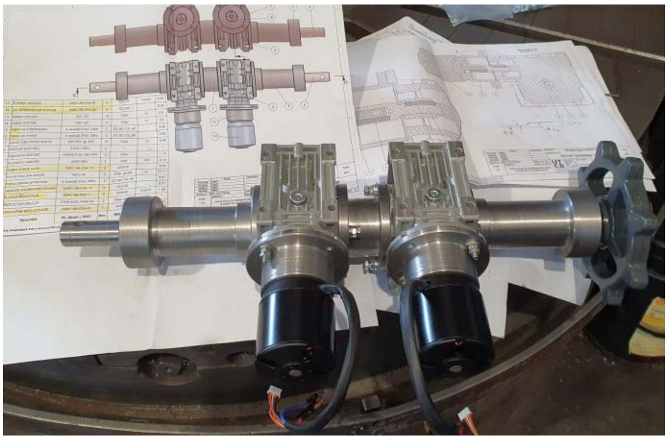

Fig. 4. Practical realization of the transmission of the electric powered transport platform

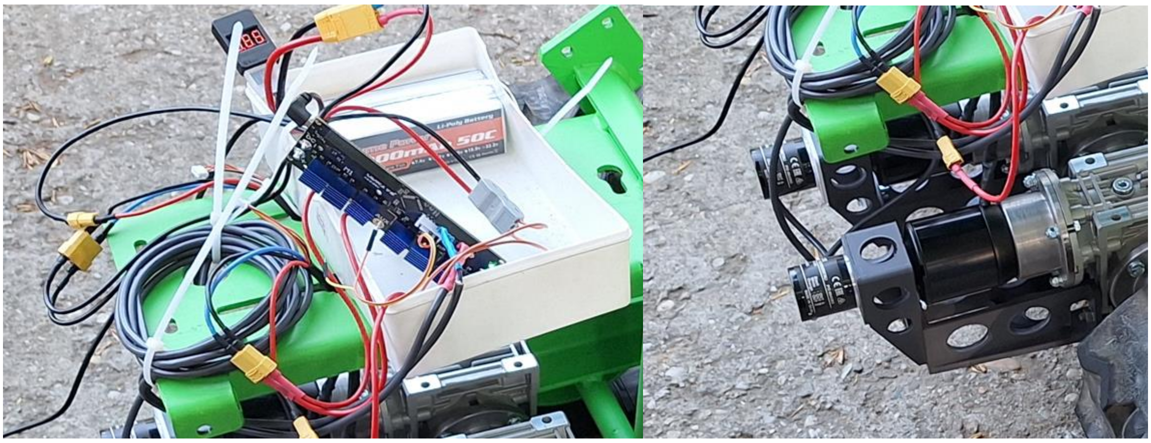

Fig. 5. Command and control module of the electric powered transportation platform

To drive the electric transport platform, Fig. 5, we used the ODrive v3.6 driver [9] which allows: position, speed and current control; Automatic identification of motor parameters (Inductance, Resistance); Real-time USB communication with the Python host program; Information for many variables including position, speed, current, control effort: extensible to expose your own variables. The command and control scheme is shown in Fig 6. For motion control we used YUMO type E6B2 -CWZ3E [13] rotary encoder with 1024P/R resolution.

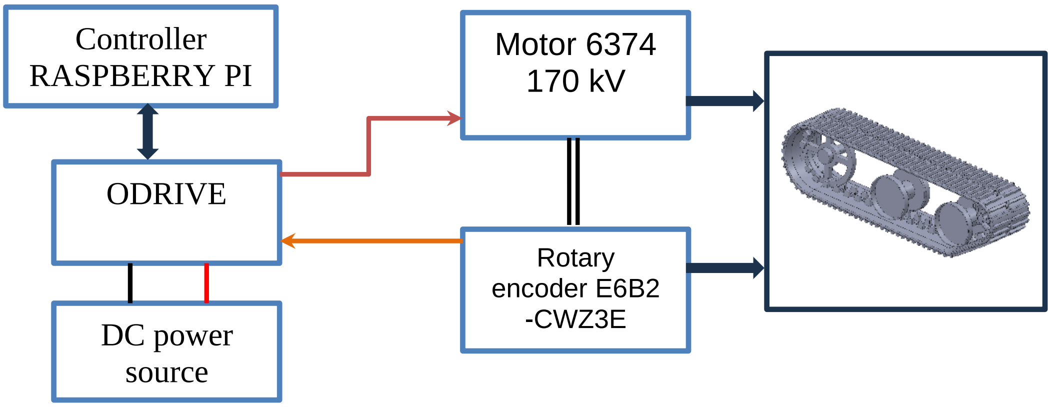

Fig. 6. Command and control scheme of the electric powered transportation platform.

The conversion from a heat engine powered transportation platform to an electric powered transportation platform fulfils the requirements for the travel speed on a construction site of about 1.0m/s as shown in the tests performed and presented in fig. 7.

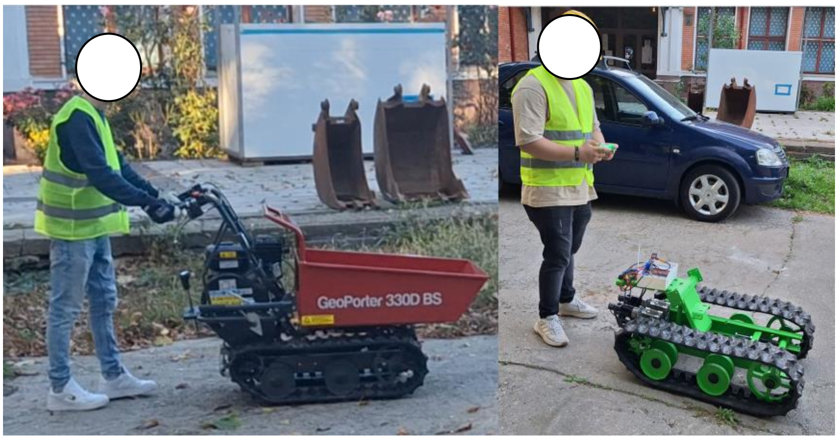

Fig. 7. Conversion of the transportation platform from thermal to electric motor drive

3. Conclusions

The electric platform for small object transportation featured in the article aligns with the future of sustainable construction. By efficiently addressing on-site logistics and minimizing environmental impact, this solution promotes sustainable practices while providing practical benefits in on-site transportation of small objects. With the right design and strategy, this platform could become a standard tool on sustainable construction sites. Electric transportation platforms align with global goals to reduce greenhouse gas emissions; reduce the time and effort required to move small objects, allowing workers to focus on important tasks; use of autonomous platforms help with repetitive tasks and reduce manual handling; reduce the risk of on-site work accidents; electric platforms are particularly well suited for urban construction sites, where noise ordinances often restrict traditional machinery.

Acknowledgements

Thank you SC CONSTRUCTII ERBASU S.A for the transportation platform provided.

References

[1] Loo, Becky P. Y., and Rosana W. M. Wong. "Towards a Conceptual Framework of Using Technology to Support Smart Construction: The Case of Modular Integrated Construction (MiC)." *Buildings* 13, no. 2: (2023): 372. https://doi.org/10.3390/buildings13020372.

[2] Akinsemoyin, Aliu, Ibukun Awolusi, Debaditya Chakraborty, Ahmed Jalil Al-Bayati, and Abiola Akanmu. "Unmanned Aerial Systems and Deep Learning for Safety and Health Activity Monitoring on Construction Sites." *Sensors* 23, no. 15 (2023): 6690. https://doi.org/10.3390/s23156690.

[3] Choi, Wonjun, Seunguk Na, and Seokjae Heo. "Integrating Drone Imagery and AI for Improved Construction Site Management through Building Information Modeling." *Buildings* 14, no. 4 (2024): 1106. https://doi.org/10.3390/buildings14041106.

[4] Harrison, Dan. "Construction Industry Technology Trends in 2024." December 5, 2023. Accessed October 15, 2024. https://olive.app/blog/construction-industry-technology-trends/.

[5] Johnson, Khari. "The Elusive Dream of Fully Autonomous Construction Vehicles." April 16, 2023. Accessed October 15, 2024. https://www.wired.com/story/the-elusive-dream-of-fully-autonomous-construction-vehicles/.

[6] Weston Robot. Accessed October 15, 2024. https://www.westonrobot.com/outdoor-robot-bunker.

[7] Robotnik. "RB-VOGUI, a collaborative robot for outdoor transport in industry." April 6, 2021. Accessed October 15, 2024. https://robotnik.eu/rb-vogui-a-collaborative-robot-for-outdoor-transport-in-industry/

[8] Movex Innovation. Cross-Country 30. Accessed October 15, 2024. https://movexinnovation.com/equipment/all-terrain-carriers/xc-30-cross-country/.

[9] Odriverobotics. Accessed October 15, 2024. https://odriverobotics.com/

[10] Geoporter 330d. Accessed October 15, 2024. https://www.geotech-pro.com/en/prodotti-geotech/geotech-geoporter-330d-power-barrow-300-kg-dumper-truck/.

[11] Briggs & Stratton. Accessed October 15, 2024. https://www.briggsandstratton.com/na/en_us/product-catalog/engines/utility-engines/xr6_5.html.

[12] Odriverobotics 6374. Accessed October 15, 2024 https://eu.odriverobotics.com/shop/odrive-custom-motor-d6374-150kv.

[13] Encoder E6B2. Accessed October 15, 2024. https://www.yumoelectric.com/6mm-24VDC-shaft-incremental-encoder-E6B2-CWZ6C-Rotary-Encoder-pd41603666.html.

ISSN 1454 - 8003
Proceedings of 2024 International Conference on Hydraulics and Pneumatics - HERVEX
November 13-15, Băile Govora, Romania

RECOVERY OF POTENTIALLY TOXIC COMPOUNDS FROM PHOSPHORIC ESTER-BASED HYDRAULIC FLUIDS (HFDR) USED IN THE MINING INDUSTRY

Adriana Mariana BORȘ[1,*], Liliana DUMITRESCU[1], Iuliana GĂGEANU[2], Alina-Iolanda POPESCU[1], Tudor Vasile BLAGA[3,4]

[1] National Institute of Research & Development for Optoelectronics / INOE 2000 – Subsidiary Hydraulics and Pneumatics Research Institute / IHP, Bucharest / Romania

[2] National Institute of Research - Development for Machines and Installations Designed to Agriculture and Food Industry - INMA Bucharest / Romania

[3] Faculty of Materials and Environmental Engineering, Technical University of Cluj-Napoca, 103-105 Muncii Boulevard, 400641 Cluj-Napoca, Romania

[4] National Institute for Research and Development of Isotopic and Molecular Technologies INCDTIM, 67-103 Donath Street, 400293 Cluj-Napoca, Romania

***** bors.ihp@fluidas.ro

Abstract: *The main trends are greater use of piston pumps and a sustained drive for greater power and efficiency. Piston pumps handle high flow rates at high hydraulic system pressures, thus providing optimal efficiency and reliability, while maintaining a compact size with high power density. For hydraulic systems, the main consequences of these trends have been increased operating pressures and temperatures for fluids. In addition to higher pressures and temperatures, fluids are expected to have a longer service life and be more resistant to oxidative and thermal degradation. Frequent recirculation can affect fluid performance, place additional stress on fluids, and shorten their lifespan. Formulations that provided acceptable fluid life and provided effective air release and foam control in the past may no longer achieve the same levels of performance. This is causing fluid developers to respond by developing new formulations that offer better performance under high temperature and pressure conditions. The challenge of increasing performance levels with lower fluid volumes and more rigorous operating conditions has been further complicated as some potential hydraulic fluid components have become unavailable or limited in the use level by changes in legislation. Original equipment manufacturers and end customers are very focused on fluid composition and are sensitive to potential non-fire hazards associated with fluid components.*

Keywords: *HFDR, fire-resistant, hydraulic fluids, phosphoric acid*

1. Introduction

In the mining sector, improving equipment reliability and operational effectiveness means reduced costs for mining. Thus, high-performance lubricants and their optimization can extend the life of lubricated components and therefore the availability of the equipment used. Reduced energy and lubricant consumption also have a positive effect on operating costs. Choosing the right hydraulic oils and corrosion-inhibiting lubricants for wire ropes is an essential but not sufficient step. Improving lubricants developed specifically for this type of industry makes mining safer, more efficient and less expensive. Therefore, the composition of these hydraulic oils is special, which takes into account the harsh working conditions and their potential contaminants that can damage the equipment. Whether it is abrasive contamination, external temperatures or oscillating movements and extremely high loads, the products used in this field have high load capacity and protection against wear, wet or dry conditions, corrosion, or the working temperature regime.
Manufacturers' recommendations for optimal product selection indicate special caution in taking into account operating conditions but also other parameters such as working time, the nature of the lubricants, their composition and especially the process and equipment for which they are used.

ISSN 1454 - 8003
Proceedings of 2024 International Conference on Hydraulics and Pneumatics - HERVEX
November 13-15, Băile Govora, Romania

The latest generation oils, special and specific to this industrial sector, mining, represent a constant challenge for both manufacturers and operators, to ensure the efficiency and reliability of the equipment necessary for the work in the field. In addition to concerns regarding sustainability strategies for energy consumption, CO2 emissions, product life cycle costs, compliance with production standards and requirements, reliability and noise reduction, resistance against external or internal influencing factors, the circularity of used lubricating and industrial oil management has also become an equally important aspect. Therefore, the specifications issued by professional manufacturing companies, hydraulic equipment manufacturers and standardization organizations provide indications on the chemical composition and physical-chemical properties of the type of hydraulic fluid, the applications, specifications and approvals in force, the benefits but also instructions on its management. These represent a way of selection and adaptability to the user's needs.

2. Materials and methods

For mining, the exploitation activity takes place in a wide thermal range (-20_150 ˚C), as such, non-flammable oils are chosen, classified ISO-L-HEES, ISO-L-HFC and ISO-L-HFDU (antioxidant / antirust / antiwear), characterized by reduced viscosity variations in relation to temperature, which ensure adequate lubrication under conditions of high thermo-mechanical stress.

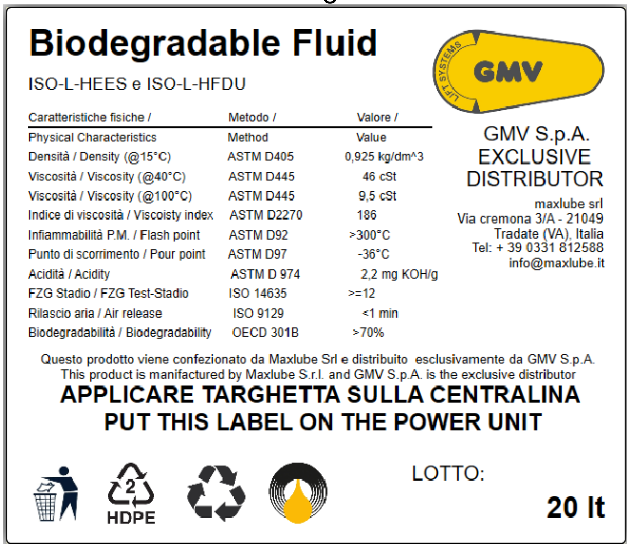

Fig. 1. Technical Data Biodegradable Hydraulic Fluid_GWV

PHYSICAL CHARACTERISTICS	METHOD	VALUE
Density	ASTM D405	0.925 Kg/dm^3
Viscosity at 40˚ C	ASTM D445	40 cSt
Viscosity at 100˚ C	ASTM D445	9,5 cSt
Viscosity index	ASTM D2270	186
Flash point	ASTM D902	>300° C
Pour point	ASTM D97	-36°C
Acidity	ASTM D974	2.2mg KOH/g
FGZ Test-Stadio	ISO 14635	≥ 12
Air release	ISO 9129	<1 min
Biodegradability	OECD 3018	>70%

Fig. 2. The physical characteristics of Biodegradable Hydraulic Fluid_GWV

Fluids with high resistance to ignition and difficult flame propagation are compounds based on phosphoric esters (HFDR), characterized by a density that slows down the response speed of the hydraulic system.
This type of high-performance hydraulic oils are designed to meet the stringent requirements of modern models from original equipment manufacturers. It must also provide protection for mobile and stationary hydraulic pumps with vanes, pistons and gears, servo valves using multi-metallic components, operating in industrial, mining and marine applications, in environmentally sensitive areas, where the impact of hydraulic oil on the environment is a real concern.
The characteristics of these hydraulic oils consist of advanced hydrolytic stability which helps prevent corrosive wear, effective oxidation stability which provides optimal performance throughout the entire operating period, they are formulated to control deposits which helps maintain system accuracy and reliability. These characteristics lead to good productivity, long system life but also low toxicity for the water fractions tested. The main role of hydraulic fluid is to transmit power, lubricate components, reduce friction, prevent corrosion, and dissipate heat.
The demanding requirements regarding machinery and equipment constantly require the fulfillment of specific requests regarding the quality of the hydraulic fluid used, requiring knowledge and experience to identify and properly select a hydraulic fluid.

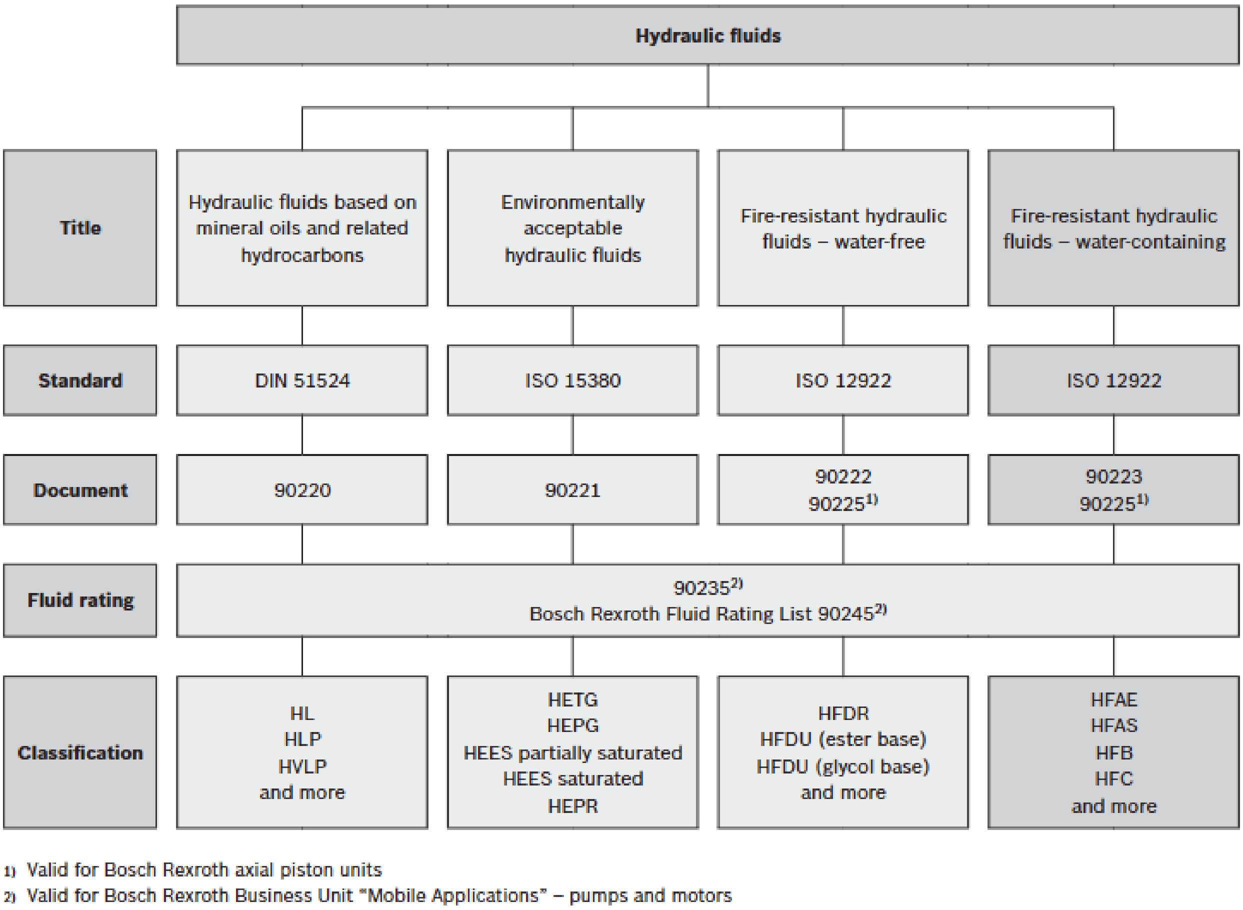

Fig. 3. Classification of hydraulic fluids - RE 90222 Fire-resistant, water-free hydraulic fluids (HFDR/HFDU); Source: Bosch Rexroth AG, RE 90223/01.2015

Water-free, fire-resistant hydraulic fluids hydraulic components are assessed on the basis of their fulfilment of the minimum requirements of ISO 12922. Hydraulic fluid suitability depends, amongst others and the viscosity factor, it being a basic property of hydraulic fluids.

ISSN 1454 - 8003
Proceedings of 2024 International Conference on Hydraulics and Pneumatics - HERVEX
November 13-15, Băile Govora, Romania

The permissible viscosity range of complete systems needs to be determined taking account of the permissible viscosity of all components and it is to be observed for each individual component. The viscosity at operating temperature determines the response characteristics of closed control loops, stability and damping of systems, the efficiency factor and the degree of wear. The optimum operating viscosity range of each component be kept within the permissible temperature range. This usually requires either cooling or heating, or both. If the viscosity of a hydraulic fluid used is above the permitted operating viscosity, this will result in increased hydraulic-mechanical losses. In return, there will be lower internal leakage losses. If the pressure level is lower, lubrication gaps may not be filled up, which can lead to increased wear. For hydraulic pumps, the permitted suction pressure may not be reached, which may lead to cavitation damage. If the viscosity of a hydraulic fluid is below the permitted operating viscosity, increased leakage, wear, susceptibility to contamination and a shorter component life cycle will result. It is required that the permissible temperature and viscosity limits are observed for the respective components.

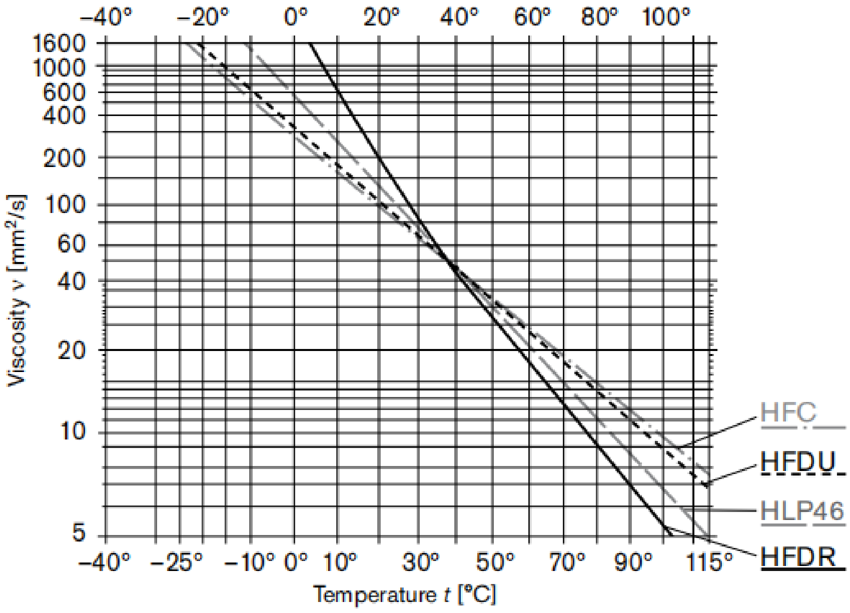

Fig. 4. Diagrams for water-free, fire-resistant hydraulic fluids in comparison to HLP and HFC (reference values, double-logarithmic representation)

Table 1: Hydraulic fluids, the viscosity temperature behaviour (V-T)

Typical viscosity data [mm²/s] at temperature	0 °C	40 °C	100 °C
HFDR	2500	43	5,3
HFDU (ester base)	330	46	9,2
For comparison HLP (see RE 90220)	610	46	7
For comparison HFC (see RE 90223)	280	46	

For hydraulic fluids, the viscosity temperature behaviour (V-T) is of particular importance. The interrelation between viscosity and temperature is described by the viscosity index (VI).

For cold testing over a period of several days, the viscosity of ester-based HFDU can increase greatly. HFDU fluid based on ester have better viscosity/temperature characteristics than mineral oil HLP (Fig. 4).
Ageing resistance is the way a water-free, fire-resistant hydraulic fluid ages depends on the thermal, chemical and mechanical stress to which it is subjected. The influence of water, air, temperature and contamination may be significantly greater than for mineral oils HLP/HVLP. High fluid temperatures (e.g. over 80 °C) result in an approximate halving of the fluid service life for every 10 °C temperature increase and should therefore by avoided. Ageing resistance can be greatly influenced and by the chemical composition of the hydraulic fluids.

3. Results

Phenomena within the lubricant layer have a great influence on lubrication, which increases with the thickness of the lubricant layer. These phenomena involve associations of molecules under the action of existing polar substances, but also through internal friction between molecules.
Thus, viscosity is very important in determining the lubricating capacity of lubricants.
Considering the chemical composition of lubricants based on phosphoric acid esters such as tricresyl phosphate, trioctyl phosphate, or diethyl ester of decanephosphonic acid, as well as polymeric tetrahydrofurans, it is necessary to process used oils, thus facilitating their regeneration and recovery process. By removing impurities and other unwanted substances, treated oils with improved quality are obtained, ready for re-introduction into the industrial circuit or for use as raw material in the petroleum industry. Thus, a wide range of aqueous liquid waste resulting from various industrial activities can be processed. The state-of-the-art facilities used are designed to efficiently manage liquid waste, ensuring the neutralization of toxic substances and minimizing the impact on the environment. The processing of used oils and aqueous waste must comply with the highest environmental and safety standards, to ensure their compliance with regulations in force.
The companies' commitment to innovation, sustainability and efficiency is reflected in every aspect of the services offered, with the companies becoming trusted partners for those who aim to manage waste responsibly and sustainably. In the specialized literature, methods and processes are described regarding concerns for recovering phosphoric acid from waste oils, being used due to its liquid state and easy injection into various equipment used in fields such as mining, agriculture, irrigation, etc. Phosphoric acid can be obtained from phosphates, commonly from apatite $Ca_5(PO_4)_3(F, OH, Cl)$ by reaction with stronger acids (sulfuric acid or nitric acid).
The anhydrous form of phosphoric acid is hygroscopic, and the hydrolysis reaction yields phosphoric acid, the by-products that arise are $CaSO_4$ and hexafluorosilicic acid H_2SiF_6.
These involve treating phosphoric acid with a mixture of at least two extraction solvents at a temperature low enough to form a clear, homogeneous extract. By controlling the temperature, a separation of the phases can be made, namely, the residual aqueous phase and the extract phase into a lower layer containing phosphoric acid and an upper layer containing solvents and separating the lower layer from the upper layer. Solvents are, for example, esters, ketones, glycol ethers and ethers, such as ethyl, butyl and amyl acetate, ethyl butyrate and cyclohexanone.
Stratification is improved by adding a small amount of purified phosphoric acid. The yield is increased by incorporating 1-5% sulfuric acid into the technical grade acid. The residual acid, after separation of the solvent extract, is acidified with sulfuric acid in an amount of 30 to 100% by weight of phosphoric acid and subjected to repeated extraction with a solvent or with a mixture of extraction solvents and a mixture of purified phosphoric and sulfuric acids.
This recovery method, however, contains some phosphoric acid impurities that are difficult to remove. One of the removal processes consists of adding alumina, calcium compounds, activated carbon dioxide, silica, or activated clay before solvent extraction. Calcium hydroxide or some phosphate-type compounds such as phosphate rock can be added to phosphoric acid to neutralize the free sulfuric acid present after treatment for better separation of the extraction phase.
The solvents used are: ethyl ether and n-butyl ether; n-butyl ether and dibutyl ether of ethylene glycol, isopropyl ether and ethyl ether, isopropyl ether and cyclohexanone, ethyl ether and

monohexyl ether of diethylene glycol, mixed mono- and di-n-butyl ethers of diethylene glycol, diethylene glycol dibutyl ether and diisobutyl ketone.
Therefore, a residual fraction from the extraction of phosphoric acid is treated in the first phase with a mixture of n-butyl ether and ethyl ether, then, the extraction phase is acidified with concentrated sulfuric acid and the mixture is extracted with a mixture of isopropyl ether and ethyl ether.
Therefore, the purification of phosphoric acid by extraction can be used in the chemical industry.
Another organic solvent-based phosphoric acid extraction process consists of adding a base of monovalent cations, such as sodium, potassium, ammonium and their derivatives or salts thereof, with phosphoric acid in a molar ratio of the monovalent cation added to the sulfate ion in the phosphoric acid of 0.5-10%. The concentration of phosphoric acid in the aqueous phase is 1.5-10.5 mol/g. The extract is washed with an aqueous solution of the same substances.
The organic solvents used are preferably ketones and ethers, for example, tributyl phosphate in pure form with the addition of a polar diluent. The method makes it possible to perform a more efficient purification of phosphoric acid by removing sulfuric acid from the separation phase. This process, like many other methods, does not have good environmental compatibility.
As such, concerns in this direction have led to another method of recovering phosphoric acid, an environmentally friendly method. This method involves the recovery of phosphoric acid in a humid environment, being a method of purifying phosphoric acid through solvent extraction.
The method targets one or more systems of ketone, ether and ester extraction agents, and the purification process mainly comprises the following steps: sequential extraction, washing and reverse extraction of crude phosphoric acid. The process consists of a pre-emulsification stage of ether solvents and carboxylates, then mixing with mineral oil and its inorganic salt and finally emulsification, homogenization and thinning to obtain the antifoaming agent - the wet medium for phosphoric acid extraction. In the purification process, the residual washing acid and the reverse extraction acid are concentrated before being recycled, so that the residual washing acid and the reverse extraction acid are controlled in relation to the phosphoric acid concentration in the corresponding extraction system. The generated residual wash acid is returned to be mixed with wet process phosphoric acid and concentrated to serve as crude phosphoric acid, and the reverse extraction acid thus generated is partially concentrated and returned to serve as wash acid.
The method is used for extraction systems of ether, ketone and ester extraction agents.
The extraction rate of phosphoric acid can be remarkably increased, the loss of phosphoric acid and the amount of acid phase circulation in the washing process are reduced, and the yield of phosphoric acid is high. The process is simple, easily controllable due to the mild conditions for separation and extraction of phosphoric acid. Production costs and energy consumption are reduced. The process does not pollute the environment, and the product obtained has a low surface tension, with a foam inhibition effect, the performance of obtaining the product is high.
The use of wet media has proven to be suitable not only for the production of phosphoric acid but also for the elimination of acidic medium foam and the inhibition of foam in the spinning, printing and dyeing industries and the like. In the wet process variant, elements such as iron, aluminum and magnesium can also be recovered. These can be expressed as oxides, from phosphoric acid with minimal phosphate losses and dilution to produce a phosphoric acid that is suitable for the production of fertilizer products such as diammonium phosphate (DAP), commercial grade phosphoric acid, superphosphoric acid and other phosphoric acid products using a continuous ion exchange approach. Furthermore, the method allows the use of lower grade phosphate rock or ore in the extraction process, which would considerably expand the potential phosphate rock reserve base for phosphate mining activities and allow for better overall utilization of resources from a given developed mining site. Phosphoric acid, produced from alumina-rich phosphate rocks, is a by-product of phosphate rock mining operations. The rock is finely ground and dispersed in sulfuric acid, and the resulting phosphoric acid contains the metal ions normally present in the treated rock.
The metal ions are then extracted from the acid by ion exchange with a water-immiscible organic sulfonic acid compound, preferably in the presence of an organophosphate or phosphonate.
After phase separation, the organic phase containing the extracted metal ions can be regenerated.

The process is particularly useful when digestion is done at a P_2O_5 concentration and temperature that produces calcium sulfate hemihydrate. By optimizing the process, production efficiency is greatly improved. The wet phosphoric acid production method is a new method of producing phosphoric acid by purifying with wet process phosphoric acid. The P_2O_5 content of wet process phosphoric acid is higher, and phosphoric acid contains a lot of SO_4^{2-} ions.

The P_2O_5 content of the acidosis liquid produced by the decomposition of phosphate ore by sulfuric acid is high. The wet process phosphoric acid and the acidolysis liquid are mixed, so that the P_2O_5 content in the mixed liquid is improved, and the content of calcium ions and sulfate radicals in the mixed liquid is reduced. The new method has a certain promoting effect on the separation of other impurities. According to the new method, mixed desulfurization is used to replace the conventional desulfurization technology with phosphoric ore paste and barium carbonate, so that the single-stage desulfurization rate can reach over 99%. Two different phosphoric acids are mixed so that SO_4^{2-} > and Ca^{2+} generate precipitates of $CaSO_4$ to eliminate SO_4^{2-}.

The optimal decontamination index (W) of the obtained mixed acidic liquid is $w(H_3PO_4)$=10-25%, while $w(SO_4^{2-})$ requires continuous monitoring. The main component of the filter residue is $CaSO_4$, and the purity is high and reaches 99%. The mixed extract for the purification of wet phosphoric acid is a mixture of n-butanol (60-70 vol%), tributyl phosphate (20-30) and methylisopropyl methanone (10-20) with high extraction and impurity removal power.

Purified phosphoric acid can be used to prepare nano-grade silver chloride by adding silver nitrate.

Purified phosphoric acid contains fluorine produced from wet process phosphoric acid which can be divided into two parts, one part is used as returned acid and the other part is used as crude phosphoric acid. This technology involves a device for producing defluorinated phosphoric acid.

The device includes 2 injection pumps, a reaction kettle, a gas-liquid separator and an absorption tower where they are sequentially connected by pipes to form a closed, circulating pipe system that is in a negative pressure state. The 2 injection pumps allow the gas in the system to flow circularly at high speed. The injection pump sucks and mixes the returned acid and sulfuric acid, then sucks a reaction liquid and sulfuric acid into the reaction vessel, where after mixing them with the gas flow, the resulting mixture is sprayed onto the liquid level of the reaction vessel. The vacuum generated by the other injection pump causes the crude phosphoric acid and the low-fluorine hot steam emitted from the reaction vessel to be sucked in and mixed.

The resulting mixture enters the gas-liquid separator, then the gas is sent to the bottom of the absorption tower, and the defluorination waste gas is led from the top of the absorption tower to the injection pump. The washing liquid is sprayed from the top of the absorption tower and the fluosilicic acid liquid is led out through the bottom of the absorption tower. This liquid flows circularly after exiting the separator, being a refined defluorinated product of phosphoric acid.

Fluorine in the form of fluoride is removed from phosphoric acid having an initial phosphate concentration of less than about 47% by determining the concentration of fluorine to be removed from the acid and the concentration of silicon in the acid. Silicon is added to the acid in an amount sufficient for the molar ratio of fluorine to be removed from the acid to silicon to the acid. The acid is concentrated so that the fluoride reacts to fluosilicic acid. By maintaining the indicated concentration ratio of fluorine to be removed and silicon, fouling of the condenser and scrubber components with deposited silica is avoided. Silicon-containing material is added to the phosphoric acid preparation process from phosphoric rocks so that the aluminum content in the wet phosphoric acid process is reduced. When the temperature of the phosphoric acid reaches the reaction temperature of 78-85°C, powdered rock phosphate and silicon-containing material are added to the phosphoric acid simultaneously. Under continuous stirring, the reaction takes place for 5-7 minutes, then concentrated sulfuric acid with a mass fraction of 98% is added and stirred to react sufficiently, and the reaction time is 1-3 hours, then filtration is performed and wet process phosphoric acid is obtained. The method is simple and easy to use, efficient and feasible for the reduction of aluminum ions in the wet phosphoric acid process. Since the discovery of their excellent anti-wear and fire resistance properties, the use of phosphate esters by industry has steadily increased (Figure 5).

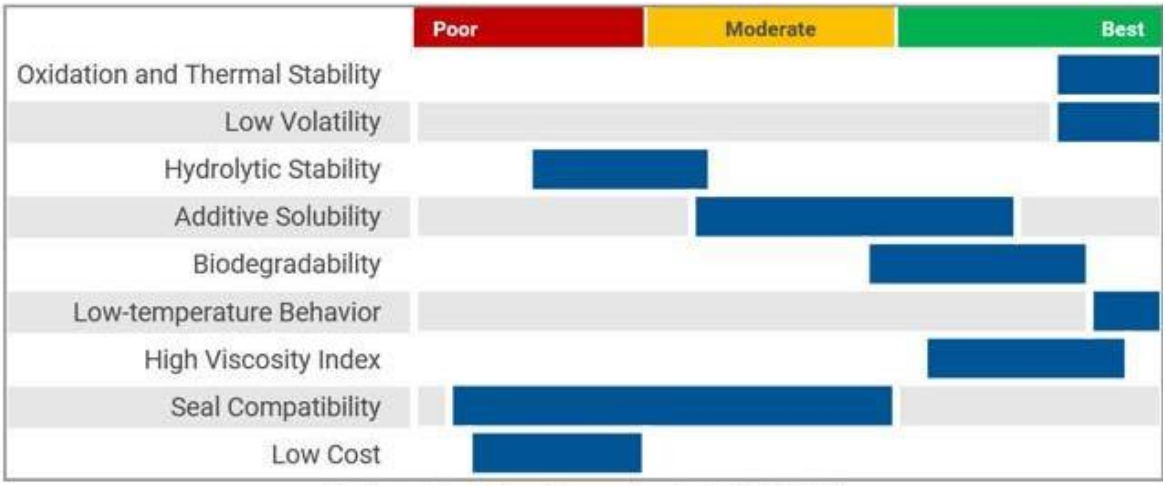

Fig. 5. Benefits and limitations of phosphate ester fluids used in industry

Source- https://www.machinerylubrication.com/Read/2480/benefits-limitations-of-phosphate-ester-fluids

Phosphate esters are primarily used as fire-resistant base materials in several applications, especially in hydraulic systems, turbines and compressors. Phosphate esters are the most fire-resistant of the non-aqueous synthetic base materials. Numerous organic phosphorus compounds, including phosphites, phosphonates, and phosphates, have found applications as additives in a variety of lubricant formulations as stabilizers, anti-wear additives, antioxidants, metal passivated, and extreme pressure additives. Only one group of phosphates, the natural trisubstituted esters of H_3PO_4, has found significant use as a synthetic base. The use of phosphoric ester-based products in hydraulic applications is still primarily dictated by fire risk considerations. Although inhibited phosphate esters possess excellent oxidation stability and inherently good anti-wear properties under critical loading conditions, they suffer from somewhat inferior hydrolytic stability.
As such, there are concerns regarding this aspect and others such as optimizing the viscosity index and reducing chemical aggressiveness compared to some conventional sealing and coating materials. These points still limit the use of phosphate ester to specialized applications where a high degree of fire resistance is required.

4. Conclusions

The paper aims to describe methods for chemical stabilization and reprocessing of residual materials from hydraulic oils used in mechanical management processes (recovery, transport and processing) of the tailings of an ore deposit using efficient technologies in order to reduce the concentration and toxicity of their composite elements. The possibility of recovering and treating phosphoric acid from hydraulic oils for use as a raw material in other processes represents a way to capitalize on them. The method described in this paper represents a new method for producing phosphoric acid by purification with wet process phosphoric acid.
The method makes it possible to perform a more efficient purification of phosphoric acid by removing sulfuric acid from the separation phase. The new method has a certain promoting effect on the separation of other impurities as well. According to the new method, the mixed desulfurization rate in a single stage can reach over 99%. The method is simple and easy to use, effective and feasible for reducing potentially toxic elements in the wet phosphoric acid process.

Acknowledgments

The work was carried out through the Core Program within the National Research Development and Innovation Plan 2022-2027, carried out with the support of the Romanian Ministry of Research, Innovation and Digitalization (MCID), project no. PN 23 05.

References

[1] European Safety and Health Commission for the Mining and Other Extractive Industries. “Requirements and Tests Applicable to Fire-Resistant Hydraulic Fluids Used for Power Transmission and Control (Hydrostatic and Hydrokinetic).” Document No. 4746/10/91 EN, European Safety and Health Commission for the Mining and Other Extractive Industries, Luxembourg, April 1994.
[2] ISO 12922:1999. “Lubricants, Industrial Oils and Related Products (Class L)—Family H (Hydraulic Systems)—Specifications for Categories HFAE, HFAS, HFB, HFC, HFDR and HFDU”.
[3] ISO 6743-4:1999. “Lubricants, Industrial Oils and Related Products (Class L)—Classification—Part 4: Family H (Hydraulic systems)”.
[4] ISO 3448:1992. “Industrial Liquid Lubricants—ISO Viscosity Classification”.
[5] RAG N 762 010. “Requirements for Fire-Resistant Hydraulic Fluid”.
[6] CETOP RP 66H. “Wick Test for Fire Resistant Fluid,” European Committee for Oils, Hydraulics and Pneumatics, Europe.
[7] ISO 15029-2:2007. “Determination of Spray Ignition Characteristics of Fire-Resistant Fluids—Part 2: Stabilized Flame Heat Release Method”.
[8] OECD 418, 2002. “OECD Guidelines for Testing of Chemicals”.
[9] ISO 3104:1994. “Transparent and Opaque Liquids; Determination of Kinematic Viscosity and Calculation of Dynamic Viscosity.
[10] ASTM D445-06, 2006”. “Standard Test Method for Kinematic Viscosity of Transparent and Opaque Liquids (and Calculation of Dynamic Viscosity)”.
[11] CETOP RP 112 H. “Fluids for Hydraulic Transmission—Mineral Oils Category HV Method for Determination of Shear Stability,” European Committee for Oils, Hydraulics and Pneumatics, Europe.
[12] DIN 51346. “Determination of the Emulsion Stability of Fire-Resistant Hydraulic Fluids Containing Water”.
[13] DIN 51587. “Testing of Lubricants; Determination of the Aging Behavior of Steam Turbine Oils and Hydraulic Oils Containing Additives”.
[14] ASTM D943-04a, 2004. “Standard Test Method for Oxidation Characteristics of Inhibited Mineral Oils.” Annual Book of ASTM Standards, Vol. 05.01, West Conshohocken, PA.
[15] DIN 51566. “Testing of Lubricants; Determination of Foaming Characteristics”.
[16] ASTM D 892-06e, 2006. “Standard Test Method for Foaming Characteristics of Lubricating Oils.” Annual Book of ASTM Standards, Vol. 05.01, West Conshohocken, PA.
[17] DIN 51381. “Testing of Lubricants and Hydraulic Fluids; Determination of Air Release Properties”.
[18] CETOP R 81H. “Compatibility of Hydraulic Fluids with Elastomeric Materials.” European Committee for Oils, Hydraulics and Pneumatics, Europe.
[19] ISO 6072:2002. “Hydraulic Fluid Power—Compatibility of Hydraulic Fluids with Elastomeric Materials”.
[20] ASTM D1744-92, 1992. “Test Method for Determination of Water in Liquid Petroleum Products by Karl Fischer Reagent.” Annual Book of ASTM Standards, ASTM International, West Conshohocken, PA.
[21] CETOP R 48H. “Method for the Evaluation of the Anti-Corrosive Properties of Water Based Hydraulic Fluids.” European Committee for Oils, Hydraulics and Pneumatics, Europe.
[22] DIN 51350/3. “Testing of Lubricants by the Shell Four-Ball Tester”.
[23] DIN 51389. “Determination of Lubricants; Mechanical Testing of Hydraulic Fluids in the Vane Cell Pump”.
[24] DIN 51354/2. “Testing of Lubricants; FZG Gear Test Rig; Method A/B, 3/90 for Lubricating Oils”.
[25] AFNOR E 48692. “Transmission Hydrauliques—Fluides—Mesure de la Filtrabilite des Fluides Difficilement Inflammables de Classes HFC et HFD”.
[26] AFNOR E 48-693. “Determination of the Compatibility of Fluids of the Same Type”.
[27] OECD 301C. “Ready Biodegradability: Modified MITI Test (I)”.
[28] OECD 305A-E. “Bioconcentration: Flow-Through Fish Test”.
[29] ISO/DIS 7745:2010. “Hydraulic Fluid Power—Fire-Resistant Fluids—Requirements and Guidelines for Use”.
[30] Rexroth A7VO28DRS (340 bar) and A8VO55DR (320 bar) combined pump test, 65–70°C, 100 hr.
[31] GMW S.p.A. “Biodegradable Fluid - ISO-L-HFDU - ISO-L-HEES”. Technical data biodegradable hydraulic fluid. Accessed October 16, 2024. https://docs.gmv.it/wp-content/uploads/simple-file-list/MULTILINGUE-FLUITRONIC-MULTILINGUAL-FLUITRONIC/ENGLISH/02b-UK-TECHNICAL-CATALOG/02-COMPONENT-SELECTION/04-VARIOUS/03-Biodegradable-Fluid-02_070-00-EN.pdf.
[32] Condur, Cosmin. “Classification of hydraulic oils. Quality specifications / Clasificarea uleiurilor hidraulice. Specificatii de calitate”. *ETIS S.R.L. website*, December 7, 2023. Accessed October 16, 2024. https://etis.ro/clasificarea-uleiurilor-hidraulice-specificatii-de-calitate/.
[33] CONEX. “Organic chemicals. CN8 / NC8 - 2023 - RO / Produse chimice organice. CN8 / NC8 - 2023 - RO”. Accessed October 17, 2024. https://www.conex.net/nc8/2023/ro/29.html.

[34] Shell plc. “Fire-resistant fluids in the metals sector”. White Paper, 2021. Accessed October 16, 2024. https://www.shell.com/business-customers/lubricants-for-business/products/shell-fire-resistant-hydraulics/_jcr_content/root/main/section/promo_copy/links/item0.stream/1686852803443/bbc96f4d59c3950ed0984f98114d1802aac09ee0/metals-fire-resistant-hydraulic-fluids.pdf.
[35] ISO 12922:2020. “Lubricants, industrial oils and related products (class L) — Family H (hydraulic systems) — Specifications for hydraulic fluids in categories HFAE, HFAS, HFB, HFC, HFDR and HFDU”.
[36] DIN ISO 15380:2020. “Lubricants, Industrial Oils and Related Products (Class L)—Family H (Hydraulic Systems)—Requirements for Categories HETG, HEPG, HEES and HEPR / Schmierstoffe, Industrieöle und Verwandte Produkte (Klasse L)—Familie H (Hydraulische Systeme)—Anforderungen für die Kategorien HETG, HEPG, HEES und HEPR”.
[37] Deutscher FSC-Standard Version 3-0: 2018.
[38] Deuster, S., and K. Schmitz. “Experimental Investigation of the Influence of Fluid Viscosity on the Efficiency of a Crawler Excavator.” Paper presented at 17th Scandinavian International Conference on Fluid Power SICFP'21, Linköping, Sweden, June 1-2, 2021.
[39] Theissen, H. “The German Market Introduction Program for Biobased Lubricants.” *Tribology Online* 5, no. 5 (2010): 225-229.
[40] DS 7-98 Hydraulic Fluids (Data Sheet), 2021. Accessed October 17, 2024. https://www.fm.com/FMAApi/data/ApprovalStandardsDownload?itemId=%7BA40610ED-2D5B-4490-A7AA-9BAC00D228D0%7D&isGated=true.

ISSN 1454 - 8003
Proceedings of 2024 International Conference on Hydraulics and Pneumatics - HERVEX
November 13-15, Băile Govora, Romania

PRELIMINARY STEPS FOR INVESTIGATING THE AIR PRESSURE INSIDE THE TYRE

Gabriel SOFRONE[1,*], Gabriel ANGHELACHE[1], Severus OLTEANU[2]

[1] National University of Science and Technology Politehnica Bucharest, Faculty of Transport

[2] National University of Science and Technology Politehnica Bucharest, Faculty of Automatic Control and Computer Science

* sofrone.gabriel@yahoo.com

Abstract: *This scientific paper presents a series of initial steps for measuring the air pressure inside the tyre. Two pressure transducers are selected for the system and presented in the paper. One of the main objectives is to verify the calibration of the transducers and confirm that they can be used for the pressure measurements. Another objective is to develop a system attached to the wheel that includes the two transducers. For the verification of the transducers' calibration, a pressure calibration rig was built, and several pressure measurements were done with the transducers connected to a pressurized enclosure. Initially, the relative errors for both transducers were significant. By repeatedly adjusting the value of the transducers' sensibilities, the errors could be lowered to acceptable values. Both measuring characteristics are quasi-linear with very small linearity errors. The paper shows that, although the measuring characteristics differ from the ones specified by the manufacturer, the transducers can be used for the proposed system. For the measuring system attached to the wheel, two modules have been developed, a central module attached to the wheel disk with bolts, and another module that will be placed inside the tyre, glued on the surface of the wheel rim. The support components for both modules were manufactured using 3D printing with a thermoplastic material (PLA).*

Keywords: *Tyre, air pressure, pressure measurement*

1. Introduction

Inner tyre pressure is a very important functional parameter of the tyre. It influences vehicle handling, fuel consumption, traction and braking performance and tyre life. In general, a low interior pressure can lead to tyre overheating. In cases of very low pressure, great deformations of tread and sidewall can appear, which lead to tyre damage [1]. Also, the pressure variation from the manufacturer's recommended pressure has a great impact on tyre life [2]. In addition, inner tyre pressure influences the rolling radius of the tyre, a fundamental parameter for vehicle dynamics. In most cases, the rolling radius is an input parameter based on formulas that do not take into consideration inner tyre pressure [3].

The study of air pressure variation inside the tyre is rarely mentioned in literature. In general, inner tyre pressure is considered constant, a value characteristic to the tyre, usually adopted or measured when the tyre is cold. An experimental way for using tyre pressure as a parameter is setting the tyre pressure at a certain value, stopping the experiment, and then readjusting the pressure after a period of tyre rolling. Paper [4] describes this method. However, there is no mention of the pressure variation between the two states of the tyre (cold tyre / warm tyre). Also, stopping the experiment for measuring may induce errors.

Another way of measuring inner tyre pressure is using a "dynamic tyre pressure sensor" [5]. The method uses a transducer mounted to the wheel, as close as possible to the wheel rotation axis. The pressure reaches the transducer via a hose connected to the tyre valve. The electrical connection between the transducer (mounted at the wheel) and the electrical transmission system (mounted in the vehicle) is achieved with a series of slip rings. This allows measurements during tyre rolling to be performed. However, the authors do not use the system for precisely measuring air pressure, only for pressure monitoring, and do not provide data for the pressure values used.

Also, the system can have large measurement errors due to the introduction of electrical noise by the sliding contact rings, making it unsuitable for accurate measurements.
“Tyre pressure monitoring system” (TPMS) is a widely used system that presents a series of versions which could be used for measuring the air pressure inside the tyre. A miniature sensor placed on the inside of the wheel rim measures the pressure and converts it into an electrical signal wirelessly sent to the car's on-board computer. Unfortunately, review of the literature showed that the system has insufficient resolution (8.3 kPa [6]) and accuracy (±7 kPa [7]).
Since the rolling radius is directly influenced by the pressure, which changes during the running of the vehicle, the pressure must be known accurately at each moment of the tyre running. Thus, one of the objectives of the paper is to develop a system attached to the wheel for measuring the pressure inside the tyre, which can be mounted on any wheel of the vehicle. The system should include two low-cost pressure transducers. Also, another objective is to verify the calibration of the included transducers and confirm they can be used for the measuring system.

2. Pressure transducers

Two transducers from NXP have been chosen for the development of the tyre air pressure measuring system: MPX5500DP and MPXH6400A. The MPX5500DP transducer is a small sized, general purpose, differential pressure transducer. The MPXH6400A transducer has a very small size and measures absolute pressure. A third transducer, the Turck PT040R pressure transducer, which is in the equipment of the Vehicle Testing Laboratory of the Department of Road Vehicles, Faculty of Transport, will also be used for the calibration check of the two chosen transducers. It was chosen as the reference transducer in the calibration process of the other two transducers. Figure 1 shows the three transducers and Table 1 shows the main parameters of interest for the chosen transducers.

Table 1: Main parameters for the chosen transducers [8,9,10]

Transducer	Relative Pressure Range [kPa]	Supply Voltage [V]	Output Voltage [V]	Sensitivity [mV/kPa]	Accuracy [%]	Price [€]
MPX5500DP	0 ÷ 500	5 ± 0.25	0.2 ÷ 4.7	9	± 2.5	18
MPXH6400A	0 ÷ 300	5 ± 0.36	0 ÷ 4.8	12.1	± 1.5	17.5
PT040R	0 ÷ 4000	11.4 ÷ 33	0 ÷ 10	2.5	± 0.3	–

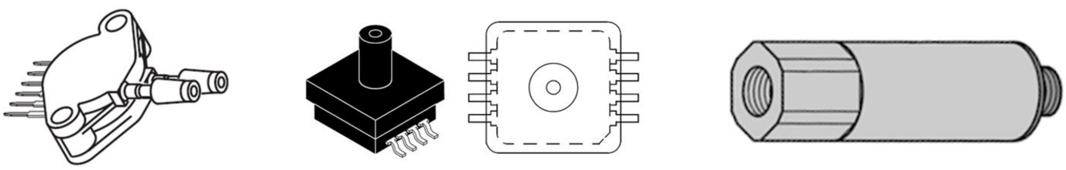

Fig. 1. Chosen pressure transducers [8,9,10]

When analysing the pressure ranges of the transducers, the MPX5500DP transducer has a pressure range suitable for the proposed application. Transducer MPXH6400A shows a maximum pressure of 300 kPa, lower than the previous transducer, but still usable for measuring the air pressure inside car tyres. The PT040R transducer has a maximum measurable pressure well above the measurement requirements of the proposed application.

3. Pressure calibration rig

To build the pressure calibration rig, a pressure enclosure was required. The enclosure should have at least two transducers connected at the same time. The measurements to check the calibration of the transducers were carried out in the Vehicle Testing Laboratory of the Road Vehicles Department. At the start of the rig development, the enclosure equipped with a pressure gauge already existed in the Department. It was modified to allow the transducers to be coupled. Only two of the five pressure outlets were used. A digital oscilloscope was used to visualize the transducer signals.

Figure 2 shows the block diagram of the rig. Particularly, the image presents the calibration of the MPX5500DP transducer. The main components of the rig are: 1 – pressure enclosure (common ramp) with five outlets and valve, 2 – plug, 3 – pressure source, 4 – pressure gauge, 5 – PT040R pressure transducer (T1), 6 – pressure transducer to be verified (T2), 7 – 24 V voltage source, 8 – 9 V voltage source, 9 – voltage step down module, 10 – Fluke 125 two-channel digital oscilloscope with internal memory. Figure 3 presents the calibration rig.

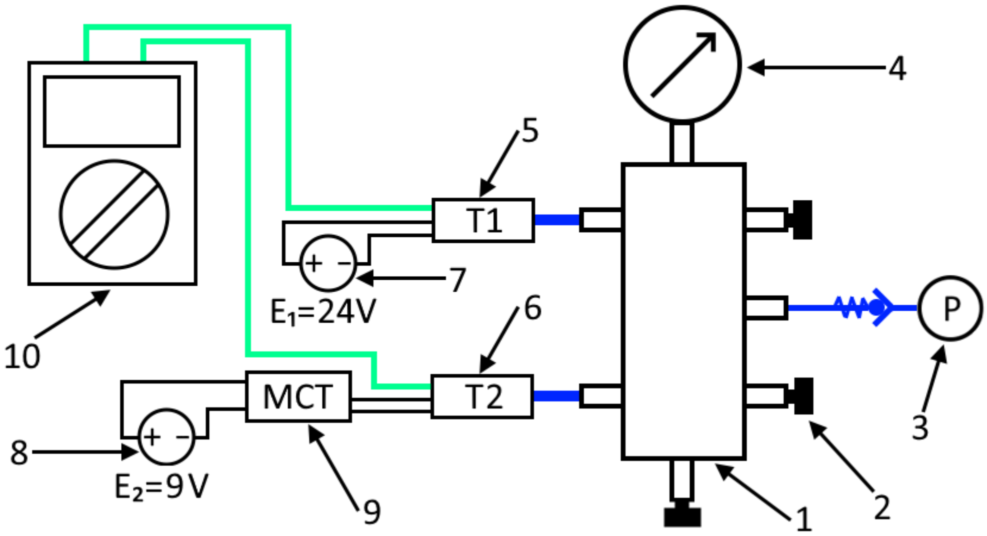

Fig. 2. Block diagram of the pressure calibration rig

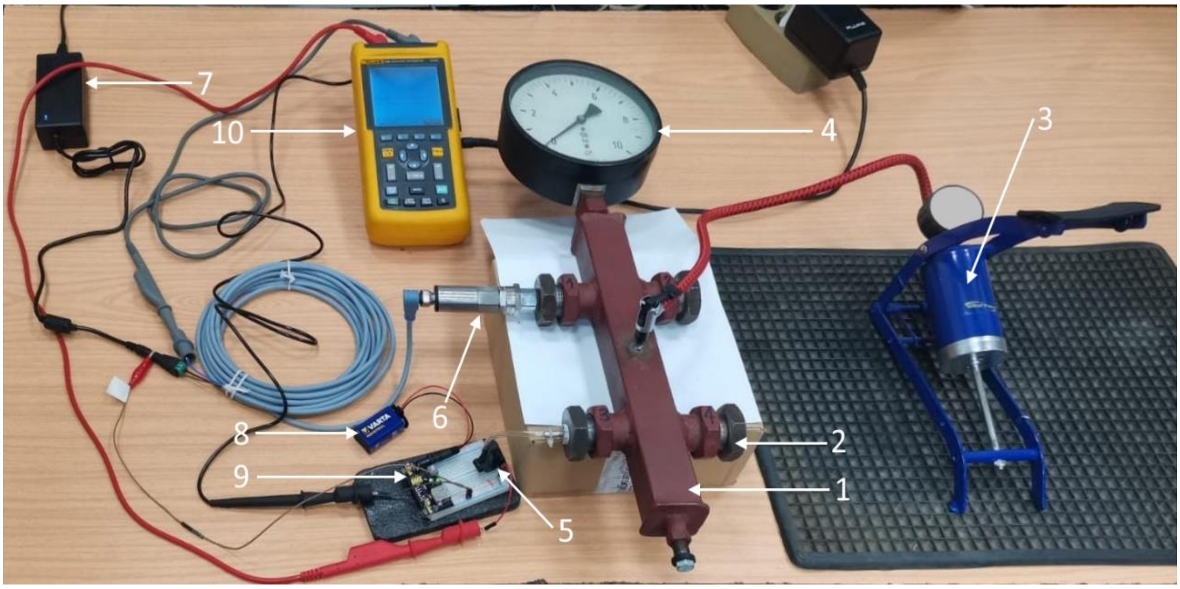

Fig. 3. Pressure calibration rig

First the calibration check of the MPX5500DP transducer was performed, then it was removed from the installation. The transducer MPXH6400A was connected and then its calibration check was performed.

The pressure source is a manually operated pump. It is connected to the enclosure's valve. The PT040R transducer is simply powered, directly from a 24V DC source. The power supply of the transducer to be verified cannot come directly from the 9V supply, as the supply voltage of the transducer is 5V maximum. Thus, a voltage step-down module is required, which supplied the MPX5500DP transducer with a voltage of 5V. The digital oscilloscope has two input channels, corresponding to the outputs of the two transducers.
For the MPX5500DP transducer, five sets of measurements were taken, ascending and descending pressure, in the range of 0 kPa to 400 kPa (relative pressure), with a 40 kPa interval between the measured values. Additionally, measurements were taken at 100 kPa and 300 kPa respectively. The pressure was read with the gauge and later verified with the readings from PT040R transducer. In the case of the MPXH6400A transducer, six sets of descending pressure measurements were performed, in the range of 100 ÷ 300 kPa with an interval between measured values of 25 kPa. For the ascending pressure measurements, the pressure was gradually increased to the desired value, then the pressure was allowed to stabilize and the two voltages were read. A similar procedure was followed for descending pressure measurements. The decrease in pressure was achieved by disconnecting the pressure source and repeatedly operating the valve.

3. Calibration results for MPX5500DP transducer

For each of the five measurements, the pressure is calculated from the obtained voltage. From this pressure, the relative error in relation to the pressure indicated by the gauge is calculated, expressed in percent. It has been observed that the relative errors obtained for the MPX5500DP transducer are very high, both in the ascending and descending measurements. The first set of ascending measurements shows relative errors in the range of 18.4 % ÷ 21.9 %. However, the variation of the relative error is not very large, with an average value of 19.9 % in the ascending measurement and 16.5 % in the descending measurement. The fact that the relative error does not show a very large variation suggests the existence of a slope error.
For the calculation of pressure, the manufacturer's sensitivity (9 mV/kPa) was used. Slope error correction involves determining the sensitivity of the transducer so that the errors become as small as possible. Through repeated attempts, the following sensitivity values were obtained for the first set of measurements: 7.28 mV/kPa (ascending), 7.37 mV/kPa (descending).

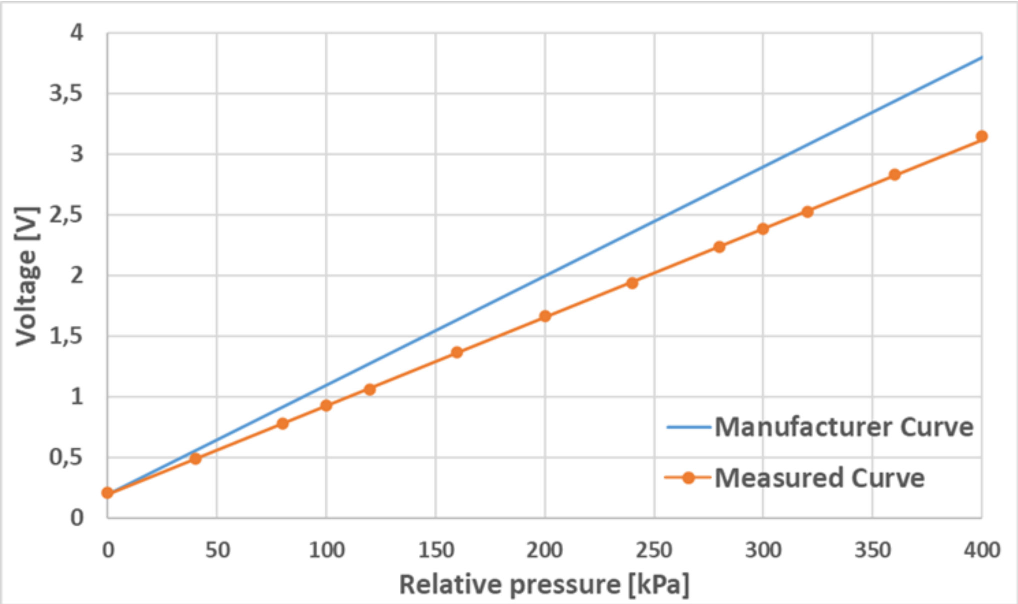

Fig. 4. Comparison between manufacturer curve and measured curve from set no.1 ascending

The overall average value of sensitivity (ascending and descending) is 7,39 mV/kPa. In this way, the MPX5500DP transducer shows very small error values in the range -0.9 ÷ 3.5%, with most of the errors being close to 1%.
For the offset of the MPX5500DP transducer expressed in voltage, an average value of 0.210 V and a range of 0.209 V ÷ 0.213 V was obtained, values close to the offset specified by the manufacturer (0.2 V).
Figure 4 shows the comparison between the characteristic obtained with the first set of measurements (the measured curve) and the characteristic provided by the manufacturer. The measured curve is quasi-linear with a very small linearity error. The figure highlights the large difference between the two characteristics, which mostly comes from the difference between the two measurement sensitivities (manufacturer and experimental).

4. Calibration results for MPXH6400A transducer

In the case of the MPX5500DP, the measurements were made in parallel with the Turck PT040R. The measurement errors of the PT040R were found to be comparable to those of the MPXH5500DP. Therefore, it was decided to verify the calibration of the MPXH6400A transducer in parallel with the MPX5500DP.
The pressure range of the MPXH6400A transducer is 0 ÷ 400 kPa, but it measures absolute pressure. Thus, at atmospheric pressure, the relative pressure value of 0 displayed by the gauge will actually represent a pressure of about 100 kPa in absolute pressure. For this reason, the pressure of 300 kPa, relative pressure at atmospheric pressure, cannot be exceeded.
From the analysis of the relative error values for the MPXH6400A transducer, the second set of measurements shows relative errors in the range of -6.2 % ÷ -4.6 %, a small error variance suggesting the existence of a slope error. To correct this error, it is necessary to determine the sensitivity of the transducer so that the errors become as small as possible. By analysing the values of all 6 sets of measurements, the actual value of the transducer sensitivity (12,75 mV/kPa) is determined. With this value the transducer pressure indications and relative errors are recalculated. The obtained pressure values are much closer to the reference values, and absolute relative errors drop below ±1% (-0.9 % ÷ 0.7 % for set two).

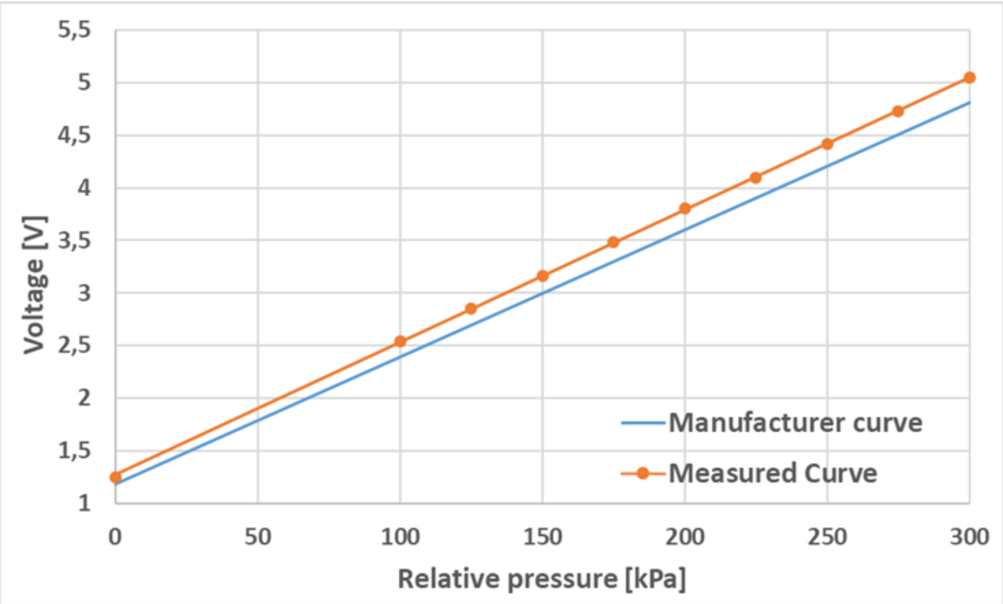

Fig. 5. Comparison between manufacturer curve and measured curve from set no.2

Figure 5 shows the comparison between the characteristic obtained with the second set of measurements and the characteristic provided by the manufacturer. For the MPXH6400A transducer there is a higher similarity of the two characteristics (very close values of transducer sensitivity and offset). However, even in this case it can be observed that at 300 kPa relative pressure, the transducer provides a voltage output signal over 5 V, above the 4.8 V limit indicated by the manufacturer.

5. Design of measuring system attached to the wheel

To be able to take measurements of the air pressure inside the tyre, it is necessary to develop a system attached to the vehicle wheel that includes the two pressure transducers detailed above and a voltage source. Since the indication of the MPXH6400A transducer changes as the supply voltage changes, it is very important that the supply voltage remains constant at 5V. This requires a voltage regulator.
The moment of inertia of the wheel should not be affected or should be kept as low as possible. Also, centrifugal forces should be limited as much as possible. This ensures the structural integrity of the assembly. With these two considerations in mind, it was decided to place the MPXH6400A pressure transducer on the inner surface of the wheel rim inside the tyre and place the other components in the centre of the wheel.
The mass of the assembly is also very important. The constructive solution for the supporting parts of the assembly components is 3D printing. In this way, it is possible to ensure adequate structural rigidity of the assembly and to reduce its mass. The assembly will be attached to the wheel by means of additional holes in the wheel disk.
To acquire the data from the two pressure transducers, it was decided to use a Raspberry Pi Pico W development board, which has an integrated Wi-Fi transmission module. Using this, the data will be transmitted to a second RaspberryPi board connected to a computer.
A pack of four AAA (R3) batteries is chosen for the power supply. Batteries have a voltage of 1.5 V at 100% state of charge, so a voltage of about 6 V will be obtained. The voltage delivered by the battery pack will be stabilized via the voltage regulator to a value of 5 V.
The measuring system will have two main modules. One module will be mounted in the centre of the wheel and the other module will be positioned on the inner surface of the wheel rim inside the tyre. Figure 6 shows the basic layout for the positioning of the two modules.

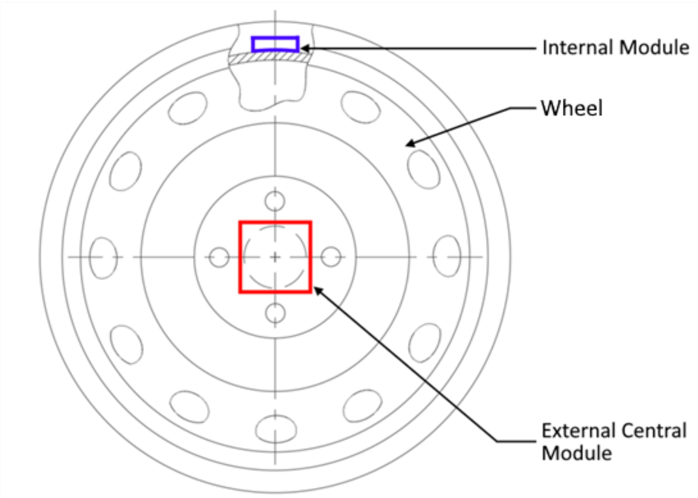

Fig. 6. Basic layout for positioning of the two modules

Figure 7 shows the functional schematic of the external central module assembly. The module base is mounted on the wheel disk's surface to support all necessary components of the module. The module has two 'stages'. The Pressure Transducer MPX5500DP is placed in the space between the outer surface of the disk and the inner surface of the base and will be bolted in place. The Rasbperry Pi board assembly is mounted to the base also by screws. For the voltage source a special socket is made in the lid of the module, where it is tightly inserted. Also, the voltage regulator is glued to the inner surface of the cover. Together with the two components the cover is attached to the module support by screws. Figure 8 presents the developed external central module.

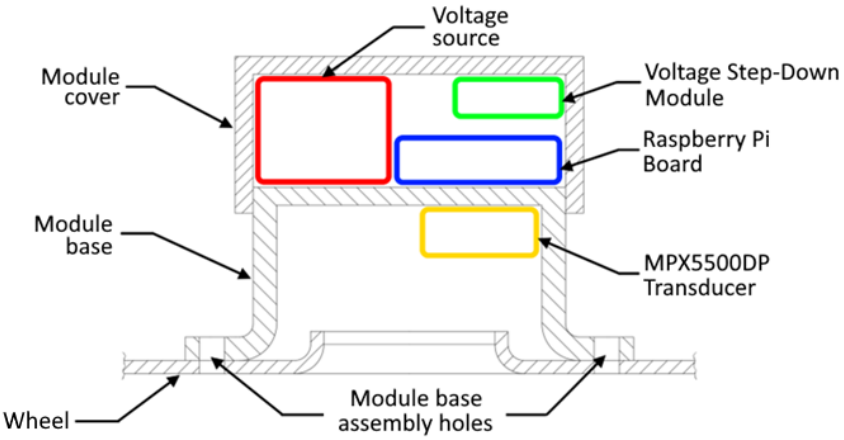

Fig. 7. External central module layout

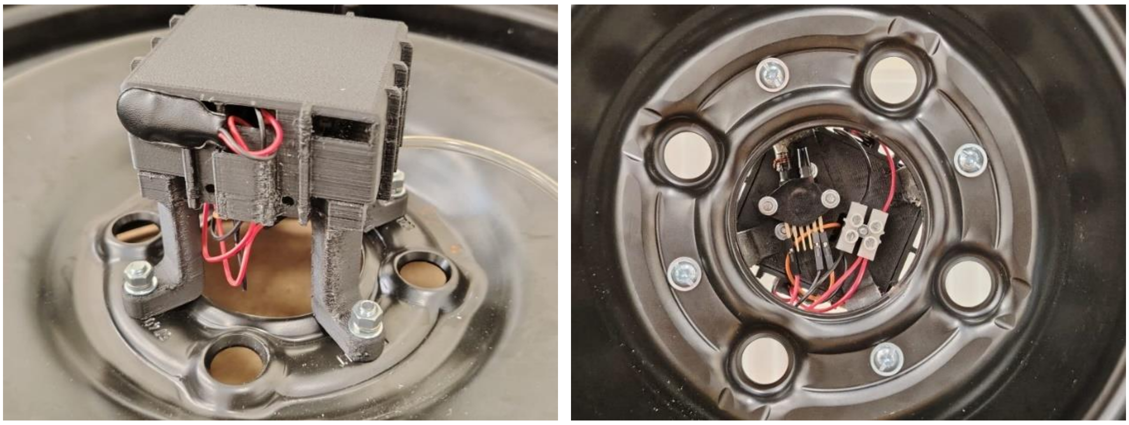

Fig. 8. External central module

Figure 9 shows the internal module assembly. On the inner surface of the wheel rim a base will be glued to support a board on which the MPXH6400A transducer will be placed. The module cover, which is assembled by means of screws, is placed over the board. At least one hole needs to be drilled in the module cover so that the transducer can measure the pressure.

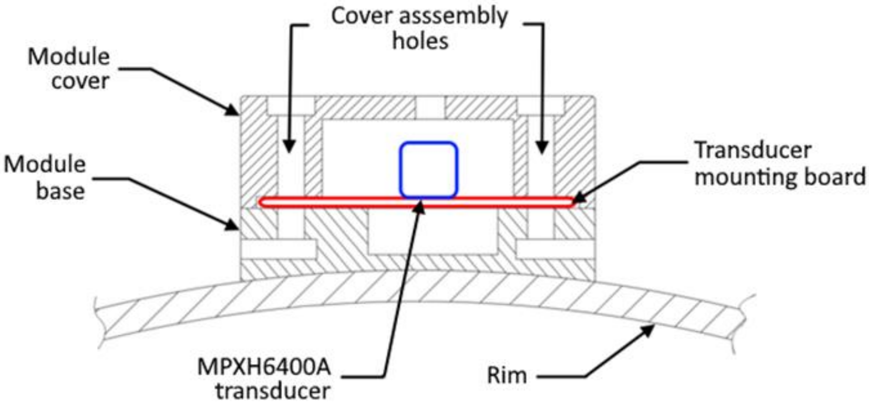

Fig. 9. Internal module layout

6. Conclusions

The selected transducers can be easily used for the given application, considering the real pressure characteristics. For the MPX5500DP transducer, there is a large difference between the two slopes of the characteristics, which shows a big difference between the actual sensitivity of the transducer and the one specified by the manufacturer.
For the MPXH6400A transducer, there is a higher similarity of the two characteristics (very close values of transducer sensitivity, small offset error). However, the transducer cannot measure above 300 kPa (relative pressure).
The measuring system attached to the wheel successfully includes all the necessary components for measuring air pressure inside the tire. It can be observed that both modules are compact, small and low mass. However, it is necessary to study the impact that the two modules have on the wheel and then to restore its dynamic balance.
A further direction of research is the influence of the position of the voltage regulator above the Raspberry Pi board. It is possible that the module and its wires create parasitic electromagnetic fields that interfere with the RaspberryPi board and its Wi-Fi module.

References

[1] Velupillai, Sankaranarayanan, and Levent Guvenc. "Tire pressure monitoring [applications of control]." *IEEE Control Systems Magazine* 27, no. 6 (December 2007): 22-25.
[2] Caban, Jacek, Paweł Droździel, Dalibor Barta, and Štefan Liščák. "Vehicle tire pressure monitoring systems." *Diagnostyka* 15, no. 3 (2014): 11-14.
[3] Jazar, Reza N. *Vehicle Dynamics: Theory and Applications*. Berlin/Heidelberg, Springer, 2008.
[4] Anghelache, Gabriel, and Raluca Moisescu. "The measurement of dynamic radii for passenger car tyre." *IOP Conference Series: Materials Science and Engineering* 252, no. (2017): 012014.
[5] Zhao, Yubo, and Ming L. Wang. "Measurement through dynamic tire pressure sensor inside the tire." *Airfield and Highway Pavements* (June 2015): 282-293.
[6] Sharma, Anil, and Jawar Singh. "Design and analysis of high performance MEMS capacitive pressure sensor for TPMS." Paper presented at the 2013 International Conference on Control, Automation, Robotics and Embedded Systems (CARE), Jabalpur, India, December 16-18, 2013.
[7] Kubba, Ali E., and Kyle Jiang. "A comprehensive study on technologies of tyre monitoring systems and possible energy solutions." *Sensors* 14, no. 6 (June 2014): 10306-10345.
[8] NXP Semiconductors. MPX5500 Series Datasheet, September 2009. Accessed December 2, 2024. https://www.nxp.com/docs/en/data-sheet/MPX5500.pdf.
[9] NXP Semiconductors. MPXH6400A Datasheet, March 2017. Accessed December 2, 2024. https://www.nxp.com/docs/en/data-sheet/MPXH6400A.pdf.
[10] Turck Industrial Automation. PT040R Datasheet, April 2014. Accessed December 2, 2024. https://plc-trade.com/pub/544998/edb-6831490-gbr-en.pdf.

ISSN 1454 - 8003
Proceedings of 2024 International Conference on Hydraulics and Pneumatics - HERVEX
November 13-15, Băile Govora, Romania

UTILIZATION OF MANURE FROM POULTRY FARMS USING THE PYROLYTIC PROCESS

Gheorghe ȘOVĂIALĂ[1,*], Ioan PAVEL[1], Gabriela MATACHE[1], Alina POPESCU[1], Vasilica ȘTEFAN[2]

[1] National Institute of Research & Development for Optoelectronics / INOE 2000 – Subsidiary Hydraulics and Pneumatics Research Institute / IHP, Bucharest

[2]The National Institute of Research – Development for Machines and Installations Designed for Agriculture and Food Industry – INMA Bucharest

* sovaiala.ihp@fluidas.ro

Abstract: The *development of a sustainable environmental strategy regarding waste management procedures in poultry farms is a major goal for all European Union countries.*
The European Union strategy aims to reduce the amount of waste generated in production processes sent to landfills, to valorize them to obtain compost and thermal energy.
The main benefits of implementing the strategy are both increasing the efficiency of activities and profitability of the field, reducing the impact on the environment, reducing costs and obstacles to recycling, and reducing pollution caused by waste, especially greenhouse gas emissions.
Within the ADER 25.3.1. Technology for valorization of poultry manure by obtaining biofertilizers rich in phosphorus, the project partners proposed to develop technology and create equipment for the processing by pyrolysis of waste from poultry farms, resulting from the activity of production farms, reproductive farms, incubation stations (animal manure: barnyard manure/chicken litter, animal tissue waste: bird carcasses, incubation waste: clear eggs, dead embryos resulting from the mirage operation, eggshells, non-viable embryos, down, non-conforming chicks resulting from hatching, technological: non-conforming eggs for the incubation operation, coming from production farms or from the incubation station, chimney cleaning sludge). Among the waste mentioned above, animal manure, with the highest contribution to technological processes in the poultry farm sectors, is best suited for energy recovery, as biomass for the production of thermal or electrical energy through the gasification process, or for obtaining solid or liquid biofuels through the pyrolysis process.

Keywords: *Pyrolysis, animal manure, biochar*

1. Introduction

Biomass is considered to be both a renewable source of energy and carbon dioxide neutralization, through the process of photosynthesis. Due to its high moisture content and sometimes low energy density, biomass is in many cases an economically unfeasible source for use as a feedstock in energy systems.
Using conversion processes such as pyrolysis, biomass can be converted into solid or liquid biofuels with up to five times the energy density [1] [2].
Currently, biomass represents an important percentage (7% of the world's primary energy consumption, according to [3] [4].
The other two major sources of unconventional energy (with higher usage shares than biomass) are nuclear energy and hydropower [5].
In other words, wind and solar energy currently account for less than 1% of global energy demand [6].
In the current context, biomass is one of the most interesting and promising resources in the category of renewable energy resources, with intensively studied energy recovery technologies. [7].
Biomass has a real potential to increase energy security in regions without abundant fossil fuel reserves, to provide alternatives to the need for liquid fuels and to reduce net carbon emissions into the atmosphere per unit of energy delivered [8].

The conversion of biomass into energy can be achieved through several pathways, which involve different processes dependent on temperature, pressure, process conditions and microorganisms. The main methods of energy recovery of biomass are: combustion; biological (biochemical) conversion; thermochemical conversion.

2. Conceptual presentation of the method and critical analysis of the main pyrolysis processes, technologies and products

Pyrolysis is a thermal decomposition process of organic matter, carried out in an inert atmosphere or in the partial absence of oxygen. There are two major differences between the pyrolysis process and the combustion process, in terms of the type of thermal process and the products of the process. First, combustion is an exothermic process that generates heat, while pyrolysis is an endothermic process that requires heat to activate the process. Second, the products of the combustion process are CO_2, water and ash, and the products of the pyrolysis process are biofuels or products for chemical recovery [9].

The name of the word comes from the Greek language and is made up of two parts: "pyro" which means fire and "lysis", which means total disintegration. Pyrolysis technology has been used since ancient times, 5500 years ago in southern and eastern Europe. The first applications were for the production of charcoal.

The Egyptians used a technique to obtain tar, necessary for boats [10], [11].

In the 18th century, the process of pyrolysis of coal was used to obtain coke (which was used in the metallurgical industry as a substitute for charcoal). In the early 1800s, the technology of coal pyrolysis was invented and applied to obtain synthesis gas, used for street lighting in London, New York and other major cities in the world [9].

Recently, due to the trends of depletion of raw material resources for petroleum products and the increase in their price, industrial-scale technologies have been developed for the conversion of unutilized waste, through pyrolysis or other processes. Pyrolysis technology is a viable alternative for the energy crisis but also for reducing pollution, being considered one of the most efficient technologies for the treatment and disposal of various wastes.

The fuels obtained from the pyrolysis process have a high energy density, have the advantage of being easy to transport and store, being a viable alternative fuel for turbines, industrial combustion applications, power plants or engines. The conversion of biomass through the industrial pyrolysis process is a technology that is in the attention of many research specialists because it can provide an alternative for energy needs and for environmental protection.

Pyrolysis is one of the most important methods of biomass conversion. Through this process, biomass is subjected to a thermal treatment of 300-1000ºC, in the absence of oxygen, producing three fuels with energy value: coal, oil and synthetic gas. Pyrolysis is the first stage encountered in thermal conversion processes, where it is followed by combustion and gasification [9].

Biomass pyrolysis is a complex process, due to the diversity, heterogeneity and thermal equilibrium for certain components. Biomass has cellulose as its main component, the decomposition of this component being the most studied in the specialized literature, being the easiest mechanism to understand [12].

Table 1 presents the stoichiometry of cellulose in pyrolysis reactions [13], [14]. Pyrolysis technology can be classified according to the conditions provided in the process, both for slow pyrolysis and for fast pyrolysis.

The **slow pyrolysis** process is carried out at low heating rates and low temperatures, with a vaporization time of 5-10 minutes [15].

Volatile organic components undergo decomposition reactions, forming coal as the main component, along with gas and bio-oil in small percentages [16]. The slow pyrolysis process does not require special conditions for processing the raw material (drying, sorting, shredding), the energy flow transmitted is lower than in the case of fast pyrolysis; the duration of the process is long, between tens of minutes and several hours.

Table 1: Stoichiometry of cellulose

Stoichiometry	**Temperature (^0C)**	**Enthalpy (kJ)**
$C_6H_{10}O_5 \rightarrow 5CO+5H_2+C$	300 1000	180 209
$C_6H_{10}O_5 \rightarrow 5CO+CH_4+3H_2$	300 1000	105 120
$C_6H_{10}O_5 \rightarrow 4CO+CH_4+C+2H_2+H_2O$	300 1000	-26 -16
$C_6H_{10}O_5 \rightarrow 3CO+CO_2+2CH4+H_2$	300 1000	-142 -140
$C_6H_{10}O_5 \rightarrow 3CO+CH_4+2C+H_2+H_2O$	300 1000	-158 -152
$C_6H_{10}O_5 \rightarrow 2CO+CO_2+CH_4+C+H_2O$	300 1000	-274 -276

Figure 1 shows the block diagram of a slow pyrolysis plant, with the main integrated components for obtaining coal, oil and synthetic gas.

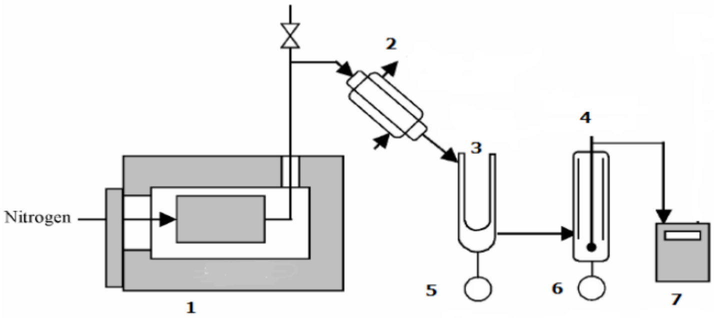

Fig. 1. Block scheme of a slow pyrolysis plant
1.Pyrolysis reactor; 2. Water-cooled condenser; 3. Secondary condenser, for additional cooling of non-condensable gases (down to -70 ºC) and oil recovery; 4. Non-condensable gas filtration device; 5. Pyrolysis oil collection container; 6. Secondary pyrolysis oil collection container; 7. Gas collection device.

The **fast pyrolysis** process takes place at high heating rates of up to 200ºC/min, largely favoring the production of bio-oil in proportions of 60-75%. The resulting coal and gas are in proportions of 15-25% [17].
Fast pyrolysis is characterized by a short vaporization time and a rapid cooling of the gases to favor the production of a high percentage of bio-oil. In integrated industrial fast pyrolysis systems, to meet the process conditions, the most used types of reactors are fluidized bed ones.
The necessary conditions for obtaining fast pyrolysis are:
• high heating rates accompanied by rapid heat transfer for biomass particles;
• crushing of the biomass raw material into particles with an equivalent diameter of less than 3 mm, since biomass has a low thermal conductivity;
• ensuring a vaporization time shorter than 2 seconds, to limit side reactions;
• temperature control around 500ºC, to maximize the percentage of bio-oil;
• rapid cooling of pyrolysis vapors, to obtain bio-oil and rapid collection of pyrolysis char, to minimize vapor cracking;
• drying the biomass to a moisture content of less than 10% [18].
An improved variant of fast pyrolysis is ultra-fast pyrolysis, which requires very high heating rates, over 1000 ºC/s and a vaporization time shorter than 1 second. The main disadvantage of this process is the catalytic effect of coal, due to which the pyrolysis oil becomes viscous and contains solid residues [19]. Figure 2 shows a fast pyrolysis plant, with the main integrated components for obtaining coal, oil and synthetic gas.

The biomass is subjected to a series of physicochemical transformations by means of the components described above, being converted into the three biofuels as a result of the technological circuit. The biomass is brought into the plant by an automatic feeding system, which introduces it into a fluidized bed reactor. Fluidization is maintained with the help of inert gas preheated to the process temperature. Primary coal is formed inside the reactor, which is carried into the main collection container. The volatile substances formed inside the reactor together with the inert gas pass through a heated cyclone (to prevent condensation), where due to the high speeds, the matter will collide several times with its walls, causing the separation of fine coal particles, which will be collected in the secondary container. The volatile matter will continue the circuit to the condenser, where a large part of the gases will condense, generating the pyrolysis oil, stored in a container located below the condenser. The non-condensed gases will continue the circuit through two purification filters, thus being prepared as synthesis gases. The gases can be transported by means of a blower to a burner that completes the heat required for the pyrolysis system, or they can be stored.

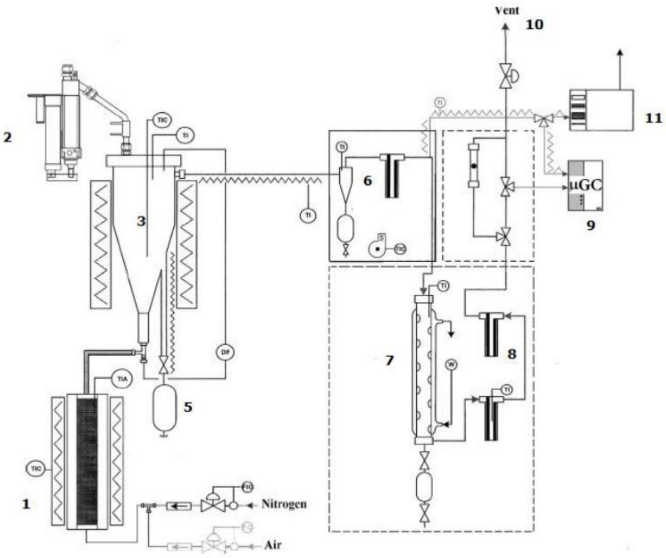

Fig. 2. Scheme of a fast pyrolysis plant [20]

1.Inert gas preheater; 2. Automatic biomass feeding system; 3. Pyrolysis reactor heated by an electrical or thermal source; 4. Secondary pyrolysis coal collection container; 5. Primary pyrolysis coal collection container; 6. Cyclone and filter for recovering fine coal particles in the heated medium; 7. Secondary condenser, for cooling non-condensable gases and recovering pyrolysis oil; 8. Filters for purifying non-condensable gases; 9. Non-condensable gas analysis station; 10. Blower for transporting gases to bottling or reuse in the thermal source of heat generation.

Depending on the parameters of temperature, heating rate and vaporization resistance, pyrolysis was differentiated into different technologies, according to Table 2, [21].

Table 2: Pyrolysis technologies, depending on the process parameters [15]

Technology	Heating speed	Vapor resistance	Temperature [^{0}C]	Main product
Carbonization	Very slow	Days	400	Coal
Conventional	Slow	300-1800 s	600	Oil, gas, coal
Fast	Very fast	0.5-5 s	650	Bio oil, gas
Ultra-fast	Very fast	<1 s	1000	Chemicals and gas
Vacuum	Medium	2-30 s	400	Bio oil
Hydro-pyrolysis	Fast	<10 s	<500	Bio oil
Methanol-pyrolysis	Fast	<10 s	>700	Chemicals

The table shows that depending on the pyrolysis technologies applied, **the three pyrolysis products** are obtained in different percentages: coal, bio-oil and synthetic gas.

Pyrolysis coal (bio-coal) is a solid product obtained from the degradation of lignin and hemicellulose during the pyrolysis process. The physicochemical properties of pyrolysis coal are dependent on a series of factors that must be analyzed: the type of reactor, the species and properties of the biomass, particle size, kinetics, heating rate, inert gas flow rate, etc. Pyrolysis coal has a high content of fixed carbon, combined with volatile matter, moisture, hydrogen and other constituents. The aromatic structure of pyrolysis coal consists of elements such as H, S, O, N and P, which are found in different proportions, depending on the species of pyrolyzed biomass. Comparing the results of the two types of pyrolysis processes - slow and fast - a higher quality is observed for the coal obtained by fast pyrolysis. Specialized studies have shown that for different temperature conditions, varying percentages of coal were obtained, at high temperatures the percentage of coal being minimal, approximately 8-10% [22].

Pyrolysis coal (biochar) can be used directly in industrial systems for the generation of heat and electricity, being a fuel with a higher thermal power and a low sulfur and nitrogen content, being the carbon-rich product obtained from biomass, such as wood, manure or vegetable residues, heated in a closed container, through the so-called thermal decomposition of organic material, with limited oxygen (O_2) supply and at relatively low temperatures (<700°C).

Biochar is an organic product rich in C, valuable for agriculture, which by incorporation improves soil fertility, sequesters carbon (C) from its gaseous compounds, ensures the filtration of water percolated into the groundwater.

The role of biochar is also highlighted by Barrow C.J., [23]: biochar attracts attention as a means of carbon capture and as a potentially valuable input for agriculture to improve soil fertility, aid sustainable production and reduce contamination of streams and groundwater.

Pyrolysis oil is an attractive product of the pyrolysis process, as it is an easy to transport, store and upgrade fuel. The highest percentage of pyrolysis oil is obtained under conditions of rapid vaporization in less than 1 second, at a reaction temperature of approximately 775 K [24].

Pyrolysis oil is viscous, corrosive and unstable, consisting of a mixture of approximately 300-400 components [25]. The viscosity of biofuel and biocrude varies greatly depending on the liquefaction conditions. The increase in viscosity can be attributed to the continuous polymerization and oxidative coupling reactions in biocrude during storage. Due to a high oxygen and water content, the calorific value is 16-19 MJ/kg, almost half that of petroleum with 40-45 Mj/kg. In order to be able to use it as a fuel, it is necessary to improve the qualities of the oil by methods such as solvent fractionation or catalytic cracking. The high water content (15-30%) generates ignition problems, a low flame and a low density of the liquid. The water content can be removed by conventional methods such as distillation [24].

The third product of the pyrolysis process, **the synthesis gas**, has as main components H_2 and CO in combination with CO_2, N_2, H_2O, alkanes and [26].

A high syngas content is obtained at higher temperatures, where tar decomposition takes place and implicitly a reduction in the percentage of coal and oil. The highest percentage of synthesis gas (76.64%) from the pyrolysis process can be obtained in plasma reactors using radio frequencies [15], [26].

The use of synthesis gas as a fuel has the advantage of producing low amounts of hydrocarbons and carbon monoxide. On the other hand, the main components of synthesis gas produce an intense combustion flame and high temperatures in engines.

2.1 Conceptual presentation of the main types of slow pyrolysis reactors

The main types of reactors designed and implemented in pyrolysis systems are diversified, depending on the specific process conditions characteristic of the respective technologies. Applications differ due to the variety of raw materials, the number of resources, the desired energy requirement, the required capacity or the desired end products to be obtained.

Pyrolysis reactors have been designed to meet specific process conditions, in order to optimize and increase the percentage of biofuel desired to be obtained. Taking into account the considerations listed above, several types of reactors can be distinguished.
Fixed bed reactors have traditionally been used to produce coal. Slow heat transfer results in low amounts of liquid following the pyrolysis process. Their technology is simple and has proven to be reliable for materials that exhibit dimensional uniformity. A disadvantage of the fixed bed reactor is given by the fact that due to the vertical movement of the solid material, the produced gas retains the components of the tar, requiring its cracking by means of other cyclone-type devices. Another disadvantage is tar deposits inside it, a fact that requires complex maintenance after use, in order not to reduce the efficiency of the system.

Thermal modules with CHAB concept

The first type of energy module with which biochar was produced was the TLUD type micro-gasification process.
In principle, the up-draft gasification process is not a biochar producer and as a result, most current installations use variants of the down-draft process.
Installations that produce both heat and biochar are divided into two categories:
- with a controlled gasification process from which biochar can also be obtained;
- with two processes in parallel: TLUD type gasification that produces thermal energy and biochar and a second subsystem, put in series in which the thermal energy produced before is used for the pyrolysis of another quantity of biomass, which produces combustible gases burned in the following those from gasification, thermal energy that can be used in thermal applications.

Installations with a controlled gasification process from which biochar can also be obtained

An example is the DRAGON type installation produced by CHIP ENERGY (USA), which can gasify a variety of biomass, produce hot water or hot air and biochar in proportion of 15-20%. Figure 3 shows the functional scheme, and Figure 4 shows the system mounted in a transportable container.

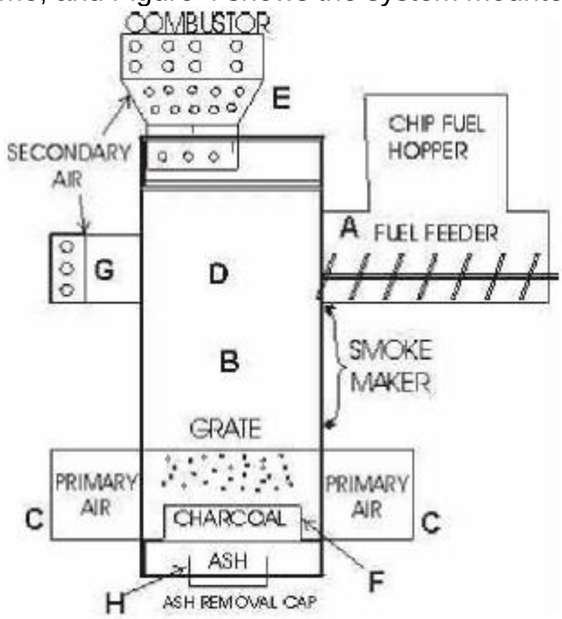

Fig. 3. DRAGON type installation functional scheme from CIP ENERGY

A. Conveyor feed hopper B. Biomass layer C. Gasification air inlet D. Generator gas collection area E. Combustion air inlet F. Biochar area G. Combustion regulation air inlet H. Ash tray

ISSN 1454 - 8003
Proceedings of 2024 International Conference on Hydraulics and Pneumatics - HERVEX
November 13-15, Băile Govora, Romania

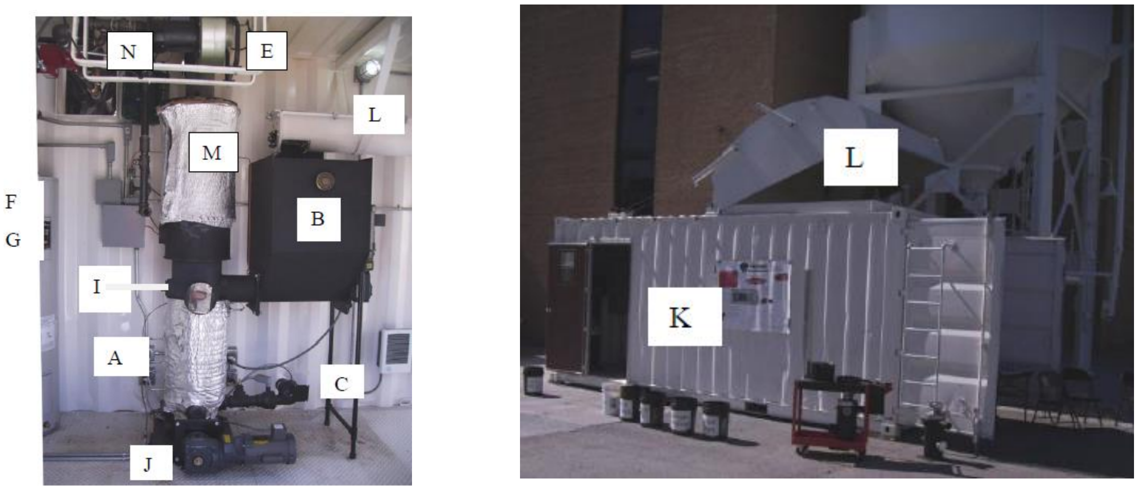

Fig. 4. DRAGON type installation from CIP ENERGY
A.60 kWt gas generator B. Biomass feed hopper C. Primary air fan D. Secondary air fan E. Draft fan F. Automatic control system G. Operator monitor J. Biochar conveyor K. Container L. External biomass hopper M Flach type steam boiler N. Hot water pump and pipes

Installations with gasification and pyrolysis processes

In order to analyze in more detail the processes that occur in this type of installations, the block scheme presented in figure 5 will be analyzed; this is the block diagram of the general structure of the thermal energy and biochar production facilities in a combined regime: gasification + pyrolysis. Biomass and air enter the system and thermal energy comes out that can be used for heating and biochar processes. The system has as component entities: the gasification reactor, the gas burner and the anaerobic pyrolysis reactor.

Fuel gases and biochar come out of the gasification reactor. The gasification gases are sent to the burner where they mix with the pyrolysis gases leaving the pyrolysis reactor. Combustion is maintained with strongly swirling combustion air and hot flue gases are produced that transfer part of their thermal energy to the pyrolysis reactor for the needs of the endothermic process, and most of it leaves the system in the form of thermal energy usable in processes of heating.

In the pyrolysis reactor, under anaerobic conditions, a pyrolysis process takes place resulting in an average of 25% biochar and 75% pyrolysis gases that are burned in the burner.

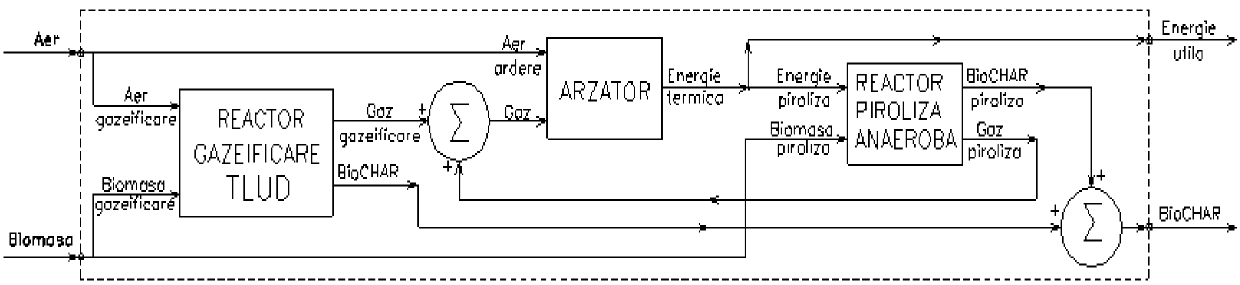

Fig. 5. Block scheme for combined energy and biochar production

A first achievement in the application of this structure is the ANILA thermal device designed by Professor RV Ravikumar, from the University of Mysore in India. The device is part of the structure with parallel reactors that produces thermal energy and biochar at household level. Figure 6 shows the functional scheme and figure 7 the operating phases of the ANILA reactor.

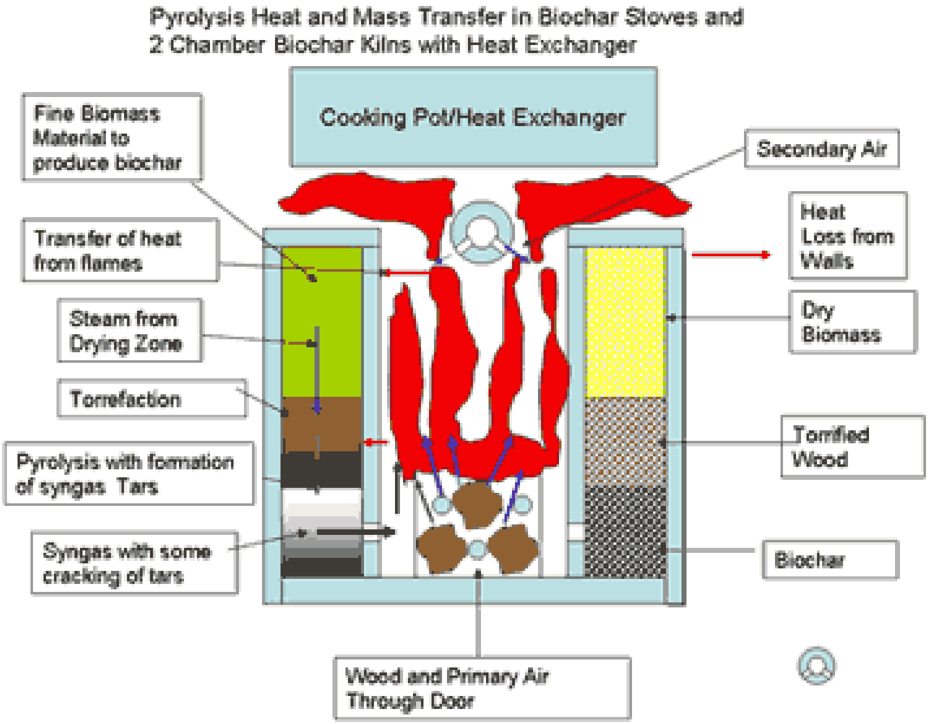

Fig. 6. Functional scheme of the ANILA type reactor

The ANILA device is a structure with two concentric reactors, in which biochar is produced, which does not enter into another combustion process. The inner reactor, intended for the micro-gasification process of the TLUD type, is filled with chopped biomass, from which, through gasification, generator gas is produced, which, through combustion, produces the heat necessary to maintain the pyrolysis of the biomass in the outer reactor.

The outer reactor, in which an anaerobic environment is maintained, is filled with biomass that will be carbonized. The wall of the inner reactor is very hot, it transmits heat to the biomass in the outer reactor which enters the anaerobic pyrolysis process. The pyrolysis gases produced pass through holes into the inner reactor, where they are completely burned in the combustion chamber, producing useful thermal energy.

It is a batch-type process with reactors mounted in parallel, which reduces the height of the installation and makes it easy to handle.

In order to obtain a quality biochar, however, it is necessary to increase the pyrolysis temperature above 500 0C, by insulating the outer wall of the pyrolysis reactor.

Another variant is the structure with reactors mounted in series, fig.8. A first demonstration achievement is the system made by Jolly Roger (2012).

It consists of a TLUD gas generator with a reactor volume of 200 l at the bottom, on which is mounted a pyrolysis reactor with a volume of 120 l heated by the combustion gases and which through the perforated bottom transfers the pyrolysis gases to the burner, contributing to the heat transfer to the pyrolysis reactor.

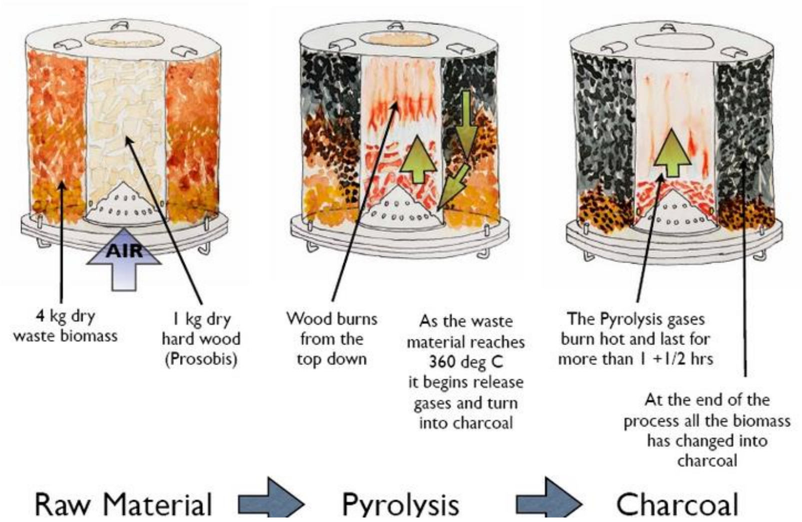

Fig. 7. Operating phases of the ANILA type system

Fig. 8. Artisanal biochar and heat production system made by Jolly Roger

Since the artisanal system was found to produce quality biochar at a low production cost, the structure and process were taken over by the company BioCharWorks (NY, USA) which designed, tested, produces and markets the systems in the family - A BIO-ENERGY CONVERTER: HYBRID 250, fig.11 - mobile system mounted on a semi-trailer and HYBRID 500, fig. 12- stationary installation.

Fig. 9. Heat and biochar production plant type HYBRID 250

Fig. 10. Heat and biochar production plant type HYBRID 500

The pyrolysis process offers a competitive alternative for the valorization of numerous sources of renewable energy, but also for the treatment and energy valorization of municipal, industrial waste, and those originating from agricultural or medical technological processes.
The pyrolysis process is considered the most environmentally friendly thermochemical process compared to combustion and incineration processes, as it has low emissions.
The pyrolysis equipment, symbolized EP, fig. 11, was designed and partially realized during the stage 2 of the ADER 25.3.1 project. Technology for capitalizing poultry droppings by obtaining biofertilizers rich in phosphorus, and its main purpose is to carry out the pyrolysis process of poultry droppings, but also of other types of materials (vegetable residues, in order to obtain biofertilizers with a high phosphorus content).

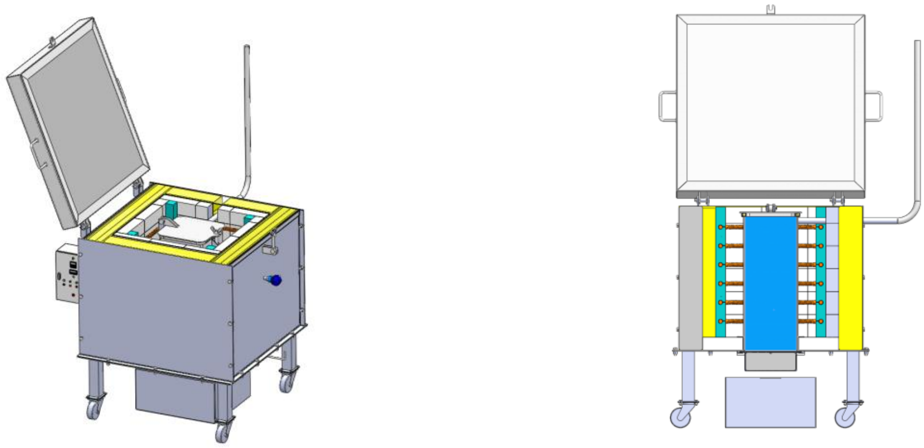

Fig. 11. Poultry waste pyrolysis equipment

The equipment for obtaining phosphorus-rich biofertilizers from poultry droppings is powered by a photovoltaic panel system and has an exhaust air purification system equipped with a pre-filter and an activated carbon filter. This system has the role of eliminating odors and possible harmful gases generated in the premises where the pyrolyzer is located.
The equipment is composed of the following subassemblies: reactor EP 1.0, combustion chamber EP 2.0, external casing EP 3.0, assembled target EP 4.0, heating system EP 5.0, collection box EP 6.0, insulation EP 7, EP 8, EP 9, control panel 10.0, air purification system 11.0.

3. Conclusions

1. Currently, biomass represents approximately 7% of the world's primary energy consumption, thus being a significant source in the global energy mix.
2. Due to their dominant weight in the technological processes of poultry farms, waste of poultry origin is suitable for processing by pyrolysis, a method that allows obtaining biofertilizers rich in phosphorus.
3. Biomass conversion through the pyrolysis process is a technology of major research interest, offering an alternative solution for both energy requirements and environmental protection; the products generated by pyrolysis have a high energy density, constituting a viable alternative for fuels.
4. Depending on the parameters of temperature, heating rate and vaporization resistance, the pyrolysis process can be adapted in different technologies to obtain, in variable percentages, the three main products of the process: coal, bio-oil and synthetic gas.
5. The physicochemical properties of char resulting from pyrolysis are influenced by numerous factors, including the type of reactor used, biomass species and characteristics, particle sizes, kinetics, heating rate, and inert gas flow.
6. Pyrolysis coal, also known as biochar, is a solid product obtained by the degradation of lignin and hemicellulose in the pyrolysis process.
7. In addition to its direct use in industrial systems for heat and electricity generation – having a superior calorific value and low sulfur and nitrogen content – pyrolysis coal (biochar) is a carbon-rich organic product. It has multiple agricultural applications, where, by incorporation into the soil, it contributes to the improvement of soil fertility, the sequestration of carbon from gaseous compounds, and ensures the filtration of percolated water to the water table.
8. The main types of equipment used to produce biochar by slow pyrolysis of biomass include: thermal modules based on the CHAB concept, controlled gasification process plants (which can also generate biochar), and fixed bed reactors.

Acknowledgments

This paper was financed by MINISTRY OF AGRICULTURE AND RURAL DEVELOPMENT – ROMANIA - MADR – Sectorial Project ADER 25.3.1 Contract no.: ADER 25.3.1 /20.07.2023 Technology for valorification poultry manure by obtaining biofertilizers rich in phosphorus.

References

[1] Marshall (Sandy), A.J., Ping F. Wu, Sang Hun Mun, and Charles Lalonde. "Commercial Application of Pyrolysis Technology in Agriculture." Paper presented by the American Society of Agricultural and Biological Engineers, Quebec Canada, July 13-16, 2014. DOI:10.13031/AIM.20141909089.
[2] Filipovici, Alexandru. *Possibilities of optimizing the industrial technologies of biomass utilization by pyrolysis / Posibilități de optimizare a tehnologiilor industriale de valorificare a biomasei prin piroliză*. PhD Thesis, 2018.
[3] Fernandes, Suneeta D., Nina M. Trautmann, David G. Streets, Christoph A. Roden, and Tami C. Bond. "Global biofuel use, 1850-2000." *Global Biogeochemical Cycles* 21 (June 2007): GB2019. DOI: 10.10.1029/2006GB002836.
[4] Field, C.B., and M.R. Raupach (eds.). *The Global Carbon Cycle: Integrating Humans, Climate and the Natural World*. Sabine, C.L., M. Heimann, P. Artaxo, D.C.E. Bakker, C.T.A. Chen, C.B. Field, N. Gruber, C. Le Quere, R.G. Prinn, J.E. Richey, P. Lankao Romero, J.A. Sathaye, and R. Valentini. "Current status and past trends of the global carbon cycle." Washington DC, Island Press, 2004.
[5] Energy Information Administration (EIA). *Annual Energy Review 2006*, US Department of Energy, 2006.
[6] Energy Information Administration (EIA). *International Primary Energy Production*, US Department of Energy, 2007.
[7] Filipovici, Alexandru., A. V. Mnerie, D. Badescu, M. Bota, S. Maris, V. Baesu, T. Slavici, and D. Ungureanu. "Agribusiness projects assessment using cost-benefit analyses." Paper presented at the 42nd International Symposium on Agricultural Engineering, Actual Tasks on Agricultural Engineering, Opatija, Croatia, February 25-28, 2014.
[8] Field, Christopher B., J. Elliott Campbell, and David B. Lobell. "Biomass energy: the scale of the potential resource." *Trends in Ecology and Evolution* 23, no. 2 (February 2008): 65–72.
[9] Rezaiyan, John, and Nicholas P. Cheremisinoff. *Gasification Technologies: A Primer for Engineers and Scientists*. CRC Press Taylor & Francis Group, 2005.
[10] Demirbas, Ayhan. "Partly chemical analysis of liquid fraction on flash pyrolysis products from biomass in the presence of sodium carbonate." *Energy Conversion and Management* 43, no. 14 (2002): 1801-1809. https://doi.org/10.1016/S0196-8904(01)00137-6.
[11] Mohan, Dinesch, Charles U. Pittman Jr., and Philip H. Steele. "Pyrolysis of wood/biomass for bio-oil: A critical review." *Energy Fuels* 20, no. 3 (March 2006): 848-889.
[12] Vand de Velden, Manon, Jan Baeyens, Anke Brems, Bart Janssens, and Raft Dewil. "Fundamentals kinetics and endothermicity of the biomass pyrolysis reaction." *Renewable Energy* 35, no.1 (January 2010): 232-242.
[13] Stull, Daniel R., Edgar F. Westrum, and Gerard C. Sinke. *The Chemical Thermodynamics of Organic Compounds*. 1st edition. John Wiley & Sons Inc., 1969.
[14] Daubert, Thomas E., and Ronald P. Danner. *Physical and Thermodynamic Properties of Pure Chemicals*. New York, Chemisphere Publishing Corporation,1992.
[15] Mohamed, Samer (ed.). *Pyrolysis.* Zaman, Chowdhury Zaira, Kaushik Pal, Wageeh A. Yehye, Suresh Sagadevan, Syed Tawab Shah, Ganiyu Abimbola Adebisi, Emy Marliana, Rahman Faijur Rafique, and Rafie Bin Johan. "Pyrolysis: A Sustainable Way to Generate Energy from Waste". IntechOpen, 2017.
[16] Bridgwater, A. V. (ed.). *Progress in Thermochemical Biomass Conversion*. Bridgwater, A.V., S. Czernik, and J. Piskoz. "An overview of fast pyrolysis." 1st edition. Wiley, 2001.
[17] Demibas, Ayhan, and Arin Gonec. "An overview of biomass pyrolysis." *Energy Source* 24, no. 5 (2002): 471-482.
[18] Bridgwater, A.V. "Review of fast pyrolysis of biomass and product upgrading." *Biomass and Bioenergy* 38 (2012): 68-94.
[19] Cornelissen T., Y. Yperman, G. Reggers, S. Schreurs, and R.Carleer. "Flash copyrolysis of biomass with polylactic acid. Part 1: Influence on bio-oil yield and heating value." *Fuel* 87 (2008): 1031-1041.
[20] Amutio, Maidar, Gartzen Lopez, Jon Alvarez, Rui Moreira, Gustavo Duarte, Joao Nunes, Martin Olazar, and Javier Bilbao. "Flash pyrolysis of forestry residues from the Portuguese Central Inland Region within the framework of the BioREFINA-Ter project." *Bioresource Technology* 129 (2013): 512-518.

[21] Antal, Michael Jerry, and Grönli Morten. "The art, science, and technology of charcoal production." *Industrial & Engineering Chemistry Research* 42 (2003): 1619-1640.
[22] Rocha, J.D., E. Olivares-Gómez, J.M. Mesa-Pérez, L.A.B. Cortez, O. Seye, and L.E. González Brossard. "The demonstration fast pyrolysis plant to biomass conversion in Brazil." Paper presented at the World Renewable Energy Congress VII (WRC 2002), Cologne, Germany, June 29 - July 5, 2002.
[23] Barrow, C.J.. "Biochar: Potential for countering land degradation and for improving agriculture." *Applied Geography* 34 (2012): 21-28.
[24] Demirbas, Ayhan. "Competitive liquid biofuels from biomass." *Applied Energy* 88 (2011): 17-28.
[25] Kantarelis, E., and A. Zabaniotou. "Valorization of cotton stalks by fast pyrolysis and fixed bed air gasification for syngas production as precursor of second generation biofuels and sustainable agriculture." *Bioresource Technology* 100 (2009): 942-947.
[26] Wei, Lin, J. Alex Thomasson, R. Mark Bricka, William D. Batchelor, Eugen P. Columbus, and James R. Wooten. "Experimental Study of a Downdraft Gasifier." Paper presented at the 2006 ASAE Annual Meeting, Boston, MA, USA, August 19-22, 2006.

SIMCENTER AMESIM-BASED OPTIMIZATION OF AN EXPERIMENTAL TEST STAND FOR ULTRA-LOW HEAD HYDRAULIC TURBINES OPTIMIZATION

Alexandru-Polifron CHIRIȚĂ[1,2,*]

[1] National Institute of Research & Development for Optoelectronics / INOE 2000, Subsidiary Hydraulics and Pneumatics Research Institute / IHP, Cutitul de Argint 14, 040558 Bucharest, Romania.

[2] Faculty of Mechanical Engineering and Robotics in Construction, Technical University of Civil Engineering Bucharest, 59 Plevnei Str., 010223 Bucharest, Romania.

* chirita.ihp@fluidas.ro

Abstract: *The aim of this paper is to simulate and optimize an experimental test stand designed for optimization of ultra-low head hydraulic turbines. By modeling various hydraulic parameters and configurations, the study seeks to identify the optimal geometry of a calibrated orifice capable of maintaining a stable water level in the upper tank, ensuring efficient operation under variable flow conditions, with a maximum flow rate of 100 L/s.*

Keywords: *Simcenter Amesim optimization, experimental test stand, ultra-low head hydraulic turbines.*

1. Introduction

In recent years, the field of hydroelectric power generation has witnessed a significant shift towards ultra-low head (ULH) hydraulic turbines. These innovative machines have been designed to operate efficiently under very low water heads, typically below 10 meters. The primary objective behind developing ULH turbines is to harness energy from small-scale and run-of-river hydropower resources that were previously considered uneconomical or impractical for traditional hydroelectric power plants.

One of the most significant advantages of ULH turbines lies in their compact design. Unlike larger, more conventional hydroelectric turbines, these machines are designed to be smaller and more agile, making them ideal for installation in confined spaces such as small-scale hydropower installations, water treatment facilities, or even residential homes. This compactness not only simplifies the installation process but also reduces visual impact on the surrounding landscape, a crucial consideration for environmentally conscious developers.

The efficiency of ULH turbines is another notable aspect that sets them apart from their larger counterparts. These machines have been optimized to achieve high efficiency rates (>90%) under low head conditions, making them an attractive option for applications where water heads are limited or variable. This improved efficiency translates directly into increased power output and reduced energy losses, further enhancing the overall viability of ULH turbines in various hydropower contexts [1, 2].

Another significant benefit associated with ultra-low head hydraulic turbines is their scalability. These machines can be designed to accommodate a wide range of capacities (from small-scale residential applications to larger commercial projects), making them an attractive option for developers seeking flexibility and adaptability in their power generation solutions. Additionally, ULH turbines are capable of operating in various flow regimes, including low-flow conditions, which makes them suitable for intermittent or variable water resources.

The environmental benefits associated with ultra-low head hydraulic turbines cannot be overstated. These machines offer a clean and renewable alternative to traditional fossil-fuel-based power generation, reducing greenhouse gas emissions and minimizing visual impact on the surrounding landscape. Furthermore, ULH turbines can help reduce energy losses in existing infrastructure by providing an efficient means of generating electricity from small-scale hydropower resources.

Despite their many advantages, ultra-low head hydraulic turbines also present some challenges that must be carefully considered during design and implementation phases. One significant limitation lies in their reduced efficiency at very low head conditions (typically < 5 m), which can limit their applicability in certain situations. Additionally, ULH turbines may struggle with variable flow rates, requiring additional control systems to maintain optimal performance [3, 4].
Ultra-low head hydraulic turbines have been successfully integrated into a variety of power generation contexts, from small-scale residential installations to larger commercial projects. Some notable examples include:

- Small-Scale Hydropower: ULH turbines are ideal for small-scale hydropower applications (e.g., residential homes, community centers) where water heads are limited or variable.
- Run-of-River Systems: These machines can be used in run-of-river systems where the flow rate is variable and water heads are low.
- Water Treatment Plants: ULH turbines have been integrated into some water treatment plants to provide power for pumping stations or other essential equipment.

Optimizing experimental test stands is crucial for ultra-low head applications as it allows researchers and engineers to accurately assess the performance of low-head hydraulic turbines under various conditions. This optimization process involves designing and testing different turbine configurations, materials, and operating parameters to achieve maximum efficiency and reliability.
The importance of optimizing experimental test stands can be attributed to several factors:

- Improved efficiency: Optimized test stands enable researchers to identify areas for improvement in turbine design, leading to increased efficiency and reduced energy losses.
- Enhanced safety: By simulating real-world conditions, optimized test stands help ensure the safe operation of low-head hydraulic turbines under various scenarios.
- Cost savings: Optimizing experimental test stands can lead to cost savings by reducing the need for expensive field testing and minimizing downtime [5, 6].

As research continues to advance, ultra-low head hydraulic turbines will likely become even more efficient and adaptable. Future developments may focus on improving efficiency at very low head conditions (typically < 5 m), enhancing control systems for variable flow rates, and exploring new applications where these machines can provide significant benefits.
Ultra-low head hydraulic turbines represent a promising development in the field of hydroelectric power generation. Their compact design, high efficiency, scalability, and environmental benefits make them an attractive option for various hydropower applications. However, careful consideration must be given to their limitations, including reduced efficiency at very low head conditions and potential challenges associated with variable flow rates.
In the near future, we expect to see increased adoption of ultra-low head hydraulic turbines in various power generation contexts, including small-scale residential installations, run-of-river systems, water treatment facilities, and commercial projects. As this technology continues to evolve, it will undoubtedly play a more prominent role in shaping our energy landscape for years to come [7, 8].

2. Material and Method

The experimental test stand was designed to replicate operating conditions for ultra-low head (ULH) hydraulic turbines, with a focus on maintaining stable water levels in the upper tank under varying flow conditions. The setup consisted of an upper tank serving as the primary water reservoir, a lower tank that received discharged water, and a centrifugal pump capable of delivering flow rates of up to 100 L/s to recirculate water from the lower tank to the upper tank. A calibrated orifice was included as the key component to control flow rate and ensure water level stability in the upper tank. Various geometries of the orifice were tested to identify an optimal design, ultimately selecting a geometry of Ø125 x 100 mm. Simcenter Amesim software was employed to model the hydraulic behavior of the test stand and simulate its performance (**Figure 1**). The simulation process began with system modeling, where components of the test stand were represented using the software's thermal-hydraulic library. Flow restrictions and orifice geometries

were defined as boundary conditions, and steady state as well as transient flow scenarios were simulated to evaluate system performance under varying conditions.
The objectives of the study are to analyze the behavior of the experimental test stand under unrestricted flow conditions, evaluate the performance of the system with specific flow restrictions applied, and investigate the impact of varying flow rates on the stability and performance of the experimental stand when flow restrictions are in place. Additionally, the study aims to assess critical parameters, including the pressure drop across the calibrated orifice, water flow rate, and maximum dissipated power on calibrated orifice.

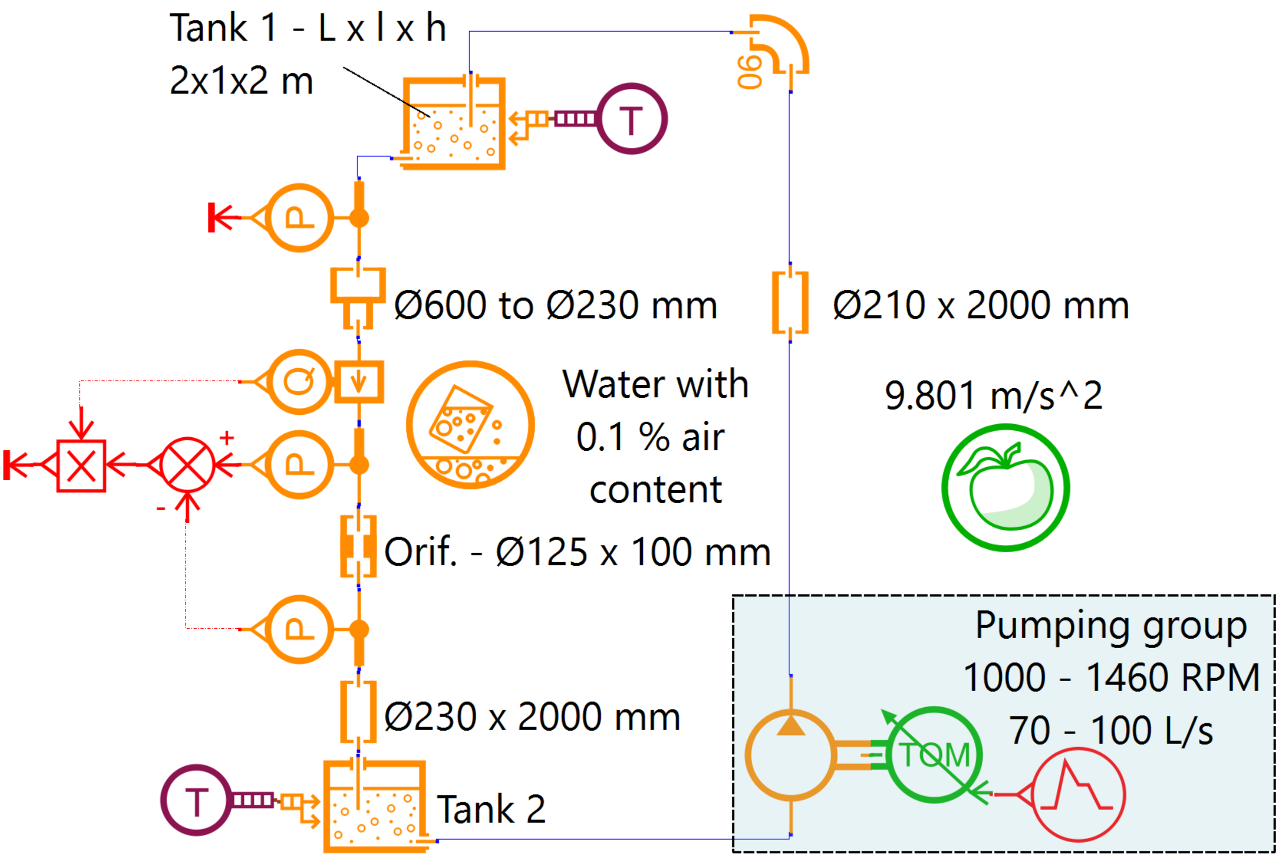

Fig. 1. Simulation network of the test stand for ultra-low head hydraulic turbines optimizations

Optimization of the system involved simulating multiple orifice geometries to identify a configuration that maintained a stable water level in the upper tank while minimizing energy losses. Key performance metrics evaluated in this study included pressure drop across the orifice, flow rate stability, power dissipation, and water level fluctuations in the upper tank.

3. Results

After running the simulation model, several graphs were plotted, related to the tree scenarios studied.
In **Figure 2,** the behavior of the experimental test stand under unrestricted flow conditions is presented. In this figure, it can be seen that the upper tank empties in less than 12 seconds through the 230 mm internal diameter pipe connecting the two basins. The water flow rate decreases because the water column pressure decreases.
Figure 3 presents the behavior of the experimental test stand under restricted flow conditions by calibrated orifice. In this figure it can be seen that the value of the flow rate pumped into the upper tank and the flow rate drained from the upper tank have the same value; also on the same graph it

can be seen that both the pressure at the base of the upper tank and the water level in it remain constant.

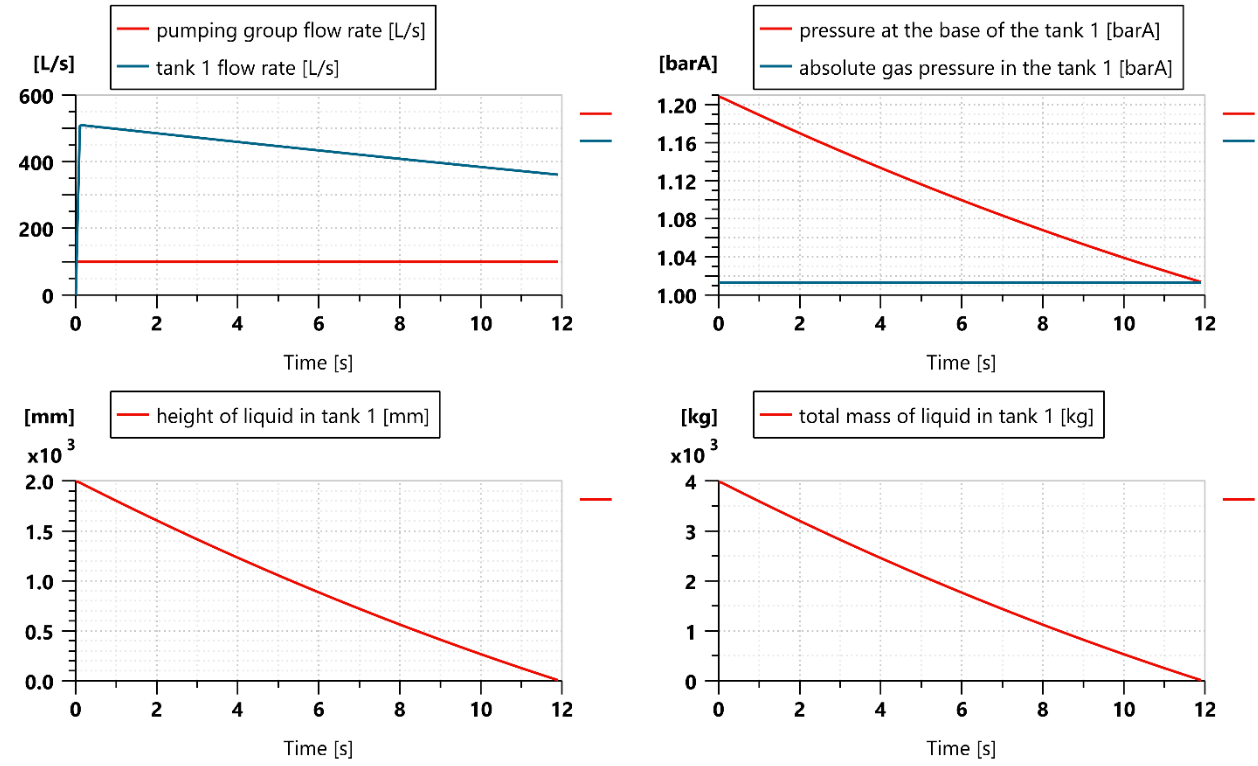

Fig. 2. Behavior of the experimental test stand under unrestricted flow conditions.

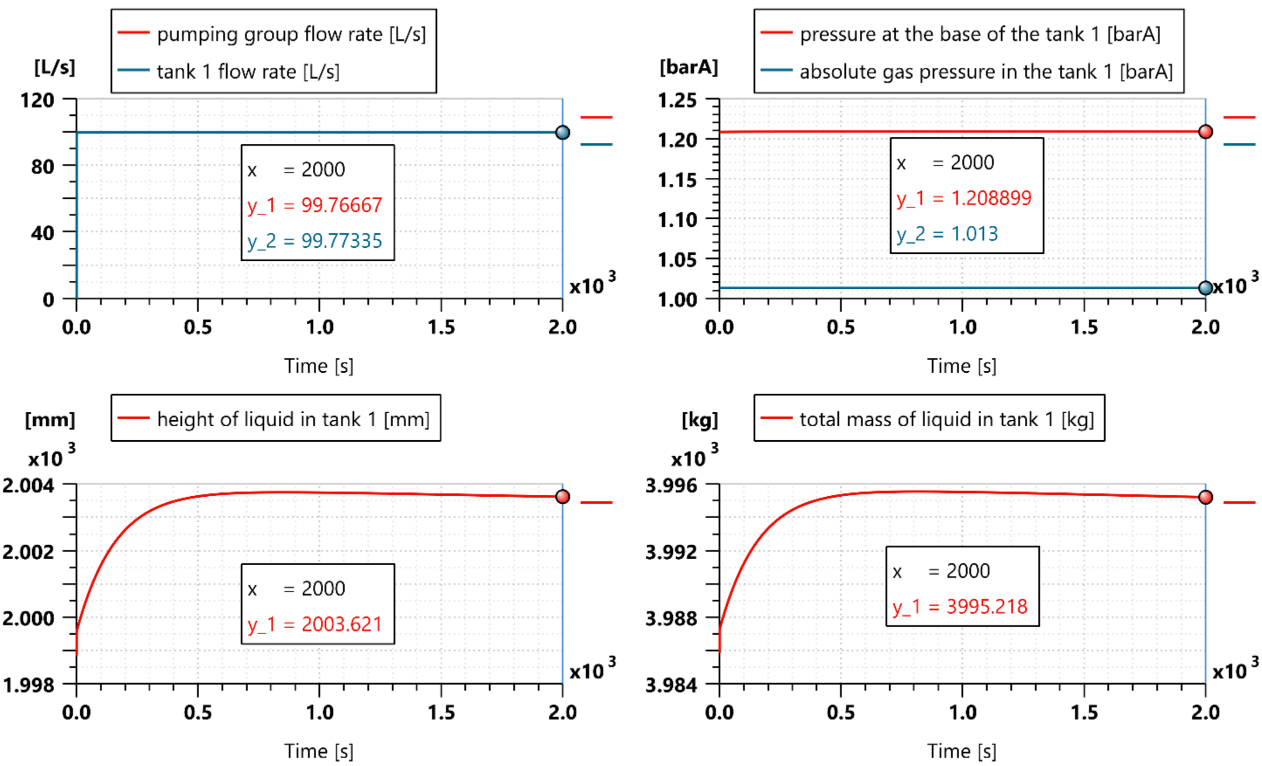

Fig. 3. Behavior of the experimental test stand under restricted flow conditions.

Figure 4 shows the behavior of the experimental test stand under restricted flow conditions and variable flow rate. In this graph, it can be seen that all parameters vary directly proportionally with the pumped flow rate, an exception being atmospheric pressure.

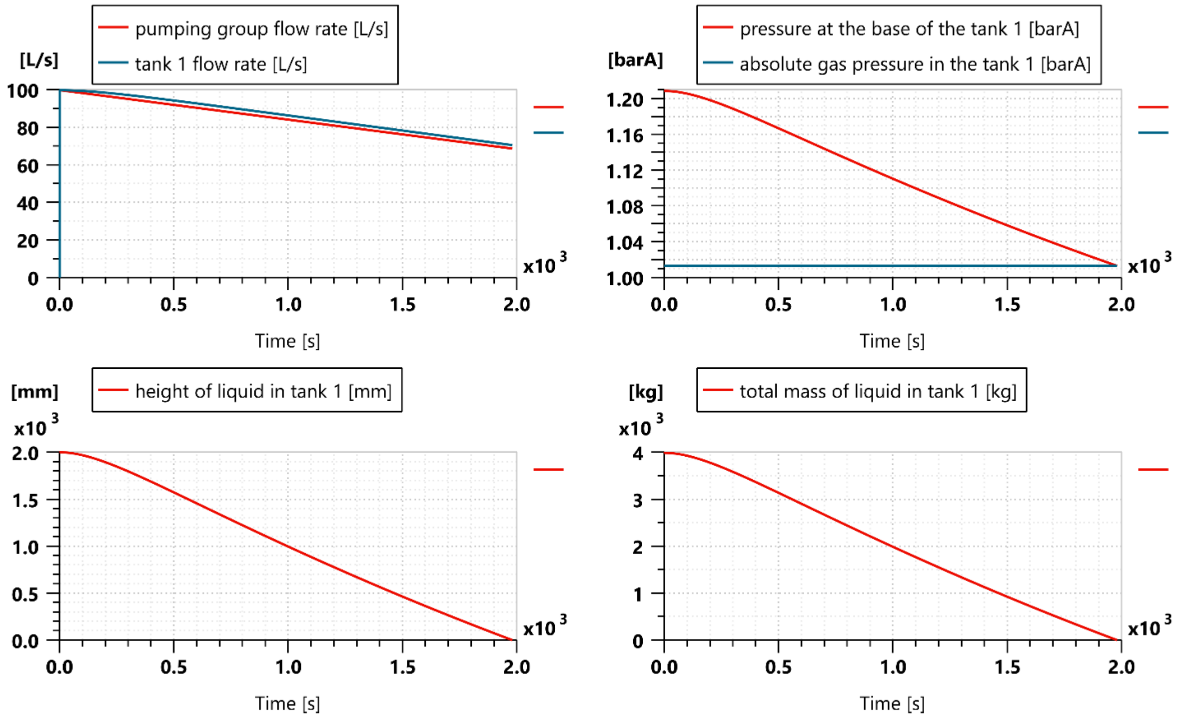

Fig. 4. Behavior of the experimental test stand under restricted flow conditions and variable flow rate.

Figure 5 shows the dependence between heights of the water column (water level) and pressure the as well as the flow rate and pressure.

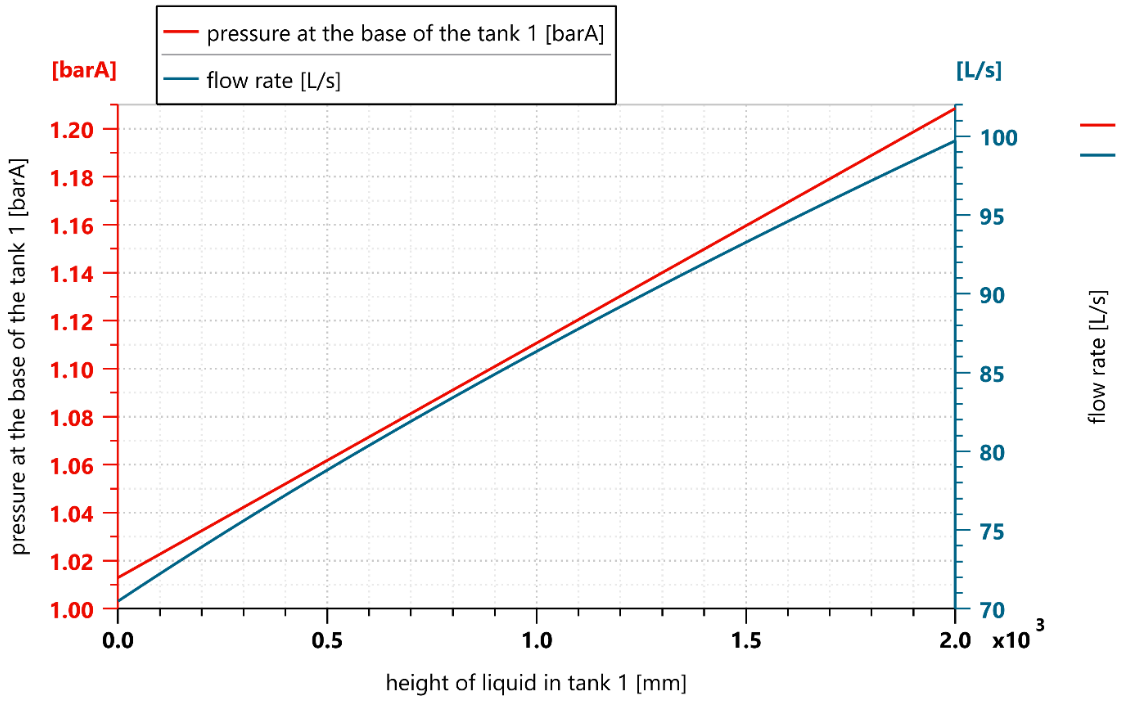

Fig. 5. Tank 1 pressure and flow rate vs. liquid height.

The time variation of the flow rate and the multiple hydraulic parameters of the calibrated orifice are presented in **Figure 6**. Most of the parameters have a variation directly proportional to the time variation of the flow rate except for the zeta coefficient whose variation is inversely proportional to the flow rate. The flow coefficient (cq) does not vary in time.

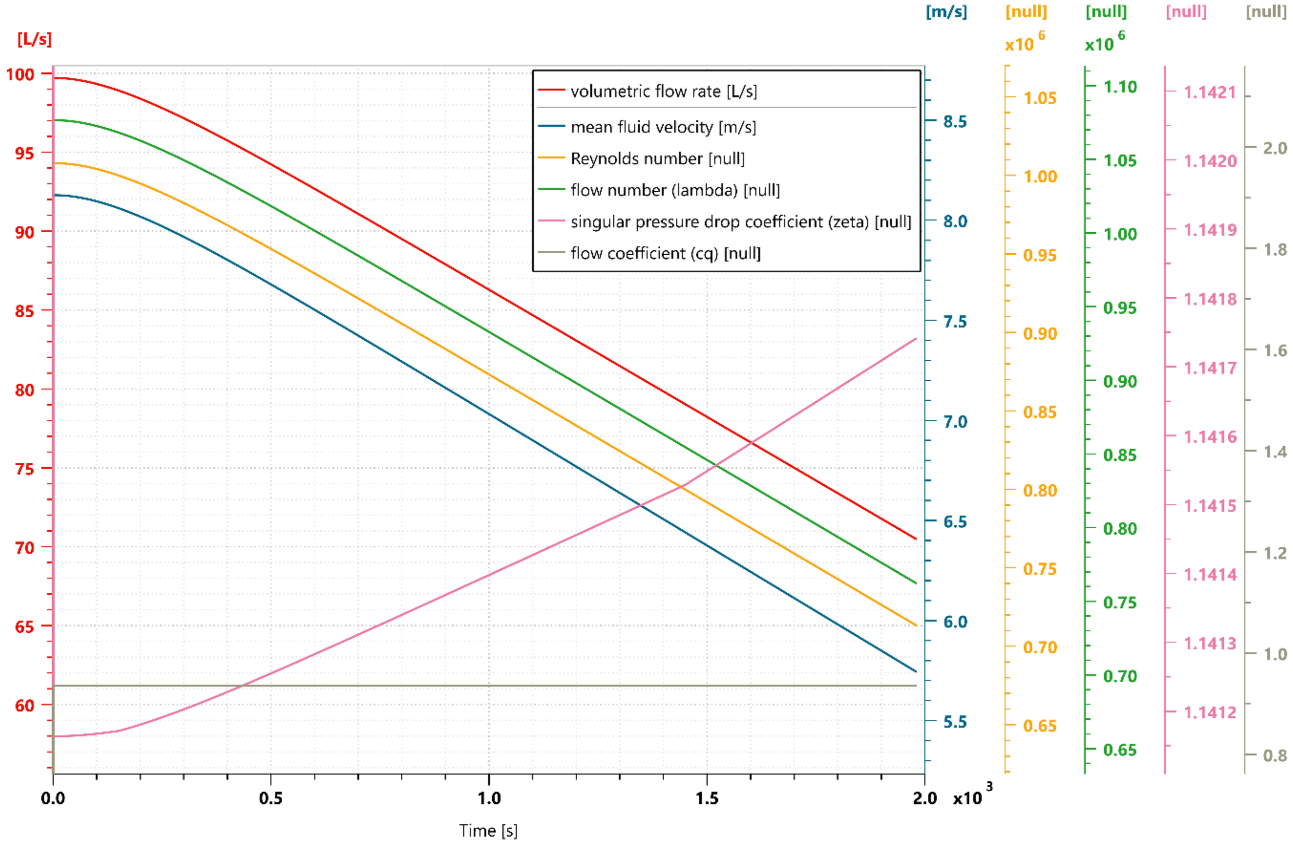

Fig. 6. The dynamics of flow rate and various hydraulic parameters through calibrated orifice.

Figure 7 illustrates the relationship between the pressure drop, the height of liquid in the upper tank, and the hydraulic power dissipated by the resistive source (calibrated orifice). The horizontal axis represents the pressure drop (in bar), while the vertical axis corresponds to the liquid height (in mm). The color gradient, ranging from blue (low values) to red (high values), indicates the power consumption in watts. **Figure 8** focuses on the relationship between the pressure drop, flow rate (Q), and the hydraulic power dissipated by the resistive source. The horizontal axis again represents the pressure drop (in bar), while the vertical axis displays the flow rate (in L/s). The color map indicates the power consumption, with values rising from blue (low power) to red (high power). The graph shows that as both the flow rate and pressure drop increase, the power rises significantly. The red zone, corresponding to the highest power values, occurs at maximum flow rates (100 L/s) and the largest pressure drops, whereas the blue areas indicate minimal power consumption at lower flow rates and pressure drops. The last two figures shows how the power required by the calibrated orifice is influenced by hydraulic parameters. **Figure 7** emphasizes the effect of the liquid height in the upper tank, which determines the potential energy influencing the power. In contrast, **Figure 8** focuses on flow rate, illustrating the dynamic influence of moving water. Despite these differences, both figures consistently show that an increase in pressure drop, whether paired with higher liquid levels or higher flow rates, leads to a substantial rise in power. Together, the graphs provide complementary insights into the hydraulic system's behavior, aiding in the optimization of the orifice geometry for stable and efficient operation in ultra-low head hydraulic turbine test stands.

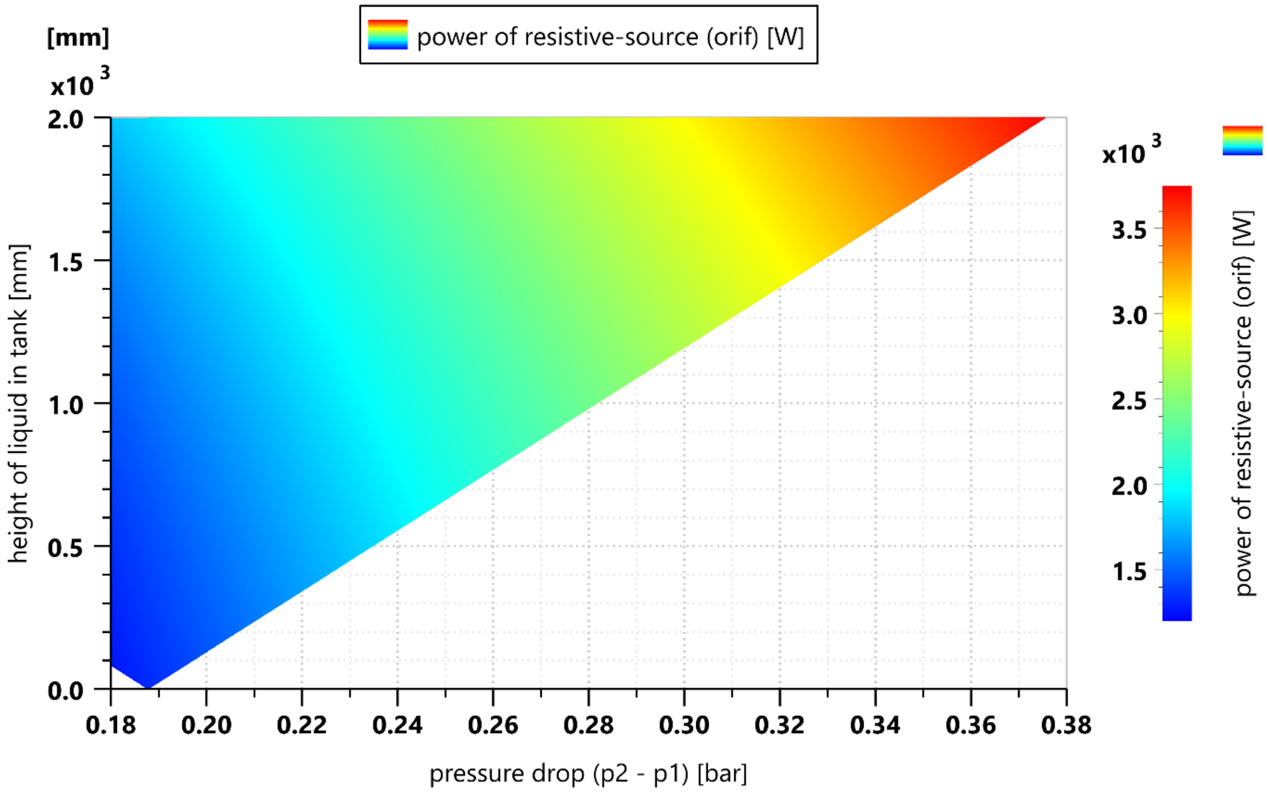

Fig. 7. The hydraulic power dissipated by the hydraulic orifice as a function of the pressure drop and the height of the liquid column.

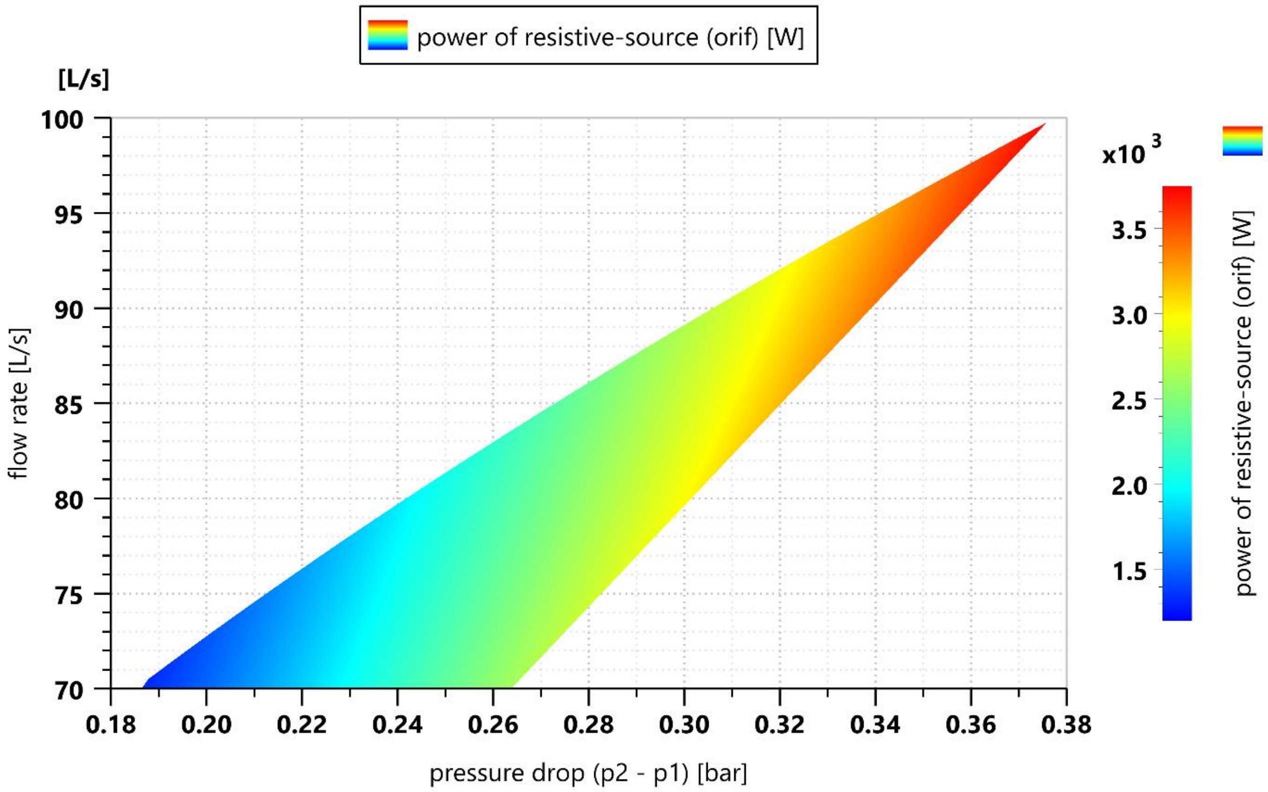

Fig. 8. Hydraulic power dissipated by the hydraulic orifice depending on pressure drop and flow rate.

4. Conclusions

The study found that a calibrated orifice with a geometry of Ø125 x 100 mm provides the most effective means of maintaining a stable water level in the upper basin. Without this calibrated orifice, the upper basin drains in under 12 seconds. However, with the orifice in place, the water level remains nearly constant, demonstrating its suitability for ULH hydraulic turbine optimization. Additionally, the pressure drop across the orifice varies between 0.18 and 0.38 bar for flow rates from 70 to 100 L/s, while the power dissipated through the orifice ranges from 1.2 to 3.7 kW. These findings underscore the orifice’s role in managing flow and energy dissipation effectively within the experimental stand.

Acknowledgments

This work was carried out through the Core Program within the National Research Development and Innovation Plan 2022-2027, carried out with the support of the Romanian Ministry of Research, Innovation and Digitalization (MCID), project no. PN 23 05.

References

[1] Chaulagain, Raj Kumar, Laxman Poudel, and Sanjeev Maharjan. “A review on non-conventional hydropower turbines and their selection for ultra-low-head applications.” *Heliyon* 9, no. 7 (July 2023): e17753.
[2] Maika, Nosare, Wenxian Lin, and Mehdi Khatamifar. “A review of gravitational water vortex hydro turbine systems for hydropower generation.” *Energies* 16, no. 14 (2023): 5394.
[3] Chaulagain, Raj Kumar, Laxman Poudel, and Sanjeev Maharjan. “Design and experimental analysis of a new vertical ultra-low-head hydro turbine with the variation of outlet flow level on the head drop section of an open canal.” *Results in Engineering* 22 (June 2024): 102240.
[4] Shamsuddeen, Mohamed Murshid, Mohammad Abu Shahzer, Min-Su Roh, and Jin-Hyuk Kim. “Feasibility study of ultra-low-head hydro turbines for energy extraction from shallow waterways.” *Heliyon* 10, no. 15, (August 2024): e35008.
[5] Yah, Nor F., Ahmed N. Oumer, and Mat S. Idris. “Small scale hydro-power as a source of renewable energy in Malaysia: A review.” *Renewable and Sustainable Energy Reviews* 72 (May 2017): 228-239.
[6] Chaulagain, Raj Kumar, Laxman Poudel, and Sanjeev Maharjan. “Experimental comparison of the upstream head using the non-rotating model of the vertical ultra-low head hydro turbine with its prototype.” Paper presented at the 11th International Symposium on Current Research in Hydropower Technologies 2023 (CRHT-XI), Kathmandu, Nepal, March 27, 2023. *Journal of Physics: Conference Series* 2629 (2023): 012018.
[7] Shamsuddeen, Mohamed Murshid, Sang-Bum Ma, No-Hyun Park, Kyung Min Kim, and Jin-Hyuk Kim. “Design analysis and optimization of a hydraulic gate turbine for power production from ultra-low head sites.” *Energy* 275 (July 2023): 127371.
[8] Timilsina, Ashesh Babu, Sean Mulligan, and Tri Ratna Bajracharya. “Water vortex hydropower technology: a state-of-the-art review of developmental trends.” *Clean Technologies and Environmental Policy* 20 (2018): 1737-1760.

ADHESION OF COLD-SPRAYED COATINGS AND THE WORKABILITY OF THE APPLIED SUBSTRATE

Medard MAKRENEK[1], Wojciech ŻÓRAWSKI[2]

[1] Kielce University of Technology, Faculty of Management and Computer Modelling, fizmm@tu.kielce.pl

[2] Kielce University of Technology, Faculty Mechatronics and Mechanical Engineering, ktrwz@tu.kielce.pl

Abstract: *Modern testing equipment for mechanical properties of materials allows for highly precise measurements of both hardness and the elasticity modulus. Advances in nanoindentation techniques, coupled with sophisticated software, make it possible to generate detailed load and unload curves. In particular, the area between the load and unload curves has been recognized as a new metric for evaluating the mechanical characteristics of a material. This area quantifies the energy absorbed during the loading process and released during unloading, which can be thought of as the 'workability' of the material. This term 'workability' is used because the value is calculated based on the area between the two curves, represented on a plane where the force (F) is plotted against the displacement of the indenter (d). The larger the area, the more work the material undergoes during deformation, thus giving an indication of its mechanical robustness and durability under stress.*

In the study, titanium coatings were applied using a cold gas spraying technique to several different metal substrates, including brass, steel, titanium, Al7075, copper, magnesium, and Al2024. Cold gas spraying was chosen because it is an effective method for depositing coatings without excessive heating, thus preserving the structural properties of both the coating and the substrate. In optimizing the spray parameters, the best conditions for coating titanium on the Al7075 alloy were identified: a spraying pressure of 40 bar, a gas temperature of 800°C, a gun traverse speed of 4 m/s, and a distance of 50 mm between the spray gun and the sample.

After the coatings were applied to the different substrates, several mechanical tests were conducted, focusing on hardness, elasticity modulus, and workability. A total of 36 nano-hardness and elasticity tests were performed on each substrate, allowing for the calculation of average values for each property. These results were summarized in a table, and a graph was plotted to illustrate the relationship between workability and elasticity. Interestingly, the experimental data points did not show a clear correlation between these two properties, indicating that the behavior of materials in terms of elasticity and workability may not be directly linked or may be influenced by other factors.

In addition to the mechanical property measurements, adhesion tests were conducted to determine how strongly the titanium coatings adhered to each substrate. The results did not show a strong correlation between adhesion strength and either workability or elasticity, suggesting that the adhesion process is likely governed by more complex factors beyond just the mechanical properties of the substrate. These discrepancies may be due to the intricate nature of the adhesion mechanisms or limitations in measurement accuracy, which could obscure any potential trends or relationships.

Keywords: *Cold Spray, hardness, elastic modulus, adhesion*

1. Introduction

Modern systems for transporting liquids or gases can interact with the materials used in their construction, such as pipelines, pumping stations, and pumps. When dealing with the transport of liquids or chemically active gases, the materials used in pipeline construction must demonstrate mechanical, chemical, and thermal resistance. To satisfy these requirements while simultaneously reducing transport system costs, thin coatings—measuring fractions of a millimetre—are applied to the substrate material. These coatings are made from materials that meet the necessary performance criteria.

Adhesion refers to the phenomenon where attractive forces between the substrate and the coating material create a durable bond. These forces arise from intermolecular interactions, including hydrogen bonds, Van der Waals forces, and electrostatic interactions. The value of adhesion forces is influenced by factors such as surface preparation and cleaning, surface roughness and topography, surface energy of the materials, and the polarity of the molecules [1]. Naturally, in addition to adhesion, maintaining the integrity of the coating itself is also crucial. The measure of a coating's integrity is the value of cohesion forces. Cohesion is the phenomenon of attraction between molecules of the same substance, which ensures that the material retains its structural integrity. In cold spray (CS) processes, numerous factors influence the value of adhesion. In their work, G. Prashar and H. Vasudev discussed methods for evaluating adhesion and identified the factors affecting its magnitude [2].These factors include gas temperature, gas type, the type of coating material, grain size and shape, and the degree of grain oxidation. Additionally, the properties of the substrate, such as hardness, temperature, and surface roughness, play a significant role.
An innovative coating application method is the thermal spray technique, specifically Cold Spray, in which the coating material is applied to the substrate without altering the properties of the deposited material layer.

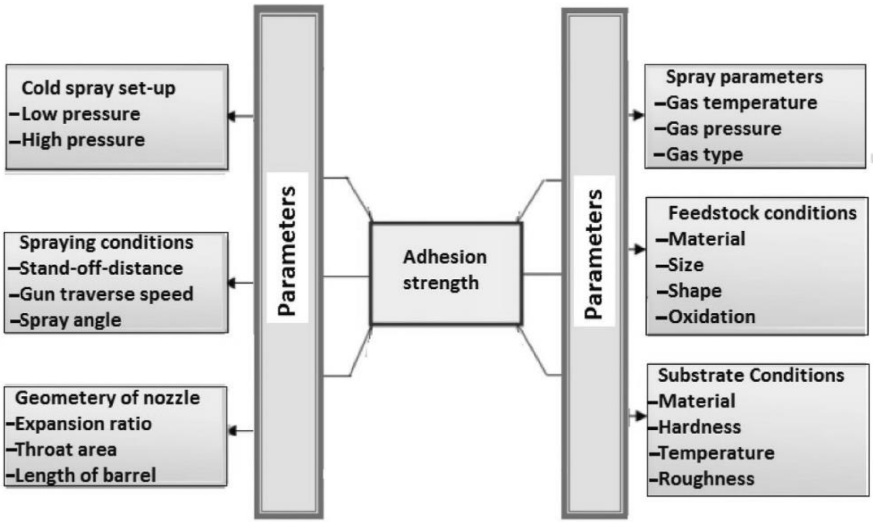

Fig. 1. Selected CS spraying parameters affecting adhesion

The essence of the Cold Spray process lies in imparting kinetic energy to the coating material particles, which, after passing through a converging-diverging nozzle, impact the substrate. When the particles reach the appropriate velocity, they adhere to the substrate, forming a coating. Depending on the coating material and the substrate, particle velocities must range from 300 to 1200 m/s. The successful deposition of the coating is determined by achieving the proper velocity—called the threshold velocity. This velocity is achieved by using a carrier gas with pressures in the range of 0.5–15 MPa. The temperature of the carrier gas is lower than the melting temperature of the feedstock material and typically ranges from 0 to 800°C. Common process gases include air, nitrogen, and helium. Figure 2 illustrates the Cold Spray process concept.
A powder of the coating material, with particle sizes ranging from 5 to 150 µm, is introduced into the gas stream. In the initial stage of the metal spray process, surface activation occurs, oxides are removed, and the substrate is cratered. In the subsequent phase of spraying, the actual coating is formed through mechanical interlocking, plugging, and the occurrence of adiabatic shear [3, 4].

Adiabatic shear instability refers to the loss of the material's shear strength, causing the deformation mechanism to shift from plastic to viscous. Therefore, the shape and size of the particles are of significant importance. In the spraying process, it is crucial for the particles to achieve sufficient kinetic energy. Particles with low mass and small size are preferred. Large particles have a greater surface area, which influences the amount of oxidized coating material. This process is undesirable from the perspective of coating formation and its adhesion to the substrate. From the perspective of the spraying process, it is preferable for the particles to have similar sizes. Such a particle size distribution ensures a precise determination of the critical velocity. As shown in Figure 2, the key component of the cold gas spraying system is the de Laval nozzle.

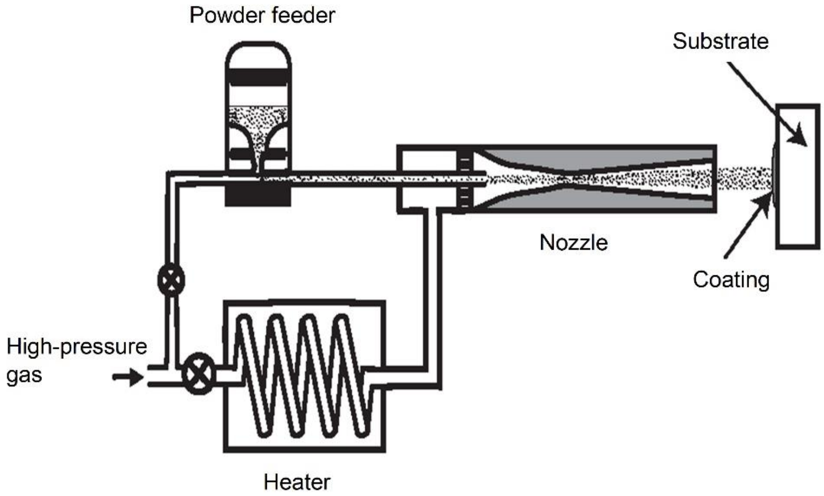

Fig. 2. The concept of cold gas spraying

The Cold Spray process is based on imparting kinetic energy to particles. To achieve this, particles are introduced into a gas stream (such as nitrogen, hydrogen, or air) before entering the nozzle, where they pass through a region of heated gas. As previously noted, the system used in the study is capable of heating the gas to 800°C. The heated gas increases the pressure at the inlet, which in turn elevates the velocity of the coating particles. After passing through the nozzle, the particle velocity can reach supersonic speeds. In the first, convergent section of the nozzle, the flow is accelerated to the speed of sound, while in the second, divergent section, the flow is further accelerated to supersonic speeds through an expansion process similar to that used in jet engines. Particles that attain high velocities, while maintaining relatively low temperatures, are directed in a solid state toward the substrate, typically at a right angle or near-right angle. The plastic deformation of the particles upon impact activates mechanisms that bind the forming coating to the substrate. These mechanisms involve jamming and plugging of the coating material with the substrate. The required particle velocity upon collision with the substrate is determined by the hardness (H) and Young's modulus (E) of both the coating material and the substrate. The Cold Spray process is fundamentally based on imparting kinetic energy to particles. In this process, particles are introduced into a gas stream—typically nitrogen, hydrogen, or air—before they enter the nozzle, where they are subjected to a region of heated gas. As previously noted, the system employed in the research is capable of heating the gas to temperatures as high as 800°C. The heating of the gas leads to an increase in pressure at the inlet, which, in turn, results in an increase in the velocity of the coating particles. After passing through the nozzle, the particles reach velocities that can exceed the speed of sound, entering the supersonic range. In the first, convergent section of the nozzle, the gas flow is accelerated to the speed of sound, where the velocity of the gas increases progressively. In the subsequent, divergent section of the nozzle, the gas is further accelerated to supersonic speeds through an expansion process, similar to the principle employed in jet propulsion systems. This acceleration of the gas stream imparts significant kinetic energy to the particles, which is crucial for the successful deposition of the coating.

Upon achieving high velocities while maintaining relatively low temperatures, the particles are directed toward the substrate in a solid state, typically at a right angle or close to a right angle. The impact of these high-velocity particles induces plastic deformation upon collision, which is a critical step in the formation of the coating. This deformation activates several key mechanisms that facilitate the bonding of the coating to the substrate. These mechanisms include jamming, where particles interlock upon impact, plugging, which refers to the filling of surface irregularities by the particles, and mechanical interlocking, where the particles become embedded within the microstructure of the substrate. Collectively, these processes contribute to the establishment of a strong adhesive bond between the coating and the substrate surface, ensuring effective coating adhesion.

The specific particle velocity required for successful deposition is influenced by the intrinsic material properties of both the coating and the substrate. These properties include hardness (H) and Young's modulus (E), both of which are vital in determining the extent of plastic deformation that can occur upon impact and, consequently, the quality of the bond that forms between the particles and the substrate. Hardness influences the resistance to deformation, while Young's modulus determines the material's ability to withstand elastic deformation. The interplay of these factors ensures that the coating adheres to the substrate with sufficient strength, thus enabling the coating to perform effectively in its intended application. Properly balancing these material properties with the correct particle velocity ensures that the coating meets the required performance characteristics, such as durability, wear resistance, and adhesion strength.

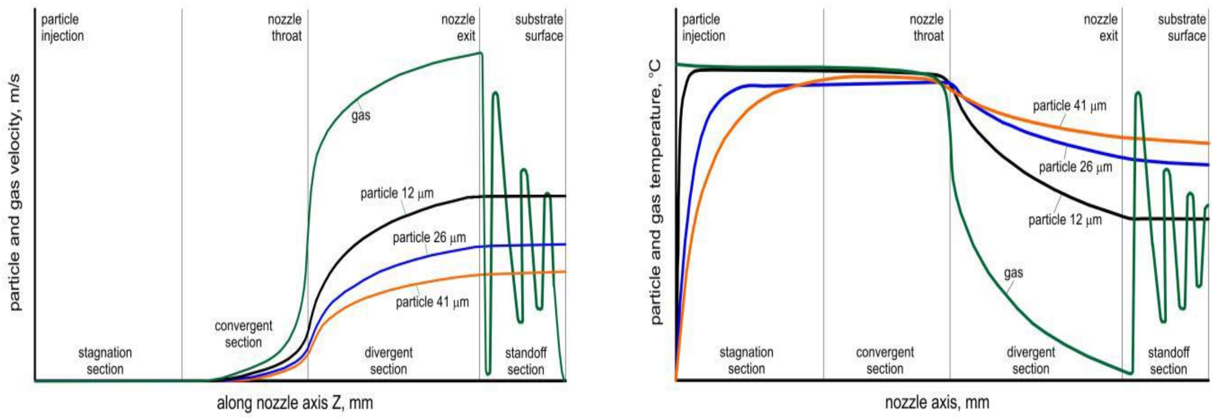

Fig. 3. The distribution of gas temperature and the velocity of the coating material particles [5]

The deposited coatings can serve a wide range of functions, each contributing to the enhancement of the substrate's properties. Functional coatings involve the deposition of a material, distinct from the substrate, onto the substrate surface to impart new functionalities, such as corrosion resistance, wear resistance, electrical conductivity, and viscosity reduction, among others. Part remanufacturing involves applying a material similar to the substrate onto a prepared surface to repair geometric defects in a component, which may have occurred due to wear, corrosion, or manufacturing imperfections. This process allows for the restoration of parts to their original shape and functionality. Additive manufacturing, enabled by cold spray technology, allows the creation of thick and very thick layers (several centimeters in thickness). This capability has opened new possibilities for producing parts with geometries close to their final form, reducing the need for post-processing and enhancing the efficiency of production.

Cold Spray, a technique introduced by Papiryn approximately 30 years ago, has become increasingly recognized, though it is still regarded as innovative in some industries [6]. Over recent years, the cold spray process has garnered significant attention due to its ability to produce dense, thick metal deposits while maintaining the purity of the sprayed powders. This is achieved without inducing phase transitions in the material—there is no formation of new phases or oxidation of the coating material during the process. As a result, the process preserves the integrity of the material properties, making it highly advantageous for various applications.

The benefits of Cold Spray technology have become widely acknowledged, particularly in fields such as aerospace, biomedicine, and energy. Its ability to deposit high-quality coatings without excessive thermal impact on both the coating and substrate materials has made it a valuable technique for producing durable, high-performance components.

2. Materials and Methods

In the experiment, the focus was placed on studying adhesion in relation to the mechanical properties of both the coating material and the substrate, while considering the values of the spray parameters. The shape and size of the coating material particles were consistent across all cases.

2.1 Research Equipment and Methodology

The equipment used in the cold gas spraying process is shown in Figure 4, highlighting the key components. As mentioned earlier, the central element of the spraying system is the de Laval nozzle (1), the gas preheating area (2), the powder material feeder, the electronic process control system for spray operation (4), and the robot that holds the de Laval nozzle and heaters, enabling precise control over the coating application process. This setup represents a typical industrial system, the Impact Innovations 5/8, in conjunction with the Fanuc M-20iA robot.

Fig. 4. The Cold Gas spraying coating system setup [7]

The adhesion value of the obtained coating was tested using a nanoindenter, applying an indentation force of 20 mN with an indenter loading and unloading rate of 40 mN/min. Based on the conducted tests, hardness (H) and Young's modulus (E) were determined. The research was carried out using a nanoindenter from NANOVEA. Measurements were performed at 36 points on cross-sectional samples of all coatings.

The adhesion of the coatings was evaluated by measuring the vacuum generated beneath a mushroom-shaped probe that was attached to the coating surface. This method involves placing the probe onto the coating, creating a sealed contact between the probe and the surface. A vacuum is then applied, and the resulting pressure difference is monitored. The degree of vacuum generated reflects the strength of the bond between the coating and the substrate. A higher vacuum indicates stronger adhesion, as it suggests that the coating is securely attached to the substrate, with minimal air gaps or separation. This technique provides valuable insights into the quality and effectiveness of the coating's adhesion properties.

Fig. 5. Vacuum pump and detachment mushroom holder

The detachment mushroom holder was adhered to the coating and subsequently detached by creating a vacuum ranging from 0 to 50 MPa. The diameter of the mushrooms used was 15 mm. Each coating was tested three times, and the result assigned to the coating was considered the average value. To characterize the morphology of the powders and their metallographic cross-sections, a scanning electron microscope (SEM, E-SEM FEI XL 30) was employed. This method allows for precise measurements of the coating's adhesion properties, with the vacuum-induced detachment force serving as a key indicator of the bond strength between the coating and the substrate. The use of SEM enabled a detailed analysis of the powder morphology and microstructure, providing valuable insights into the coating's characteristics and quality at the microscopic level.

2.2 Coatings and Substrate Types

Titanium powder with a particle size distribution shown in Figure 6 was selected as the coating material. For the spraying process, titanium particles with a granulometry range of 20–70 µm were chosen. The average particle size was approximately 31.5 µm. The Ti particles were approximately spherical in shape.

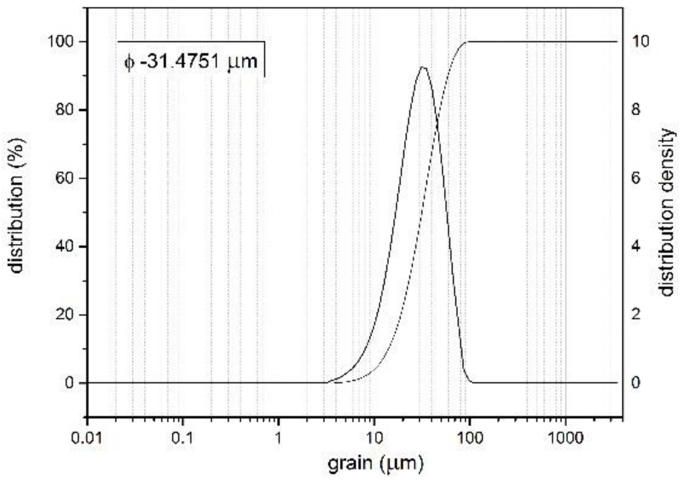

Fig. 6. The granulometric distribution of Ti particles

Seven metal plates were selected as substrates for the application of the titanium coating. These substrates were rectangular plates, each measuring 25 x 3 x 0.5 cm, which provided an adequate surface area for uniform coating deposition. To ensure optimal adhesion between the coating and the substrate, the metal plates underwent surface preparation processes before coating. Specifically, the substrates were sandblasted to increase surface roughness, which is crucial for enhancing the mechanical interlocking between the coating and substrate. Additionally, the plates were degreased to remove any oils, contaminants, or residues that could interfere with the coating process and adhesion quality.

Table 1 presents a detailed list of the materials used for the substrates, including their corresponding Young's modulus (E), which is a critical parameter in evaluating the mechanical properties of the substrate material. Young's modulus provides insights into the material's stiffness, which plays an important role in determining the behavior of the coating during the deposition process and under operational conditions.

Table 1: List of substrate materials

Substrate	E [GPa]
Al2024	175,0±11,0
Al7075	155,0±9,0
Brass	110,0±7,5
Copper	120,0±8,0
Magnesium	1,0±0,1
Steel	210,0±7,6
Titanium	150,0±8,0

To ensure the accuracy and reliability of the experimental results, all measurements were carried out using a single, consistent machine setup. This approach minimized variability in the testing conditions, contributing to the precision of the obtained data and making the results more comparable across different tests. The values of Young's modulus (E) were measured using the NANOVEA nanoindenter.

2.2 Selection of Experimental Parameters - G. Taguchi's Statistical Method

The Taguchi method is a structured approach to experimental design aimed at process optimization and the creation of high-quality systems. It reduces the number of experiments needed while maintaining precision and consistency. This approach, based on factorial design, utilizes an orthogonal array—a set of experiments performed under different conditions—to assess and optimize the selected factors (variables). Known for its simplicity, effectiveness, and reliability, the Taguchi method is widely used in optimization tasks [8, 9].
The Taguchi design utilizes a loss function, which is transformed into a signal-to-noise (S/N) ratio to assess the deviation between experimental outcomes and desired targets. The S/N ratio is calculated as the ratio of the mean response to its standard deviation, serving as a tool to pinpoint the optimal settings for each factor to improve performance. In S/N analysis, performance characteristics are classified into three categories: lower-the-better, higher-the-better, and nominal-the-better. Additionally, statistical analysis, often through analysis of variance (ANOVA), is employed to identify the most significant variables. By combining the Taguchi design with ANOVA, a powerful method for determining the optimal process conditions is achieved.
The S/N ratio represents the relationship between the mean (signal) and the standard deviation (noise) and is influenced by the quality characteristics of the product or process being optimized. Commonly used S/N ratios include nominal-is-best (NB), lower-the-better (LB), and higher-the-better (HB).
In the conducted experiment, the HB procedure was chosen due to the goal of achieving the highest possible adhesion value of the coating to the substrate.
Funkcha S/N przybiera postać

$$S/_N = -10log_{10}\frac{1}{n}\sum_{i=1}^{1}\frac{1}{y_i^2} \tag{1}$$

where y is the measured quantity.
The selection of parameters was carried out for a coating made of titanium on a titanium substrate. In the experiment, controlled parameters and their value ranges were chosen, which are presented in Table 2.

Table 2: The set of cold gas spray parameters

T [ºC]			p [bar]			d [mm]			V [mm/s]		
700	750	800	30	37	45	30	40	50	300	400	500

The selection of parameters for the deposition of a titanium coating on a titanium substrate was carried out using industrial statistics based on the Genichi Taguchi method. One of the main advantages of this method is the significant reduction in the number of experiments required, along with the flexibility to adjust the parameter values in real-time. Four controlled parameters were chosen: temperature (T), pressure (p), velocity (V), and distance (d), with each parameter having three possible values. Without the application of the Taguchi method, the total number of combinations would be $3^4 = 81$, which is a substantial number of experiments. However, by applying the Taguchi statistical method, the number of experiments was reduced to just 9. The experimental design and its details are presented in Table 3. This approach not only saves resources but also streamlines the process of determining the optimal conditions for the coating deposition.

Table 3: Experimental plan according to Taguchi

Trial no.	Input parameters			
	T [ºC]	p [bar]	d [mm]	V [mm/s]
1.	700	30	30	300
2.	700	37	40	400
3.	700	45	50	500
4.	750	30	40	500
5.	750	37	50	300
6.	750	45	30	400
7.	800	30	50	400
8.	800	37	30	500
9.	800	45	40	300

After completing the parameter selection, a verification experiment was carried out to assess the effectiveness of the chosen parameter values in controlling the spray process. In this phase, the experiment aimed to confirm whether the selected conditions would produce the desired coating properties, such as optimal adhesion, uniformity, and thickness. This verification step helped ensure that the process was operating within the intended specifications and provided insights into any potential adjustments needed for further optimization.

3. Results and Discussion

According to formula (1), the calculated S/N (ETA) function and its solution are presented in Figure 7. Each input parameter was assigned specific values (Table 2). After completing the full set of experiments in accordance with Table 3, a statistical analysis was performed to determine the optimal values of temperature (T), pressure (p), velocity (V), and distance (l), and their influence on the S/N function was analyzed. The primary factor determining the quality of the experiment was the adhesion of the coating to the substrate.

For temperature, the value of the ETA function increases with rising temperature and reaches its maximum at a temperature of 800°C. A similar approach was used to determine the optimal pressure (p), which did not reach saturation within the designated range. The highest ETA value occurred at a pressure of 45 bar. An analogous procedure was followed for the spray distance (l) and velocity

ISSN 1454 - 8003
Proceedings of 2024 International Conference on Hydraulics and Pneumatics - HERVEX
November 13-15, Băile Govora, Romania

(V). The ETA diagram for the distance l shows that the value for a distance of 50 mm is close to saturation. Similarly, in the analysis of ETA for the spray head velocity, the maximum value of the analyzed function was found at the extreme value of 500 mm/s, within the range of 300 to 500 mm/s.

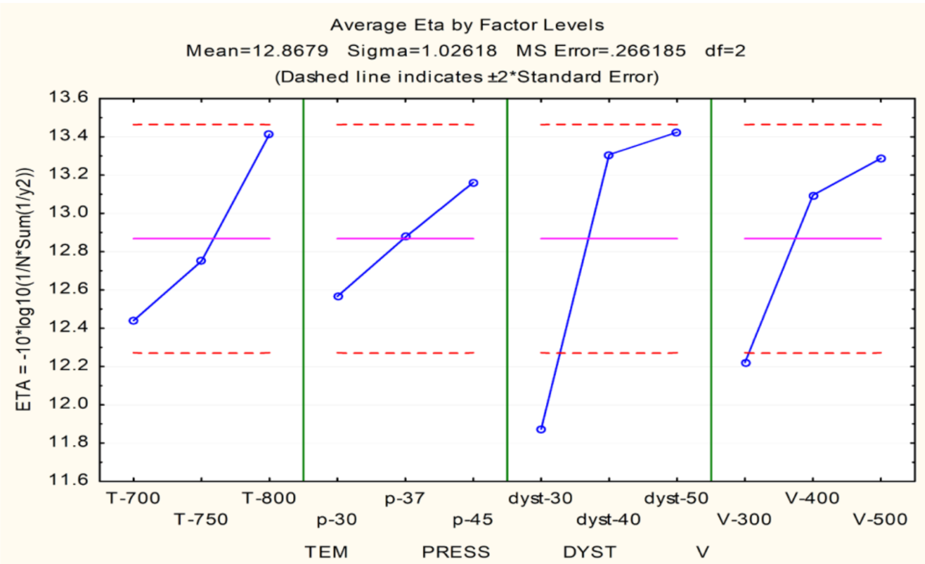

Fig. 7. Diagram of the values of the process control parameters for cold gas spraying

In optimizing the spray parameters, the best conditions for coating titanium onto titanium were identified: a gas temperature of 800°C, a spraying pressure of 45 bar, a distance of 50 mm between the spray gun and the sample, and a traverse speed of 500 mm/s. The selection of parameter ranges was mainly determined by the capabilities of the spraying equipment. Despite the identification of the optimal values within the specified range, the analysis suggests that higher values for temperature and pressure could potentially improve the process further.
The following Figure 8 presents selected cross-sections of the sprayed coating, obtained under the statistically chosen parameters that control the coating application process. The coating is uniform, showing no cracks or porosity. A clear interface between the coating and the substrate is visible, exhibiting the typical mechanical bonding features such as jamming and interlocking of the coating material with the substrate. To assess the quality of the deposited coating, control measurements of hardness (H) and Young's modulus (E) were carried out on cross-sectional specimens. These measurements are critical in evaluating the mechanical performance of the coating and its adhesion to the substrate.

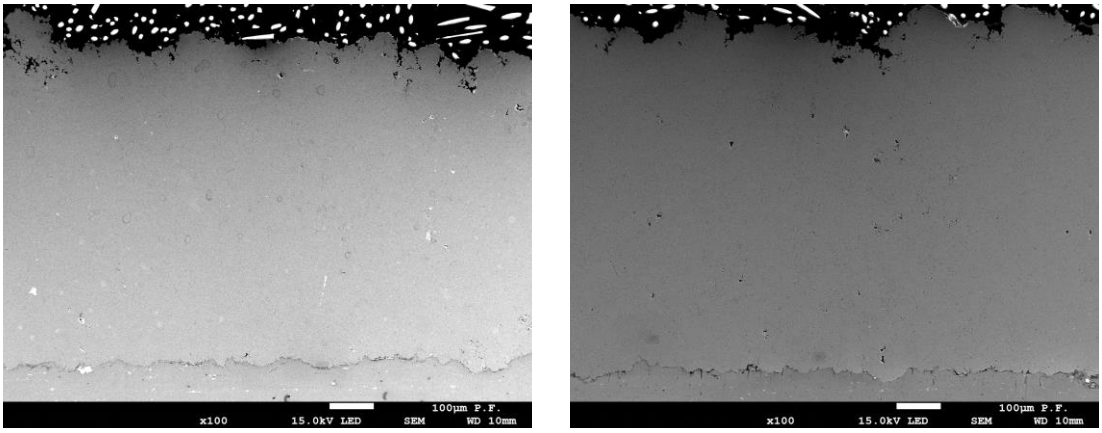

Fig. 8. Cross-section of the coating and substrate of the Ti coating on Ti.

The obtained results fluctuated around the mean with an error of less than 6%. This result was considered satisfactory.
The adhesion test for each coating was repeated three times, with the adhesion value taken as the average. The results were collected and graphically presented in Figures 9 and 10.

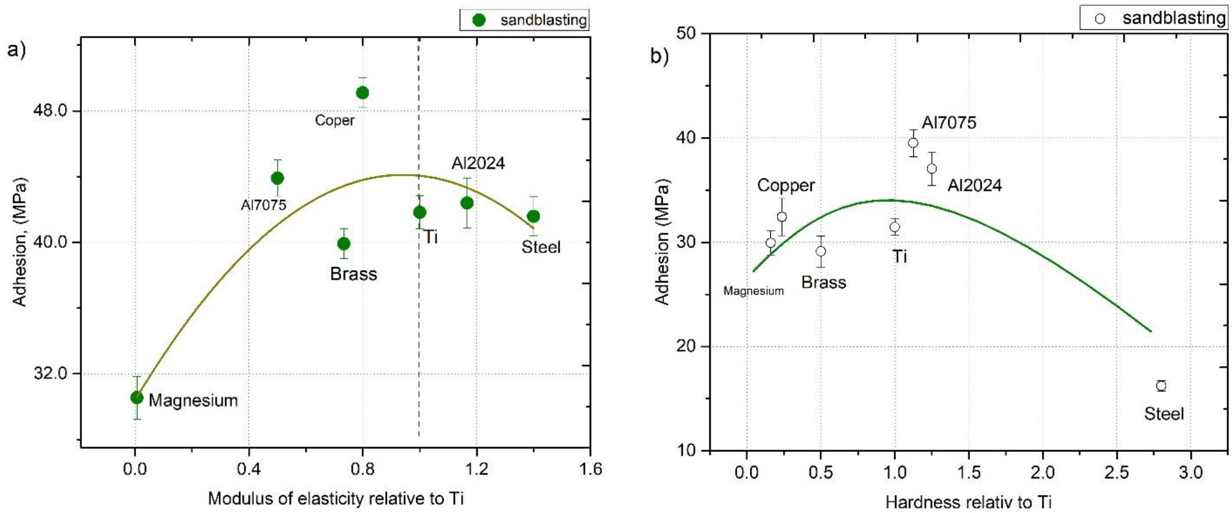

Fig. 9. a) Adhesion of the examined coatings as a function of Young's modulus (E),
b) Adhesion as a function of hardness (H)

The horizontal axes of the graphs are scaled with respect to the values of Young's modulus (E) and hardness (H) for titanium, where both the hardness and the modulus of elasticity are assigned a value of one. In Figure 9a, the adhesion values are lowest for magnesium, highest for copper, and then decrease for steel. The relationship between hardness and adhesion is expected to follow a similar trend. However, in this case, the adhesion for steel deviates significantly from the values observed for other substrates. This is due to the considerably higher hardness and Young's modulus of the titanium coating compared to the steel substrate. This difference arises from the insufficient kinetic energy of the particles impacting the steel surface, which is unable to induce the surface deformation necessary for mechanical interlocking. Analyzing Figure 9, it can be concluded that the modulus of elasticity might be replaced by another material parameter that better characterizes the behavior of the material in the context of adhesion formation.

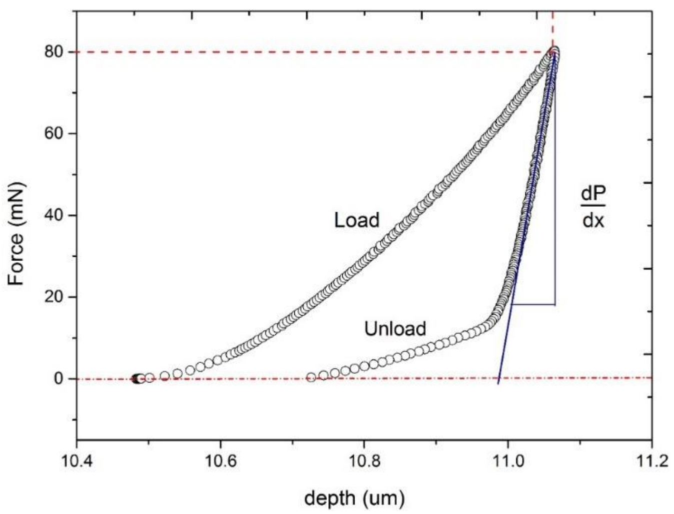

Fig. 10. The curves obtained in the hardness testing process using the indentation method

The elastic modulus is calculated from the initial slope of the unload curve, with the subsequent portion of the curve being disregarded. Some materials exhibit a very short unload curve, which reflects the almost unchanged indentation depth during indentation testing. In certain cases, the load curve reaches zero, indicating that the indentation in the material is significantly smaller than its maximum dimensions. This relationship suggests an alternative approach to plasticity, considering not only the shape of the curve but also the area enclosed by it.

Figure 10 presents the shape of the load and unload curves obtained during the indentation test. The area under the load curve represents the work done by the indenter in achieving the applied load force. The area under the unload curve reflects the work done by the material as it expels the indenter. The difference between the work performed by the indenter and the material is referred to as "workability" in this context. Integration under the curves was carried out to calculate the amount of work done, and the results are presented in Figure 11.

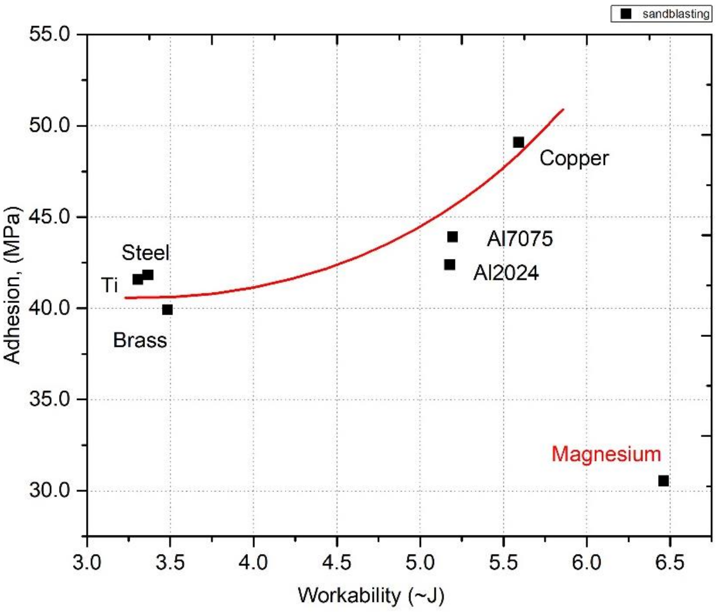

Fig. 11. Adhesion as a function of "workability"

It can be concluded that the relationship between adhesion and "workability" better reflects reality than the correlation between adhesion and Young's modulus. A correlation study was conducted between the Young's modulus and the "workability" values of the investigated coatings. The correlation coefficient was found to be -0.7±0.4, thus justifying the use of "workability" in further analysis.

4. Conclusion

A statistical optimization of the process of applying titanium coatings to various metal substrates was conducted. As a result of measuring the adhesion of titanium coatings on metal substrates with diverse mechanical properties, the highest adhesion value was observed in the case of copper. In contrast, the adhesion value for magnesium substrates was relatively low. There is a clear correlation between the adhesion results and the Young's modulus and "workability." Further analysis of adhesion in relation to Young's modulus and hardness leads to the conclusion that predicting the values of control parameters is effective for substrates whose Young's modulus and hardness values do not differ from those of the tested coating by more than 30%.
Analyzing the relationship between the examined variables (Fig. 9a and 12) confirms that the introduced parameter "workability" more accurately describes the material's behavior during the coating process using the cold spray technique.

When selecting the process parameters for cold gas spraying, it is important to choose the range of variability for the controlling parameters such that, in the statistical analysis (using the G. Taguchi method), the signal-to-noise (S/N) function reaches its extremum within the investigated range. This ensures that the process optimization results in the most favorable conditions for achieving the desired coating properties.

Acknowledgments

The authors would like to express their sincere gratitude to the organizers for selecting them to participate in the conference and for inspiring and creative discussions in a friendly atmosphere.

References

[1] HMS. “Adhesion of materials - bonding strength and methods of increasing it” / “Adhezja materiałów – siła sklejania i metody jej zwiększania”. *HMS Blog*, October 27, 2023. Accessed December 8, 2024. https://hms-steel.pl/adhezja/.

[2] Prashar, Gaurav, and Hitesh Vasudev. “A comprehensive review on the analysis of adhesion strength of cold spray deposits.” *Results in Surfaces and Interfaces* 16 (August 2024): 100263. https://doi.org/10.1016/j.rsurfi.2024.100263.

[3] Moridi, Atieh, Seyyed Mostafa Hassani-Gangaraj, Mario Guagliano, and Ming Dao. “Cold spray coating: review of material systems and future perspectives.” *Surface Engineering* 30, no. 6 (2014): 369-395.

[4] Małachowska, Aleksandra, Marcin Winnicki, and Andrzej Ambroziak. “Prospects of Low Pressure Cold Spray” / “Perspektywy natryskiwania niskociśnieniowego metodą Cold Spray.” *Przegląd Spawalnictwa - Welding Technology Review* 84, no. 10 (2012): 2-6.

[5] Winnicki, Marcin, Tomasz Piwowarczyk, and Aleksandra Małachowska. “General Description of Cold Sprayed Coatings Formation and of Their Properties.” *Bulletin of the Polish Academy of Sciences. Technical Sciences* 66, no. 3 (2018): 301-310. DOI: 10.24425/123436.

[6] McCune, R. C., A. N. Papyrin, J. N. Hall, W. L. Riggs II, and P. H. Zajchowski. *An exploration of the cold gas-dynamic spray method for several materials systems*. United States, National Center for Manufacturing Sciences, 1995.

[7] Soboń, Dominika. *Analysis of the effect of laser processing on the properties of Ti and Ti-6Al-4V coatings sprayed with cold gas / Analiza wpływu obróbki laserowej na właściwości powłok Ti i Ti-6Al-4V natryskanych zimnym gazem*. Doctoral dissertation. Kielce University of Technology, 2024.

[8] Taguchi, G., and Y. Wu. *Introduction to off-line quality control* (2nd ed.). Central Japan Quality Control Association, 2002.

[9] Van Dum Vu, H., et al. “Statistical optimization of process parameters using the Taguchi method: A review.” *Journal of Manufacturing Science and Engineering* 142, no. 2 (2020): 1-12.

ISSN 1454 - 8003
Proceedings of 2024 International Conference on Hydraulics and Pneumatics - HERVEX
November 13-15, Băile Govora, Romania

CONSIDERATIONS REGARDING THE IMPLEMENTATION OF HYDROSTATIC TRANSMISSIONS IN WIND TURBINE POWER TRANSMISSION SYSTEMS

Liliana DUMITRESCU[1], Alexandru-Polifron CHIRIȚĂ[1], Radu-Iulian RĂDOI[1], Ștefan-Mihai ȘEFU[1], Adriana Mariana BORȘ[1], Ionaș Cătălin DUMITRESCU[1,*], Eugen MARIN[2]

[1] National R&D Institute for Optoelectronics, Subsidiary Hydraulics and Pneumatics Research Institute Bucharest / Romania, dumitrescu.ihp@fluidas.ro

[2] National Institute of Research-Development for Machines and Installations Designed to Agriculture and Food Industry - INMA, Bucharest / Romania, emarin@inma.ro

Abstract: *Hydrostatic systems are characterized by the possibility of generating and transmitting large forces and moments, which are more difficult to achieve mechanically or electrically. The hydraulic energy generator (pump) can be connected to the drive element (hydraulic motor) with rigid or flexible pipes, which allows the latter to be located at a distance from the pump. If this principle is applied to a wind turbine, it results that the electric generator, which is usually located in the nacelle and is mechanically driven, can also be mounted on the ground and driven by a hydraulic motor. In this way, the mass located in the turbine nacelle decreases significantly, and the hydrostatic transmission also brings other advantages, related to maintenance, speed regulation, hydraulic energy storage, etc. The article presents a proposal for a hydrostatic transmission for a low-power wind turbine (below 100 kW).*

Keywords: *Wind turbine, hydrostatic transmission, nacelle, mass, simulation, electric generator*

1. Introduction

In recent decades, the perspective of depletion of fossil fuel resources, their increasing price and the problems related to pollution from the combustion of these fuels have led to an increasing exploitation of renewable or "green" resources. Among these, wind energy and solar energy have stood out, their exploitation capacities increasing annually by significant percentages. In 2023, this increase was 36%, with installed capacity reaching 473 GW. In addition to reducing pollution, another positive aspect of the exploitation of renewable resources is the large number of people employed in the field; thus, in 2023, 13.7 million people were involved, an increase of 8% compared to the previous year. The exploitation of renewable energy sources contributes 13% to Total Final Energy Consumption, in 2023, the same percentage as in the previous year.
Regarding wind energy, Europe had a total installed capacity of 272 GW at the end of 2023, of which 18.3 GW were added in 2023. In Romania, these values are 3.1 GW and 72 MW respectively, with wind energy covering 14% of the country's electricity consumption [1, 2].
In terms of wind energy conversion means, horizontal axis wind turbines have proven to be the most suitable, both for onshore and offshore installation; in the latter category, the largest turbine commissioned in 2024 has a capacity of 26 MW. The nacelle of this turbine is located at a height of 185 m and weighs around 1000 tonnes; a significant part of this weight is the electric generator and the mechanical transmission between the wind rotor and the generator, as well as the auxiliary systems.
In recent years, in addition to the cost of materials used in wind turbines, environmental issues have become increasingly important; this concerns pollution associated with the manufacture of components, as well as their transport by sea or land and their installation at the intended location, all of which are proportional to the mass of the turbine [3].
This is why reducing the suspended mass in the nacelle becomes increasingly important as the capacity of wind turbines increases. Moving the generator and mechanical transmission to the base of the turbine reduces the total weight of the nacelle, but also the weight of the supporting tower and

the base in which it is mounted. According to [4], for a 3 MW turbine, replacing the transmission lightens the nacelle by approx. 35%, and the weight of the tower will be reduced by a percentage between 33 and 50%. Even if these values cannot be scaled for current turbines of higher power, it is obvious that the weight reductions, and implicitly the costs of manufacturing, transportation, etc., are significant [5, 6].
Even though in the past the issue of reducing the cost of wind turbines was not so current, concerns regarding the realization of hydrostatic transmissions for wind turbines can be found since the 1980s, increasing with the installed power. Thus, the first significant achievement is the SWT-3 turbine, with a power of 3 MW, produced by the Bendix Corporation, and put into operation in 1980. The hydrostatic transmission was realized with 14 fixed-capacity hydraulic pumps and 18 variable motors. Between the rotor and the hydraulic pumps, as well as between the hydraulic motors and the electric generator, speed amplifiers with gears were mounted.
The Norwegian company ChapDrive AS took a step forward by using an all-hydraulic transmission, without mechanical speed amplification. For this, it used a low speed hydraulic pump, fixed displacement, and a high speed hydraulic motor with variable displacement, which drives the generator. The turbine was developed in various power variants, with tests being carried out on models from 50 kW to a turbine with a power of 900 kW; the next step was the design of a variant with a power of 5 MW.
Interest in the field of hydrostatic transmissions for wind turbines can also be found in Germany, at RWTH Aachen, where a transmission testing and simulation platform has been developed [7].

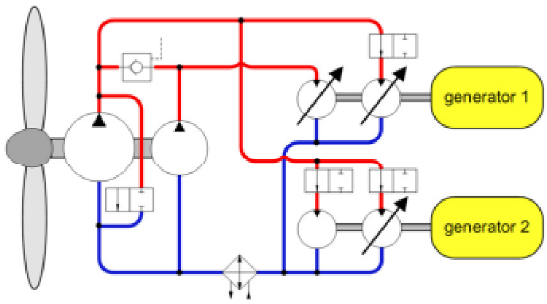

Fig. 1a. Hydrostatic transmission simulation platform for 1 MW wind turbines

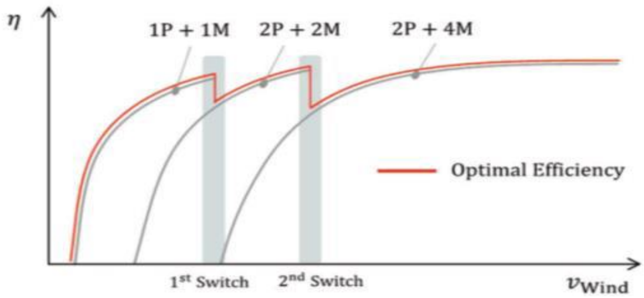

Fig. 1b. Overall system efficiency

The functional model consists of 2 fixed displacement hydrostatic pumps, one of which has a capacity 4 times greater than the other. 2 electric generators are driven by 2 hydraulic motors; of the 4 motors, 3 motors are fixed displacement and one has variable displacement. The latter is used alone at low wind speeds; at higher speeds the other drive motors are also introduced into the circuit.

2. Material and method

As shown, reducing the suspended mass has beneficial effects in several directions (economic, ecological, etc.). The importance of this solution increases as we consider larger turbines.
In any case, if the electric generator is to be placed on the ground, the energy of the wind rotor will have to be transmitted to the generator; the solution can be mechanical, hydraulic or a mix between the two types. As a rule, the purely mechanical transmission is used for low powers, while the hydrostatic transmission can also be used for high powers (even off-shore turbines, in the order of MW). It is also mandatory that a hydrostatic transmission has a component that allows the modification of the driving speed of the electric generator; most of the time, this component is a variable displacement motor (figure 2).

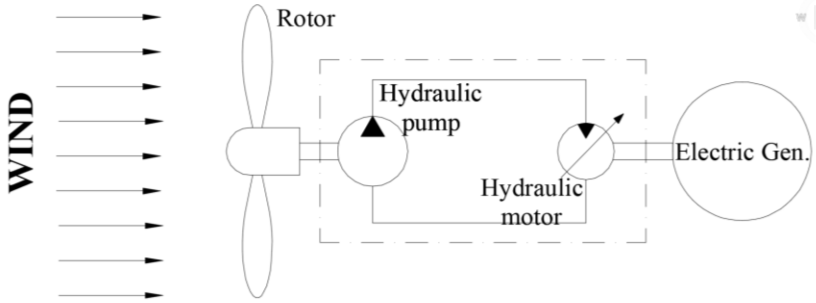

Fig. 2. Schematic diagram of a hydrostatic transmission for wind turbines

The Research Institute for Hydraulics and Pneumatics in Bucharest considered the creation of a mixed transmission, composed of 2 open-circuit hydrostatic transmissions and a mechanical transmission between them. The 2 hydrostatic transmissions are located in the nacelle, respectively on the ground, and the mechanical connection between them is made using a tubular shaft.
The first hydrostatic transmission, with the symbol HST1, is located in the turbine nacelle and acts as a speed amplifier; thus, the wind rotor drives an orbital hydraulic motor which in this case acts as a pump, with a displacement of 1000 cm^3/rev. The pump driven by the rotor transmits energy to a motor with a capacity of 34 cm^3/rev, both hydraulic machines having a fixed displacement. In this way, the speed of the wind rotor is amplified by approx. 30 times.
The hydraulic motor is coupled to a mechanical shaft, which transmits the rotational movement to the second hydraulic circuit (HST2); the shaft drives a fixed pump, with a displacement of 34 cm^3/rev. The pressurized fluid is transferred to a variable hydraulic motor, with a maximum capacity of 49 cm^3/rev, which drives the electric generator. By changing the displacement of the hydraulic motor, the constant generator drive speed is maintained.
The turbine simulated in AMESIM has a nominal power of 42 kW at a wind speed of 10 m/s and a corresponding speed of 100 rpm. For this power, a wind rotor with a diameter of 15 m is required, and the transmission shaft has a length of approx. 10 m.

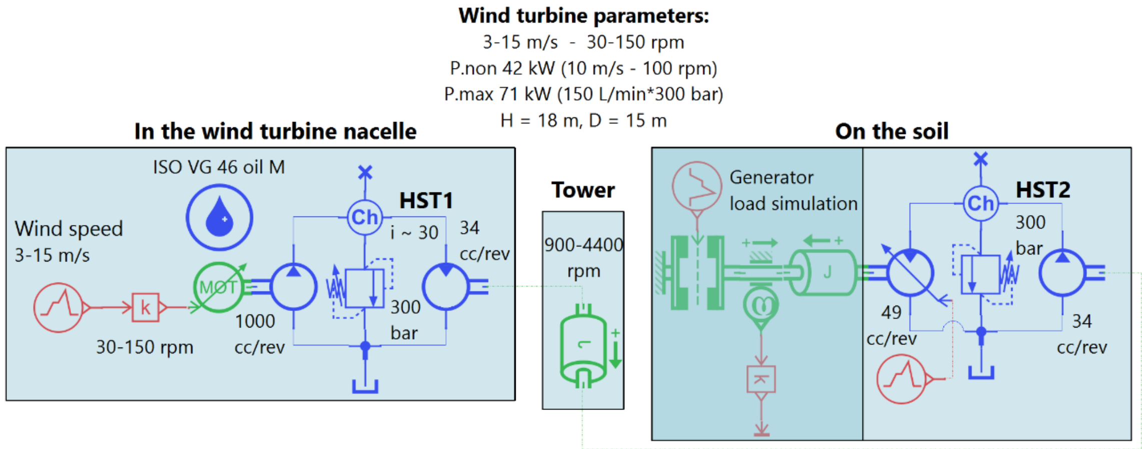

Fig. 3. Numerical simulation network of the wind turbine equipped with hydrostatic transmissions

3. Results & discussion

After running the simulation program of the turbine operation, having the wind speed as a variable parameter, the graphs in figures 4 and 5 resulted.
These graphs show the variation of the main parameters of the wind turbine depending on the wind speed. This parameter influences the power, which is proportional to the rotor speed, but also to the generator drive motor speed.

The turbine produces 42 kW at a wind speed of 10 m/s, which drives the turbine rotor at 100 rpm; at this speed, the variable hydraulic motor in HST2 has a speed of approx. 3000 rpm. The simulations were performed up to a wind speed of 15 m/s, at which the turbine has a power of 71 kW and a drive speed of the HST2 pump of 4400 rpm. At a wind speed of 15 m/s, the rotor rotates at 150 rpm.

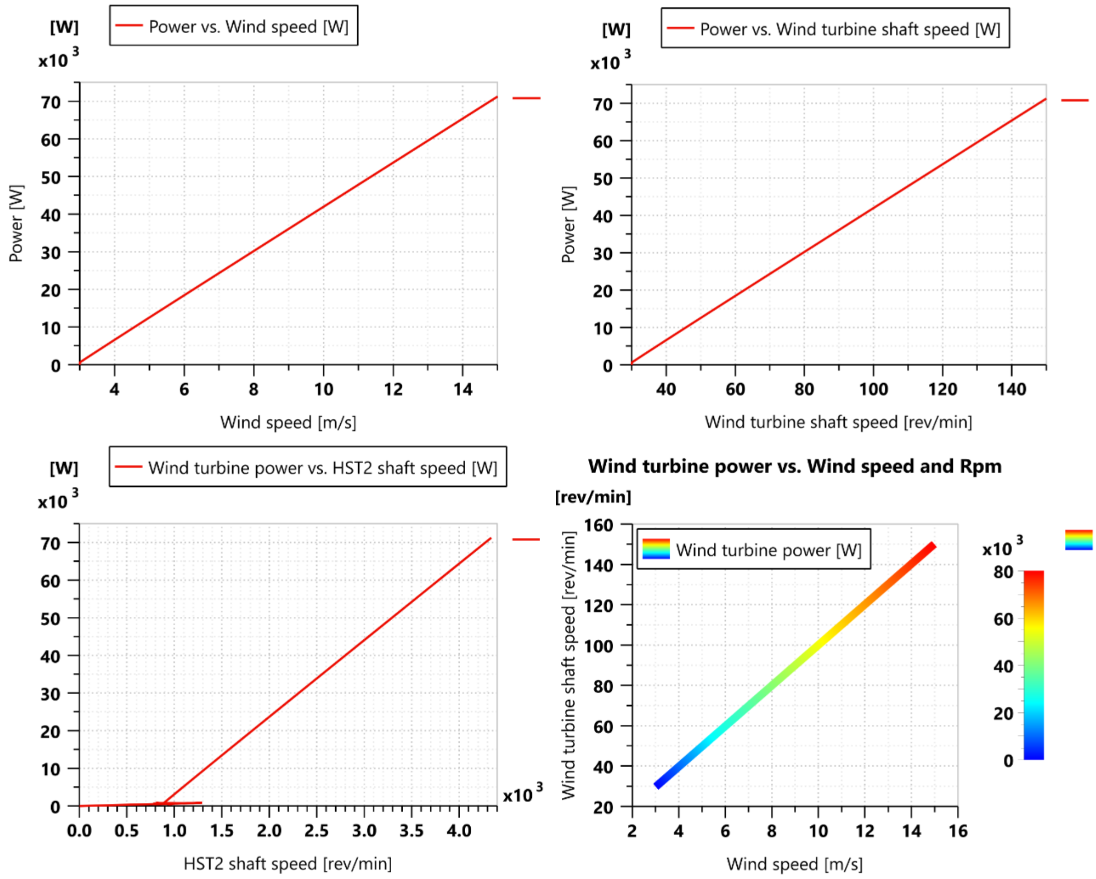

Fig. 4. Power as a function of wind speed, wind turbine shaft speed and speed of the hydraulic pump in the structure of HST2

At the electric generator level, it is of great importance that the drive speed and frequency are kept constant, at values of 3000 rpm and 50 Hz respectively. This is achieved by continuously changing the capacity of the hydraulic motor. The results for the 2 parameters are presented in figure 5.

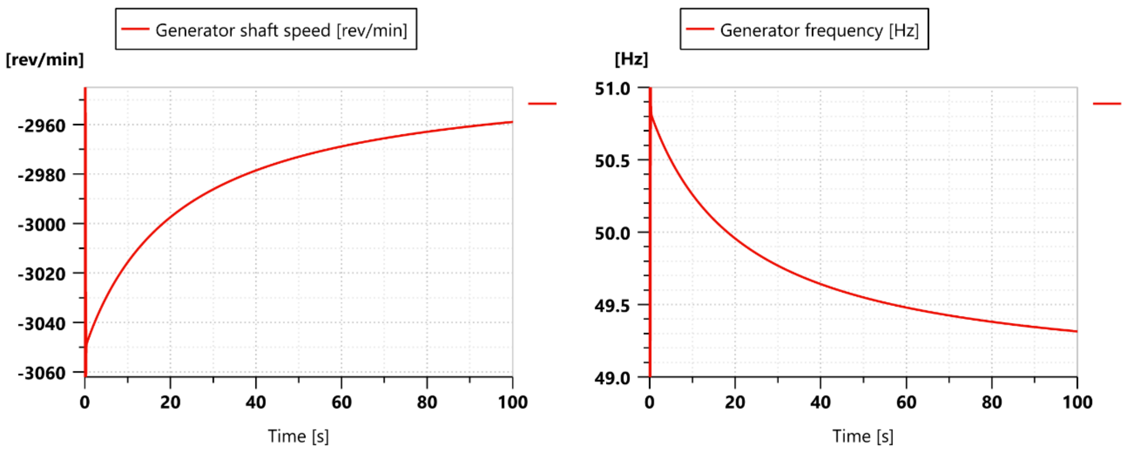

Fig. 5. Speed of the synchronous electric generator and its frequency

As can be seen from the first graph in the figure above, the generator speed varies by max. 60 rpm, which represents a deviation of less than 2%; as for the current frequency, it shows the same percentage variation around 50 Hz.

4. Conclusions

The use of hydraulic drives in applications for the production, transmission and storage of energy from renewable sources have application potential and are in continuous development.
There are various architecture solutions of hydrostatic transmissions and it must fulfil two important objectives: on the one hand, the management of large powers, up to over 10 MW at the present time, and on the other hand, the reduction of mass at the nacelle level.
The normally used mechanical power transmission can be easily replaced by a hydromechanical hybrid power transmission technology in wind power application.
In the proposed solution, the energy transmission is done mechanically-hydraulic; an open hydraulic circuit is placed in the turbine nacelle, which has the main role of amplifying the rotor speed, considered to be in the range of 30…150 rpm. The amplification ratio is 30. Thus, by means of a low-mass transmission shaft, the energy is transmitted to the second hydraulic circuit, which contains a variable hydraulic motor, which drives the electric generator, located on the ground, at a constant speed.
With this solution, both the generator drive speed and the frequency are maintained constant, with a deviation of less than 2%, which recommends the solution for implementation.
The proposed hydrostatic power transmission system for wind turbines has several advantages, such as reducing the suspended mass of the turbine, reducing the cost of the transmission system, and improving the general efficiency of the system.

Acknowledgments

The work was carried out through the Core Program within the National Research Development and Innovation Plan 2022-2027, carried out with the support of the Romanian Ministry of Research, Innovation and Digitalization (MCID), project no. PN 23-05.

References

[1] REN21 - Renewable Energy Policy Network for the 21st Century. “Renewables 2024. Global Status Report”, 2024. Accessed October 2, 2024. https://www.ren21.net/gsr-2024/.
[2] GWEC – Global Wind Energy Council. “Global Wind Report 2023”, *GWEC.NET*, August 28, 2023. Accessed October 13, 2024. https://gwec.net/globalwindreport2023/#download.
[3] Rajaei, Mozhdeh, and James M. Tinjum. “Life cycle assessment of energy balance and emissions of a wind energy plant.” *Geotechnical and Geological Engineering* 31, no. 6 (2013): 1663–1670.
[4] Roggenburg, Michael, Helber A. Esquivel-Puentes, Andrea Vacca, Humberto Bocanegra Evans, Jose M. Garcia-Bravo, David M. Warsinger, Monika Ivantysynova, and Luciano Castillo. “Techno-economic analysis of a hydraulic transmission for floating offshore wind turbines.” *Renewable Energy* 153 (June 2020): 1194-1204.
[5] Qin, Chao, Elijah Innes-Wimsatt, and Eric Loth. “Hydraulic-electric hybrid wind turbines: Tower mass saving and energy storage capacity.” *Renewable Energy* 99 (December 2016): 69-79.
[6] Jonkman, J., S. Butterfield, W. Musial, and G. Scott. “Definition of a 5-MW reference wind turbine for offshore system development.” National Renewable Energy Laboratory. Technical Report NREL/TP-500-38060, February 2009. Accessed October 23, 2024. https://core.ac.uk/download/pdf/71321186.pdf.
[7] Vukovic, Milos, and Hubertus Murrenhoff. “The next generation of fluid power systems.” *Procedia Engineering* no. 106 (2015): 2-7.

http://hervex.ro